Università degli Studi di Ferrara

DOTTORATO DI RICERCA IN "FISICA"

CICLO XXVII

COORDINATORE Prof. Vincenzo Guidi

Eni Carbon Silicates as crystalline and mesoporous hybrids for gas sensing

Settore Scientifico Disciplinare FIS/01

Dottorando	**Tutore**
Dott. Fabbri Barbara	Prof. Vincenzo Guidi

Anni 2012/2014

"La crisi è la più grande benedizione per le persone e le nazioni, perché la crisi porta progressi.
La creatività nasce dall'angoscia come il giorno nasce dalla notte oscura.
E' nella crisi che sorge l'inventiva, le scoperte e le grandi strategie.
Chi supera la crisi supera sé stesso senza essere superato.
Chi attribuisce alla crisi i suoi fallimenti e difficoltà, violenta il suo stesso talento e dà più valore ai problemi che alle soluzioni.
La vera crisi, è la crisi dell'incompetenza.
L'inconveniente delle persone e delle nazioni è la pigrizia nel cercare soluzioni e vie di uscita.
Senza crisi non ci sono sfide, senza sfide la vita è una routine, una lenta agonia.
Senza crisi non c'è merito.
E' nella crisi che emerge il meglio di ognuno, perché senza crisi tutti i venti sono solo lievi brezze.
Parlare di crisi significa incrementarla, e tacere nella crisi è esaltare il conformismo.
Invece, lavoriamo duro.
Finiamola una volta per tutte con l'unica crisi pericolosa, che è la tragedia di non voler lottare per superarla".

Albert Einstein

Contents

Introduction

A sensor is a device that detects events or changes in quantities and provides a corresponding output, generally as an electrical or optical signal. Sensors are used in everyday objects for innumerable applications; from common uses such as temperature, pressure or flow monitoring to particular purposes such as DNA selection.

Nowadays, in order to satisfy market demands, materials and devices for sensors production must be increasingly miniaturized, eco-friendly, energetically efficient, reliable multitasking, and low-cost, then the research in material and technological sciences have gained a huge development to reach the expectations. Moving towards these requirements, hybrid nanomaterials are a fundamental alternative choice with respect to well-established materials, such as metals, ceramics or plastics cannot fulfill all technological desires for the various new applications. The interest in hybrid materials composed of organic and inorganic units arises from the possibility of combining the advantages of both components, that is, mechanical, structural, and hydrothermal stability of the inorganic compound and the flexibility and functionality of the organic one, favorable for catalyzing consecutive or cascade reactions.

Indeed the objective of this thesis, which arises from a collaborative research project between Eni Spa and the Department of Physics and Earth Science of University of Ferrara, was to implement innovative hybrid materials referred to as ECS (Eni Carbon Silicate) in gas sensors manufacturing, in order to investigate first of all if the materials are suitable for film deposition, then if these films are electrically active, and finally if ECS represent an improvement for gas sensing field.

Until now, the experience of Sensors and Semiconductors Laboratory (LSS) has been focused on chemoresistive gas sensors based on metal-oxides semiconductors, completely inorganic. So, concerning the research in materials science, it is obvious that the employment of hybrids has represented a new challenge for LSS, especially because in ECS powders, with respect to the most hybrid materials, organic and inorganic compounds are perfectly merged each other in a complex structure: in fact, new crystalline phases ECSs have every silicon involved in one Si-C covalent bond, and they are obtained by using different bis-silylated organic precursors as silica source, without surfactant agent and $NaAlO_2$ is the source of aluminum. The presence of aluminum plays a relevant role favoring the crystallization of ECS's. The novelty of these materials concerns their structures, crystalline aluminosilicate scaffoldings with long-range 3D order, which distinguish them from the previously reported amorphous and "crystal-like" silica-based PMOs (periodic mesoporous organosilicas). This is the result of an high refined development of hybrids synthesis started from zeolites, since hybrids add variable chemical modification to the repertoire of zeolites, which are well established as heterogeneous catalysts, ion exchangers, and molecular sieves with many different pore architectures. These new materials could have very interesting properties, allowing the preparation of new functional active sites with tunable geometrical and chemical properties. Partial incorporation of organic groups into zeolites by using a reactant mixture of silsesquioxane together with a conventional silica has strong limitations. It can only be applied to zeolites with metal cations (e.g., NaX) or prepared using organic structure-directing agents that can be extracted by ion exchange (e.g., Beta) to avoid high-temperature treatment, which is deleterious for the organosilica group. Grafting silsesquioxanes onto preformed zeolites failed because most of the SiOH groups are located in the intercrystalline mesoporous regions.

A more successful approach for synthesizing hybrid zeolites involves using bis-silylated organic precursors as silica source. However, the much lower than expected organic content indicates that the Si–C bonds undergo hydrolysis. In any case, incorporation of methylene groups within the zeolite framework (an isomorphous substitution of –O– by –CH$_2$–) is still debated because of the impossibility to distinguish a methylene group in the framework from one in the amorphous impurities that are usually present. A breakthrough in the synthesis of crystalline aluminosilica-based hybrid organic–inorganic porous materials occurred in 2008 with the advent of ECSs.

Regarding the research in technological science nowadays solid-state devices have evolved rapidly improving the quality and decreasing the processing and operating costs. From this point of view, metal-oxide gas sensors, well-known at LSS, represent an achievement thanks to their attractive features as discrete reliability and repeatability of the measurement, very high sensitivity even at low gas concentration, low costs of manufacturing and small dimensions that allow a suitable integration for different uses making gas sensors fundamental in several fields, such as environmental monitoring, medical diagnoses, safety systems and industrial process control. Despite this, sensors based on metal-oxides provide high power consumption which supports chemical reaction at the surface, and very low response at room temperature characterized by an irreversible behavior. In fact the sensing mechanism of metal-oxide gas sensors relies on variations of the electrical resistance, due to the interactions of the functional material with oxygen and gas molecules at the surface, it is fundamental to know the dimensions of both the grains and the film to compare them with the length scale of surface interactions. For the majority of metal-oxide semiconductors, the variation of film's electrical resistance induced by bulk/surface charge transfer is promoted by using high temperatures. Despite the significant performances of these devices, thermal-activation entails high power consumption, lower durability and safety risk in presence of flammable gases. Then, room temperature operation is an extremely valuable goal in gas sensing research, due to intrinsic safety of sensors working in harsh or industrial environment, moreover it is interesting to reduce power consumption and consequently the size of associated electronics. In recent years, photo-activation mechanism has represented a precious alternative to achieve room temperature gas sensing.

Therefore the goal of this thesis first of all was to produce a sensors using ECS powders as functional materials then, due to their low temperature of processing, to verify their possible operation at room temperature.

The PhD thesis is organized in four Chapters and three Appendixes. In Chapters 1 and 2, based on previous works of Gomez-Romero P., Sanchez C., Kilckebick G., Hoffamann F., and Fröba M., hybrid materials and in particular PMOs are respectively investigated. Indeed, it was necessary to carry out a deepened study starting from the origins of organic-inorganic materials, thus to classify them examining their synthesis processes and properties, and then to search suitable examples to compare ECSs powders, main object of this work. Seeing as ECS synthesis resembles that of PMOs, ordered mesoporous organosilica hybrid materials are discussed. Starting from their classification and synthesis, it was fundamental to argue in particular PMOs which are the closer precursors of ECSs. Thus, these which in turn have been fully explored.

Among materials belonging to ECS family, the six powders provided by Eni to LSS are analyzed in Chapter 3 together with a brief discussion on chemoresistive gas sensors. The explanation of design and operating processes of these devices will make clear the project development. Then, in Chapter 3 the experimental setup and the characterization techniques used are explained.

In Chapter 4 the research method and results are reported: the Chapter is divided in two parts regarding the preliminary tests and the use of ECS powders as functional materials for sensing films. Finally the results are discussed and a possible interpretation of sensing mechanism is suggested.

List of publications

The research activity carried out by the PhD student involved all key aspects regarding the study and the realization of solid state devices for gas sensing: the use of innovative materials, such as organic-inorganic hybrids and non-oxide semiconductors, but also the deepening about new properties of well-known metal-oxides; then the design of enabling technologies alternative to alumina substrates and the study of new applications for gas sensors.

The collaborative research project regarding organic-inorganic nanoscale powders, Eni Carbon Silicates (ECS), as functional material is the subject of this PhD thesis. Films produced with these powders resulted electrically active showing a remarkable sensitivity to some target gases returning in stable, fast, and perfectly reversible signals obtained at room temperature. From the point of view of the sensing field, this is a revolutionary result and a contribution will be submitted to a high value journal. In parallel, by using powders of non-oxide semiconductors as functional material in the production of printing pastes, photo-conductivity and surface chemical activity were investigate discovering a good selectivity of these powders to other relevant gases. In this way, new scenarios for sensing material have been opened in alternative to metal-oxide semiconductors. In parallel a study regarding the use of porous silicon as a substrate for the production of chemo-resistive gas sensors has been developed, in order to limit power consumption and to increase adsorbing area and response performances, such velocity and reversibility. Finally, the possible applications of sensors produced were deepened in order to design portable devices for monitoring, in particular the response of the devices in the presence of gaseous emissions associated with cardiopulmonary diseases and colon cancer, thus emissions from polluting sites and factory.

Articles and proceeding published during the PhD and not included in this thesis are listed to follow. Respective abstracts of published papers are collected in Appendix C.

Papers

[J01] V. Guidi, M.C. Carotta, B. Fabbri, S. Gherardi, A. Giberti, C. Malagù, Array of sensors for detection of gaseous malodors in organic decomposition products, Sensors and Actuators B 174 (2012) 349– 354

[J02] A. Giberti, M.C. Carotta, B. Fabbri, S. Gherardi, V. Guidi, C. Malagù, High-sensitivity detection of acetaldehyde, Sensors and Actuators B 174 (2012) 402– 405

[J03] B. Fabbri,S. Gherardi,A. Giberti,V. Guidi,C. Malagù, Sensing of gaseous malodors characteristic of landfills and waste treatment plants, JOURNAL OF SENSORS AND SENSOR SYSTEMS 3, 61–67, 2014

[J04] A. Giberti, B. Fabbri, A. Gaiardo, V. Guidi, C. Malagù, Resonant photoactivation of cadmium sulfide and its effect on the surface chemical activity, Applied Physics Letters 104, 222102 (2014)

[J05] C. Malagu', B. Fabbri, S. Gherardi, A. Giberti, V. Guidi, N. Landini, G. Zonta, Chemoresistive gas sensors for detection of colorectal cancer biomarkers, Sensors 2014, 14, 18982-18992

[J06] A. Giberti, D. Casotti, G. Cruciani, B. Fabbri, A. Gaiardo, V. Guidi, C. Malagù, G. Zonta, S. Gherardi, Electrical conductivity of CdS films for gas sensing: Selectivity properties to alcoholic chains, Sensors and Actuators B 207, (2014) 504-510

[J07] B. Fabbri, A. Gaiardo, A. Giberti, V. Guid, C. Malagù, A. Martucc, M. Sturaro, G. Zonta, S. Gherardi, Chemoresistive properties of photo-activated thin and thick ZnO films, submitted to Sensors and Actuators B

[J08] G. Zonta, G. Anania, B. Fabbri, A. Gaiardo, S. Gherardi, A. Giberti, V. Guidi, N. Landini, C. Malagu', Detection of colorectal cancer biomarkers in the presence of interfering gases, submitted to Sensors and Actuators B

Contributions (oral/poster) to conferences/workshops

[P01] B. Fabbri, A. Giberti, V. Guidi, C. Malagù, Sensing of typical gaseous malodors in organic decomposition products, IMCS 2012 – The 14th International Meeting on Chemical Sensors, Norimberga (Germania), 20-23 maggio 2012, Proceeding DOI 10.5162/IMCS2012/P2.1.4 1339 – 1342, oral presentation (B. Fabbri)

[P02] B. Fabbri, S. Gherardi, A. Giberti, V. Guidi, C. Malagù, Sensing of gaseous malodors in landfills and waste treatment plants, AMA Conference 2013 – Sensor, Norimberga (Germania), 14-16 maggio 2013, Proceeding DOI 10.5162/sensor2013/E7.3, oral presentation (B. Fabbri)

[P03] B. Fabbri, A. Gaiardo, A. Giberti, V. Guidi, C. Malagù, A. Martucci, M. Sturaro, Electrical, optical and sensing properties of photo-activated ZnO thin films, Eurosensors 2014, Brescia (Italy), 7-10 settembre 2014, Procedia Engineering 87 (2014) 148 – 151, poster

[P04] B. Fabbri, A. Gaiardo, V. Guidi, C. Malagù, A. Giberti, Photo-activation of cadmium sulfide films for gas sensing, Eurosensors 2014, Brescia (Italy), 7-10 settembre 2014, Procedia Engineering 87 (2014) 140 – 143, poster

[P05] G. Zonta, B. Fabbri, A. Giberti, V. Guidi, C. Malagù, Detection of colorectal biomarkers in the presence of interfering gases, Eurosensors 2014, Brescia (Italy), 7-10 settembre 2014, Procedia Engineering 87 (2014) 596 – 599, poster

[A01] B. Fabbri, S. Gherardi, A. Giberti, V. Guidi, C. Malagù, Sensing of gaseous malodors in landfills and waste treatment plants, Book of abstract AISEM 2013, Brescia, 5-7 febbraio 2013, oral presentation (B. Fabbri)

[A02] V. Guidi, B. Fabbri, A. Giberti, C. Malagù, M. C. Carotta, S. Gherardi, Sensing of gaseous malodors characteristic of landfills and waste treatment plants, 5th GOSPEL Workshop, Oita, Japan, 26-29 maggio 2013, oral presentation (V. Guidi)

[A03] C. Malagù, M.C. Carotta, B. Fabbri, S. Gherardi, A. Giberti, Thick film technology for chemical sensor, FisMat 2013, Milano (Italy), 9-13 settembre 2013, Book of abstract #382, oral presentation (V. Guidi)

[A04] A. Giberti, C. Malagù, B. Fabbri, V.Guidi, E. Della Gaspera, A. Martucci, Electro-optical characterizations of zinc oxide nanoparticles: an evidence for light-assisted desorption of oxygen, The 15th International Meeting on Chemical Sensors, Buenos Aires (Argentina), 16-19 marzo 2014, Book of Abstract IMCS 2014, oral presentation (A. Giberti)

[A05] B. Fabbri, S. Gherardi, A. Giberti, V. Guidi, C. Malagù, G. Zonta, Chemoresistive gas sensors for detection of colorectal cancer biomarkers, The 15th International Meeting on Chemical Sensors, Buenos Aires (Argentina), 16-19 marzo 2014 Book of Abstract IMCS 2014, poster

[A06] B. Fabbri, V. Boldrini, G. Calabrese, A. Gaiardo, A. Giberti, V Guidi, C. Malagù, F. Spizzo, G. Zonta, S. Gherardi, Mesoporous silicon gas sensor: design, fabbrication and conduction model, accettato come poster ad AISEM 2015, Trento (Italy), 3-5 febbraio 2015, poster

[A07] A. Gaiardo, A. Giberti, V Guidi, P. Bellutti, C. Malagù, B. Fabbri, G. Zonta, S. Gherardi, Tin (IV) sulfide chemoresistivity: a possible new gas sensing material, accettato come poster ad AISEM 2015, Trento (Italy), 3-5 febbraio 2015, poster

Capther 1
Organic – Inorganic Hybrid Materials

Research and development of novel organic-inorganic hybrid materials and nanocomposites with extraordinary properties has become one of the most expanding fields in materials chemistry in recent years. One reason for this trend is that this class of materials bridges various scientific disciplines and combines the best attributes of the different worlds in one system. The compounds formed often possess exciting new properties for future functional materials and technological applications. Natural materials act as a model for these systems and many examples for biomimetic approaches can be found in the development of hybrid materials [1]. At the same time, the requirements of future technologies act as a driving force for the research and development of these materials.

All along, scientists have tried to reproduce Nature and in particular its ability of self-structuring on the atomic level. Indeed, since atoms condense in ordered systems because in that way they reach the minimum energy configuration, natural materials present complex, hierarchical architecture at sizes ranging from a few nanometers to several micro- to millimeters. Moreover, in Nature one can find materials that assemble this remarkable feature towards the possibility to combine organic and inorganic components in so-called hybrid materials. This efficient integration allows the being of objects characterized both by miniaturization, a maximum of elementary functions in a small volume, and hybridization between organic and inorganic parts, optimizing complementary properties, functions, and hierarchy [1-3]. Achieving original hybrid nanomaterials means to develop complex systems of various shapes with mastery at different length scales of composition, structure, porosity, functionality, and morphology, so different fields are synergistically coupled in a cross-cutting approach. Combining chemical and processing strategies, different functional hybrid nanomaterials can be constructed, in order to obtain dedicated materials for specific applications [4, 5].

1.1 Introduction to Hybrid Materials

1.1.1 Definition

The term hybrid material is used for many different systems spanning a wide area of different materials, such as crystalline highly ordered coordination polymers, amorphous sol–gel compounds, materials with and without interactions between the inorganic and organic units. The most wide-ranging definition is the following: a hybrid material is a material that includes two moieties blended on the molecular scale. Commonly one of these compounds is inorganic and the other one organic in nature.

The concept of "organic-inorganic hybrid" materials has more to do with chemistry than with physical mixtures. They can be broadly defined as compounds with organic and inorganic components, intimately mixed. Indeed, hybrids are either homogeneous systems derived from monomers and miscible organic and inorganic components, or heterogeneous systems (nanocomposites) where at least one of the components' domains has a dimension ranging from Å to several nanometers [6].

Thus, as the size of interacting particles gets reduced in going from mixtures to composite materials, the importance of the interface in determining final properties grows, and as we move towards nanocomposite materials, where components interact at a molecular level. The terms hybrid material and nanocomposite are often confused because there is no clear borderline between these materials. The term nanocomposite is used if one of the structural units, either the organic or the inorganic, is in a defined size range of 1–100nm. Therefore there is a gradual transition between hybrid materials and nanocomposites, because large molecular building blocks for hybrid materials, such as large inorganic clusters, can already be of the nanometer length scale. Moreover, commonly the term nanocomposites is used if discrete structural units in the respective size regime are used and the term hybrid materials is more often used if the inorganic units are formed in situ by molecular precursors, for example applying sol–gel reactions.

Scientists and engineers realized early on that mixtures of materials can show superior properties compared with their pure counterparts. Of course, hybrid materials cannot be obtained simply by teaching organic molecules to sit on an inorganic support. Organic functions on inorganic supports have to be organized and have to be orchestrated in their action, which often involves sophisticated chemistry and a structuring and patterning of the inorganic partner at molecular dimensions [5].

1.1.2 Origins and development

The origin of hybrid materials did not take place in a chemical laboratory but in nature. Many natural materials consist of inorganic and organic building blocks distributed on the (macro)molecular or nanoscale. In most cases the inorganic part provides mechanical strength and an overall structure to the natural objects while the organic part delivers bonding between the inorganic building blocks and/or the soft tissue. Typical examples of such materials are crustacean carapace, mollusk shells (Figure 1.1), bone or teeth tissues.

The concepts of bonding and structure in such materials are intensively studied by many scientists to understand the fundamental processes of their formation and to transfer the ideas to artificial materials in a so-called biomimetic approach. The special circumstances under which biological hybrid inorganic–organic materials are formed, such as ambient temperatures, an aqueous environment, a neutral pH and the fascinating plethora of complex geometries produced under these conditions make the mimicking of such structures an ultimate goal for scientists. In particular the study of biomineralization and its shape control is an important target of many scientific studies. This primarily interface-controlled process still reveals many questions, in particular how such a remarkable level of morphological diversity with a multiplicity of functions can be produced by so few building blocks. In addition to questions concerning the composition of the materials, their unique structures motivate enquiry to get a deeper insight in their formation, often not only because of their beauty but also because of the various functions the structures perform. A complex hierarchical order of construction from the nanometer to the millimeter level is regularly found in nature, where every size level of the specific material has its function which benefits the whole performance of the material. Furthermore these different levels of complexity are reached by soft chemical self-assembly mechanisms over a large dimension, which is one of the major challenges of modern materials chemistry.

Although it is not known the original birth of hybrid materials exactly, it is clear that the mixing of organic and inorganic components was carried out in ancient world.

Nautilus shell

Nacre diffraction grating
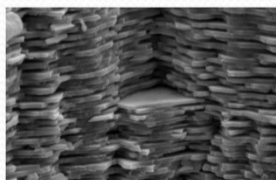
Scheme

SEM image

Biominelarization of the Nacre of Shell

Structure of Abalone Nacre

1 μm

CaCO₃

CaCO₃

Water-Soluble Polymer (Acidic proteins)

Water-Insoluble Polymer (Chitin/Silk-fibroin-like proteins)

Illustration of the Formation Process

Ca²⁺ Ca²⁺ Ca²⁺

Interaction

Biomacromolecules

Control of Crystal Growth by Combination of Insoluble Polymer (matrices) and Water-Soluble Polymer (additives)
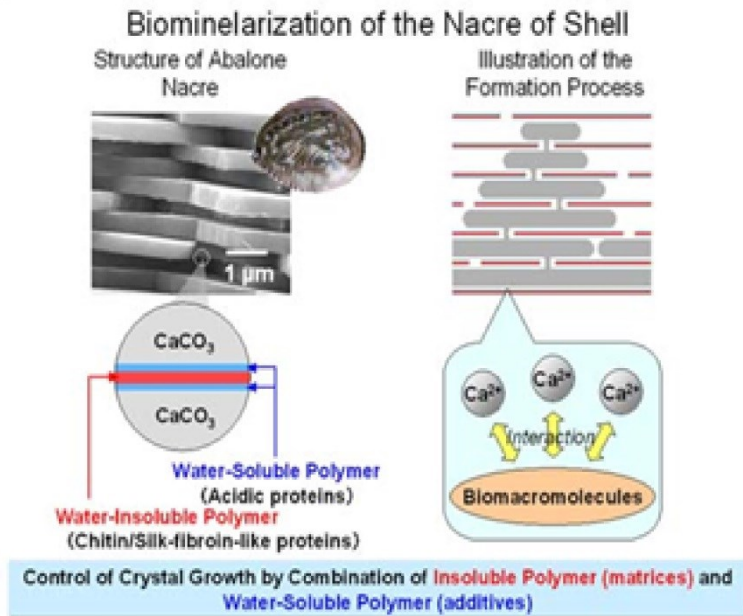
Figure 1.1. Nacre, also known as mother of pearl, is an organic-inorganic composite material produced by some molluscs as an inner shell layer. Nacre is composed of hexagonal platelets of aragonite (a form of calcium carbonate) 10–20 μm wide and 0.5 μm thick arranged in a continuous parallel lamina. These layers are separated by sheets of organic matrix composed of elastic biopolymers. This mixture of brittle platelets and the thin layers of elastic biopolymers makes the material strong and resilient. This design at multiple length sizes greatly increases it stoughness, making it almost as strong as silicon. Nacre appears iridescent because the thickness of the aragonite platelets is close to the wavelength of visible light. These structures interfere constructively and destructively with different wavelengths of light at different viewing angles, creating structural colours [7-8].

An striking example about this regards ancient Maya fresco paintings: they are characterized by bright blue, an hitherto unknown pigment which came to be known as Maya blue, and ochre colors that had been miraculously preserved (see Figure 1.2 a). In addition to its beautiful tones, the most remarkable feature of Maya blue was its durability. Maya blue is indeed a robust pigment, not only resisting biodegradation, but showing also unprecedented stability when exposed to acids, alkalis and organic solvents. The pigment is not a copper mineral, nor is it related to natural ultramarine, ground Lapis Lazuli or Lazurite as originally thought. Maya blue is a hybrid organic-inorganic material with molecules of the natural blue dye known as indigo encapsulated within the channels of a clay mineral known as palygorskite. It is a man-made material that combines the color of the organic pigment and the resistance of the inorganic host, a synergic material, with properties and performance well beyond those of a simple mixture of its components [3, 9-13].
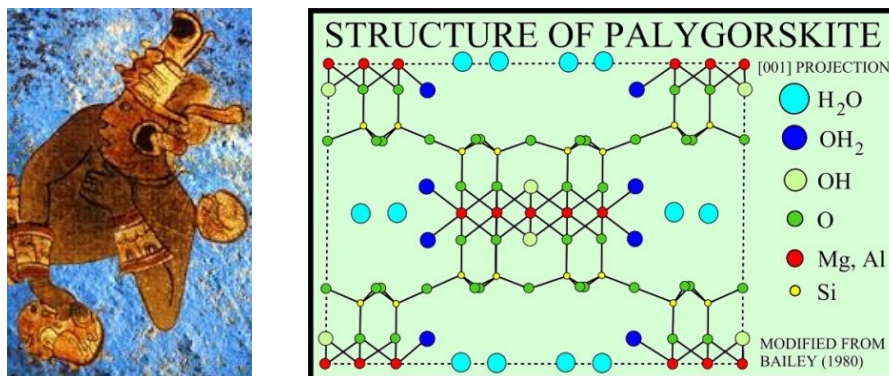
Figure 1.2. a) Wall painting about a warrior with Blue Maya on the background; b) Schematic representation of palygorskite structure.

The structure of palygorskite (Figure 1.2 b), of ideal formula $Si_8(Mg_2Al_2)O_{20}(OH)_2(OH_2)_4 \cdot 4H_2O$, can be described in terms of a multi-layer structure, each layer formed by an octahedral sheet of MgO_6 surrounded by two tetrahedral sheets of SiO_2[1]. The tetrahedral in each sheet present a periodic inversion of the apical oxygen, thus resulting in a discontinuous octahedral sheet which defines channels 6.4 x 3.7 Å sized. Such channels are filled by weakly bound, non-structural (zeolitic) water while magnesium and aluminium cations complete their coordination with tightly-bound water molecules (structural water). So, water molecules and further organic molecules can be trapped in the channels, as Maya blue in which molecules of the natural blue indigo are encapsulated within the channels of palygorskite [2, 14, 15].

Therefore, hybrid materials or even nanotechnology is not an invention of the last decade but was developed a long time ago. The deliberate effort to combine properties of organic and inorganic components in a single composite material is an old challenge starting with the beginning of the industrial era [13]. Indeed, it was only at the end of the 20th and the beginning of the 21st century that it was realized by scientists, in particular because of the availability of novel physico–chemical characterization methods, the field of nanoscience opened many perspectives for approaches to new materials.

The combination of different analytical techniques gives rise to novel insights into hybrid materials and makes it clear that bottom-up strategies from the molecular level towards materials' design will lead to novel properties in this class of materials. Some of the earliest and best known organic-inorganic admixtures are certainly derived from the paint and polymer industries, where inorganic pigments or fillers are dispersed in organic components (solvents, surfactants, polymers, etc.) to yield or improve optical and mechanical properties.

Apart from the use of inorganic materials as fillers for organic polymers, such as rubber, it was a long time before much scientific activity was devoted to mixtures of inorganic and organic materials. One process changed this situation: the sol–gel process. This process was developed in the 1930s using silicon alkoxides as precursors from which silica was produced. In fact this process is similar to an organic polymerization starting from molecular precursors resulting in a bulk material. Contrary to many other procedures used in the production of inorganic materials this is one of the first processes where ambient conditions were applied to produce ceramics. The control over the preparation of multicomponent systems by a mild reaction method also led to industrial interest in that process. In particular

---

[1] Si^{4+} can be substituted by Al^{3+} or Fe^{3+}, whereas Mg^{2+} can be substituted by Al^{3+}, Fe^{2+}, Fe^{3+} or rarely by Li^+, Cr^{3+}, Mn^{2+}, Ni^{2+}, Cu^{2+} and Zn^{2+}.

the silicon based sol–gel process was one of the major driving forces what has become the broad field of inorganic–organic hybrid materials. The reason for the special role of silicon was its good process ability and the stability of the Si—C bond during the formation of a silica network which allowed the production of organic-modified inorganic networks in one step. Inorganic–organic hybrids can be applied in many branches of materials chemistry because they are simple to process and are amenable to design on the molecular scale [5].

The development of hybrid organic-inorganic materials stemmed from several different areas of chemistry, but exploded only very recently with the birth of soft inorganic chemistry processes ("Chimie Douce"), where mild synthetic conditions open a versatile access to chemically designed hybrid organic-inorganic materials. Later on, research shifted towards more sophisticated nanocomposites with higher added values. Nowadays the field of organic-inorganic materials has grown to include a large variety of types, extending to other fields as diverse as molecular and supramolecular materials or polymer chemistry. Furthermore, a very significant trend has been the growing interest in functional hybrids, which broadens the field even further. Thus, in addition to structural hybrid materials bringing the best of glass and plastics together, there is a quickly expanding area of research on functional materials in which mechanical properties are secondary – though certainly not unimportant – and the emphasis is on chemical, electrochemical, or biochemical activity, as well as on magnetic, electronic, optical or other physical properties, or a combination of them [13].

1.1.3 Types and classification

The variety of hybrid materials is too large, and growing, to allow for a systematic grouping criterion. A first basic classification could arrange material types according to the approximate dimensions of their organic and inorganic components.

The arrangement presented in Figure 1.3 provides a first general overview of the area, spanning from molecular to extended organic-inorganic combinations. In this respect the graph also shows the greater richness of the field in the twilight region of supramolecular and nanostructured materials, forming a broad continuum between molecular and solid state chemistry. The predominant phase in the hybrid, i.e. organic-inorganic vs. inorganic-organic materials depending on whether the extended, host or matrix phase were organic or inorganic respectively. Such classification has been conveniently used to categorize a particular type of polymer-based hybrid, although it could be difficult to generalize due to the abundance of intermediate cases and to the indistinct use of both terms in the literature, where the label organic-inorganic is most commonly used in a generic way.

On the other hand, a more detailed and widely used classification distinguishes hybrid materials on the base of the nature of the interface or the interactions between organic and inorganic components. The particular nanostructure, the degree of organization and the properties that can be obtained for hybrid materials certainly depend on the chemical nature of their components, but they are also heavily influenced by the interaction between these components [7, 13, 17].
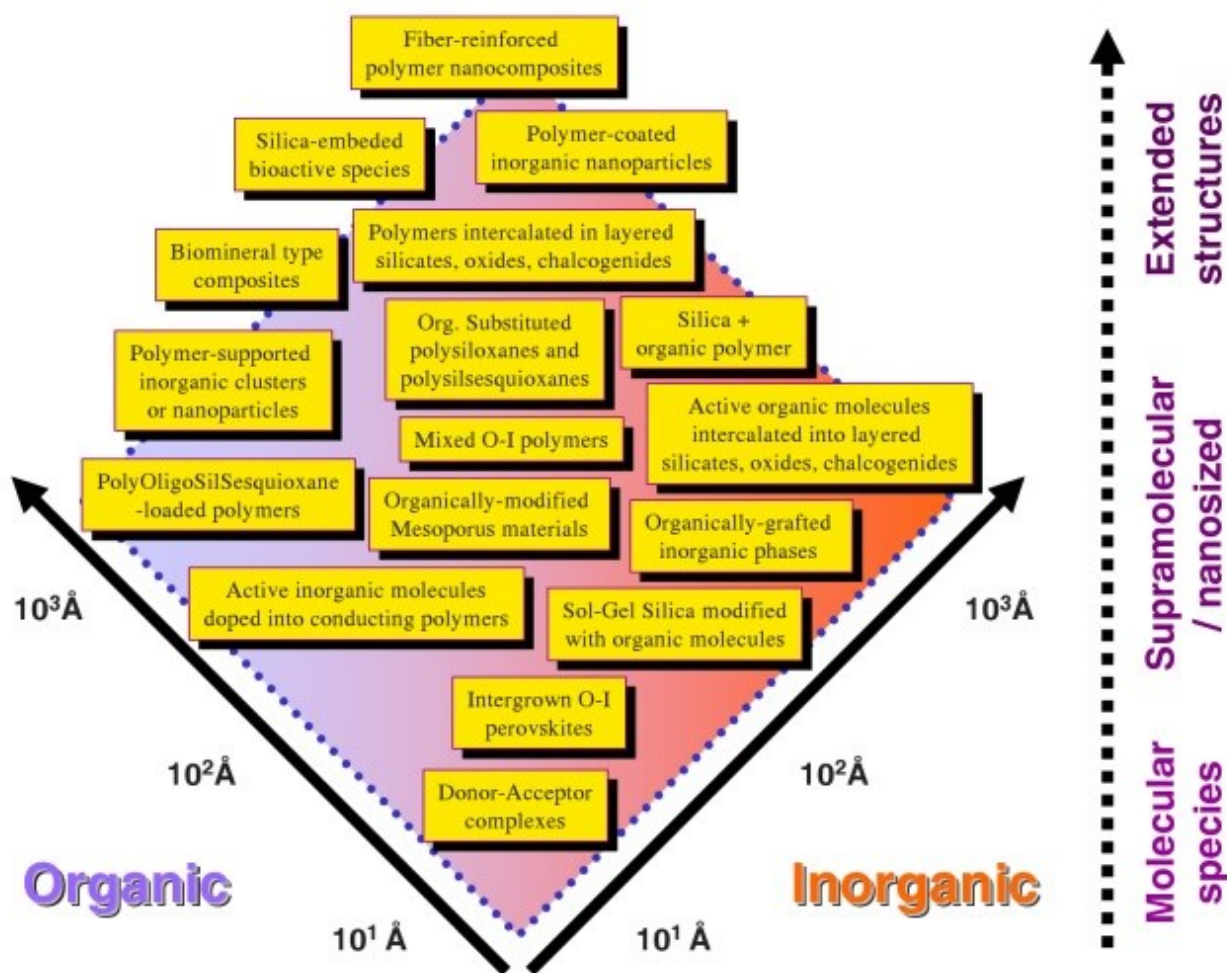
Figure 1.3. Examples of general types of hybrids spreading on a field of organic and inorganic dimensions are showing. The field of hybrid organic-inorganic materials has bloomed at the interface of many conventional disciplines, and is producing an amazing variety of materials and applications, ranging from molecular and supramolecular structures, to cluster-polymer adducts, sol-gel hybrids, or to nanocomposite materials based on extended phases [16].

Class I corresponds to all the systems where no covalent or iono-covalent bonds are present between the organic and inorganic components. In such materials, the various components only exchange weak interactions (at least in terms of orbital overlap) such as hydrogen bonding, van der Waals contacts, π–π interactions or electrostatic forces. On the contrary, in Class II materials, at least a fraction of the organic and inorganic components are linked through strong chemical bonds (covalent, iono-covalent or Lewis acid-base bonds). The chemical strategy followed for the construction of class II hybrid networks depends of course on the relative stability of the chemical links that associate the different components.

In addition to the bonding characteristics, structural properties can also be used to distinguish between various hybrid materials. An organic moiety containing a functional group that allows the attachment to an inorganic network can act as a network modifying compound because in the final structure the inorganic network is only modified by the organic group. If a reactive functional group is incorporated the system is called a network functionalizer. The situation is different if two or three of such anchor groups modify an organic segment; this leads to materials in which the inorganic group is afterwards an integral part of the hybrid network.
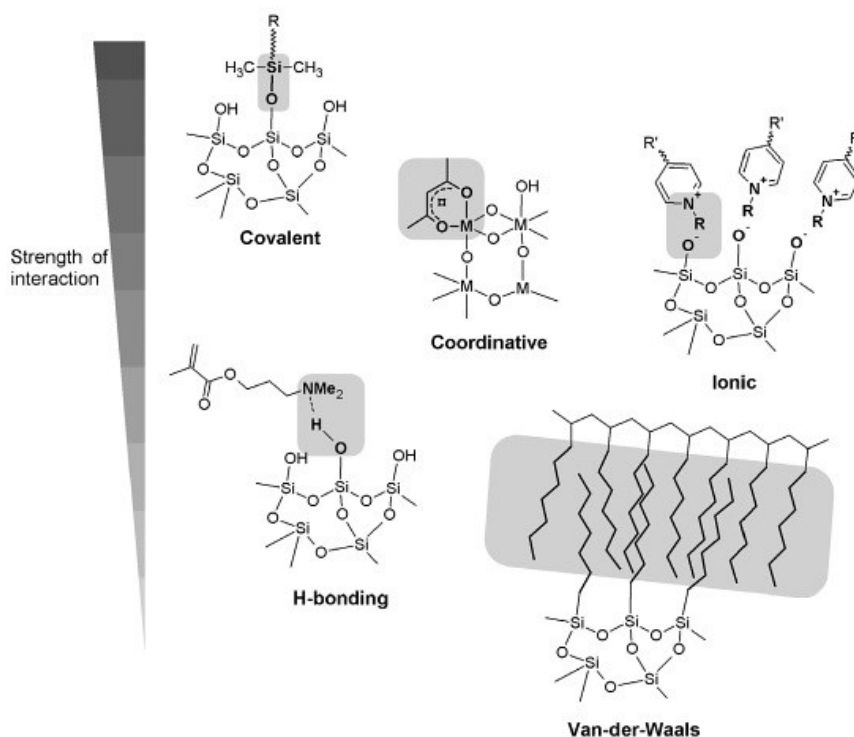
Figure 1.4. Selected interactions typically applied in hybrid materials and their relative strength [5].

Because of the gradual change in the strength of chemical interactions (Figure 1.4) it becomes clear that there is a steady transition between weak and strong interactions. The energetic categorization of different chemical interactions depending on their binding energies. In addition to the bonding characteristics structural properties can also be used to distinguish between various hybrid materials.

Blends are formed if no strong chemical interactions exist between the inorganic and organic building blocks. One example for such a material is the combination of inorganic clusters or particles with organic polymers lacking a strong (e.g. covalent) interaction between the components (Figure 1.5 a). In this case a material is formed that consists for example of an organic polymer with entrapped discrete inorganic moieties in which, depending on the functionalities of the components, for example weak crosslinking occurs by the entrapped inorganic units through physical interactions or the inorganic components are entrapped in a cross linked polymer matrix. If an inorganic and an organic network interpenetrate each other without strong chemical interactions, so called interpenetrating networks (IPNs) are formed (Figure 1.5 b), which is for example the case if a sol–gel material is formed in presence of an organic polymer or vice versa. Both materials described belong to class I hybrids. Class II hybrids are formed when the discrete inorganic building blocks, e.g. clusters, are covalently bonded to the organic polymers (Figure 1.5 c) or inorganic and organic polymers are covalently connected with each other (Figure 1.5 d) [5].

A basic classification of the most common types of organic-inorganic materials normally includes the following three main groups: intercalation compounds, organic derivatives of inorganic solids, and sol-gel hybrid materials. Moreover, there are other organic-inorganic materials not included in this classification, as for instance: (i) compounds based on amines or organo-ammonium species associated with silica or metal-oxide substrates, that are intermediates in the synthesis of zeolites, ALPOs, MCMs and other micro- and meso-porous materials, and (ii) organic polymer-based hybrids such as those formed between conducting polymers and polyoxometalate oxide-clusters [13].
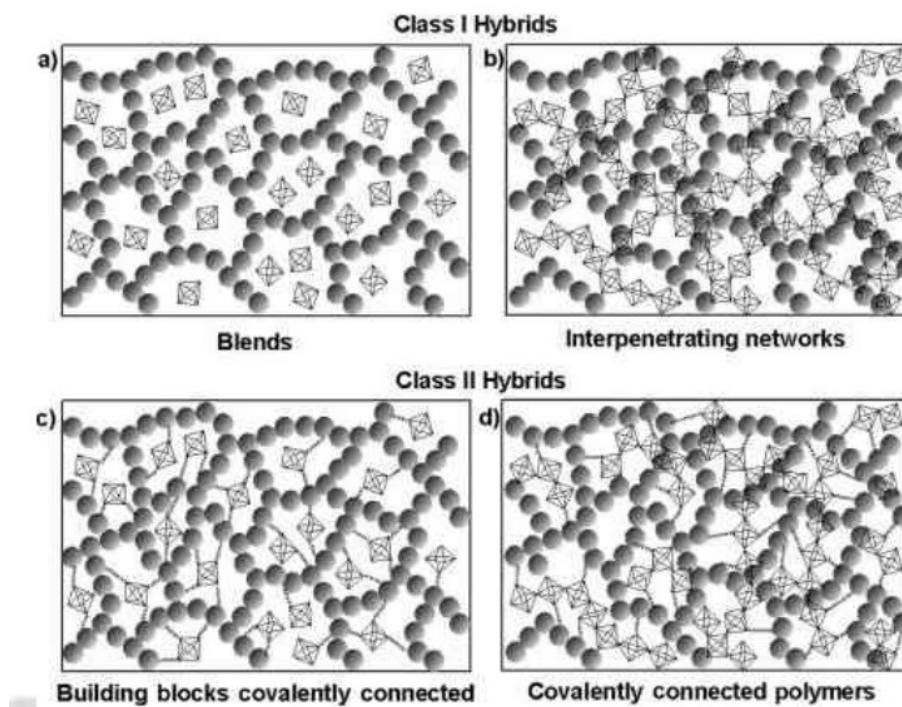
Figure 1.5. The different types of hybrid materials [5].

1.2 Design and construction of Hybrid Materials

Independently of the types or applications, and in addition to the nature of the interface between organic and inorganic components, an important feature in the tailoring of hybrid networks concerns the chemical pathways that are used to design a given hybrid material. But, the design and synthesis of hybrid materials depend markedly on the type of hybrid sought. Class I and II hybrids differ radically in the type of synthetic approaches adequate to their successful preparation.

1.2.1 Synthesis strategies

In principle two different approaches can be used for the formation of hybrid materials: either well-defined preformed building blocks are applied that react with each other to form the final hybrid material in which the precursors still at least partially keep their original integrity or one or both structural units are formed from the precursors that are transformed into a novel (network) structure (see path *A* in Figure 1.6).

As mentioned above building blocks at least partially keep their molecular integrity throughout the material formation, which means that structural units that are present in these sources for materials formation can also be found in the final material. At the same time typical properties of these building blocks usually survive the matrix formation, which is not the case if material precursors are transferred into novel materials. So, well-defined nano-objects, can be obtained via the controlled reactivity of molecular precursors that allows mastering of nucleation, growth, and aggregation processes. Beside the molecular building blocks mentioned, nanosized building blocks, such as particles or nanorods, can also be used to form nanocomposites.

The building block approach has one large advantage compared with the in situ formation of the inorganic or organic entities: because at least one structural unit (the building block) is well-defined and usually does not undergo significant structural changes during the matrix formation, better structure–property predictions are possible. Furthermore, the building blocks can be designed in such a way to give the best performance in the materials' formation, for example good solubility of inorganic compounds in organic monomers by surface groups showing a similar polarity as the monomers.

Contrary to the building block approach the in situ formation of the hybrid materials is based on the chemical transformation of the precursors used throughout materials' preparation. Typically this is the case if organic polymers are formed but also if the sol–gel process is applied to produce the inorganic component. In these cases well-defined discrete molecules are transformed to multidimensional structures, which often show totally different properties from the original precursors. Generally simple, commercially available molecules are applied and the internal structure of the final material is determined by the composition of these precursors but also by the reaction conditions. Therefore control over the latter is a crucial step in this process, changing one parameter can often lead to two very different materials. Hence, the final performance of the derived materials is strongly dependent on their processing and its optimization [5,18-20].

Four main strategies, divided on the two principle approaches, are schematized in Figure 1.6 (path *B-E*).

❖ **Strategies from molecular precursors** correspond to soft chemistry-based routes including conventional sol-gel chemistry, the use of specific bridged and polyfunctional precursors, hydrothermal synthesis including the synthesis of coordination polymers.

Many of the classical inorganic solid state materials are formed using solid precursors and high temperature processes, which are often not compatible with the presence of organic groups because they are decomposed at elevated temperatures. Hence, these high temperature processes are not suitable for the in situ formation of hybrid materials. Reactions that are employed should have more the character of classical covalent bond formation in solutions. One of the most prominent processes which fulfill these demands is the sol–gel process. However, such rather low temperature processes often do not lead to the thermodynamically most stable structure but to kinetic products, which has some implications for the structures obtained. For example low temperature derived inorganic materials are often amorphous or crystallinity is only observed on a very small length scale, i.e. the nanometer range [5].

● **Conventional sol-gel chemistry** pathways (path *B*) are performed from simple precursor or via the use of specific bridged and polyfunctional precursors . Hybrid networks are obtained through hydrolysis of organically modified metal alkoxides or metal halides condensed with or without simple metallic alkoxides. The solvent may or may not contain a specific organic molecule, a biocomponent or polyfunctional polymers that can be crosslinkable or that can interact or be trapped within the inorganic components through a large set of fuzzy interactions (H-bonds, π–πinteractions, Van der Waals). These strategies are simple, low cost and yield amorphous nanocomposite hybrid materials. These materials that exhibit an infinity of microstructures can be transparent and easily shaped as films or bulks. However, they are generally polydisperse in size and locally heterogeneous in chemical composition.
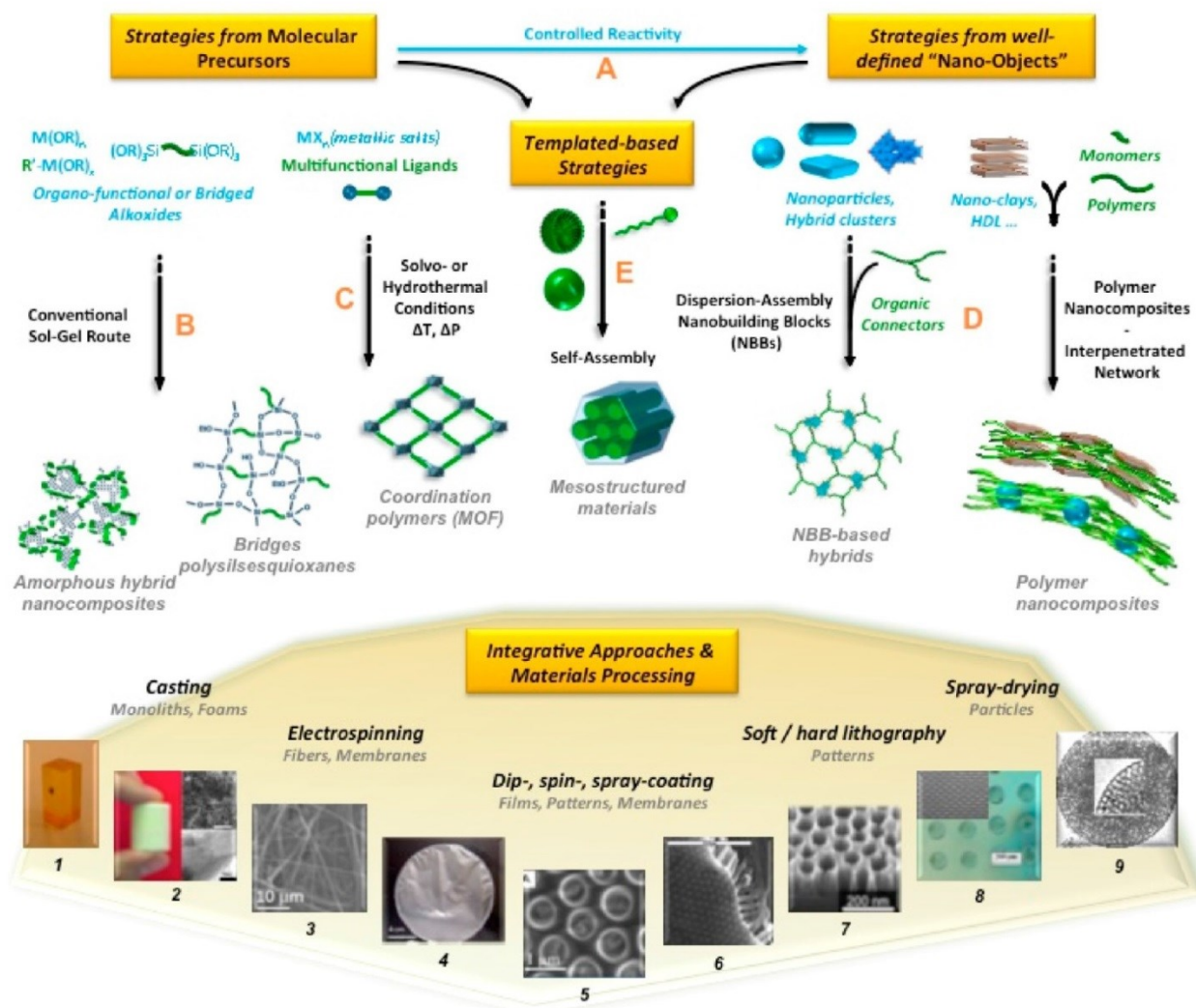
Figure 1.6. Framework of the general strategies associated to the molecular design and construction of functional inorganic and hybrid nanomaterials. Top: chemical pathways. Bottom: processing approaches and some examples of resulting materials: From left to right on the bottom, some examples of materials resulting from these approches [18].

Better understanding and control of the local and semi-local structure of these materials and their degree of organization are important issues, especially if tailored properties are sought for. In particular, two main approaches are used to achieve such control. The first consists of bridged precursors of silsesquioxanes $X_3Si\text{-}R'\text{-}SiX_3$ (R' is an organic spacer and X = Cl, Br, -OR) where the chemical tailoring of the organic bridge which allow the making of homogeneous molecular hybrid organic-inorganic materials. The second oneincludes all aspects of hydrothermal synthesis performed at moderates temperatures (20 – 200°C) in polar solvents [13, 18, 19].

- **Hydrothermal synthesis** (path *C*) allows to obtain more crystallized materials. The presence of organic templates had given rise to numerous microporous hybrid materials as organically templated zeolites that have already led to an extensive number of applications. Metal Organic Frameworks (MOFs) are coordination polymers built from telechelic or polyfunctional spacers tht coordinate metallic centers or link in situ generated metal containing small oligomers such as metallic oxo-clusters [18].

❖ **Strategies from well-defined nano-objects** correspond to the hybridization of typical building block should consist of a well-defined molecular or nanosized structure and of a well-defined size and shape, with a tailored surface structure and composition. In regard of the preparation of functional hybrid materials the building block should also deliver interesting chemical or physical properties, in areas like conductivity, magnetic behavior, thermal properties, switching possibilities, etc. All these characteristics should be kept during the material formation, for example the embedment into a different phase. Building blocks can be inorganic or organic in nature, but because they are incorporated into another phase they should be somehow compatible with the second phase [5, 19].

- **The assembling of well-defined nanobuilding blocks** (NBB, path *D*): a suitable method to reach a better definition of the inorganic component consists in the use (via assembly or intercalation or intercalation and dispersion) of perfectly calibrated preformed objects that keep their integrity in the final material. These NBB can be clusters, organically pre- or post- functionalized nanoparticles (metallic oxides, metals, chalcogenides, etc ...), nanocore-shells or layered compounds able to intercalate organic components. NBB can be capped with polymerizable ligands or connected through organic spacers, like telechelic molecules or polymers, or functional dendrimers. The use of highly pre-condensed species presents several advantages: they exhibit a lower reactivity towards hydrolysis or attack of nucleophilic moieties than metal alkoxides. The nanobuilding components are nanometric and monodispersed, and with perfectly defined structures, which facilitate the characterization of the final materials. The variety found in the nanobuilding blocks (nature, structure, and functionality) and links allows one to build an amazing range of different architectures and organic-inorganic interfaces, associated with different assembling strategies. Moreover, the step-by-step preparation of the materials usually allows for a high degree of control over their semi-local structure [13, 18, 19].

❖ **Template-based strategies** correspond to procedures based on self assembly of amphiphilic molecules or polymers coupled with sol-gel polymerisation (see Figure 1.6 path *E*). In the last ten years, a new field has been explored, which corresponds to the organization or the texturation of growing inorganic or hybrid networks, templated by organic structure-directing agents. The success of this strategy is also clearly related to the ability that materials scientists have to control and tune hybrid interfaces. In this field, hybrid organic-inorganic phases are very interesting, due to the versatility they demonstrate in the building of a whole continuous range of nanocomposites, from ordered dispersions of inorganic bricks in a hybrid matrix to highly controlled nanosegregation of organic polymers within inorganic matrices. In the latter case, one of the most striking examples is the synthesis of mesostructured hybrid networks. More recent strategies consist in the use of alkoxysilylated surfactant templated growths with bridged silsesquioxanes as precursors. This approach yields a new class of periodically organized mesoporous hybrid silicas with organic functionality within the walls.

This nanoporous materials present a high degree of order and their mesoporosity is available for further organic functionalization surface grafting reactions. Another possibility is the combination between the "nanobuilding block approach" and "templated assembling" will have a paramount importance in exploring the theme of "synthesis with construction". Indeed, such materials exhibit a large variety of interfaces between the organic and the inorganic components (covalent bonding, complexation, electrostatic interactions, etc.).

These NBB with tunable functionalities can, through molecular recognition processes, permit the development of a new vectorial chemistry [13, 18, 19].

1.2.2 Integrative approaches and material processing

The synthesis strategies (paths *A−E*) reported mainly offer the control of materials structures and textures from nanoscopic and mesoscopic to submicronic ranges (from 1 Å to 500 Å). The micrometer range can be easily reached by including other templating strategies. In fact, an important area with respect to potential applications of hybrid materials and nanocomposites is the ability to design these materials on several length scales, from the molecular to the macroscopic scale. Because the processing of hybrid materials is more similar to that of organic polymers than to classical inorganic materials, such as ceramic or metal powders, based on the solvent-based chemistry behind the materials there is a variety of methods that can be adapted for their processing on the macroscopic scale. One has to distinguish between different applications to identify the best processing strategies.
Because of the tunable rheology of the colloidal dispersions, materials can be engineered through many processing methods (see Figure 1.6 bottom) used for organic polymers, among which are casting of monoliths or membranes, films deposition methods (dip-coating, spin coating, spray coating), fiber drawing (via extrusion, pulling, or electrospinning), electrochemical deposition, (soft) or (hard) lithography based techniques (dip-pen, X-ray, two photon adsorption (TPA) lithography), aerosol or spray, electro-spray processing, inkjet printing, electron beam writing, nanoimprinting, etc. Recently, the coupling of these synthesis procedures with a top-down approach such as RIE (reactive ion etching) plasma processing allowed building ever more sophisticated materials. All these integrative strategies are indeed opening new avenues for the tailored construction of hierarchically structured inorganic and hybrid materials [18].

Two different techniques can be identified for a structural control on the nanometer length scale: the top-down and the bottom-up approach. The top-down approach forms the nanostructures from larger objects by physical or chemical methods and is more engineering-related, while the bottom-up approach relies on self-organization (also called self-assembly) of molecules or nanometer sized compounds. The latter process is for many scientists the more elegant way to form large complex hierarchical structures. In a bottom-up approach many reaction details have to be understood and controlled. Therefore, this process, although very promising, is yet only understood for quite small molecules and there are only some promising techniques that can already be applied for large scale technological applications. Self-assembly is the major principle of the controlled formation of structural building blocks. It means nothing other than the spontaneous organization of unorganized systems to a complex structure, which is first of all an art to break and generate specific interactions and to work against entropy. There are several basic principles that have to be taken into account for a self-assembly process: the structure and shape of the building blocks, their interactions like the attractive and repulsive forces, their interactions with solvents, the environment where the reaction is carried out and diffusion processes. Two principles are employed in the synthesis of hybrid materials, the self-assembly of the building blocks of the material itself and the use of templates that can self-assemble and form a shape which is applied in the preparation of a material. Such templates are used in technology since a long time, for example as porogenes but it was only recently that they found a widespread use in the formation of hybrid materials.

26

Templates can fulfill various purposes, for example they can fill space and/or direct the formation of specific structures. Templates that fill space have been technologically used in materials processing for a long time; examples are porogenes for the formation of foam-like materials or single molecules that are employed in zeolite synthesis. In both examples the templates are removed after their use to form the pores in the material.
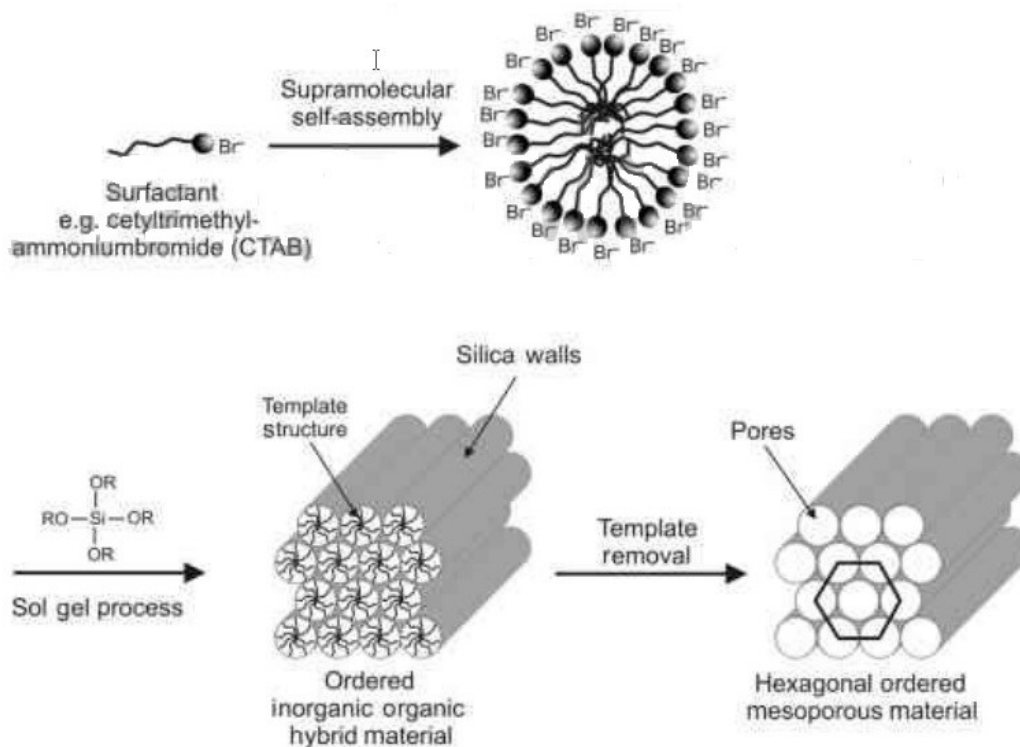

Figure 1.7. Formation of well-ordered mesoporous materials by a templating approach [13].

Templates for the synthesis of hybrid materials can be preformed structures such as dendrimers or nanoparticles that form 2-D or 3-D ordered structures. Furthermore the supramolecular self-organization of single molecules into larger 2-D and 3-D structures can also be employed as a template. One example is the application of amphiphilic surfactants that organize into micelles and more complicated 3-D arrangements such as hexagonal arranged rod-like structure, cubic interpenetrating networks or lamellar structures, increasing the surfactant concentration. The latter are not usually used for structural engineering because they collapse after removal of the template. The structures formed, that are dependent on parameters such as the concentration of the surfactants in the solvent, the temperature and sometimes the pH, consist of hydrophobic and hydrophilic regions and the interfaces between them which are applied in the formation of solid materials, primarily by sol–gel process (Figure 1.7). As long as the organic surfactants are still incorporated in the formed inorganic matrix the materials can be considered as inorganic–organic hybrid materials. After removal of the template which commonly occurs by calcinations at temperatures above 450°C, the materials are purely inorganic in nature. Probably the most prominent example of the use of single organic (macro)molecules and their 3-D assembly as templates for inorganic and hybrid materials is the use of surfactants in the formation of nano- and mesostructured materials porous materials. Recently the silicate or metal oxide walls of the mesoporous materials were substituted by hybrid materials formed by bridged silsesquioxanes and so-called periodically mesoporous organosilicas (PMOs) were formed [5]. These will be discussed in detail in the second chapter.

1.3 Properties and applications

1.3.1 General properties

The most obvious advantage of inorganic–organic hybrids is that they can favorably combine the often dissimilar properties of organic and inorganic components in one material (Table 1.1). The many possible combinations of components provides the opportunity to invent an almost unlimited set of new materials with a large spectrum of known and as yet unknown properties.

Table 1.1. Comparison of general properties of typical inorganic and organic materials [5].

Properties	Organics (polymers)	Inorganics (SiO₂, transition metal oxides (TMO))
Nature of bonds	covalent [C—C], van der Waals, H-bonding	ionic or iono-covalent [M—O]
T_g	low ($-120\,°C$ to $200\,°C$)	high ($\gg 200\,°C$)
Thermal stability	low ($<350\,°C$–$450\,°C$)	high ($\gg 100\,°C$)
Density	0.9–1.2	2.0–4.0
Refractive index	1.2–1.6	1.15–2.7
Mechanical properties	elasticity plasticity rubbery (depending on T_g)	hardness strength fragility
Hydrophobicity	hydrophilic	hydrophilic
Permeability	hydrophobic ±permeable to gases	low permeability to gases
Electronic properties	insulating to conductive redox properties	insulating to semiconductors (SiO₂, TMO) redox properties (TMO) magnetic properties
Processability	high (molding, casting, film formation, control of viscosity)	low for powders high for sol–gel coatings

A driving force in the area of hybrid materials is the possibility to create multifunctional materials, probably the most intriguing property of hybrid materials that makes this material class interesting for many applications is their processing. Examples are the incorporation of inorganic clusters or nanoparticles with specific optical, electronic or magnetic properties in organic polymer matrices.

Because the compositional variations are carried out on the molecular scale a gradual fine tuning of the material properties is possible. One important subject in materials chemistry is the formation of smart materials, such as materials that react to environmental changes or switchable systems, because they open routes to novel technologies, for example electroactive materials, electrochromic materials, sensors and membranes, biohybrid materials, etc.

The desired function can be delivered from the organic or inorganic or from both components. One of the advantages of hybrid materials in this context is that functional

organic molecules as well as biomolecules often show better stability and performance if introduced in an inorganic matrix.

Properties of hybrid materials are usually changed by modifications of the composition on the molecular scale. If, for example, more hydrophobicity of a material is desired, the amount of hydrophobic molecular components is increased. In sol–gel materials this is usually achieved if alkyl- or aryl-substituted trialkoxysilanes are introduced in the formulation. Hydrophobic and lipophobic materials are composed if partially or fully fluorinated molecules are included.

Contrary to pure solid state inorganic materials that often require a high temperature treatment for their processing, hybrid materials show a more polymer-like handling, either because of their large organic content or because of the formation of crosslinked inorganic networks from small molecular precursors just like in polymerization reactions. These materials can be shaped in any form in bulk and in films. In many cases the precursors for hybrid materials and nanocomposites are quite expensive and therefore the preparation of bulk materials is economically not feasible, but their quite simple processing into coatings and thin films can be one solution to this disadvantage. Applying such coatings to cheaper supports can be advantageous. Indeed, although from an economical point of view bulk hybrid materials can currently only compete in very special areas with classical inorganic or organic materials, e.g. in the biomaterials sector, the possibility of their processing as thin films can lead to property improvements of cheaper materials by a simple surface treatment, e.g. scratch resistant coatings [5].

Mechanical properties, such as toughness or scratch resistance, are tailored if hard inorganic nanoparticles are included into the polymer matrix. One of the most prominent passive features of hybrid materials already used in industry are decorative coatings obtained by the embedment of organic dyes in hybrid coatings. Another advantage of hybrid materials is the increased mechanical strength based on the inorganic structures. Scratch-resistant coatings for plastic glasses are based on this principle. Since it is possible to include more than one function into a material by simply incorporating a second component with another property into the material formulation, in the case of scratch-resistant coatings, for example, additional hydrophobic or antifogging properties can be introduced.

Furthermore, the materials' building blocks can also deliver an internal structure to the material which can be regularly ordered. While in most cases phase separation is avoided, phase separation of organic and inorganic components is used for the formation of porous materials.

1.3.2 From properties to functional devices

Numerous new applications in the field of advanced materials science are related to functional hybrids. Thus, the combination at the nanosize level of active inorganic and organic or even bioactive components in a single material has made accessible an immense new area of materials science that has extraordinary implications in the development of multi-functional materials. The chemical nature of this emerging class of hybrids varies wildly, from molecular and supramolecular adducts to extended solids, mineral or biomineral phases. These functional hybrids are considered as innovative advanced materials, and promising applications are expected in many fields: optics, electronics, ionics, energy storage and conversion, mechanics, membranes, protective coatings, catalysis, sensors, biology, etc.. Many interesting new materials have already been prepared with mechanical properties tunable between those of glasses and those of polymers, with improved optical properties, or with improved catalytic or membrane based properties. For example, hybrid materials having

excellent laser efficiencies and good photostability, very fast photochromic response, very high and stable second order non-linear optical response, or being original pH sensors and electroluminescent diodes have been reported in the past five years. And some hybrid products have already entered the applied field and the market. Examples include organically doped sol-gel glassware sold by Spiegelau, sol-gel entrapped enzymes sold by Fluka, or the one million TV sets sold annually by Toshiba, the screens of which are coated with hybrids made of indigo dyes embedded in a silica/zirconia matrix, interestingly, a 21 st century material which brings us echoes of ancient Maya Blue [13, 19].
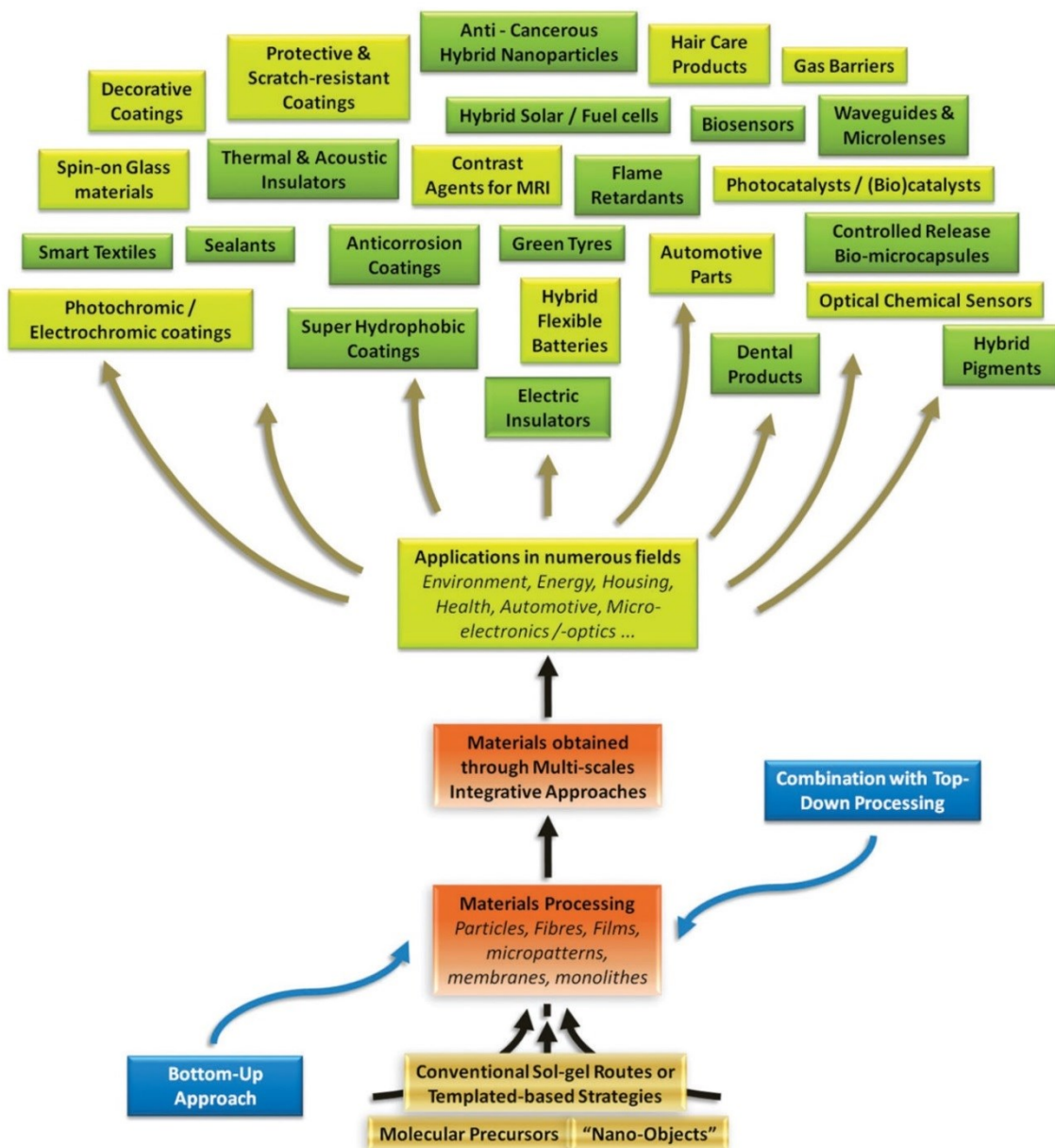
Figure 1.8. Schematic representation of hybrid materials on both the academic and industrial scenes [19].

Nanocomposite based devices for electronic and optoelectronic applications include light-emitting diodes, photodiodes, solar cells, gas sensors and field effect transistors. While most of these devices can also be produced as fully organic polymer-based systems, the composites with inorganic moieties have important advantages such as the improvement of

long-term stability, the improvement of electronic properties by doping with functionalized particles and the tailoring of the band gap by changing the size of the particles. The enhancement of mechanical and thermal properties of polymers by the inclusion of inorganic moieties, especially in the form of nanocomposites, offers the possibility for these materials to substitute classical compounds based on metals or on traditional composites in the transportation industry or as fire retardant materials for construction industry. Medical materials are also one typical application area of hybrid materials, as their mechanical properties can be tailored in combination with their biocompatibility, for example nanocomposites for dental filling materials. A high content of inorganic particles in these materials provides the necessary toughness and low shrinkage, while the organic components provide the curing properties combined with the paste-like behavior. Additional organic groups can improve the adhesion properties between the nanocomposites and the dentine.

Composite electrolyte materials for applications such as solid-state lithium batteries or supercapacitors are produced using organic–inorganic polymeric systems formed by the mixture of organic polymers and inorganic moieties prepared by sol–gel techniques. In these systems at least one of the network-forming species should contain components that allow an interaction with the conducting ions. This is often realized using organic polymers which allow an interaction with the ions, for example via coordinative or by electrostatic interactions. One typical example is proton conducting membranes which are important for the production of fuel cells The application of hybrid composites is interesting for these systems because this membrane is stable at high temperatures compared with pure organic systems.

In the next sections electrical properties and applications will be discussed in order to understand electron transport mechanism in such materials which hereafter could result useful also for sensing properties investigations.

1.3.3 Electronics

The potential for new technological opportunities and reduced product cost has fueled recent efforts to replace crystalline silicon as the active component in electronic devices. Recently, the effort to introduce semiconducting organic materials within practical electronic devices has opened the possibility of depositing semiconducting components at near room temperature and therefore on a range of substrates, including those that are large area, organic-based and flexible. The organic-based materials, when fully developed, are expected to enable such technologies as electronic newspapers, smart cards and fabric, inexpensive ID tags and similar flexible, low-cost products. The advances in mobility have been enabled by the development of new organic semiconductors, as well as by new techniques to better order the molecules on surfaces. After approximately 25 years of development, the room-temperature mobility values in organic thin film devices have reached $\sim 1 cm^2 V^{-1} s^{-1}$ (approximately the value of mobility for the best amorphous Si material, but still several orders of magnitude lower than crystalline silicon). While great progress has been made in improving the mobility of organic materials, the room-temperature mobility appears to be limited by the weak intermolecular interactions (i.e., generally van der Waals interaction) in molecular materials and the ability to organize and order the chains in polymer-based materials.

Organic-inorganic hybrids offer attractive opportunities for many electronic applications, because they can combine useful attributes of both organic and inorganic materials within a single molecular scale composite. Organic components provide, for example, lightweight and flexible mechanical properties, ease of deposition, and the ability to tailor efficient

luminescence. Inorganic materials, on the other hand, may contribute higher electrical mobility (as a result of the strong covalent bonding within these systems), band gap tunability, and thermal/mechanical stability.

The family of potential organic-inorganic hybrids is vast, among these a lot of functional hybrid consists of at least one amorphous component. But this section will primarily focus on the metal halide-based perovskite family, since this is currently one of the most thoroughly studied crystalline hybrid systems with respect to potential electronic device applications.

Crystalline hybrids are particularly interesting because of the ability to conveniently correlate structure-property relationships, thereby providing a mechanism for understanding and tailoring properties. Additionally, the good solubility and relatively low-melting and boiling points for the metal halide component of the perovskites provide for a range of low-cost film deposition options [13].

1.3.3.1 Organic-Inorganic Perovskites

The basic AMX_3 hybrid perovskite structure consists of a three-dimensional network of corner-sharing small metal cation (M), halide anion (X) and organic large cations (A) occupying the 12-fold coordinated sites between the octahedra of structure MX_6 (Figure 1.9). The size of the cation A is an important aspect for the formation of a closed packed perovskite structure, since this cation A must fit into the space composed of the four adjacent octahedra which are connected together through shared corners. So, the three-dimensional (3D) confinement for the A cation site limits the types of organic cations that can be incorporated within the 3D perovskite structure. In these organic/ inorganic halides, the organic cations are small and are typically restricted to methylammonium, ethylammonium and formami-dinium. The integration of larger molecules with terminal cationic groups within the inorganic framework have also been demon-strated in some cases. The metal cations are typically divalent metal ions such as Pb^{2+}, Sn^{2+} and Ge^{2+} while the halide anions are I^-, Cl^- and Br^-. Several examples of cubic or distorted organic-inorganic perovskites include $(CH_3NH_3)PbX_3$ (X=Cl, Br, I), $(CH_3NH_3)SnI_3$, $(CH_3NH_3)SnBr_3$, and $(NH_2CH=NH_2)SnI$. Layered perovskite structures can also be formed and are structurally derived from the 3D AMX_3 structure by taking n-layer thick cuts from along a particular crystallographic direction of the structure and stacking these slabs in alternation with organic cation layers. Several possibilities for the perovskite slab orientation include <100>, <110>, and <111> cuts. The single layer (n=1) <100>-oriented layered perovskites are the simplest and most widely studied perovskites and contain single MX_4^{2-} layers, where M is a divalent metal and X is a halide [13, 21].

The flexible structural and chemical characteristics of the organic-inorganic perovskites provide for a wide range of interesting and potentially useful physical properties. Interesting magnetic properties, for example, arise in many of the layered hybrid perovskites with first-row transition metals in the inorganic layers, as a result of the low (and tunable) dimensionality of the structures. While magnetic and structural properties are quite notable for the hybrids, this review will focus on optical and electrical properties since these are currently most relevant for electronic device applications.
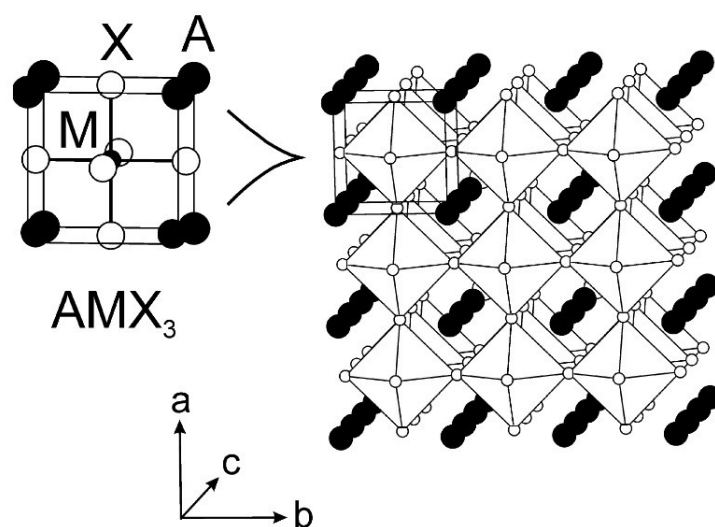
Figure 1.9. Schematic representations of basic perovkite structure (on the left) and how the structure extends in three dimensions (on the right).

Many of the layered hybrid perovskites, especially those containing germanium(II), tin(II), or lead(II) halide sheets, resemble multilayer quantum well structures, with semiconducting inorganic sheets alternating with wider band gap (i.e. highest occupied molecular orbital to lowest unoccupied molecular orbital, HOMO-LUMO gap) organic layers (Figure 1.12). Making substitutions on either the metal or halogen site modifies the band gap of the inorganic layers (well depth), while the width of the barrier and well layers can easily be adjusted by changing the length of the organic cations and the number of perovskite sheets between each organic layer, respectively. In the hybrid structures with semiconducting inorganic sheets and simple organic cations (i.e. aliphatic or single ring aromatic moieties), the conduction band of the inorganic layers is generally below that of the organic layers and the valence band of the inorganic layers is similarly above that of the organic layers (Figure 1.10 a). Therefore, the inorganic sheets act as quantum wells for both electrons and holes. Alternatively, if larger band gap metal halide sheets are integrated with more complex, conjugated (i.e. smaller HOMO-LUMO gap) organic cations, the well and barrier layer roles can be reversed (Figure 1.10 b). Given appropriate modifications of the chemistry of the organic and inorganic layers, the band gaps for the organic and inorganic layers can also be offset (Figure 1.10 c), leading to a type II heterostructure, in which the wells for the electrons and holes are in different layers. The self-assembling structures share many of the interesting electronic characteristics of quantum well structures prepared by "artificial" techniques, such as molecular beam epitaxy (MBE), and are therefore expected to yield similarly interesting optical and electrical characteristics [13, 21].

As for optical properties, the electrical characteristics of the hybrid perovskites are likely to be substantially influenced by the incorporation of more complex organic cations. For organic cations with relatively small HOMO-LUMO gaps, transport in the organic cation layer may be achievable. In these systems, the inorganic framework should provide a means of templating the conformation and orientation of the oligomeric or dye-containing cation. Given the importance of molecular ordering to the mobility and transport characteristics of organic semiconductors in TFTs and related devices, this templating capability should prove quite significant. Presently, however, the transport properties within the organic component of hybrid perovskites have not been rigorously explored.
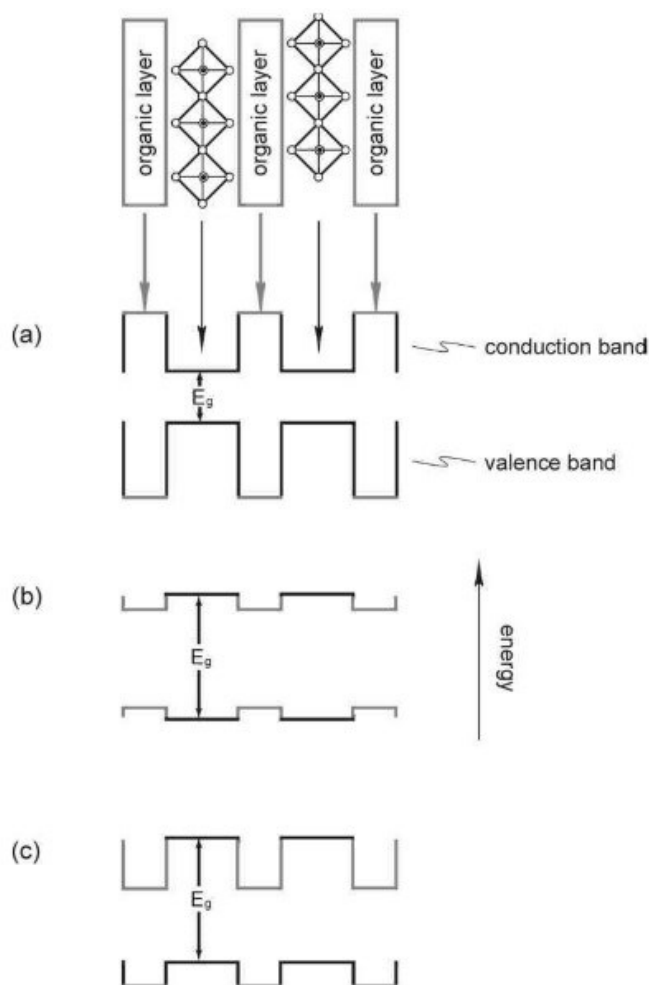
Figure 1.10. Schematic organic-inorganic perovskite structure and several possible energy level schemes that can arise within these structures.

The recent development of organic-inorganic halide perovskite materials as light harvesters in solid-state sensitized solar cells has led to reports of impressive variety of photovoltaic architectures [22-25].

1.4 Sensing hybrid materials

So far, gas sensing materials can be classified mainly into two types, namely, inorganic semiconductor metal oxides (SMOs) and organic conducting polymers (CPs) materials. The conventional gas sensors based SMOs like doped or undoped SnO_2, TiO_2, ZnO, WO_3 or Fe_2O_3 have been well studied to detect most of reducing gases and they are considered interesting for their good response, low cost and simple sensing methods [26]. However, there still exist some problems with them, for example high working temperature, thus resulting in high energy or power consuming or latent safety trouble. Therefore, much effort has been focused on the development of the sensors with low power operating at low temperature or room temperature. Alternatively, the gas sensors based on conducting polymers such as polythiophene (PPT), polypyrrole (PPy) and polyaniline (PANI), have also received considerable interest as effective materials for room temperature chemical sensors. However, conducting polymers also have their own shortcomings such as low thermal stability, low response and long response time for gas sensors, which can hinder their potential applications in future [27, 28] It is believed that the combination of nanosized metal

oxides and conducting polymers could be expected to be an effective approach to solve the above problems [29, 30].

1.4.1 Introduction to hybrid sensors

Sensor is a transducer that converts one form of energy into another suitable form amenable for further processing. Although numerous types of sensors have been well established in industries, agriculture, medicine and many other fields, the development of sensing materials with high sensing capabilities is still proceeding at an unprecedented rate.

Inorganic and organic compounds have been proposed as sensing materials, and have gained increasingly development, respectively, due to some particular advantages. Inorganic compounds behave generally high chemical and thermal stability that allows their application under different operating conditions, and they can be obtained by cheap processes and be easily deposited in thin or thick film form by different techniques. On the other hand organic compounds are characterized by a synthetic versatility and reactivity, which makes it possible to modulate the molecular structure of the sensing materials to enhance the selectivity toward a target analyte. Additionally, in the fields of sensors, the organic sensing materials such as conducting polymers (polyaniline (PANI), polypyrrole (PPy), and polythiophene (PTP), etc.) can show response to target analytes at room temperature or low temperature, which has a convenient operating and attractive prospect [29]. Nevertheless, the drawbacks for single inorganic or single organic sensing materials, namely, high operating temperature and low selectivity for inorganic sensing materials, and poor chemical stability and mechanical strength for organic sensing materials, could restrict their practical application. The researches have proved that the mechanical strength and chemical stability can be enhanced by the addition of inorganic particles into the organic materials to form hybrids. Following this idea, the most general approach has been the exploitation of the inorganic compound as protective matrix where the organic moiety, which is the sensing component, is dispersed by different techniques. A different and more intriguing approach, on the other hand, can be that in the hybrid materials, both components cooperate in the sensing mechanisms, resulting in enhanced performances. Therefore, in the past decades, the organic/inorganic hybrid materials with different combinations of the two components, expected to obtain new kind composite materials with synergetic or complementary behaviors, have received more and more attentions worldwide and become attractive for many new electronic, optical, magnetic or catalytic applications since their properties or performances can be improved, considering the possibility to combine the advantages of organic and inorganic counterparts. As far as sensor applications concerned, many reports have been published based on the organic/inorganic hybrid sensing materials for the applications in gas sensors, humidity sensors, ultraviolet sensors, strain sensors, and other sensors. In past decade research, various organic/inorganic hybrids were prepared including PTP/SnO_2, PPy/SnO_2, PANI/SnO_2, PPy/WO_3, PTP/WO_3, PPy/ZnO, PANI/ZnO and PPy/Fe_2O_3, and investigated their gas sensing performances to several toxic or harmful gases such as NH_3, H_2S, NO_2, methanol, ethanol and acetone. Gas sensing tests showed that the hybrids possessed better gas sensing performances compared with the single component at room temperature or low temperature, implying theirs potential application for gas sensors. Experimental data also showed the hybrids had higher thermal stability than the pure polymers, which was beneficial to theirs potential applications as chemical sensors.

The organic/inorganic hybrid gas sensing materials have gained more attention, however, the sensor performances, such as stability, repeatability and recovery speed, still need to be improved

in further research. Meanwhile, the hybrids take on benign foreground in ultraviolet (UV) sensors, strain sensors, electrochemical immunosensor and fluorescent chemosensor, therefore it is attractive to apply organic/inorganic hybrid in these fields. Moreover, development of the hybrids from two components to three or more components should be promising in improving the sensor performances and expanding their application field [30].

1.4.2 Sensing films of hybrid materials

The sensor is generally fabricated into film form, namely thin film form and thick film form. The thin film sensor can be fabricated by several methods. For example, the $(PPy)xMoO_3$ thin films were fabricated by an ex situ intercalation process. The host MoO_3 films were first deposited on LaAlO3 (LAO) single crystal substrates by using a chemical vapor deposition (CVD) method followed by the intercalation of PPy into the MoO_3 films. The PANI/inorganic nanocomposite thin films were deposited over such PSS film by electrostatic self-assembly and in situ chemical oxidation polymerization combined technique using a dip-coater at anout 10 °C. An in situ UV-irradiation method was used to prepare TiO_2 NPs/PPy composite thin films on alumina substrate as resistive type humidity sensors. The precursor composite solution consisting of TiO_2 NPs and pyrrole (Py) was firstly spin-coated on an alumina substrate with a pair of comb-like electrodes to form thin films, and then the films were polymerized under the irradiation of UV light (254 nm) for 10 min. The thick film sensor can be fabricated by a coating method. A proper amount of sample powder was lightly ground with several drops of terpineol in an agate mortar to form slurry. Then, the slurry was coated onto the outside surface of the alumina tube containing two Au electrodes and four Pt wires on both ends of the tube. The film form sensor was also fabricated by electrochemically deposited method, spincoat method, electrostatic self-assembly technique, and dip-coat technique. Additionally, the test samples to be used as a sensor was also prepared in pellet form by using an applying press [30].

1.4.3 Humidity hybrid sensors

Humidity sensors have been widely used in industrial production, environment monitoring and protection, storage, human comfort, etc., and a great variety of materials have been investigated as humidity-sensing materials [31-42]. Similar to other chemical sensor, the high performance humidity sensors also are required to have linear response, high response, fast response time, chemical and physical stability, wide operating humidity range and low cost. For this purpose, the humidity sensing materials include organic/inorganic composites have been studied. Su et al. [43]. fabricated resistive-type humidity sensors through in situ photopolymerization of pure PPy and TiO_2 nanoparticles/PPy (TiO_2 NPs/PPy) composite thin films on an alumina substrate. The sensor based TiO_2 NPs/PPy composite thin films, with the TiO_2 NPs addition of 0.0012 g, showed the higher response, much better linearity in its semi-logarithmic response curve and smaller hysteresis in the range of 30–90% RH than the sensor composed of PPy alone, which could be well explained by the finding that the impedance in a low humidity range continued to decrease with the doping of TiO_2 NPs as a photoinitiator in the fabrication process, and, in the composite films, the naked TiO_2 NPs had a more electrically active surface, and therefore were able to adsorb more water molecules than the PPy alone [44]. Li et al. [45] in situ synthesized sodium polystyrenesulfonate (NaPSS)/ZnO organic/inorganic nanocomposite and be used to prepare thin film humidity sensors. The logarithm of the impedance of sensor based on composite film changed linearly by four-orders of magnitude over almost whole humidity range (11–97% RH).

The sensors based on nanocomposites showed higher response, better linearity, small hysteresis (<2% RH) and quicker response (2 s for absorption and desorption, respectively) than sensors prepared with NaPSS. It was proposed that the improvement in sensing properties resulted from the introduction of inorganic ZnO and the formation of nanocomposites at nanoscale. Parvatikar et al. [46] synthesized conducting PANI/WO$_3$ composites by 'in situ' deposition technique by placing fine graded WO$_3$ in polymerization mixture of aniline. High temperature conductivity measurements showed thermal activated behavior. The change in resistance with respect to percent relative humidity (RH) was observed. The almost linear response of PANI/WO$_3$ (50 wt% of WO$_3$ in PANI) to the broad range of humidity (ranging between 10 and 95% RH) proved to be a competent material as humidity sensor. Suri et al. [47] reported the PPy/_-Fe$_2$O$_3$ nanocomposites in the pellet form were used as humidity sensor, which showed better humidity sensing as compared with _-Fe$_2$O$_3$ and higher response with higher PPy concentration. Wang et al. [48] investigated the humidity sensing properties of the RMX/BaTiO$_3$ composite material made of obtained by mixing nanocrystal BaTiO$_3$ and polymer quaternary acrylic resin (RMX). The humidity sensor made of the composite material showed better humidity sensing properties than the BaTiO$_3$ sensor such as higher response and smaller humidity hysteresis. Parvatikar et al. [49] synthesized PANI/Co$_3$O$_4$ composites by an in situ chemical polymerization method with ammonium persulfate ((NH_4)$_2$S$_2$O$_8$) as an oxidizing agent. This was a single-step polymerization process for the direct synthesis of the emeraldine salt phase of the polymer. High temperature conductivity measurements showed thermally activated behavior. The almost linear response of PANI/Co$_3$O$_4$ (50% Co$_3$O$_4$ in PANI) composites to a broad humidity range (10–95%) proved this to be a competent material for humidity sensing. Singla et al. [50] reported the PANI/Mn$_3$O$_4$ composite doped with perchloric acid, sulfuric acid, ortho-phosphoric acid, acetic acid and acrylic acid as sensing materials to determine relative humidity in the range of 20–90%. Relative humidity measurement had been related with the change in resistance of doped composite samples. Each acid doped PANI/Mn$_3$O$_4$ showed an increase in resistance as relative humidity increases, however the response was found to dependent on the type of dopant anions. The response of each composite was found to be almost linear with the humidity but the composites doped with organic acids had found to be more sensitive than those with inorganic dopants. Due to the linear increase in resistance, composites doped with organic acids could act as humidity sensor.

References

[1] Sanchez C., Arribart H., Giraud Guille M. M., Biomimetism and bioinspiration as tools for the design of innovative materials and systems, Nature Materials 4 (4), 277 (2005)

[2] Sanchez C., Julian B., Belleville P., Popall M., Application of hybrid organic-inorganic nanocomposites, Journal of Materials Chemistry 15 (35-36), 3559 (2005)

[3] Fahmi A., Pietsch T., Mendoza C., Cheval N., Functional hybrid materials, Materials Today 12 (5), 44-50 (2009)

[4] Sanchez C., Boissiere C., Cassaignon S., Chaneac C., Durupthy O., Faustini M., Grosso D., Laberty-Robert C., Nicole L., Portehault D., Ribor F., Rozes L., Sassoye C., Molecular Engineering of Functional Inorganic and Hybrid Materials, Chemistry of Materials 26, 221-238 (2014)

[5] Kickelbick G., Hybrid Materials. Synthesis, Characterization, and Applications, 2007 Wiley-VCH Verlag GmbH & Co. KGaA, Weinheim, ISBN: 978-3-527-31299-3

[6] Bensaude-Vincent B., Arribart H., Bouligand Y, Sanchez C., Chemists and the school of nature, New Journal of Chemistry 1, 1-5 (2002)

[7] Kato T., Sakamoto T., Nishimura T., Macromolecular Templating for the Formation of Inorganic-Organic Hybrid Structures. MRS Bulletin 35 (2010) 127-132.

[8] Kato T., Sugawara A., Hosoda N., Calcium Carbonate-Organic Hybrid Materials, Advanced Materials 14 (2002) 869

[9] Sanchez C. Ribot F., Design of hybrid organic-inorganic materials synthesized via sol-gel chemistry, New Journal of Chemistry 18 (10), 1007 (1994)

[10] Van Olphen H., Maya blue: a clay-organic pigment?, Science 154 (3749) 645-6 (1966)

[11] Yacamán M. J., Rendon L., Arenas J., Serra M. C., Maya Blue Paint: An Ancient Nanostructured Material, Science 273 (5272) 223-5 (1996)

[12] http://www.azulmaya.com/

[13] Gómez-Romero P., Sanchez C., Functional Hybrid Materials, 2004 Wiley-VCH Verlag GmbH & Co. KGaA, Weinheim, ISBN: 978-3-527-30484-4

[14] Doménech A., Doménech-Carbó M.T., Osete-Cortina L., Montoya N., Application of solid-state electrochemistry techniques to polyfunctional organic–inorganic hybrid materials: The Maya Blue problem, Microporous and Mesoporous Materials 166 (2013) 123–130

[15] http://pubs.usgs.gov/of/2001/of01-041/htmldocs/clays/seppaly.htm

[16] Abdul Khalil H.P.S., Jawaid M., Hassan A., Paridah M.T., Zaidon A., Oil Palm Biomass Fibres and Recent Advancement in Oil Palm Biomass Fibres Based Hybrid Biocomposites, 2012 Composites and Their Applications, Prof. Ning Hu (Ed.), ISBN: 978-953-51-0706-4, InTech, DOI: 10.5772/48235. Available from: http://www.intechopen.com/books/composites-and-their-applications/oil-palm-biomass-fibres-and-recent-advancement-in-oil-palm-biomass-fibres-based-hybrid-biocomposites

[17] Judeinstein P., Sanchez C., Hybrid organic–inorganic materials: a land of multidisciplinarity, Journal of Materials Chemistry 6 (1996) 511

[18] Sanchez C., Boissiere C., Cassaignon S., Chaneac C., Durupthy O., Faustini M., Grosso D., Laberty-Robert C., Nicole L., Portehault D., Ribot F., Rozes L., Sassoye C., Molecular Engineering of Functional Inorganic and Hybrid Materials, Chemistry of Materials 26 (2014) 221−238

[19] Sanchez C., Belleville P., Popalld M., Nicole L., Applications of advanced hybrid organic–inorganic nanomaterials: from laboratory to market, Chemical Society Review 40 (2011) 696–753

[20] Grosso D., Ribot F., Boissiere C., Sanchez C., Molecular and supramolecular dynamics of hybrid organic–inorganic interfaces for the rational construction of advanced hybrid nanomaterials, Chemical Society Review, 40 (2011), 829–848

[21] Boix P. P., Nonomura K., Mathews N., Mhaisalkar S. G., Current progress and future perspectives for organic/inorganic perovskite solar cells, Materials Today 17 (2014) 16-23

[22] Mitzi D. B., Synthesis, Structure, and Properties of Organic-Inorganic Perovskites and Related Materials, in Progress in organic chemistry, 2007, John Wiley & Sons, 1-122

[23] Takahashi Y., Obara R., Nakagawa K., Nakano M., Tokita J., Inabe T., Tunable Charge Transport in Soluble Organic–Inorganic Hybrid Semiconductors, Chemical Materials 19 (2007) 6312–6316

[24] Bi D., Yang L., Boschloo G., Hagfeldt A., Johansson E. M. J., Effect of Different Hole Transport Materials on Recombination in $CH_3NH_3PbI_3$ Perovskite-Sensitized Mesoscopic Solar Cells, Journal of Physical Chemistry Letters 4 (2013) 1532−1536

[25] Xing G., Mathews N., Sun S., Sien Lim S., Ming Lam Y., Grätzel M., Mhaisalkar S., Chien Sum T., Long-Range Balanced Electron and Hole-Transport Lengths in Organic-Inorganic $CH_3NH_3PbI_3$, 342 (2013) 344-347

[26] Carotta M.C., Guidi V., Malagù C., Vendemiati B., Martinelli G., Gas sensors based on semiconductor oxides: basic aspects onto materials and working principles, Mater. Res. Soc. Symp. Proc. 828 (2005) 173–184

[27] Van de Leur R.H.M., Van der Waal A., Gas and vapor detection using polypyrrole, Synthetic Metals 102 (1999) 1330–1331

[28] Wallace G.G., Spinks G.M., Kane-Maguire A.P., Tesdale P.R., Conductive Electroactive Polymers: Intelligent Materials Systems, CRC Press, London, 2002

[29] Ma X.F., Mang W., Li G., Chen H.Z., Bai R., Preparation of polyaniline–TiO_2 composite film with in situ polymerization approach and its gas-sensitivity at room temperature, Materials Chemistry and Physics 98 (2006) 241–247

[30] Wang S., Kang Y., Wang L., Zhang H., Wang Y., Wang Y., Organic/inorganic hybrid sensors: A review, Sensors and Actuators B 182 (2013) 467– 481

[31] Sakai Y., Sadaoka Y., Matsuguchi M., Humidity sensors based on polymer thin films, Sensors and Actuators B 85 (1996) 35–36.

[32] Harsányi G., Polymeric sensing films: new horizons in sensorics, Materials Chemistry and Physics 43 (1996) 199–203.

[33] Suresh Raj A.M.E., Magadalane C.M., Nagaraja K.S., Zinc(II) oxide–yttrium(III) oxide composite humidity sensors, Physica Status Solidi A 191 (2002) 230–234.

[34] Jain M.K., Bhatnagar M.C.,. Sharma G.L, Effect of Li doping on ZrO_2–TiO_2 humidity sensors, Sensors and Actuators B 55 (1999) 180–185.

[35] Xu C.N., Miyasake K., Watanabe T., Humidity sensors using manganese oxides, Sensors and Actuators B 46 (1998) 87–96.

[36] Bayhan M., Hashemi T., Brinkman A.W., Sintering and humidity sensitive behavior of the $ZnCr_2O_4$–K_2CrO_4 ceramic system, Journal of Materials Science 32 (1997) 6619–6623.

[37] Traversa E., Ceramic sensors for humidity detection: the state-of-the art and future developments, Sensors and Actuators B 23 (1995) 135–156.

[38] Montesperelli G., Pumo A., Traversa E., Gusmano, Bearzotti A., Montenero A., Traversa G.G., Sol–gel processed TiO_2-based thin films as innovative humidity sensors, Sensors and Actuators B 25 (1995) 705–709.

[39] Yeh Y.C., Tseng T.Y., Chang D.A., Electrical properties of TiO_2–$K_2Ti_6O_{13}$ porous ceramic humidity sensor, Journal of the American Ceramic Society 73 (1990) 1992–1998.

[40] Wu L., Wu C.C., Wu M.M., Humidity sensitivity of Sr (Sr,Ti)O_3 ceramics, Journal of Electronic Materials 19 (1990) 197–200.

[41] T. Nitta, Z. Terada, S. Hayakawa, Humidity sensitive electrical conduction of MgCr2O4–TiO2 porous ceramics, Journal of the American Ceramic Society 63 (1980) 295–299.

[42] Farahani H., Wagiran R., Hamidon M. N., Humidity Sensors Principle, Mechanism, and Fabrication Technologies: A Comprehensive Review, Sensors 14 (2014) 7881-7939

[43] Su P.G., Huang L.N., Humidity sensors based on TiO_2 nanoparticles/polypyrrole composite thin films, Sensors and Actuators B 123 (2007) 501–507

[44] Chalkova E., Fedkin M.V., Wesolowski D.J., Lvov S.N., Effect of TiO_2 surface properties on performance of Nafion-based composite membranes in high temperature and low relative humidity PEM fuel cells, Journal of the Electrochemical Society 152 (2005) A1742–A1747

[45] Li Y., Yang M.J., She Y., Humidity sensors using in situ synthesized sodium polystyrenesulfonate/ZnO nanocomposites, Talanta 62 (2004) 707–712

[46] Parvatikar N., Jain S., Khasim S., Revansiddappa M., Bhoraskar S.V., Ambika Prasad M.V.N., Electrical and humidity sensing properties of polyaniline/WO_3 composites, Sensors and Actuators B 114 (2006) 599–603.

[47] Suri K., Annapoorni S., Sarkar A.K., Tandon R.P., Gas and humidity sensors based on iron oxide–polypyrrole nanocomposites, Sensors and Actuators B 8 (2002) 277–282.

[48] Wang J., Yan W.P., Zhang J.C., Qiu F.B., Zhang T., Liu G.F., Xu B.K., Property analysis and humidity sensitivity of the composite material of $BaTiO_3$ and RMX, Materials Chemistry and Physics 69 (2001) 288–291

[49] Parvatikar N., Jain S., Kanamadi C.M., Chougule B.K., Bhoraskar S.V., Ambika Prasad M.V.N., Humidity sensing and electrical properties of polyaniline/cobalt oxide composites, Journal of Applied Polymer Science 103 (2007) 653–658

[50] Singla M.L., Awasthi S., Srivastava A., Humidity sensing using polyaniline/Mn_3O_4 composite doped with organic/inorganic acids, Sensors and Actuators B 127 (2007) 580–585

Capther 2
Ordered Mesoporous Organosilica Hybrid Materials: from PMO to ECS

The general interest in developing hybrid materials arises from the expectation that the assembly of organic and inorganic building blocks in a single material can combine their particular advantages. That is, first of all the manifold chemical functionality of the organic component combined with the chemical, mechanical, and thermal robustness of the inorganic part, which is itself functionally very limited. Through this symbiosis, materials are formed whose properties differ significantly from those of the single, isolated components; completely new properties of these hybrid materials can emerge. This is valid in particular for porous materials, that is, for those with high surface-to-volume ratios. Although also compact composite and hybrid materials exhibit modified bulk properties, such as density, hardness, elasticity, and so on, the actual advantage of porous hybrid materials arises out of the number of and accessibility to localized functional or interacting centers. Of course, this can be realized better the larger the interface and the more functional centers are placed at this interface. To give only two examples: Tuning the polarity of the pore surfaces by integrating organic components into an inorganic matrix is supposed to extend the spectrum of materials that are optimized for a particular chromatographic problem. Furthermore, by functionalizing an inorganic host material with organic functionalities like CZC multiple bonds, alcohols, thiols, carboxylic or sulfonic acids, amines, etc., for instance, chemical or biochemical reactions can be carried out on a stable, solid, stationary inorganic matrix. Three pathways are available for the synthesis of porous hybrid materials based on (organo-)silica units: (1) the subsequent modification of the pore surface of a purely inorganic silica material (grafting), (2) the simultaneous condensation of corresponding silica and organosilica precursors (co-condensation), and (3) the incorporation of organic groups as bridging components directly and specifically into the pore walls by the use of bis- or multi-silylated single-source organosilica precursors [creation of (periodic) mesoporous organosilicas; PMOs] [1].

2.1 Porous Hybrid Materials

2.1.1 Definition and classification

A solid is called porous, when it contains pores, i.e. cavities, channels or interstices, chich are deeper than they are wide. A porous material can be described in two ways, by the pores or by the pore walls. Some porous materials are based on agglomerated or aggregated powders in which the pores are formed by interparticle voids, while others are based on continuous solid networks.

For most applications the pore size is of major importance. However, pore sizes are not susceptible to precise measurement, because the pore shape is usually high irregular, leading to a variety of pore sizes within one single material. Nevertheless, the use of three different pore size regimes was recommended by IUPAC:

- Micropores, with diameters smaller than 2 nm;

- Mesopores, with diamteers between 2 and 50 nm;
- Macropores, with diameters larger than 50 nm.

This nomenclature is not arbitrarily chosen, but is associated with the different transport mechanisms occurring in the various types of pores, i.e. molecular diffusion and activatd transport in micropores; while in mesoporores Knudsen transport[2], surface diffusion and capillary condensation are the major mechanisms; and in macropores, bulk diffusion and viscous flow dominate.

As already mentioned, a wide variety of porous inorganic frameworks is known (Figure 2.1). Today, zeolites or MOFs are the most prominent examples for microporous materials. Mesoporous solids with pore sizes between 2 and 50nm can be found for example in aerogels, pillared clays and M41S materials, while macroporous solids are for example glasses, foams or inverse opal structures.
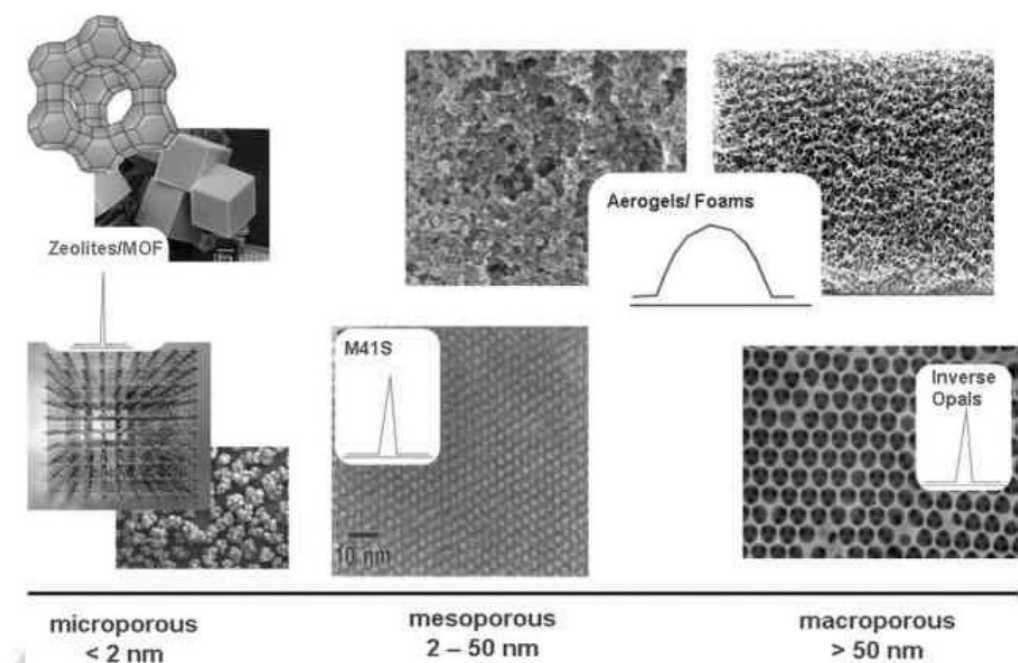
Figure 2.1: Different porous materials classified according to their pore size and pore size distribution [2].

In addition, these materials can be distinguished by the arrangement of the pores – periodic or random – and the pore radii distribution, which can range from either narrow with a rather uniform pore size distribution to quite a broad distribution. Not only pore size distribution and pore diameters are of interest for applications, but also the connectivity of the pore system or its dimension is of high interest. Porous channel systems, e.g. the ones in M41S phases, may be one-dimensional (1-D) as found for the hexagonally organized pore systems with their long channels, or 3-D as found for a cubic ordered pore structure. In addition to the dimensionality of the pore system, two different surfaces must be distinguished in porous materials. The outer or exterior surface is an outward curving surface (convex) with a completely different reactivity as the inward curving surface (concave) that is typically found in the interior of the pores. This effect is of importance for functionalization reactions [2].

With an organic modification of porous solids a wide field of porous hybrid materials can be obtained that, by the combination of inorganic and organic building blocks, benefit from the

---

[2] Knudsen diffusion occurs when the mean free path is relatively long compared to the pore size, so molecules collide frequently with the pore wall.

properties of both parts; an approach which already has been performed on a wide variety of different matrices. The organic groups can be placed selectively on the internal and/or the external pore surfaces or even within the pore walls. The organic modification in principle permits a fine tuning of materials properties, including surface properties such as hydrophilicity/hydrophobicity or potential interaction to guest molecules. In addition, the surface reactivity can be altered and the surface can be protected by organic groups with respect to chemical attack, but also bulk properties, e.g. mechanical or optical properties can be changed. This flexibility in choosing organic, inorganic or even hybrid building blocks allows one to control the materials properties to optimize them for each desired applications.

2.1.2 Synthesis of Porous Hybrid Materials based on Organo-Silica Units

The development of porous materials with large specific surface areas is currently an area of extensive research, particularly with regard to potential applications in areas such as adsorption, chromatography, catalysis, sensor technology, and gas storage [3].

Among these, mesoporous organic–inorganic hybrid materials, a new class of materials characterized by large specific surface areas and pore sizes between 2 and 15 nm, have been obtained through the coupling of inorganic and organic components by template synthesis. The incorporation of functionalities can be achieved in three ways (Figure 2.2): by subsequent attachment of organic components onto a pure silica matrix (grafting), by simultaneous reaction of condensable inorganic silica species and silylated organic compounds (co-condensation, one-pot synthesis), and by the use of bis- or multi-silylated single source organosilica precursors that lead to periodic mesoporous organosilicas (PMOs).
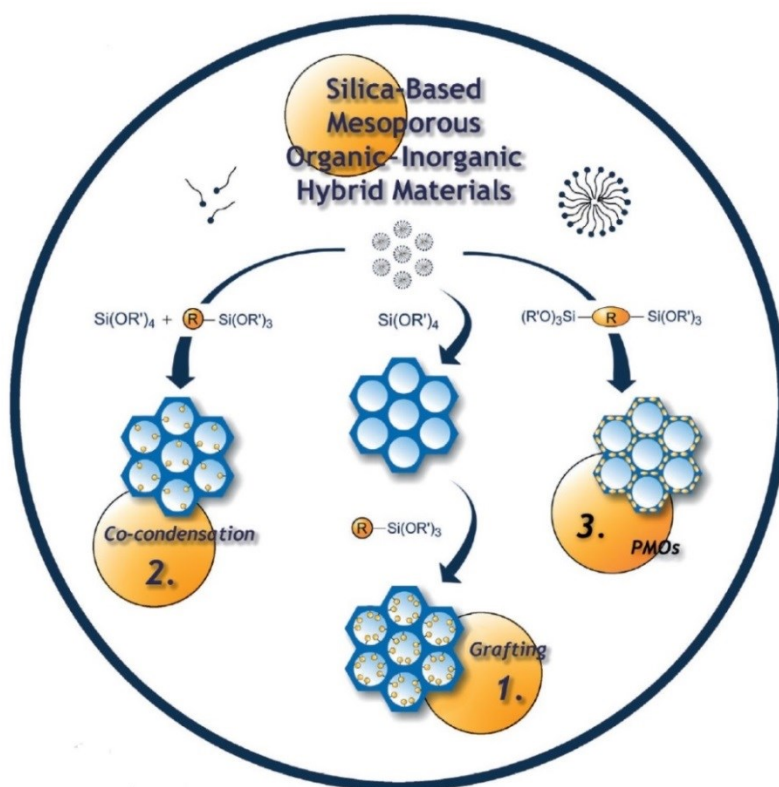
Figure 2.2. Diagram of the three synthetic approaches used for silica-based mesoporous organic-inorganic hybrid materials [3].

2.1.2.1 Postsynthetic Functionalization of Silica: Grafting

Grafting refers to the subsequent modification of the inner surfaces of mesostructured silica phases with organic groups. This process is carried out primarily by reaction of organosilanes of the type $(R'O)_3SiR$, or less frequently chlorosilanes $ClSiR_3$ or silazanes $HN(SiR_3)_3$, with the free silanol groups of the pore surfaces (Figure 2.3). In principle, functionalization with a variety of organic groups can be realized in this way by variation of the organic residue R. This method of modification has the advantage that, under the synthetic conditions used, the mesostructure of the starting silica phase is usually retained, whereas the lining of the walls is accompanied by a reduction in the porosity of the hybrid material (albeit depending upon the size of the organic residue and the degree of occupation). If the organosilanes react preferentially at the pore openings during the initial stages of the synthetic process, the diffusion of further molecules into the center of the pores can be impaired, which can in turn lead to a nonhomogeneous distribution of the organic groups within the pores and a lower degree of occupation. In extreme cases (e.g., with very bulky grafting species), this can lead to complete closure of the pores (pore blocking). The process of grafting is frequently erroneously called immobilization, which is a term that we believe should be reserved for adsorptive methods (e.g., the removal of toxic or environmentally relevant contaminants by adsorbent materials, or the separation of proteins and biocatalysts by restriction of the freedom of movement) [1, 3].
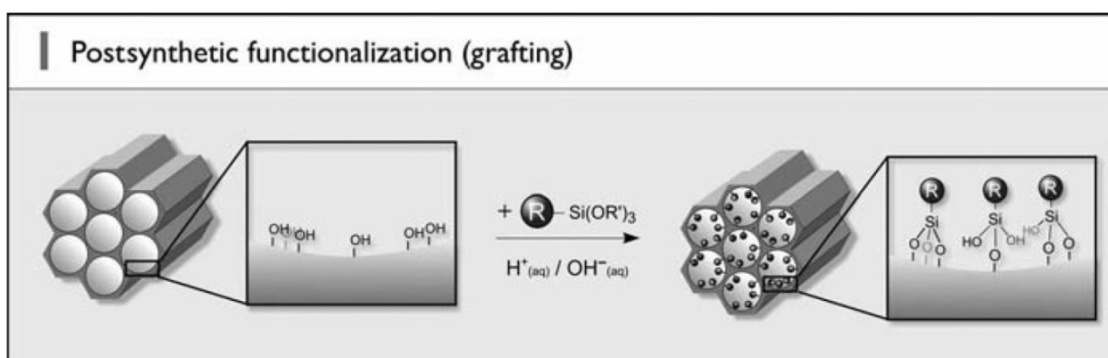
Figure 2.3. Grafting (postsynthetic functionalization) for organic modification of mesoporous pure silica phases with terminal organotrialkoxysilanes of the type $(R'O)_3SiR$. R =organic functional group [1].

2.1.2.2 One-pot Synthesis (Direct Synthesis): Co-Condensation

An alternative method to synthesize organically functionalized mesoporous silica phases is the co-condensation method (one-pot synthesis). It is possible to prepare mesostructured silica phases by the co-condensation of tetraalkoxysilanes [$(RO)_4Si$ (TEOS or TMOS)] with terminal trialkoxyorganosilanes of the type $(R'O)_3SiR$ in the presence of structure-directing agents leading to materials with organic residues anchored covalently to the pore walls (Figure 2.4). By using structure-directing agents known from the synthesis of pure mesoporous silica phases (e.g., MCM or SBA silica phases), organically modified silicas can be prepared in such a way that the organic functionalities project into the pores. Since the organic functionalities are direct components of the silica matrix, pore blocking is not a problem in the co-condensation method. Furthermore, the organic units are generally more homogeneously distributed than in materials synthesized with the grafting process. However, the co-condensation method also has a number of disadvantages: in general, the degree of mesoscopic order of the products decreases with increasing concentration of $(R'O)_3SiR$ in the reaction mixture, which ultimately leads to totally disordered products.
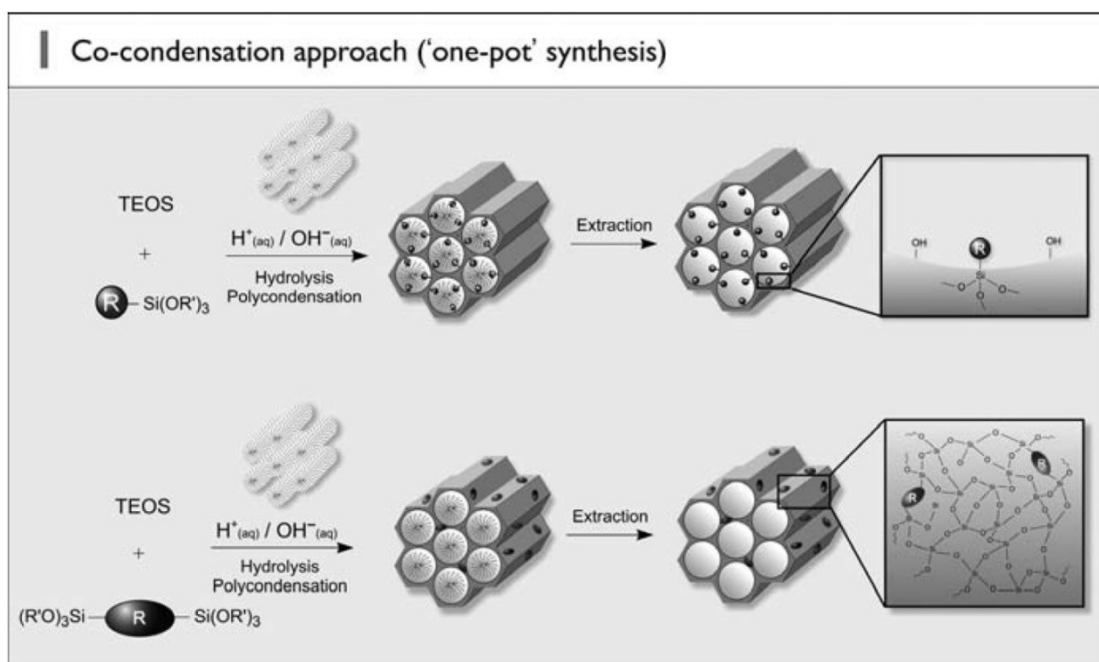
Figure 2.4. Co-condensation method (direct synthesis) employing TEOS and a terminal organotrialkoxysilane (top) or TEOS and an organo-bridged silsesquioxane (bottom) as mixed precursors for the organic modification of mesoporous pure silica phases. R = organic functional group [1].

Consequently, the content of organic functionalities in the modified silica phases does not normally exceed 40 mol%. Furthermore, the proportion of terminal organic groups that are incorporated into the pore-wall network is generally lower than would correspond to the starting concentration of the reaction mixture. These observations can be explained by the fact that an increasing proportion of

$(R'O)_3SiR$ in the reaction mixture favors homocondensation reactions—at the cost of cross-linking co-condensation reactions with the silica precursors. The tendency towards homocondensation reactions, which is caused by the different hydrolysis and condensation rates of the structurally different precursors, is a constant problem in co-condensation because the homogeneous distribution of different organic functionalities in the framework cannot be guaranteed. Moreover, an increase in loading of the incorporated organic groups can lead to a reduction in the pore diameter, pore volume, and specific surface areas. A further, purely methodological disadvantage that is associated with the co-condensation method is that care must be taken not to destroy the organic functionality during removal of the surfactant, which is why commonly only extractive methods can be used, and calcination is not suitable in most cases [1, 3].

2.1.2.3 Single-Source Precursor Method: PMO

The synthesis of organic–inorganic hybrid materials by hydrolysis and condensation reactions of bridged organosilica precursors of the type $(R'O)_3SiRSi(OR')_3$ has been known for a long time from sol–gel chemistry. In contrast to the organically functionalized silica phases, which are obtained by postsynthetic or direct synthesis, the organic units in this case are incorporated in the three-dimensional network structure of the silica matrix through two covalent bonds and thus distributed totally homogeneously in the pore walls. These materials, which are obtained as porous aero- and xerogels, can have large inner surface areas of up to 1800 m^2g^{-1} as well as high thermal stability but generally exhibit completely disordered pore systems with a relatively wide distribution of pore radii. The transfer of the concept of the structure-directed synthesis of pure silica mesophases by surfactants to the

bissilylated organosilica precursors described above allows the construction of a new class of mesostructured organic–inorganic hybrid materials—periodic mesoporous organosilicas (PMOs)—in which the organic bridges are integral components of the silica network (Figure 2.5). In contrast to amorphous aero- and xerogels, PMOs are characterized by a periodically organized pore system and a very narrow pore radius distribution. The first PMO was synthesized in 1999 by three research groups working independently of one another. PMO materials are considered as highly promising candidates for a series of technical applications, for example, in the areas of catalysis, adsorption, chromatography, nanoelectronics, or the preparation of active compound release systems [1, 3].
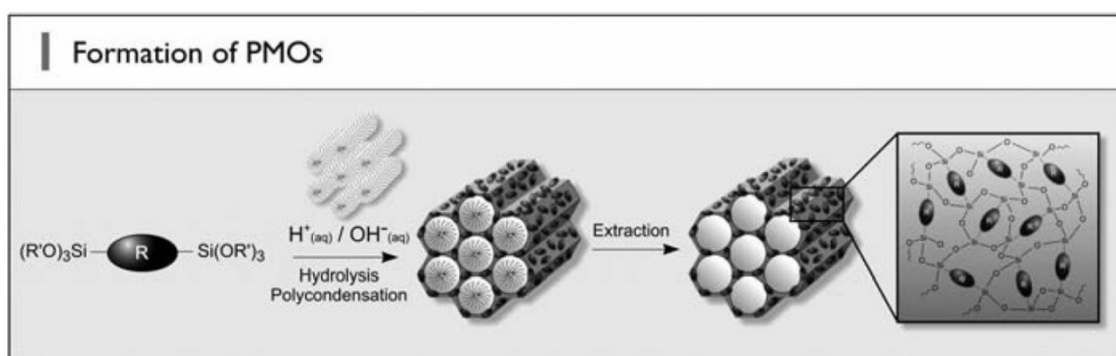
Figure 2.5. General synthesis pathway to PMOs that are constructed from bis-silylated organic bridging units. R = organic bridge [1] .

2.2 Periodic Mesoporous Organosilca (PMO)

2.2.1 Introduction to PMOs

The third method to prepare ordered mesoporous hybrid materials utilize bridged silsesquioxane precursors of the type ($(R'O)_3Si$–R–$Si(OR')_3$; R: organic bridging group, R': methyl or ethyl), i.e. precursors which are capable of undergoing cross-linking reactions and concurrently carry the organic functionality R a priori on board, so to speak (see Figure 2.5), leading to materials in which the density of the organic functional groups cannot be higher. The fact that the organic groups are covalently bonded and embedded in these bis-silylated compounds leads to mesostructured hybrids in which the organic groups are an integral part of the pore walls, meaning that the framework itself is modified. In these materials inorganic and organic parts are completely homogeneously mixed at the molecular scale within the whole sample. This is different from the materials which are produced by the grafting or co-condensation method, in which a more or less unaffected pure inorganic substrate is lined-up at the interface to the pores with organic groups they might be probably better described as materials with mixed compartments.

The first report of PMOs with crystal-like pore walls comes from Inagaki et al. [8]. The powder X-ray diffraction (XRD) pattern of the benzene-bridged PMO arises the existence of a periodicity of 7.6 Å on the molecular scale. This crystal-like organization of the organic bridges within the pore walls (a model of the pore walls is shown in Figure 2.6) was confirmed by HRTEM images [8], which showed numerous lattice fringes along the pore axis and also indicated a separation distance of 7.6 Å. The product resulted thermally stable up to 500°C.
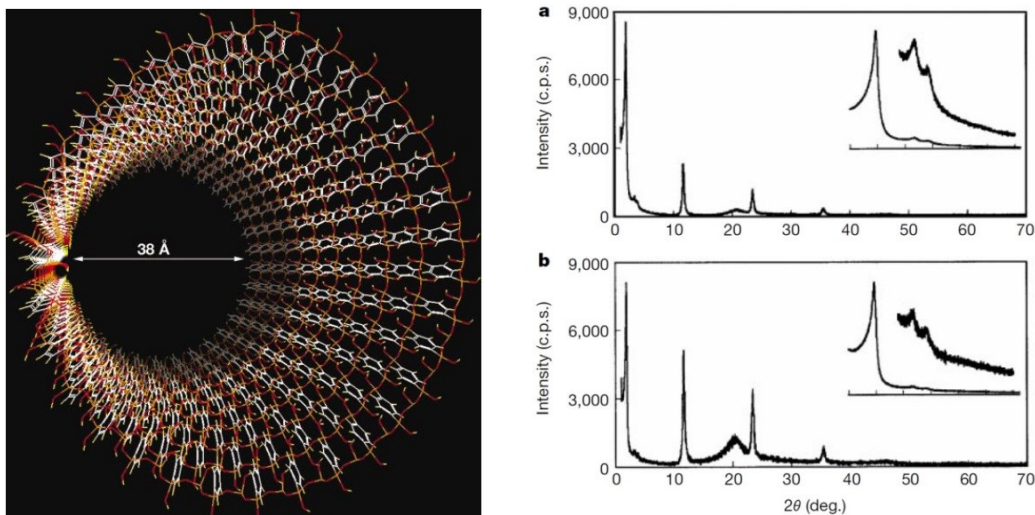
Figure 2.6. Pore surface model of the of mesoporous benzene-silica discovered by Inagaki et al. (on the left). Benzene rings are aligned in a circle around the pore, fixed at both sides by silicate chains. The silicate is terminated by silanol (Si-OH) at the surface. Hydrophobic benzene layers and hydrophilic silicate layers array alternately at an interval of 7.6 Å along the channel direction. Silicon in orange; oxygen in red; carbon in, white; hydrogen in yellow. Powder X-ray diffraction patterns of mesoporous benzene-silicas (on the right). a) Material after removal of surfactants; b) As-made material containing surfactants. Patterns in the low-angle region (1 < 2θ < 7) are shown magnified in the insets. These materials have both mesoscale (d = 45.5, 26.0 and 22.9 Å) and molecular-scale (d = 7.6, 3.8 and 2.5 Å) periodic structures [8].

PMO hybrids were created by applying the concept as that for the surfactant directed synthesis of ordered mesoporous silica to covalently bonded organic–silica scaffolds, which was stimulated by successful research on organosilsesquioxane gels.

The well-defined mesopores of PMOs can be controlled in the diameter range of 1.5–30 nm by the appropriate selection of template surfactants and additives used in the polycondensation process. While ionic surfactant templates have been preferably used to prepare conventional PMOs, large-pore PMOs with different symmetry of mesostructures have been successfully synthesized by the use of amphiphilic block copolymer templates and the addition of salts. A wide variety of organic moieties (R) are available for structural control and functionalization in the design of PMOs.

In the meantime, a significant number of different precursors were successfully converted into PMO materials; Figure 2.7 shows a small selection of some representatives, providing only an overview of chemical classes: short-chained saturated alkylene (1) or unsaturated alkenylene (2) groups, cyclic (3) or branched (4) multi-silylated compounds, those with aromatic (5,6) as well as heterocyclic (7,8) and polycyclic (9)
aromatic compounds, aromatic compounds with substituents that can be easily further modified (10,11), ethers (12), units with extended conjugated p-systems (13), and chiral groups (14,15).

Meanwhile, further PMOs with crystal-like pore walls were synthetized. Apparently, precursors which are rather very rigid, linear/symmetric and do not carry too long/bulky substituents favour the formation of crystal-like pore walls. Note that the term 'crystal-like' instead of 'crystalline' is used because (i) the organic bridges do not have to possess strict translational symmetry, they can be slightly tilted with respect to each other, and (ii) the silica part of the pore walls do not possess longe-range order.
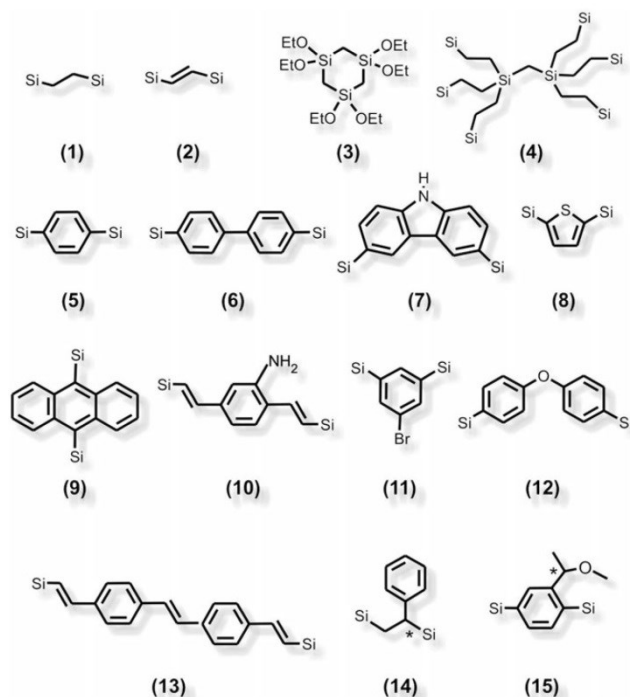
Figure 2.7. Overview of the organosilica precursors that have been converted into PMOs. Terminal Si atoms: Si=Si(OR)₃ with R=CH₃, C₂H₅.

The preparation of PMOs is associated with two main challenges which should not be concealed: Firstly, most of the precursors are not commercially available and their synthesis can be very demanding. Secondly, it turned out that the precursor has to fulfill certain structural requirements in order to result in a PMO material, meaning that by far not all bis-silylated compounds are convertible into PMOs. In some cases the 'dilution' of the reaction mixture with pure inorganic precursors (TMOS/TEOS) is helpful, although at the (disproportionate) cost of the density of organic groups.

In summary, the conceptual placement of PMOs within the class of silica-based organic-inorganic porous materials is due:

1) in contrast to completely amorphous aero- and xerogels, PMOs are characterized by a periodically organized pore system and a very narrow pore radius distribution;
2) some PMO precursors, in particular those with rigid, inflexible organic bridges, exhibit the tendency to undergo (at least partially) self-assembling processes on the molecular scale, too, which may give rise to PMOs that are not only ordered with respect to their channel system but exhibit additionally a crystal-like arrangement of their organic bridges within the pore walls;
3) with some exceptions it is usually not possible to remove the SDAs from the composite material by calcination due to the limited thermal stability of the organic moieties;
4) with increasing length of the organic bridge the hydrophobicity of the PMO precursor will increase; this can cause an interference with the SDAs, and in the worst case can lead to a massive disturbance of the liquid-crystalline phase, which may finally result in an unordered (or nonperiodic) mesoporous organosilica material with a spaghetti- or worm-like arrangement of the pores.

2.2.2 Properties and sensing applications of PMOs

The ordered and uniform porosity of mesoporous organic–inorganic hybrid materials may have the following advantages:

- the narrow pore size distribution is useful in all size selective applications (sieve effect), for instance chromatography or catalysis;
- the absence of slit-like or bottle-neck pores guarantees a fast and efficient mass transport of species with appropriate sizes (i.e., those that are smaller than the pore diameter) within these materials, which is advantageous, for instance, for sorption applications like wastewater treatment;
- regarding the field of host–guest chemistry the regular arrangement of the pores provides opportunities to design materials with completely new properties, for instance, those in which guest molecules or clusters of semiconductors are adsorbed in a uniform manner and orientation and thus may show interesting collective properties like nonlinear optical behavior or special magnetic coupling effects; this may be of particular interest for PMO thin films and monoliths [1].

PMOs exhibit several unique features built into their structure:

- high loading of organic groups,
- insignificant pore blocking,
- chemical reactive sites in the pore wall,
- homogeneously distributed groups,
- easily modified physical and chemical properties by flexible tuning of the organic bridge,
- high surface area, uniform pore and channel size with nanoscale dimensions.

In particular, uniform pore size distribution, porosity and ordered pore arrangement are maintained even after modification. The self-assembly mesoporous silica materials can be made in a variety of morphologies like powders, thin films, fibers, spheres, and monoliths. However the mesoporous silica thin films are believed as an ideal morphology for electronic and optical devices [11].

The special features of mesoporous silica thin films have attracted considerable attention because of their potential applications as molecular sieves, catalysts, adsorbents, optical devices, and sensor devices [12–22]. The use of mesoporous silica material for separation and sensor devices is interesting because the large surface area of mesoporous material, which can be as high as $1100 m^2 g^{-1}$, allows especially good gas access [22–27]. Recently, a number of studies have been performed that aim to modify the mesoporous hexagonal structure and increase the potential applicability of these materials for highly selective gas sensor and catalytic.

Regard gas sensors, an interesting study was carried out by B. Yuliarto et al. [11]. They used ordered benzene-silica hybrid material dip-coated onto n-type silicon, with SiO_2 and Si_3N_4 layers as a substrate. An alternating modulated LED (930 nm,1 kHz) beamwas irradiatedonthe reverse side of the semiconductor to induce an AC photocurrent. A volume flow controller and multi-port valve controlled the VOCs during measurement. The N_2 gas is used as the carrier gas for gas response measurement. In Figure 2.8 one can observe that the increase of photocapacitive current indicates a change of the positive surface potential, due to physical adsorption and interaction between the VOCs and the mesoporous silica layer.

B. Yuliarto et al. showed a selectivity of benzene molecule improvement for benzene–silica hybrid mesoporous thin film with respect to pure mesoporous silica. In the latter, there are many Si-O- and silanol (-Si-OH) bonds on the inner surface, which makes it hydrophilic material. Although the methanol is different from water, it is still easier to be absorbed into the Si-O- or Si-OH through hydrogen bond compared to the benzene. This phenomenon is according to the experimental results, where better absorption and reaction of methanol with the pure mesoporous silica compared to the benzene yield higher sensitive response of methanol than that of benzene. Moreover, in the benzene–silica hybrid mesoporous material, the densities of Si-O- and silanol (-Si-OH) bonds should be dramatically decreased because of the replacing of the benzene silica in a crystalline super lattice structure. The inner surface of the benzene–silica hybrid mesoporous transfers from hydrophilic into hydrophobic, which allows the mesoporous structure to be accessed easier by the organic molecules compared to the inorganic compound. As a result, the benzene which consists of organic molecules would be easily absorbed than methanol through the interaction among the benzene group within the inner surface of the benzene–silica mesoporous pores. However, the decrease of surface area after modification of mesoporous silica by benzene chain produces lower sensitive response compared to the cases of pure mesoporous silica sensor. Therefore, when the methanol is exposed into the benzene–silica hybrid mesoporous film, it is only absorbed and reacted with the silica part of wall pore. On the other hand, when the benzene exposed into the benzene–silica hybrid mesoporous, the benzene molecules react not only with the silica part, but also with the benzene chain in the wall pore [11].
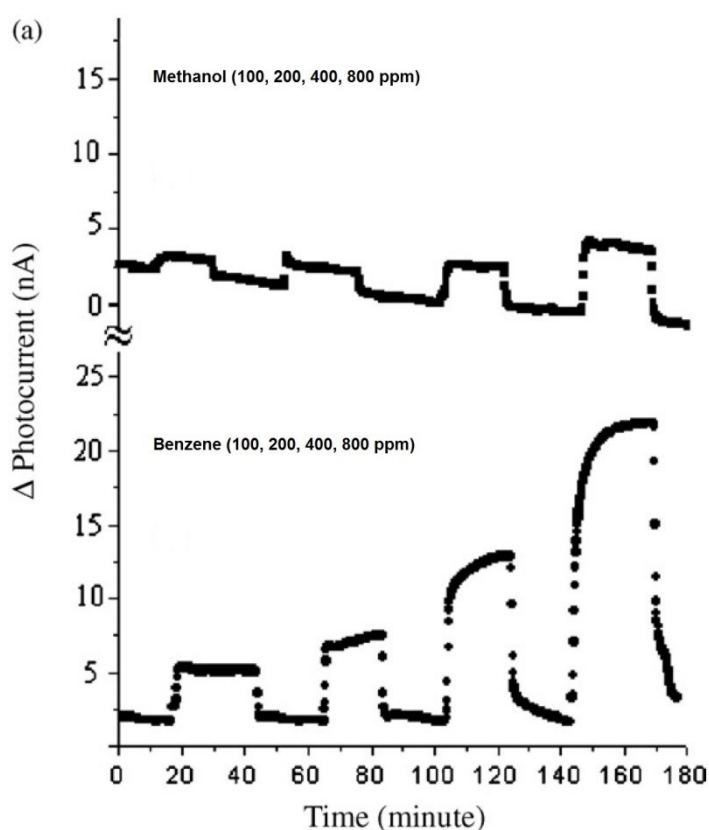
Figure 2.8. Response dynamic on exposure to increasing benzene, and methanol at 100, 200, 400 and 800 ppm of benzene–silica hybrid mesoporous [11].

50

2.3 Eni Carbon Silicates

The synthesis of aluminosilcate hybrids with organic groups fused within a crystalline framework is a daunting mission which has eluded many workers. Hybrids add variable chemical modification to the repertoire of zeolites, which are well established as heterogeneous catalysts, ion exchangers, and molecular sieves with many different pore architectures [27]. Such materials can combine the advantages of inorganic (thermal, mechanical and structural stability) and organic parts (possibility for functionalization and high flexibility).

ECSs (Eni Carbon Silicates) represet a new class of crystalline hybrid organic–inorganic. The novelty of these materials concerns their structures, crystalline aluminosilicate scaffoldings with long-range 3D order, which distinguishes them from the previously reported amorphous and ''crystallinelike'' silica-based PMOs (Periodic Mesoporous Organosilicas) [28-30]. ECS synthesis resembles that of PMOs, i.e., low crystllization temperature and sylated organic precursors as silica source, except that no surfactants are used and $NaAlO_2$ is the source of aluminium [27].

2.3.1 From zeolites to ECS

The increasing demand for materials with innovative properties has driven research to tailor their chemical and physical characteristics. Silicates and metal silicates are a group of compounds which can produce two- or three-dimensional crystalline structures, compact or porous (zeolites), lamellar (micas and clays) or linear. Amon these, zeolites and zeolite-like materials have been of great relevance in the evolution catalysts and in the separation of mixtures of different molecules; indeed they conjugate properties, such as ordered porous structure and active site environment geometry, which are typical of biological catalysts, with the robustness and the stability of inorganic materials. Zeolites, however, can be more than just aluminosilicates. Isomorphous substitution of Al and Si in the three dimensional lattice of tetrahedra by other tri- and tetravalent elements such as boron and heavier metals (e.g. iron, titanium and germanium) has extended the zeolite versatility to ever developing fields of application. Another important modification is the incorporation of organic functions within the zeolite framework because it would open up new opportunities for modulating hydrophilic/hydrophobic character useful for adsorption and catalysis. In addition, new functionalities and active sites would be useful, e.g., in acid/base catalysis. In order to improve the potentiality of zeolites, several years ago, different research groups began preparing hybrid organo–inorganic porous compounds [4]. Covalent organic incorporation in zeolites has been attempted, with varying success, since the beginning of the 1990s. Postsynthesis treatment of preformed aluminosilicates by grafting organosilanes of the general formula $R-Si(EtO)_3$, wherein R is an organic group capable of complexing transition metals, was scarcely successful [31]. It was found that the functionalization practically does not occur within the micropores but only in the mesopores and on the external surface. In fact, it is reported that the functionalization of ultra-stabilized Y zeolites, with organosilanes bearing metal complexes, occurred at the inter-crystalline mesoporous region. Others arrived at the same conclusion after functionalizing a series of Y zeolites with varying amounts of mesopores (generated by steaming) [32]. More interesting was the co-condensation approach, which provide organic functionalized molecular sieves (OFMSs) by replacing a part of the conventional silica source (e.g., TEOS) with an organosilane (e.g., phenethyltrimethoxysilane, aminopropyltrimethoxysilane, mercaptopropyltrimethoxysilane) in the reaction mixture. In this way, the group $(-O)_3Si$ is incorporated in the zeolitic framework, whereas the organic group is situated inside the zeolitic porous system. Although successful,

this protocol suffers from a severe drawback: it can be applied only for functionalizing zeolites, synthetized in the purely inorganic system (A, X, Y) or those (Beta) from which the organic directing agent (SDA) used for their crystallization needs be removed by chemical extraction and not by high-temperature thermal treatments which would otherwise also cause the destruction of the anchored organic group. As a matter of fact, all the work was done using zeolite Beta, from which the tetraethylammonium was removed by repeated treatments with acetic acid/water solutions [33, 34].

Hybrid zeolite-type materials can be prepared by pillaring with bridged silsesquioxanes to give so-called 2D zeolites [35] which form spontaneously during synthesis (for example MWW-type zeolites [36]), or by post-synthesis treatments of preformed 3D structures as in the case of germanosilicate UTL [37]. Two ways exist so far: in a case a MWW-type precursor was pillared with 1,4-bis-(triethoxysilyl)-benzene (BTEB) [38], and in the second a layered UTL-type phase was pillared with bridged silsesquioxanes of various complexity [39]. This approach is attractive because the porosity of the pillared materials can be tailored by selecting the type and amount of bridged silsesquioxanes used. Moreover, the organic groups of the pillars can be functionalized by post-synthesis treatments to produce bi-functional catalysts. These new materials could have very interesting properties, allowing the preparation of new functional active sites with tunable geometrical and chemical properties. In this regard, the first opportunity was offered by the discovery of an ordered mesoporous silica [40], which appeared to be an attractive substrate for anchoring organic groups to the inorganic backbone. These interesting results have stimulated the curiosity to explore the possibility of preparing truly crystalline hybrid silicates, since they would open the access to a new class of materials with a better defined geometry and improved stability.

There remains a final intriguing approach for synthesizing structured hybrid porous materials using bridged silsesquioxanes. In an early stage, the organic molecules were grafted to the silica network by direct and secondary syntheses. Several research groups have described the synthesis of known zeolites where a minor portion (25%) of the bridging oxygen atoms (Si–O–Si) were substituted by methylene groups (Si–CH_2–Si) into the framework using bis-(triethoxysilyl)-methane [$(RO)_3Si$–CH_2–$Si(OR)_3$] (BTEM) as a silica source [47-51]. Although these examples demonstrate the possibility of incorporating small organic moieties in the microporous silica framework, they should still be considered small variations of the parent-zeolites (LTA, MFI, ITQ-21, beta and X). Moreover, this substitution is feasible from an energetic point of view [52] and supported by physical–chemical observations, incorporation of the organic groups in the accompanying amorphous phase, rather than in the zeolite framework, cannot be ruled out [51]. More recently, organic functionalities were incorporated into the silica structure using bis-silylated organic precursors (1,4-bis-(triethoxysilyl)-benzene), to give the so called "periodic mesoporous organosilicas" (PMO's) [3, 6, 53]. Among this kind of organo-silicates, some PMO's with crystalline-like pores were described, starting from the pioneering work of Inagaki et al. who prepared a mesostructured material using BTEB in the presence of a surfactant, octadecyltrimethylammonium chloride, NaOH and water, under hydrothermal conditions at temperatures close to 100°C [8]. The solid thus obtained is characterized by a system of mesopores with regular dimensions organized according to a regular two-dimensional hexagonal pattern, analogous to that found in the well-known aluminosilicates or silicons called MCM-41. Unlike these, charcterized by completely amorphous walls, PMO shows a regular alternation of organic and inorganic regions with a spacing of ca. 7.6 Å along the direction of the channels, corresponding to the length of the bridged silsesquioxane moiety, [38] This feature is common to all PMOs, which cannot be considered as truly crystalline phases, lacking in all cases 3D order.

Careful inspection of the structural models reported for PMOs reveals that the condensation of bridged silsesquioxanes inevitably leads to the formation of compact structures. This was recently demonstrated for the sole crystalline hybrid silicate reported so far, obtained from the bis-silylated anthracenyl precursor.

In the exploratory syntheses of hybrid organic–inorganic aluminosilicates, Eni research group was able to obtain several new crystalline phases referred to as ECS (Eni Carbon Silicate) in which all the silicon atoms are covalently bonded to carbon atoms. ECS phases, constituting a new class of crystalline organic–inorganic hybrid materials, have been synthesized for the first time and deeply characterized. New materials, having every silicon involved in one Si-C bond, have been obtained by using different bis-silylated organic precursors as silica source, without templates or surfactant agent. The presence of aluminum plays a relevant role favoring the crystallization of ECS's. Until now, several ECS powders have been synthetized and they show high surface area consistent with a porous architecture.

Therefore, one can conclude that an additional component, the simplest being a tetrahedron (e.g., $[SiO_4]$ or $[AlO_4]$) is required for preparing porous crystalline structures that furnishes a (intra-layer) spacer between $[CSiO_3]$ tetrahedra. In fact, the addition of $NaAlO_2$ to the reaction mixture gave a new family of crystalline microporous hybrid organic–inorganic aluminosilicates, with integral Si–C bonds and, as expected, $[AlO_4]$ tetrahedra acting as spacers among the $[CSiO_3]$ groups [28].

2.3.2 ECS synthesis

2.3.2.1 Origins and development

The possibility of preparing crystalline hybrid silicates was explored by starting from the synthesis procedure described by Inagaki et al. [8], trying to understand the role of the surfactant and the organo-silica source (BTEB) in the formation of the structure. Hybrid mesoporous silicates were synthetized by adding 1,4-bis(triethoxysilyl)benzene to an acqueous solution containing octadecyltrimethylammonium chloride, as surfactant, and soda. The materials obtained with this process have hexagonal pore distribution with a constant lattice of 52.5 Å and walls which delimit the pores with a structural periodicity equal to 7.6 Å along the direction of the channels (see Figure 2.6). The X-ray powder diffraction patterns in Figure 2.9, both in presence of surfactant and not, show three reflections at low angular values ($2\theta < 4.0°$), with $2\theta = 1.94°, 3.40°, 3.48°$, corresponding to distances between planes $d = 45.5, 26.0, 22.9$ Å and four reflections in the region $10° < 2\theta < 50°$, with $2\theta = 11.64°$, $23.40°, 35.92°, 47.87°$ corresponding to $d = 7.6, 3.8, 2.5$ and 1.9 Å. A further reflection was localized at about $20.5°$ of 2θ, but it was large and badly defined.

The role of the surfactant was the ordering the channel's array, while BTEB was the only responsible for the long range order within the pore walls [28, 58]. In fact, in absence of surfactant it was possible to obtain a material (ECS-4) having an X-ray powder diffraction pattern similar to that reported by Inagaki et al., but without any peak at very low 2θ angles, as reported in Figure 2.10 [28].

Explorative syntheses performed by using BTEB and by adding an aluminum source led to the crystallization of a new material named ECS-1. The XRD pattern is clearly different with respect to those characterizing the previously described materials (Figure 2.10). ECS organic-inorganic hybrid silicates, obtained starting from this synthesis process, were characterized by an X-ray diffraction patterns with reflection exclusively at angular values higher than $4.7°$ of 2θ. From this result the investigation was expanded by changing the

synthesis parameters. In particular, with BTEB other two new ECS phases (ECS-2 and ECS-3) were synthesized by subtle variations of the Si/Al molar ratio or upon replacing NaOH by KOH in the reactant mixture. Furthermore, other three crystalline phases were obtained using BTEBP (ECS-5), BTEEB (ECS-6) and BTMP (ECS-7) as silica sources. The following conditions are particularly preferred to obtain crystalline organo alumino-silicates: (i) relatively low Si/Al molar ratio (<10), (ii) alkali metal ions (Na and/or K), (iii) concentrated gels (optimal H_2O/Si molar ratio = 11), and (iv) low crystallization temperature (<140 °C). These phases were extensively characterized in order to assess the integrity of the bis-silylated organic moieties, evaluate their porous properties, determine their structural characteristics and assess their thermal behavior [28].

Laboratory XRD patterns of the ECS phases are reported in Figure 2.9 and show that all the phases synthesized in the presence of aluminum are crystalline with distinctive XRD patterns. As already mentioned, only ECS-4, synthesized from BTEB without $NaAlO_2$, shows an XRD pattern similar to that of the PMO phase described by Inagaki et al. [8], but without any reflections in the low-angle region.
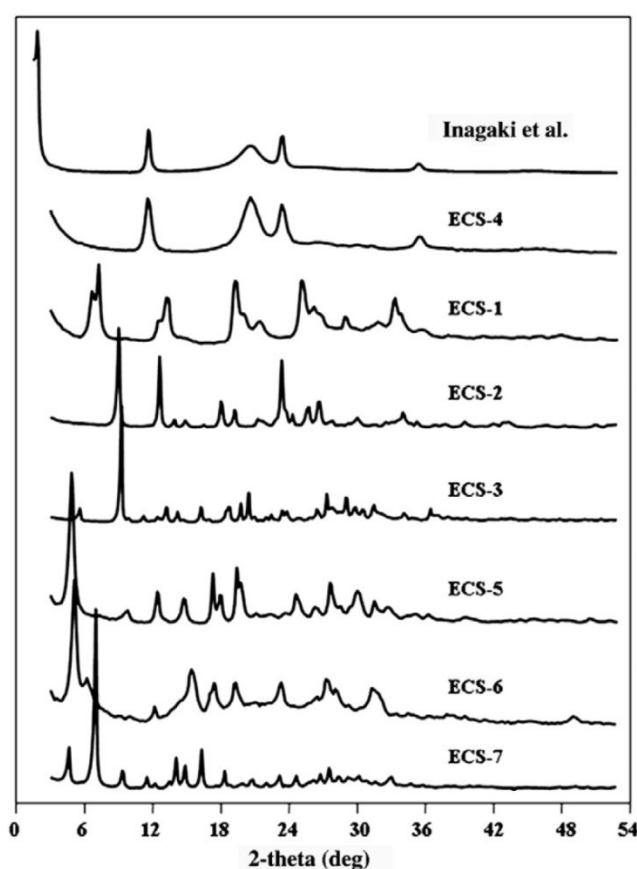
Figure 2.9. Laboratory X-ray powder diffraction patterns of the ECS's compared with the PMO of Inagaki et al. [28].

More precisely, ECS-4 exhibits the same structural periodicity, but without any ordering of the pores. Therefore, this material cannot be considered strictu sensu crystalline, and the lack of three-dimensional order for the structure should be a consequence of the absence of Al in the synthesis. In fact, three crystalline phases (ECS-1, ECS-2 and ECS-3) were synthesized using BTEB when $NaAlO_2$ was present.

^{29}Si and ^{13}C MAS NMR analyses confirm that in all cases the bis-silylated organic groups maintain their integrities[3]. In fact, ^{29}Si MAS NMR spectra (Figure 2.10 a) display resonances with chemical shifts in the -45 to -85 ppm range. This chemical shift is attributed to silicon atoms exhibiting one C–Si bond and is well separated from the shift range for "Q tetrahedra" in zeolites with variable Al contents (-90 to -120 ppm). Only a low signal at -93 ppm chemical shift is observed for ECS-2, attributed to sodalite impurity by XRD analysis. ^{27}Al MAS NMR spectra reveal that all the hybrid materials contain mainly four-coordinate aluminum sites (Figure 2.10 b); signals near 50 and 0 ppm are assigned to AlO_4 and AlO_6 sites, respectively [28].
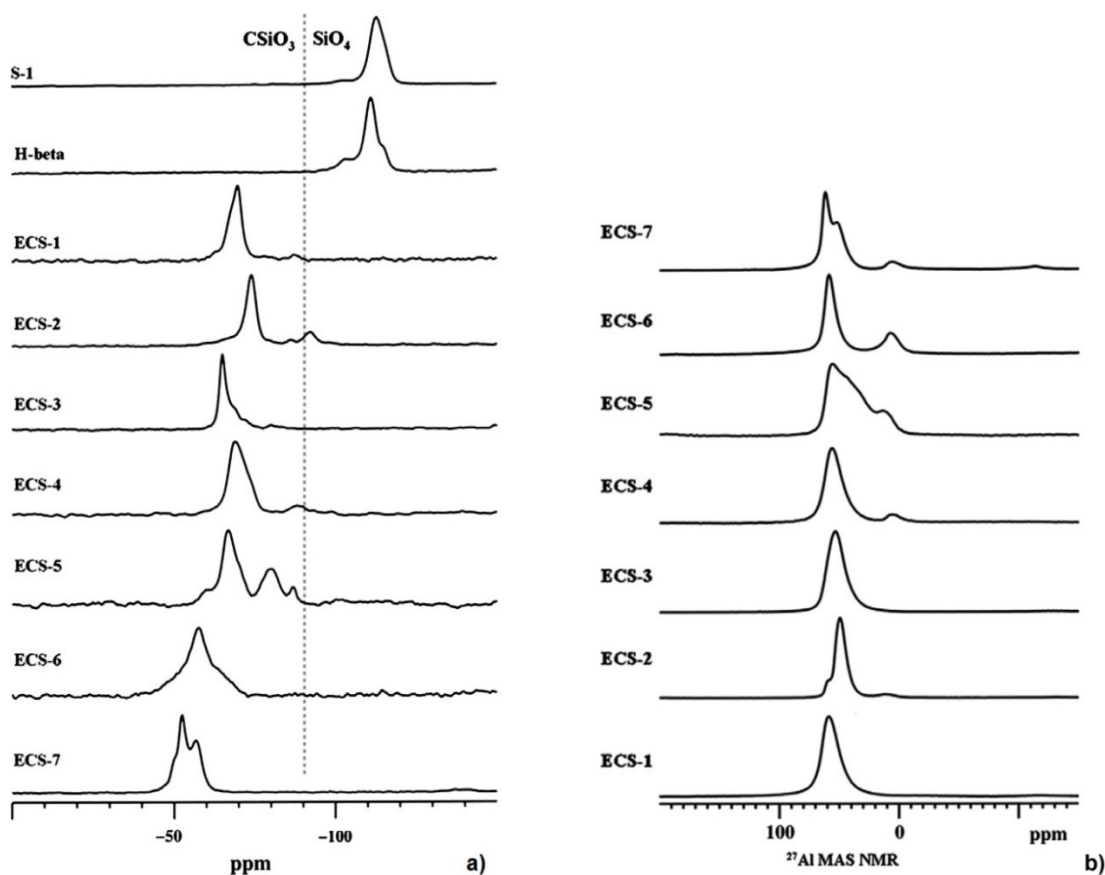
Figure 2.10. a) ^{29}Si-MAS-NMR spectra of the ECS's compared with those of highly siliceous silicate-1 and H-beta (Si/Al=12), and b) ^{27}Al-MAS-NMR spectra of ECS's. [28].

2.3.2.2 Final ECS synthesis process

Eni Carbon Silicates, characterized by a three-dimensional crystalline structure in which the disilane is integrally incorporated, were obtained by hydrothermal treatment, at relatively low temperatures and lengthy times, of a reaction mixture containing the disilane, sodium aluminate ($NaAlO_2$), NaOH and/or KOH and demineralized water [55]. The process for preparing the hybrid silicates and metal-silicates described in patents [55, 56] comprises:

1) adding a disilane having formula

$$X_3Si\text{-}R\text{-}SiX_3$$

---

[3] ^{29}Si and ^{13}C MAS NMR analyses allow to reveal the presence of Si-C bonds. It is known that in ^{29}Si-MAS-NMR spectroscopy, the chemical shift of sites of the $Si(OT)_{4-x}(OH)_x$ type, where $T=Si$ or Al and x ranges from 0 to 3, is within the range of -90 and -120 ppm [42], whereas the chemical shift of sites of the $C\text{-}Si(OT)_{3-x}(OH)_x$ type, where x ranges from 0 to 2, i.e. silicon atoms bound to a carbon atom, is lower, in absolute value, than -90 ppm, ranges, for example, from -50 and -90 ppm [8, 39].

wherein R is an organic group[4] with a number of carbon atoms lower or equal to 20, and X is a substituent which can be hydrolyzed, to an acqueous mixture containig at least one hydroxide of at least one metal cation Me selected from alkaline and/or alkaline-earth metals, and possibly one or more sources of one or more elements T selected from elements belonging to groups IIIB, IVB, VB, and transition metals, with a molar ratio Si/(Si + T) in said structure higher or equal than 0.5 and lower than 1;

2) maintaining the mixture under hydrothermal conditions, at autogenous pressure, for a time sufficient for forming a solid material;
3) recovering the solid and drying it.

The hybrid silicates and metal-silicates are characterized by the following formula:

$$SiO_{1.5} \cdot x\, TO_2 \cdot y/n\, Me \cdot z\, C$$
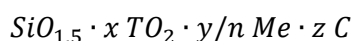
wherein Si is the silicon contained in the structural unit, T is at least one element selected from elements belonging to groups IIIB, IVB, VB, and transition metals, Me is at least one cation of having a valence n, C is carbon, x ranges from 0 to 1, y ranges from 0 to 1, z ranges between 0.5 and 10.

Two aspects influence this apparently simple synthesis procedure. The first is related to the crystallization temperature, kept constant at 100 °C. This temperature is a compromise between that need to have a sufficiently high crystallization rate (at 80–90 °C the crystallization is very slow or does not take place at all) and that causing Si–C bond hydrolysis. Indeed, excessively low temperatures are unfavorable for the hydrolysis, but also slow down the condensation reaction of the disilane molecules jeopardizing the crystallization of some ECS phases. Beside, increasing the temperature above 100 °C the hydrolysis reaction is accelerated and under strongly basic conditions favors Si–C bond rupture, leading to the formation of [SiO$_4$] tetrahedra in a solution with high concentrations of Al and alkali metal ions, ideal conditions for crystallizing inorganic low-silica zeolites (e.g. sodalite, analcime, cancrinite), which can therefor and lower than e become prevalent product [28, 34, 57]. The second more critical aspect concerns the poor water solubility of the organosilane precursors (which become water soluble after hydrolysis of the alkoxy groups). To facilitate basic conditions for the organosilane, the surface contact between the two phases was maximized by accurately mixing them and performing the hydrothermal treatment in oscillating autoclaves. Precursor alkoxy hydrolysis is then the rate determining step with very long crystallization times (weeks). In any case, careful preparation of the reagent mixtures and controlled crystallization conditions gave reproducibly well-crystallized ECS phases with only trace amounts (if any) of non-hybrid zeolites. When the syntheses are performed in the presence of the bridged silsesquioxane and NaAlO$_2$ only, ECS materials were obtained with low Si/Al molar ratios (1.33–2.00). Although not fully explored yet, the decrease of the trivalent metal content was found possible but rather difficult. For instance, syntheses conducted with a second conventional source of silica (TEOS) led to the formation of phases similar to those reported by Okamoto et al. [58] and successively by us (ECS-4) [28], using the synthesis procedure for PMO's [8] without surfactants. Likely, these results are due to the higher rate of hydrolysis of TEOS with respect to the disilane precursors, resulting in polymerization and segregation of the inorganic component. Because of the

---

[4] The hydrocarbon group is an aliphatic or aromatic group, possibly substituted with groups containing heteroatoms. The aliphatic groups are linear or branched, saturated or unsaturated. R is selected from le following groups: -CH$_2$-, -CH$_2$CH$_2$-, linear or branched –C$_3$H$_6$-, linear or branched –C$_4$H$_8$-, -C$_6$H$_4$-, -CH$_2$-(C$_6$H$_4$)-CH$_2$, -C$_2$H$_4$-(C$_6$H$_4$)-C$_2$H$_4$-C$_2$H$_4$-, -CH=CH-, -CH=CH-CH$_2$-, CH$_2$-CH=CH-CH$_2$-.

difficulties associated with the use of a conventional source of silica, the replacement of Al with B, a well-known approach in the field of zeolites, will be discussed in the following section [34].

2.3.2.3 The role of boric acid

The experimental evidences highlight the positive effects on the crystallization of ECS phases resulting from the addition of boric acid in the reaction mixture. In particular, ECS are obtained containing boron in a mixture with one or more elements T different from boron, selected from elements of groups IIIB, IVB, VB, and transition metals, and among these, also new ECS phases.

Then, in this case ECS silicates and metal-silicates are characterized by the following formula:

$$SiO_{1.5} \cdot x\,YO_2 \cdot y/n\,Me \cdot z\,C$$
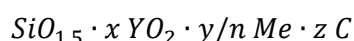
wherein *Si* is the silicon contained in the structural unit, *Y* is boron at least one element *T* selected from elements belonging to groups IIIB, IVB, VB, and transition metals, *Me* is at least one cation of having a valence *n*, *C* is carbon, *x* ranges from 0 to 1, *y* ranges from 0 to 1, *z* ranges between 0.5 and 10.

In all the silicates and metal-silicates obtained with the process described above, the molar ratio *T/B* is preferably greater than 0 and less 10, and even more preferably varies within the range of 5-10. If there are more elements *T*, said molar ratio *T/B* corresponds to the ratio between the sum of the moles of said elements *T* and the moles of *B* [58].

Although present in high amounts in the reaction mixtures (SiO_2/B_2O_3 = 2.30–4.60) only traces of B were detected in the products (SiO_2/B_2O_3 = 40–100) and, most importantly, it can be removed from the samples by mild washing with diluted NaOH solution without appreciably affecting crystallinity. This means that it is very likely that B did substitute a small fraction of Al in the inorganic fraction of the structure of ECS's, even though it cannot be excluded that part of the B is adsorbed on the external surface of the crystals and/or of the amorphous phase present in small amounts in the samples. Nevertheless, its presence is crucial because it significantly accelerates the crystallization rate of the various ECS materials, improving at the same time their crystallinity and phase purity compared to the analogous phases prepared without H_3BO_3. These evidences likely indicate that boric acid has a catalytic role in the crystallization of ECS's and some recent papers may suggest possible explanations. In particular, the addition of H_3BO_3 was reported to have such a role (a) in the self-organization of silica producing mesoporous materials whose morphology depends on the synthesis conditions [64] and (b) in the organization of bridged silsesquioxanes (1,4-bis-(triethoxysilyl)-benzene and 2,5-bis-(triethoxysilyl)-thiophene) in PMO's prepared in the presence of non-ionic surfactants (e.g. Pluronic P123, PLGE) [64, 65]. In all cases, the syntheses were performed under mild acidic conditions while the crystallization of ECS's occurs without the use of surfactants and under strong basic conditions in which borate anions, $[B(OH)_4]^-$, are mostly present. To account for the increase of the crystallization rate of ECS's, therefore, it is necessary to consider that the reaction mixture is composed by an emulsion of bis-silylated organic precursor in water and that the rate determining step of the reaction is probably given by the hydrolysis of the Si–OR groups and the transport of the hydrolyzed moieties in water solution, where the crystallization takes place. Therefore, it is likely that the role of borate ions is to promote these fundamental steps of the reaction, by binding to the molecules present on the surface of the droplets and thus

favoring their transport in aqueous solution, where they can be easily hydrolyzed and made available for the crystallization of the ECS phases [34].

The diffractograms of ECS 13 and 14 in presence and in absence of boric acid within the synthesis process are shown below in Figure 2.11 and 2.12. The ECS 13 X-ray powder pattern indicated with line A in Figure 2.11, reveals the formation of extremely crystalline ECS 13 prepared by adding 0.70 g of H_3BO_3, whereas the diffractograms indicated with lines B and C, relating to the sample obtained without boric acid heated for 7 and 14 days, respectively show that for low crystallization times the ECS 13 phase is accompanied by significant quantities of amorphous phase and reflections with a significantly greater width than those present in the sample prepared in the presence of boric acid.
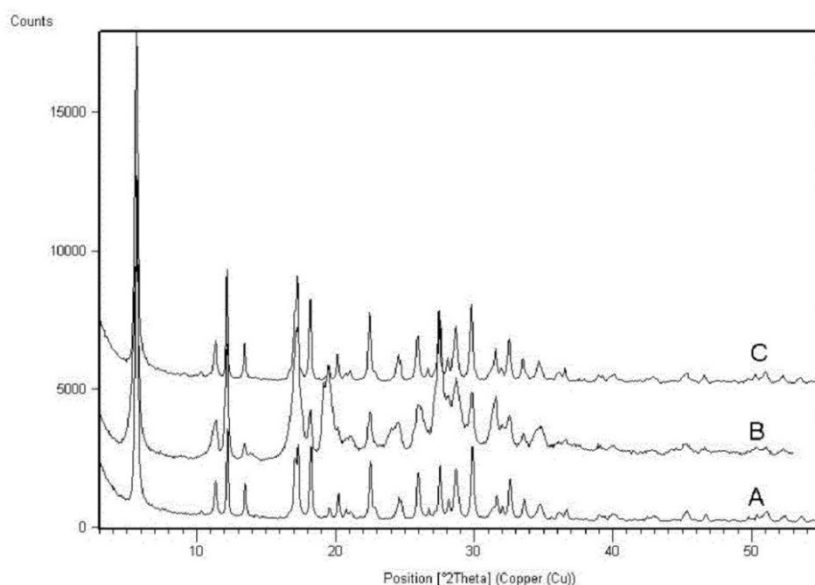
Figure 2.11. X-ray powder diffraction patterns for ECS 13 A) in presence of boric acid, B) without boric acid and heated to 100°C for 7 days, and C) without boric acid and heated to 100°C for 14 days [57].

This indicates the reduced dimension of the crystals and/or their extremely defective nature. An ECS13 having a quality comparable, in terms of crystallinity and sizes of the crystals, to that obtained with boric acid, is only obtained after 14 days of crystallization, a much longer time with respect to the 5 days necessary for crystallization in the presence of boric acid.
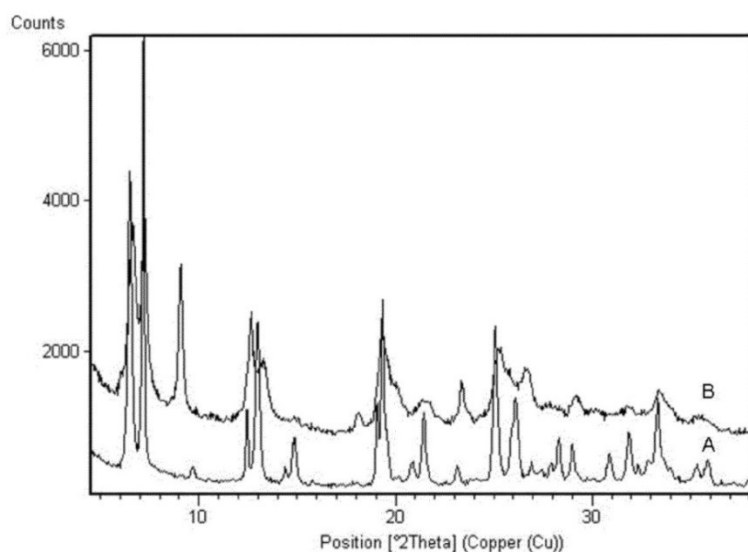
Figure 2.12. X-ray powder diffraction patterns for ECS 14 A) in presence of boric acid, and B) without boric acid [57].

The ECS 14 X-ray powder pattern indicated with line A in Figure 2.12, reveals the formation of well-crystallized ECS 14 prepared by adding 1.32 g of H_3BO_3, whereas the diffractogram indicated with lines B, shows that the product is only partially crystallized and that the non-identified crystalline phase only incidentally present have reflections coinciding with or close to those present in the XRD spectrum of ECS 14 phase [67].

Finally, ^{29}Si-MAS-NMR analysis of the hybrid matal-silicates ECS 13, prepared from 2,6-bis-(triethoxysilyl)naphthalene, and ECS 14, prepared from 1,4-bis-(triethoxysilyi)benzene, containig boric acid allows the presence of Si-C bonds to be revealed, in particular show signals whose chemical shift drops to absolute values lower than -90 ppm, in particular from -40 to -90 ppm [34, 57].

2.3.2.4 Thermal behaviour

Obviously, the high organic content of ECS's makes them less thermally stable than classical inorganic zeolites. As a consequence, analogously to other microporous materials such as zeolites [43], understanding the thermal behaviour of ECS's structure is of crucial importance for applying them as catalysts or for producing thin films for applications in gas sensing and light harvesting [44]. In fact, the unstable organic moieties can lead to structural collapse or breakdown which compromises shape-selective catalytic processes. In addition, the low Si/Al molar ratios of ECS's, with the required high amounts of extra-framework cations [6, 11, 12], could compromise the structural stability. A parallel can be made with zeolites, where a high Si/Al molar ratio affords greater thermally stable than their low-silica counterparts [43]. In this context, zeolite beta is one of the most representative examples. Commercial zeolite beta (Si/Al = 13) is reportedly stable up to 750 °C with structural breakdown at 850 °C [45], while its monoclinicdominant natural counterpart tschernichite (Si/Al = 2.5) under-goes structural breakdown with complete amorphitization at 350 °C [13, 46].

The TG analysis carried out with the samples described above showed a weight loss at low temperature (T < 350 °C), associated to the elimination of residual solvent adsorbed on the surface and in the pores, followed by a second significant loss due to the decomposition of the organic groups (Figure 2.13). The later occurs above 350 °C, the onset of the decomposition being dependent on the nature of the organic group as well as on the overall composition of the framework [28].
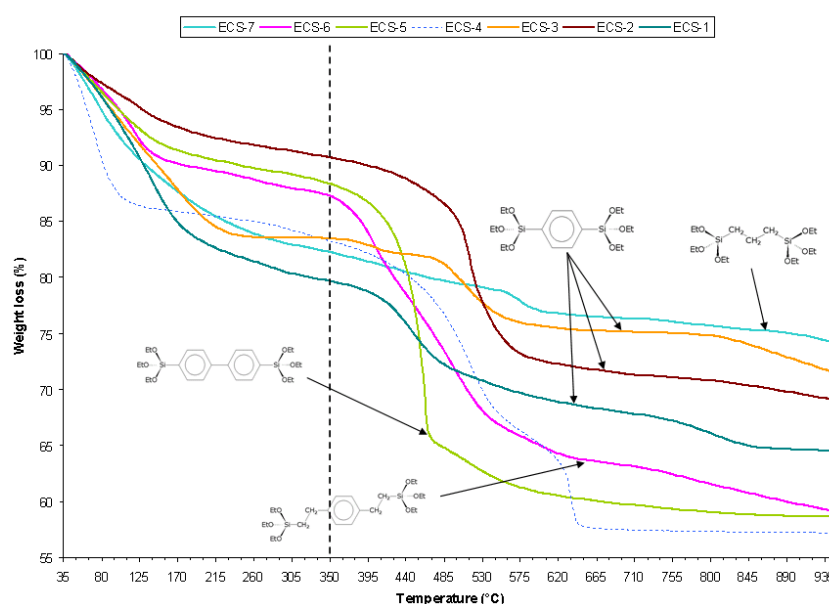
Figure 2.13. Thermal curves for some ECSs powders [image provided by Eni].

The deepened TG-MS analysis of ECS-3 could be representative with respect to the thermal behavior of Eni Carbon Silicates. TG-MS in Figure 2.14 showed three different weight loss events [13]. In the DTA curve, the first weight loss (15.8 wt.%) was accompanied by a slightly endothermic very broad peak, associated with the elimination of water molecules from the ECS-3 porosity, as clearly indicated by the masses detected during heating (Figure 2.15). The second weight loss was accompanied by two exothermic peaks, near 360 and 430 °C, the latter being sharp and very strong. These features are associated with atomic masses of 18, 44 and 78. structural degradation occurred by: (i) combustion of the organic moiety (18 = H2O, 44 = CO2), supported by consumption of molecular oxygen (amu 32) (Figure 2.14); (ii) elimination of integral benzene molecules (amu 78). The third weight loss which occurred at high temperature (over 700 °C) likely involved the decomposition of compounds (e.g. coke, Na/K carbonates) formed during the earlier thermal event. In conclusion, thermal analysis guided the selection of temperatures for in situ XRD and revealed that most of the adsorbed water was lost at 250 °C.

ECS-3 maintained a high degree of crystallinity up to 150 °C, as found by in situ X-ray powder diffraction analysis in air. At this temperature, 37 wt.% of the initial water molecules were still trapped in the ECS-3 porosity and the unit cell volume was smaller by only about 3.8%. At 200 °C the long-range structural order was dramatically affected, while short-range order was not. The large loss in XRD pattern quality was consistent with a structural collapse.
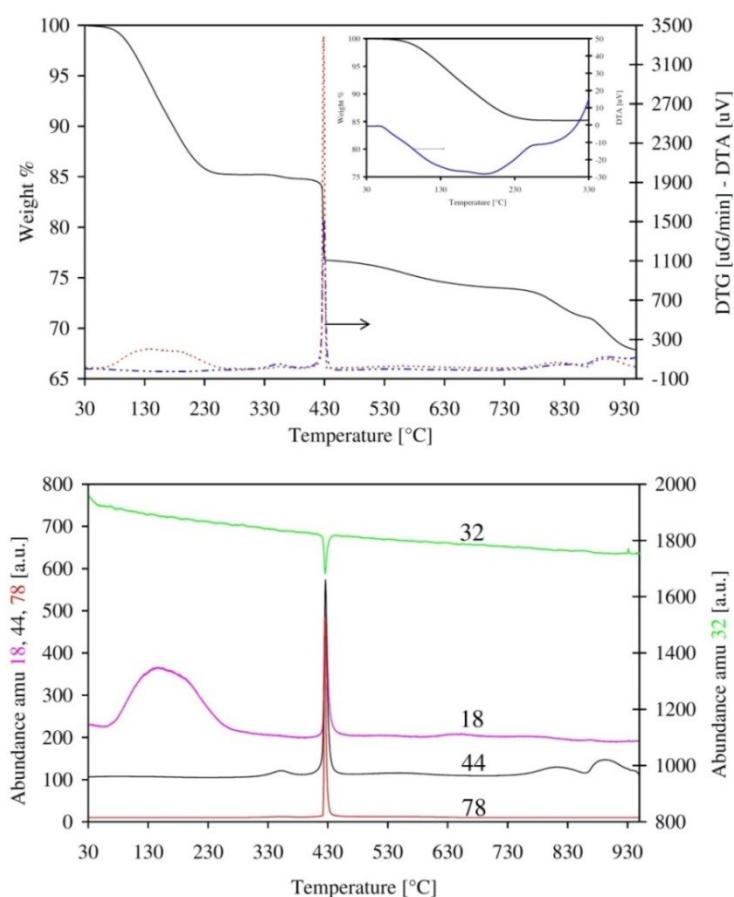
Figure 2.14. Thermal curves (above) and individual mass patterns (below) for ECS-3. Above: TG, DTG, and DTA curves. The inset shows the portion of the thermal curve between 30 and 330 °C evidencing the endothermic peak related to the water molecules escape from the ECS-3 porosity. Below: patterns for masses 18 (H_2O), 32 (O_2), 44 (CO_2) and 78 (benzene) detected during the heating ramp [29].

Structural collapse of ECS-3 at 200 °C (in air) was associated with a large decrease in the textural properties (and specific surface area). The reason for this is uncertain. It is

suggested that this mainly results from a change in the position of the pendant phenyl group, formed via one-sided Si–C cleavage, which blocks the aperture of the sinusoidal channel's pore mouth. The mechanism proposed for Si–C rupture involves an initial proton transfer from nearby water molecules to the phenylene bridging groups with formation of Q3 Si and Si-phenyl groups. This hypothesis is supported by the N_2 adsorption/desorption measurement after degassing the sample at 200 °C in vacuum. In this case, ECS-3 maintains its crystal structure and textural properties. This indicates that removal of water molecules increases the ECS-3thermal stability.
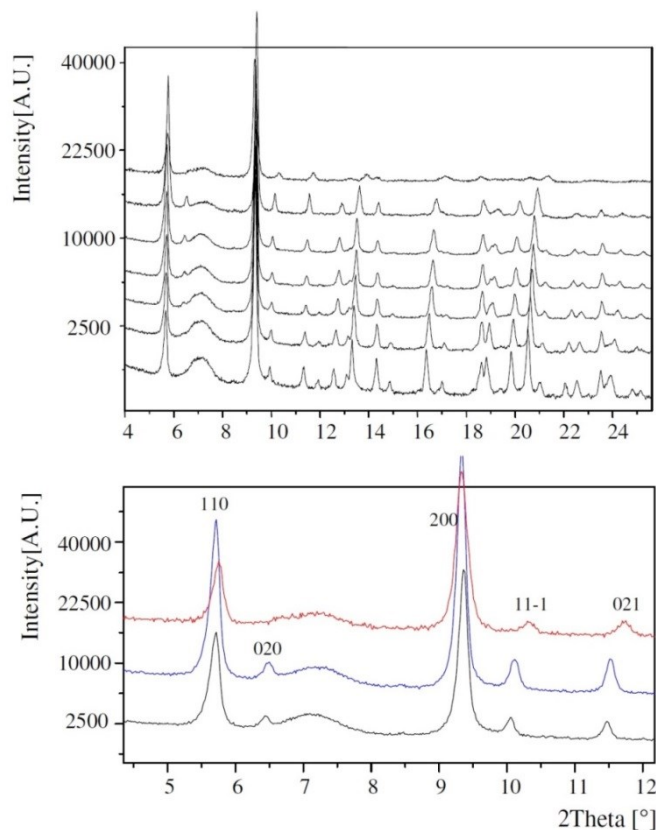
Figure 2.15. Above: comparison of ECS-3 powder diffraction patterns at (from bottom) room temperature, 50, 75, 100, 125, 150 and 200 °C. Below: portion of the pattern of ECS-3 at 125 (bottom), 150 (middle) and 200 °C (top) along with the indexes of the main reflections [29].

2.3.3 ECS family

At present the ECS family of materials consists of some 20 different phases obtained by varying the nature of the bridging organic group, the alkali metal ion and the synthesis conditions. Crystal structures were determined for several hybrids. In particular, ECS-2, ECS-3 and ECS-17 synthesized with BTEB possess 3D ordered structures with stacks of aluminosilicate layers covalently bonded to each other by phenylene rings. The aluminosilicate layers consist of [AlO$_4$] tetrahedra bound to four different [CSiO$_3$] tetrahedra, confirming that they act as spacers between the silsesquioxane units and give low density structures with different pore systems [27, 28, 69]. When the syntheses are performed in the presence of the bridged silsesquioxane and NaAlO, ECS materials crystallize as aluminosilicates with low Si/Al atomic ratios (1.33 in ECS-3 and 2.00 in ECS-2 and ECS-17). Attempts to decrease the Al content inthe structure by adding a conventional silica source (TEOS) is possible, provided that opportune measures are taken for compensating the mismatch between the rates of hydrolysis of the two silica sources. On the other hand, quite interesting results were obtained when attempting to substitute (at least partially) Al by B, in

analogy with what is usually done in zeolites. The complete replacement of $NaAlO_2$ by H_3BO_3 led to the formation of partially ordered phases, such as ECS-4 with BTEB, while equimolar amounts of the two sources in the reaction mixture (with BTEB and NaOH) gave ECS-14 [67]. The structure of ECS-14 resembles that of AlPO-5, a microporous aluminophosphate with the AFI framework type, characterized by a 12MR linear channel system running parallel to [001].44 This encouraging result prompted to continue using boric acid for synthesizing new ECS's and to improve the crystallization of known phases [69, 70].

References

[1] Hoffmann F. , Fröba M., in The Supramolecular Chemistry of Organic-Inorganic Hybrid Materials, editors K. Rurack and R. Martinez-Manez, 2010 John Wiley & Sons, 39-111

[2] Kickelbick G., Hybrid Materials. Synthesis, Characterization, and Applications, 2007 Wiley-VCH Verlag GmbH & Co. KGaA, Weinheim, ISBN: 978-3-527-31299-3

[3] Hoffmann F., Cornelius M., Morel J., Fröba M., Silica-Based Mesoporous Organic–Inorganic Hybrid Materials, Angewandte Chemie Int. Ed. 45 (2006), 3216–3251

[4] Čejka J., Corma A., Zones S., Zeolites and Catalysis, Synthesis, Reactions and Applications, 2010 Wiley-VCH Verlag GmbH & Co. KGaA, Weinheim, ISBN: 978-3-527-32514-6

[5] Mizoshita N., Tani T., Inagaki S., Syntheses, properties and applications of periodic mesoporous organosilicas prepared from bridged organosilane precursors, Chemical Society Review, 40 (2011), 789–800

[6] Hoffmann F. , Fröba M., Vitalising porous inorganic silica networks with organic functions—PMOs and related hybrid materials, Chemical Society Review, 40 (2011), 608–620

[7] Mehdi A., Reye C., Corriu R., From molecular chemistry to hybrid nanomaterials. Design and Functionalization, Chemical Society Review, 40 (2011), 563–574

[8] Inagaki S., Guan S., Ohsuna T., Terasaki O., An orderedmesoporous organosilica hybrid material with a crystal-like wall structure, Nature, 416 (2002), 304-307

[9] Melde B. J., Johnson B. J., Charles P. T., Mesoporous Silicate Materials in Sensing, Sensors, 8 (2008), 5202-5228

[10] Férey G., Serre C., Devic T., Maurin G., Jobic H., Llewellyn P. L., De Weireld G., Vimont A., Daturif M., Changg J., Why hybrid porous solids capture greenhouse gases?, Chemical Society Review, 40 (2011), 550–562

[11] Yuliarto B., Kumai Y., Inagaki S., Zhou H., Enhanced benzene selectivity of mesoporous silica SPV sensors by incorporating phenylene groups in the silica framework, Sensors and Actuators B 138 (2009) 417–421

[12] Mizoshita N., Goto Y., Maegawa Y., Tani T., Inagaki S., Tetraphenylpyrene-Bridged Periodic Mesostructured Organosilica Films with Efficient Visible-Light Emission, Chemistry of Materials 22 (2010) 2548–2554

[13] Maegawa Y., Mizoshita N., Tani T., Inagaki S., Transparent and visible-light harvesting acridone-bridged mesostructured organosilica film, Journal of Materials Chemistry, 20 (2010) 4399–4403

[14] Goto Y., Mizoshita N., Ohtani O., Okada T., Shimada T., Tani T., Inagaki S., Synthesis of Mesoporous Aromatic Silica Thin Films and Their Optical Properties, Chemistry of Materials 20 (2008) 4495–4498

[15] Scott. B.J., Wirnsberger G., Stucky G. D., Mesoporous and mesostrucutred materials for optical applications, Chemistry of Materials 13 (2001) 3140-3150

[15] Mizoshita N., Yamanaka K., Hiroto S., Shinokubo H., Tani T., Inagaki S., Energy and Electron Transfer from Fluorescent Mesostructured Organosilica Framework to Guest Dyes, Langmuir 28 (2012) 3987−3994

[16] Alvaro M., Benıtez M., Cabeza J. F., Garcıa H., Leyva A., Electrochemiluminescence of a Periodic Mesoporous Organosilica Containing 9,10-Diarylanthracene Units, Journal of Physical Chemistry C 111 (2007) 7532-7538

[17] Mizoshita N., Ikai M., Tani T., Inagaki S., Hole-Transporting Periodic Mesostructured Organosilica, Journal of American Chemistry Society 131 (2009) 14225–14227

[18] Yuliarto B., Zhou H.S., Yamada T., Honma I., Asai K., Preparation of tin modified silica mesoporous films, Stud. Surf. Sci. Catal. 146 (2003) 81–84

[19] Zhao X.S., (Max) Lu G.Q., Millar G.J., Advances in mesoporous molecular sieve MCM-41, Ind. Eng. Chem. Res. 35 (1996) 2075–2090

[20] Nguyen S.V., Szabo V., Trong On D., Kaliaguine S., Mesoporous silica supported $LaCoO_3$ perovskites as catalysts for methane oxidation, Microporous Mesoporous Mater. 54 (2002) 51–61

[21] Nam K.H., Tavlarides L.L., Synthesis of a high-density phosphonic acid functional mesoporous adsorbent: application to chromium(III) removal, Chem. Mater. 17 (2005) 1597–1604

[22] Li G., Kawi S., MCM-41 modified SnO_2 gas sensors: sensitivity and selectivity properties, Sens. Actuators B 59 (1999) 1–8

[23] Innocenzi P., Martucci A., Guglielmi M., Bearzotti A., Traversa E., J.C. Pivin, Mesoporous silica thin films for alcohol sensors, J. Eur. Ceram. Soc. 21 (2001) 1985–1988

[24] Zhou H.S., Yamada T., Asai K., Honma I., Uchida H., Katsube T., NO gas sensor based on surface photovoltage system fabricated by self-ordered hexagonal mesoporous silicate film, Jpn. J. Appl. Phys. 40 (2001) 7098–7102

[25] Yamada T., Zhou H.S., Uchida H., Tomita M., Ueno Y., Honma I., Asai K., Katsube T., Application of a cubic-likemesoporous silica film to a surface photovoltage gas sensing system, Microporous Mesoporous Mater. 54 (2002) 269–276

[26] Shimizu Y., Hyodo T., Egashira M., Mesoporous semiconducting oxides for gas sensor application, J. Eur. Ceram. Soc. 24 (2004) 1389–1398

[27] Bellussi G., Montanari E., Di Paola E., Millini R., Carati A., Rizzo C., Parker Jr W.O., Gemmi M., Mugnaioli E., Kolb U., Zanardi S., ECS-3: A Crystalline Hybrid Organic–Inorganic Aluminosilicate with Open Porosity, Angewandte Chem. Int. Ed. 51 (2012) 666-669

[28] Bellussi G., Carati A., Di Paola E., Millini R., Parker Jr. W. O., Rizzo C., Zanardi S., Crystalline hybrid organic-inorganic alumino-silicates, Microporous and Mesoporous Materials 113 (2008) 252-260

[29] Zanardi S., Parker Jr. W. O., Carati A., Botti G., Montanari E., On the thermal behaviour of the crystalline hybrid organic-inorganic aluminosilicate ECS-3, Microporous and Mesoporous Materials 172 (2013) 200-205

[30] Zanardi S., Bellussi G., Carati A., Di Paola E., Millini R., Parker Jr. W. O., Rizzo C., On the crystal structure solution and characterization of ECS-2, a novel microporous hybrid organic-inorganic material, Studies in Surface Science and Catalysis 174 (2008) 965–968

[31] Corma A., Iglesias M., del Pino C. , Sánchez F., New rhodium complexes anchored on modified USY zeolites. A remarkable effect of the support on the enantioselectivity of catalytic hydrogenation of prochiral alkenes, Journal of Chemical Society, Chemical Communication, (1991) 1253-1255

[32] Cauvel A., Brunel D., Di Renzo F., Moreau P., Fajula F., Functionalization of Y zeolites with organosilane reagents, Studies in Surface Science and Catalysis, 94 (1994), 286

[33] Jones C.W., Tsuji K., Davis M. E.. "Organic-Functionalized Molecular Sieves as Shape-Selective Catalysts." Nature 393 (1998) 52-54

[34] Zanardi S., Bellussi G., Parker Jr. W. O., Montanari E., Bellettato M., Cruciani G., Carati A., Guidetti S., Rizzo C., Millini R., The role of boric acid in the synthesis of Eni Carbon Silicates, Dalton Trans. 43 (2014) 10617-10627

[35] Roth W. J., Nachtigall P., Morris R. E. , Čejka J., Two-dimensional zeolites: Current status and perspectives Chem. Rev., 2014

[36] Millini R., Perego G., Parker Jr. W. O., Bellussi G., Carluccio L., Layered structure of ERB-1 microporous borosilicate precursor and its intercalation properties towards polar molecules, Microporous Mater., 1995, 4, 221

[37] Roth W. J., Shvets O. V., Shamzhy M., Chlubná P., Kubů M., Nachtigall P., Čejka J., Postsynthesis transformation of three-dimensional framework into a lamellar zeolite with modifiable architecture, J. Am. Chem. Soc., 2011, 133, 6130.

[38] Corma A., Dıaz U., Garcıa T., Sastre G., Velty A., J. Am. Chem. Soc., 2010, 132, 15011.

[39] Opanasenko M., Parker Jr. W. O., Shamzhy M., Montanari E., Bellettato M., Mazur M., Millini R., Čejka J., J. Am. Chem. Soc., 2013, 136, 2511.

[40] Kresge C.T., Leonowicz M., Roth W.J., Vartuli J.C., Beck J.C., Nature 359 (1992) 710–712.

[41] Lim M.H., Blanford C.F., Stein A., J. Am. Chem. Soc. 119 (1997) 4090–4091.

[42] Fowler C.E., Lebeau B., Mann S., Chem. Commun. (1998) 1825–1826.

[43] Burkett S.L., Sim S.D., Mann S., Chem. Commun. (1996) 1367–1368.

[44] Mercier L., Pinnavaia T.J., Adv. Mater. 9 (1997) 500–503.

[45] Feng X., Frixell G.E., Wang L-Q., Kim A.Y., Liu J., Kemner K.M., Science 276 (1997) 923–926.

[46] Van Rhijn W.M., De Vos D.E., Sels B.F., Bossaert W.D., Jacobs P.A., Chem. Commun. (1998) 317–318.

[47] Yamamoto K., Sakata Y., Nohara Y., Takahashi Y., Tatsumi T., Science, 2003, 300, 470.

[48] Yamamoto K., Nohara Y., Domon Y., Takahashi Y., Sakata Y., Ple´vert J., Tatsumi T., Chem. Mater., 2005, 17, 3913.

[49] Yamamoto K., Tatsumi T., Chem. Mater., 2008, 20, 972.

[50] Díaz U., Vidal-Moya J.-A., Corma A., Microporous Mesoporous Mater., 2006, 93, 180.

[51] Su B. L., Roussel M., Vause K., Yang X. Y., Gilles F., Shi L., Leonova E., Ede´n M., Zou X., Microporous Mesoporous Mater., 2007, 105, 49.

[52] Astala R., Auerbach S. M., J. Am. Chem. Soc., 2004, 126,1843.

[53] Fujita S, Inagaki S., Chem. Mater., 2008, 20, 891.

[54] Goto Y., Ohsuna T., Mizoshita N., Tani T., Inagaki S., Solid State Sci., 2011, 13, 729.

[55] Bellussi G., Carati A., Rizzo C., Diaz Morales U., Zanardi S., Parker W. O., Millini R., Organic-inorganic hybrid silicates and metal-silicate having an ordered structure, WO 2008/017513 A2

[56] Bellussi G., Carati A., Rizzo C., Diaz Morales U., Zanardi S., Parker W. O., Millini R., Organic-inorganic hybrid silicates and metal-silicate having an ordered structure, US 2010/0191009

[57] Bellussi G., Carati A., Millini R., Rizzo C., Zanardi S., Process for preparing organic-inorganic hybrid silicates and metal-silicates with an ordered structure and new hybrid silcates and metal-silicates, WO 2013/098261 A1

[58] Okamoto K., Goto Y., Inagaki S., J. Mater. Chem., 2005, 15, 4136.

[59] Engelhardt G., Michel D., High resolution Solid-State NMR of silicates and zeolites, Wiley, 1987, 148-149

[60] Cruciani G., J. Phys. Chem. Sol. 67 (2006) 1973.

[61] Tani T., Inagaki S., J. Mater. Chem. 19 (2009) 4451.

[62] Millini R., Perego C., Parker Jr. W.O., Flego C., Girotti G., Stud. Surf. Sci. Catal. 154 (2004) 1214.

[63] Alberti A., Cruciani G., Galli E., Millini R., Zanardi S., J. Phys. Chem. C 111 (2007) 4503.

[64] Ding S., Liu N., Li X., Peng L., Guo X., Ding W., Langmuir, 2010, 26, 4572.

[65] Cho E.-B., Mandal M., Jaroniek M., Chem. Mater., 2011, 23, 1971.

[66] Cho E.-B., Park J., Jaroniek M., J. Phys. Chem. C, 2013, 117, 21441.

[67] Bellussi G., Millini R., Montanari E., Carati A., Rizzo C., Parker Jr. W. O., Cruciani G., de Angelis A., Bonoldi L., Zanardi S., A highly crystalline microporous hybrid organic-inorganic aluminosilicate resembling the AFI-type zeolite, Chem. Commun, 48 (2012) 7356-7358

[68] Opanasenko M., Parker Jr. W. O., Shamzhy M., Montanari E., Bellettato M., Mazur M., Millini R., Cejka J., Hierarchical hybrid organic-inorganic materials with tunable textural properties obtained using zeolitic-layered precursor, J. Am. Chem. Soc. 136 (2014) 2511-2519

[69] Bellettato M., Bonoldi L., Cruciani G., Flego C., Guidetti S., Millini R., Montanari E., Parker Jr. W. O., Zanardi S., Flexible structure of a thermally stable hybrid aluminosilicate built with only the three-ring unit, J. Phys. Chem. C 118 (2014) 7458-7467

[70] Bellussi G., Carati A., Rizzo C., Millini R., New trends in the synthesis of crystalline microporous materials, Catalysis Science & Technology, 3 (2013) 833-857

Capther 3
Eni Carbon Silicates as sensing films: materials and methods

This thesis is the result of a collaboration project between Eni Spa and the Department of Physics and Earth. Science of the University of Ferrara. In particular, two academic groups were involved: the Sensors Group, managed by Prof. Vincenzo Guidi, and Mineralogy Group, managed by Prof. Giuseppe Cruciani. The main goal of this project was to investigate the possibility of using the Eni Carbon Silicates powders, synthetized by Eni, as a functional material for the production of films to implement in gas sensing devices.

The purpuoses of the project can be summarized as follows:

➢ to create a homogeneous and compact paste using ECS powders;

➢ to carry out morphological, chemical, structural, and thermal characterizations both for powders and pastes;

➢ to employ thick film technique in order to deposite the pastes onto alumina substrates;

➢ to investigate the possibility of using ECS materials as sensing films through electrical characterization.

Eni has made available six organic-inorganic hybrid aluminosilicates, two for each organic parent compound: ECS 4 and ECS 14 (precursor BTEB), ECS 5 and ECS 9 (BTEBP), ECS 12 and ECS 13 (BTENaph). The synthesis processes of these powders were deepened in the previous capter, here the background provided by Eni about the six ECSs (4, 14, 5, 9, 12, 13), the knowledge about chemorestive gas sensors resulting from Sensors Group experience and the characterizations methods used by Mineralogy Group will be discussed in order to understand the reasons of research activity planning.

3.1 ECS powders: preliminar knowledges

ECS materials were synthesized using 1,4-bis-(triethoxysilyl)-benzene (BTEB), 2,6-bis-(trimethoxysilyl)-naphthalene (BTEN) and 4,4′-bis-(triethoxysilyl)-biphenyl (BTEBP) (all from JSI Silicone Co., Korea) as silica sources. Sodium aluminate ($NaAlO_2$), boric acid (H_3BO_3) and NaOH were used as aluminum, boron and alkaline sources, respectively.

The reactant mixtures were prepared by adding the required amount of bridged silsesquioxane to a solution obtained by dissolving NaOH and $NaAlO_2$ in demineralized water. When required, H_3BO_3 was added after the dissolution of NaOH. The resulting mixture was charged into a stainless steel oscillating autoclave and heated under autogenous pressure at 100 °C for the desired time. Once cooled to room temperature, the solid product was separated from the mother liquors, washed with de-mineralized water and dried overnight at 100 °C. The detailed synthesis processed, published in a dedicated international patents [1-3], is reported in the previous capther.

In this section, ECSs preliminary information, in particular for crystalline powders, will be introduce because of major interest for the investigations.

3.1.1 Powders by BTEB precursor: ECS 14 and 4

A brief summary of main features for precursor BTEB, ECS 4 and ECS 14 is shown in the following Table 3.1.

Table 3.1. Precursor BTEB, ECS 4, and ECS 14.

	BTEB	ECS 4	ECS 14
Formula	(Et)$_3$-O-Si-Benzene-O-Si-(Et)$_3$	SiAl$_{0.01}$K$_{0.02}$C$_{2.95}$	SiAl$_{0.9}$Na$_{0.5}$C$_3$O$_{3.5}$x1.8 H$_2$O
Excitation λ (nm)	270		
Emission λ (nm)	289	306, 350	290
State		Amorphous	Crystalline
Area (m^2/g)		360	20
Stability (°C)		300	300
H$_2$O (%w)		5	15.7
Morphology		Not done	Hexagonal plates
Channels (Å)		/	~ 7, linear

ECS 14 was synthesized hydrothermally at 373 K in a stainless steel rotating autoclave from an alkaline aqueous reaction mixture containing BTEB, sodium aluminate (NaAlO$_2$), sodium hydroxide (NaOH) and boric acid (H$_3$BO$_3$) [4]. A white crystalline product was isolated, washed repeatedly with demineralized water and dried at 373 K. TG-DTA-MS analysis revealed that ECS 14 was stable up to 375 °C (Figure 3.1). Above this temperature, two well-separated weight losses occurred with the complete structural breakdown due to the combustion and removal of the phenylene moieties.
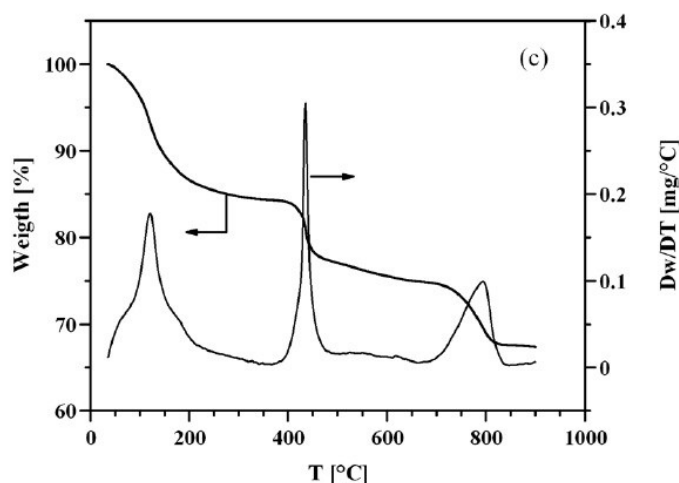
Figure 3.1. TG and DTG profiles collected on ECS 14 [5].

Similar to ECS 3 [6, 7] ECS 14 crystallizes as hexagonal micrometer-sized platelets (Figure 3.2), which provided an initial guess for the crystal system; as a matter of fact, the XRD pattern (Figure 3.3) was indexed on a hexagonal unit cell (refined unit cell parameters were: a = 14.21306(3), c = 27.2081(1) Å, V = 4759.97(3) Å^3) and the systematic absence indicated P6/mcc as the most probable space group. The density of ECS 14 was measured to be 1.84 g cm^{-3}.
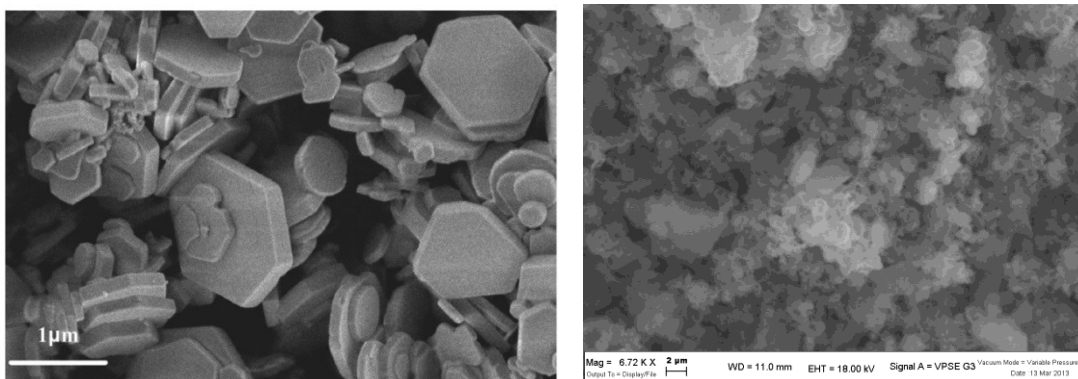
Figure 3.2. SEM micrograph of ECS 14 powder showing the hexagonally-shaped platelets (on the left) [4], and of amorphous ECS 4 powder obtained in the course of research activity (on the right).
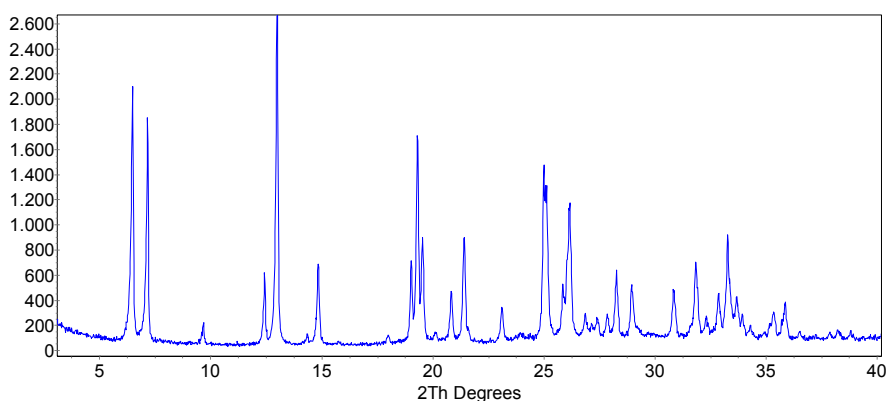
Figure 3.3. Diffractogram of ECS 14 powder, as provided by ENI.

Projection down [010] reveals indeed a layered material, composed of organic–inorganic layers stacked along [001] and bonded together by sodium ions (Figure 3.4). Projection along [001] evidences a one-dimensional system of linear channels with 12-MR openings. This projection has already been found in the structures of the AFI-type: the aluminophosphate AlPO-5 and purely siliceous SSZ-24. The similarities with the AFI framework type are not limited to the [001] projection. The layers of ECS-14 can be built from the subunit of the AFI structure consisting of four interconnected sheets of tetrahedral and by incorporating phenylene rings between the second and the third sheets (Figure 3.5). Different from AlPO-5, where sheets of AlO_4 and PO_4 tetrahedra alternate along [001], in ECS-14 the phenylene group imposes the O_3SiC tetrahedra to be adjacent and bonded to AlO_4 tetrahedra forming two sheets above and below the layer.

Each SiO_4 tetrahedron is bonded to three AlO_4 tetrahedra, the latter being completed by a fourth O atom bonded to the Na(2) ion located between layers. Each Na(2) ion is tetrahedrally coordinated to four AlO_4 sites, belonging to couples in two adjacent layers, with a rather short Na–O distance (1.926(2)Å). The occupancy of the Na(2) was refined to ~70%. An additional Na(1) ion was found in the (2/3,1/3,z) special position, leading to an overall content of ~14 Na atoms per unit cell, far below the content necessary for compensating the charge of the 24 Al atoms present in the unit cell.

69
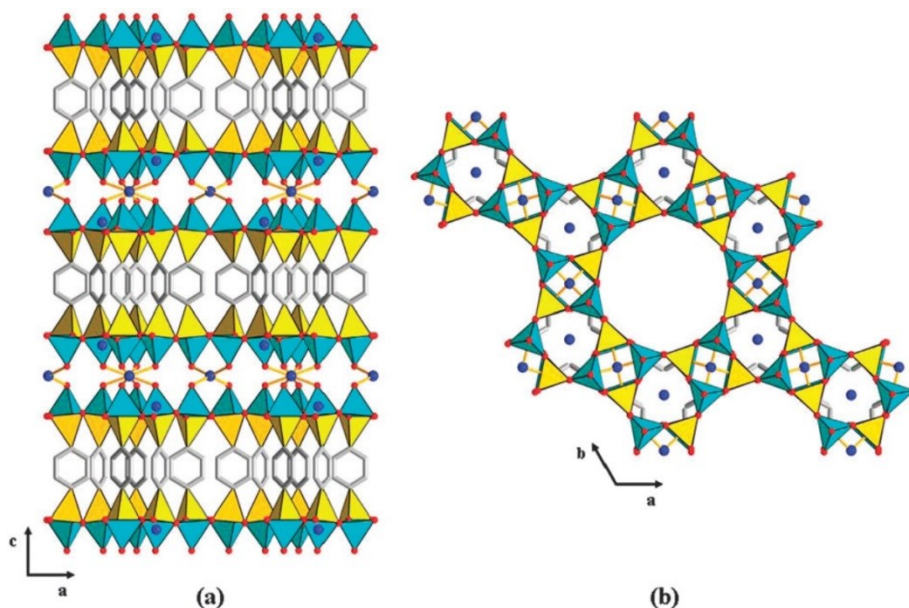
Figure 3.4. Projections of the structure of ECS 14 down [010] (a) and [001] (b) [SiO₃C] tetrahedra in gold, [AlO₄] tetrahedra in cyan, phenylene rings in grey, oxygen atoms in red and sodium atoms in blue. H atoms and H₂O molecules are omitted for clarit [4].

It is worth noting that the stacking of layers along [001] in ECS-14 is different compared to that of AFI structure. Figure 3.4 shows that layer stacking in AFI occurs by a translation of ~8.5 Å (i.e. the unit cell parameter c) along [001]. Differently, in ECS-14 each layer is related to the adjacent one by a rotation of 180° around the binary axis located at z=1/4. In this way, the six phenylene rings of adjacent layers appear to be rotated by 30° around the axis of the channel along the [010] projection [4, 5].
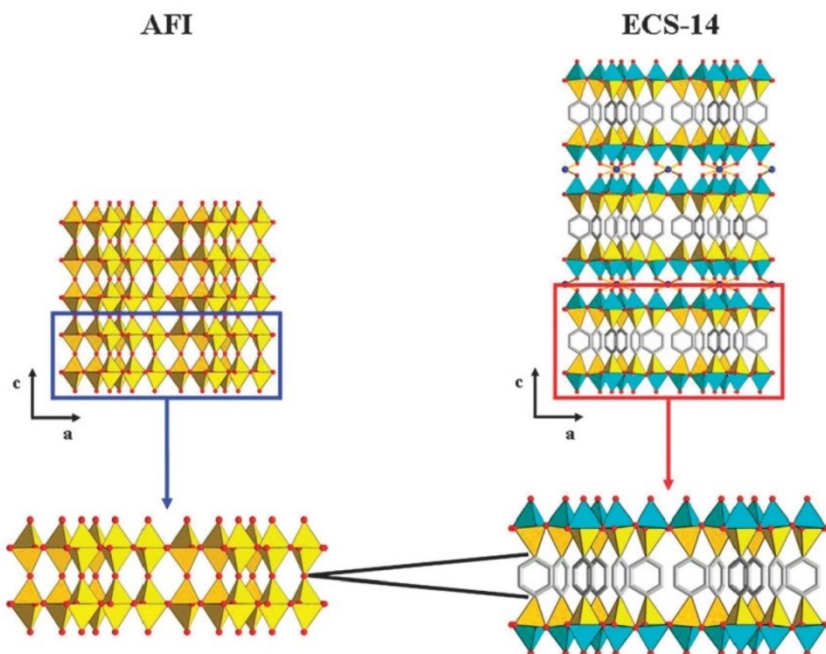
Figure 3.5. Representations of the structures of SSZ-24 (top left) and ECS 14 (top right) down [010] showing that the hybrid organic–inorganic layer is built through the insertion of phenylene rings between two layers of silica tetrahedra (bottom). ([SiO₄] and [SiO₃C] tetrahedra in gold, [AlO₄] tetrahedra in cyan, phenylene rings in grey, oxygen atoms in red and sodium atoms in blue.)[4].

About ECS 4, given that its amorphous state (see Figure 3.2), there are no published papers and one has to bring information only from patents [1, 2], because in the first ECSs

publication [8] ECS 4 was synthesized from BTEB without $NaAlO_2$. In the absence of the surfactant, it was possible to obtain ECS 4 having an X-ray powder diffraction pattern similar to PMO reported by Inagaki et al. (see Figure 2.10) but without any reflection peak at very low-angle region. Then, ECS 4 exhibits the same structural periodicity, but without any ordering of the pores. It was concluded that the role of the surfactant was the ordering the channel's array, while BTEB was the only responsible for the long range order within the pore walls. Therefore, this material cannot be considered strictu sensu crystalline, and the lack of three-dimensional order for the structure should be a consequence of the absence of Al in the synthesis [8]. From Table 3.1, one can observe that ECS 4 powder used for this research activity has a larger active surface than ECS 14, but the same stability temperature (see Figure 2.14).

3.1.2 Powders by BTEBP precursor: ECS 5 and 9

A brief summary of main features for precursor BTEBP, ECS 5 and ECS 9 is shown in the following Table 3.2.

Table 3.2. Precursor BTEBP, ECS 5, and ECS 9.

	BTEBP	ECS 5	ECS 9
Formula	**(Et)$_3$-Si-O-Biphenyl-R-O-Si-(Et)$_3$**	**SiAl$_{0.78}$Na$_{0.69}$O$_{.15}$ C $_{5.55}$**	**SiO$_{1.5}$C$_6$H$_4$**
Excitation λ (nm)	**259**		
Emission λ (nm)	**310**	**318**	**378**
State		**Crystalline**	**Amorphous**
Area (m^2/g)		**25**	**299**
Stability (°C)		**< 200**	**/**
H$_2$O (%w)		**15**	**hydrofobic**
Morphology		**Square plates < 500 nm**	**Not done**
Channels (Å)		**/**	**/**

The TG/DTG traces of ECS 5, reported in Figure 3.6 showed an initial important weight loss associated with the elimination of structural water (i.e. not adsorbed on the surface of the crystals). The TG analysis showed a weight loss at low temperature (T < 350 °C), associated to the elimination of residual solvent adsorbed on the surface and in the pores, followed by a second significant loss due to the decomposition of the organic groups. The later occurs above 350 °C, the onset of the decomposition being dependent on the nature of the organic group as well as on the overall composition of the framework [5, 8]. This thermal behavior is in line with that observed for the other ECS phases.

Concerning the powder morphology, TEM investigation showed square–shape platelets (Figure 3.7) [5], whereas HRTEM analysis showed an interlayer spacing (~ 19 Å) significantly larger than that predictable by simply replacing the phenylene groups by biphenylene in the ECS-2 structure (~ 15 Å) [8]. According to the HRTEM observations, the inorganic layer is much thicker, and therefore more complex, than that found in ECS 2 (Figure 3.7).
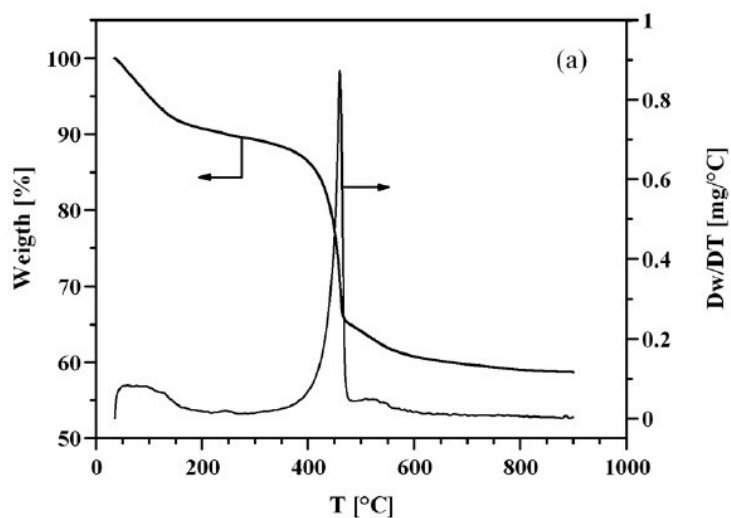
Figure 3.6. TG and DTG profiles collected on ECS 5 [5].

When the surface area of ECS 5 is considered together with the evidences of the HRTEM analysis, it is possible to hypothesize that the inorganic layers are characterized by the presence of pores accessible to small molecules and therefore much larger than the 6-membered rings found in the inorganic layer of ECS-2 [8].
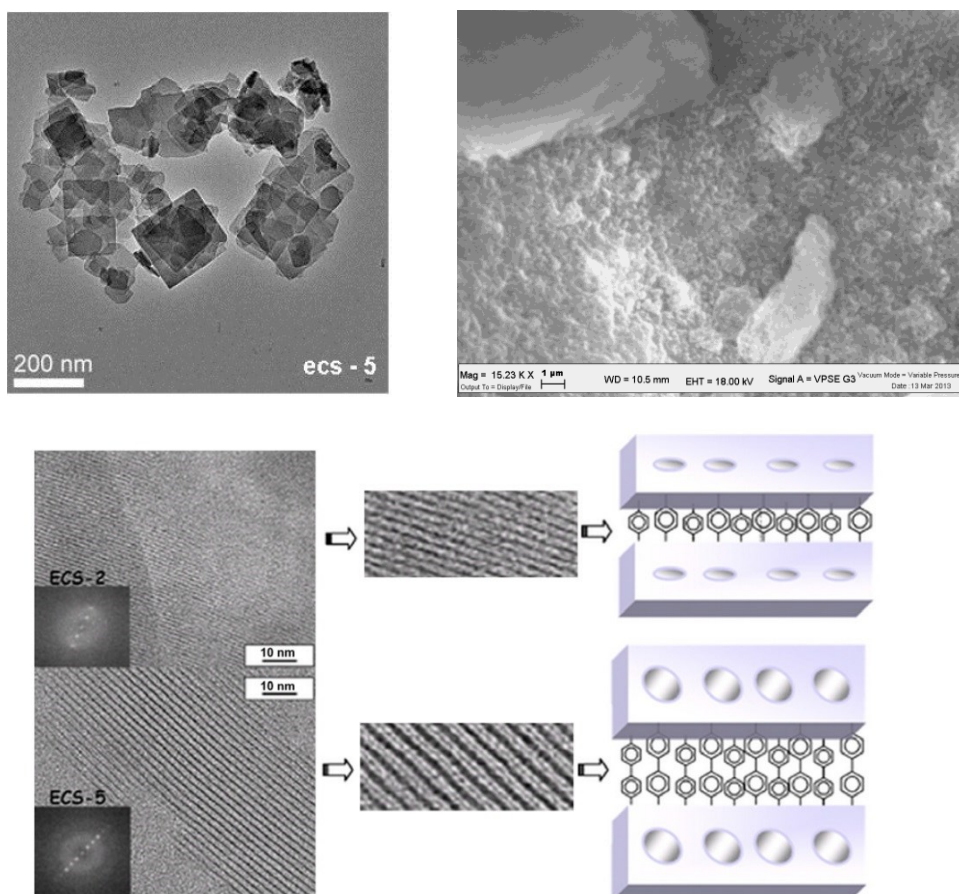
Figure 3.7. TEM micrograph of ECS 5 showing the square-shaped platelets (above left) [7], and SEM of amorphous ECS 9 powder (above right).High resolution transmission electron micrographs of ECS 5 powder compared to ECS 2 (below left). Porous ECS 5 structure (below right) hypothesized speculating on the basis of TEM analysis.

Laboratory XRD patterns of the ECS 5, reported in Figure 3.8, shows a crystalline phase.
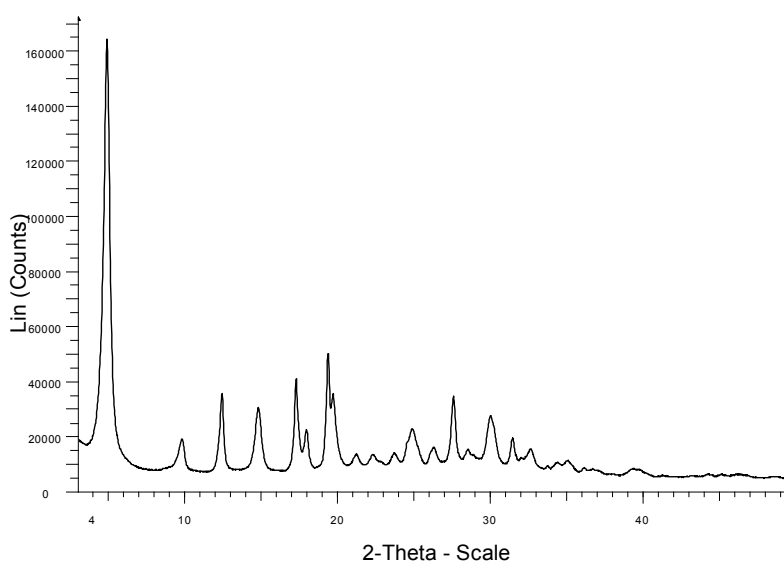
Figure 3.8. Diffractogram of ECS 5 powder, as provided by ENI.

Regard to ECS 9, characterized by amorphous phase (see Figure 3.7), there are no further published information more than those reported in Table 3.2.

3.1.3 Powders by BTENaph precursor: ECS 12 and 13

A brief summary of main features for precursor BTENaph, ECS 12 and ECS 13 is shown in the following Table 3.3.

Table 3.3. Precursor BTENaph, ECS 12, and ECS 13.

	BTENaph	ECS 12	ECS 13
Formula	$(Et)_3$-Si-O-Naftalene-R-O-Si-$(Et)_3$	$SiO_{1.5}C_6H_3$	$Na_{0.7}[SiAl_{0.7}O_4(C_5H_4))]x_{2.2}H_2O$
Excitation λ (nm)	277		
Emission λ (nm)	331, 346, 362	400	348
State		Amorphous	Crystalline
Area (m²/g)		515	43
Stability (°C)		Not done	< 200
H₂O (%w)		hydrofobic	13
Morphology		Not done	Square plates < 500 nm
Channels (Å)		/	~ 4, linear

BTENaph in presence of $NaAlO_2$ formed the new ECS 13 phase. The TG/DTG traces of ECS 13, reported in Figure 3.9, shows an initial important weight loss associated with the elimination of structural water. The decomposition of the organic components occurs above ~350 °C as for ECS 5. This thermal behavior is in line with that observed for the other ECS phases.
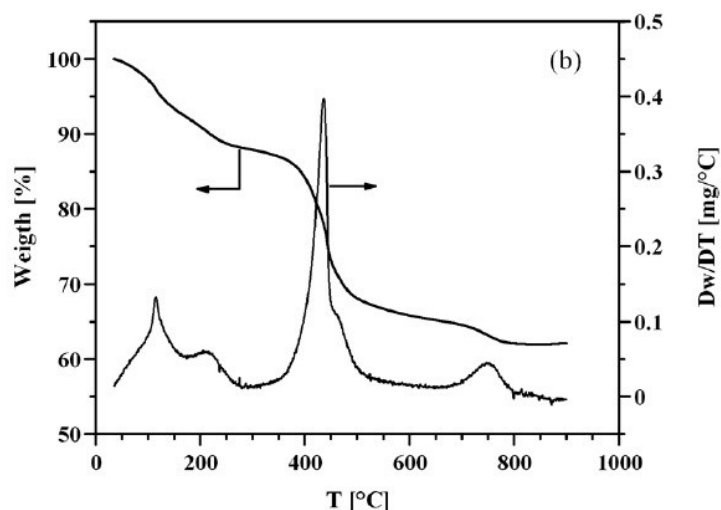
Figure 3.9. TG and DTG profiles collected on ECS 5 [5].

TEM investigation on ECS 13 powder showed square–shape platelets (Figure 3.10) [5]. In most cases it crystallized poorly or was accompanied by other unidentified by-products, but the use of H_3BO_3 led to a positive result. In fact, comparison of XRD patterns of highest quality samples (Figure 3.11) synthesized in the Si/Al and in the Si/Al/B systems confirmed their high crystallinity but even that the addition of H_3BO_3 leads to the formation of pure ECS 13 (i.e. without traces of the unidentified phase observed in the samples prepared in the Si/Al system) with larger-sized crystallites, as evidenced by the different sharpness of the reflections in the patterns [5]. A tetragonal unit cell with parameters a = 10.240 and c = 31.119 Å was obtained starting from the high resolution synchrotron powder diffraction data.
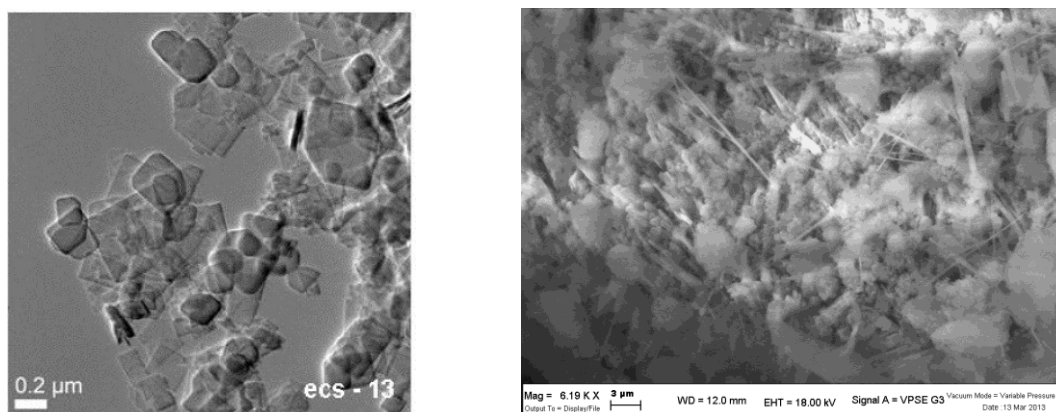
Figure 3.10. TEM micrograph of ECS 13 powder showing the square-shaped platelets (on the left) [7], and SEM of amorphous ECS 12 powder obtained in the course of research activity (on the right).

The crystal structure of ECS 13 is shown in Figure 3.12. The [100] projection reveals indeed that it is formed by composite organic–inorganic layers, which stack in the same manner as found in ECS 14. Inside the inorganic layer, each $[CSiO_3]$ tetrahedron is bonded to three distinct $[AlO_4]$ tetrahedral in such a way that they form the upper and lower parts of the layer. These layers, in turn, stack along [001] and are bonded together by tetrahedrally coordinated Na ions.
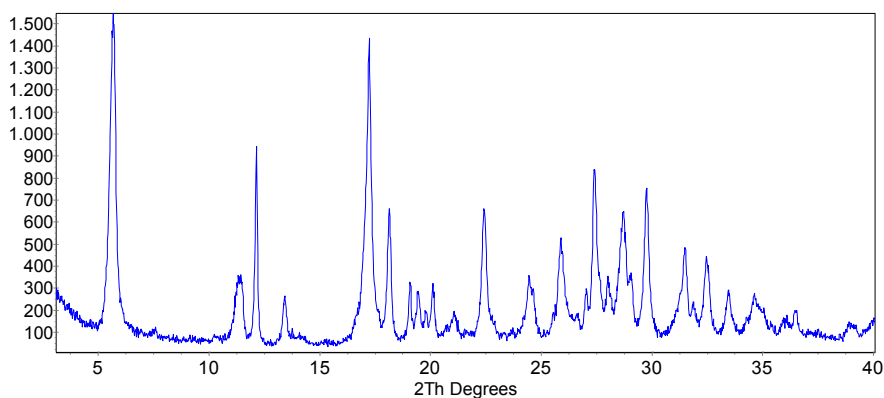
Figure 3.11. Diffractogram of ECS 13 powder (synthetized without boric acid), as provided by ENI.

The similarities between the two phases are however limited to this, as the two layers have completely different structures. In the case of ECS 14, the [001] projection is identical to that of aluminophosphate AlPO-5, or its purely siliceous counterpart SSZ-24, both having the AFI framework type structure [4]. On the other hand, the [001] projection of the layer composing the ECS 13 recalls, at first sight, that of another aluminophosphate known as AlPO-C, characterized by a 2D pore system composed by 8-ring linear channels running along [001] interconnected with highly distorted 8-ring channels running along [100].
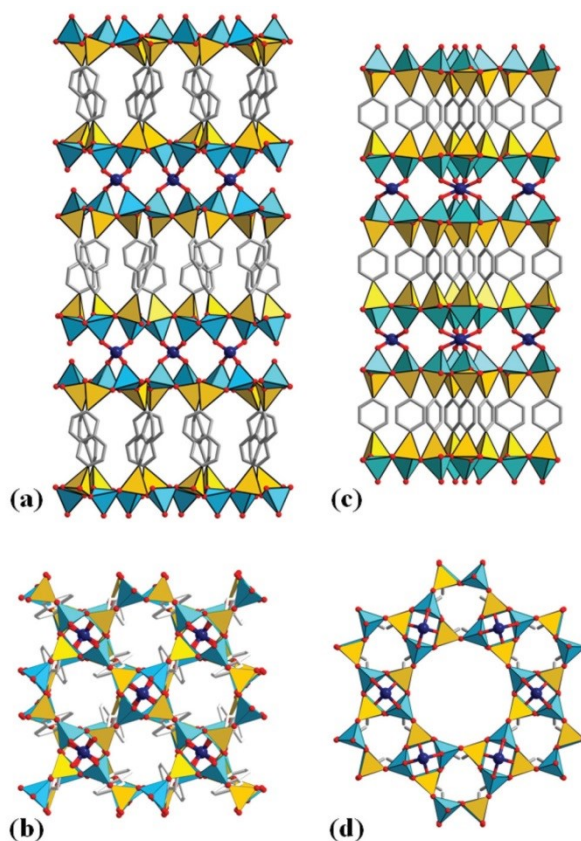
Figure 3.12. (a) [100] and (b) [001] projections of the structure of ECS 13 compared to the [110] (c) and [001] (d) projections of the structure of ECS 14. [CSiO₃] tetrahedra in yellow, [AlO₄] tetrahedra in light blue, organic groups in grey, Na/Si atoms in the interlayer in blue. Extra framework cations, water molecules and hydrogen are omitted for the safe of clarity [5].

The similarity between the two structures is limited to the two-dimensional [001] projection, but they differ for the different relative orientation of the tetrahedra. The [001] projection of

75

ECS 13 shows, indeed, the presence of 8-ring windows in the inorganic layer, but they do not give rise to the formation of channels because of the orientation of the naphthalene groups in the organic layers.

3.2 Gas sensors background

The research activity of Sensors Group of Department of Physics and Earth Science (University of Ferrara) is based on the study of chemoresistive gas sensors, involving all key aspects linked to the development of solid state devices for gas sensing: synthesis and characterizations of functional materials, such as metal oxides and non-oxides semiconductors; the design and characterizations of different substrates, such as alumina and silicon, the study of film deposition techniques and innovative applications for gas sensors. Analysis of electrical transport models through several materials have been carried out and compared to experimental evidence.

Starting from this background, first of all it was necessary to verify the possibility of handling ECS powders and to create a suitable film for implementation in sensing devices. Thus, possible electrical tests could be carried out to investigate electric transport properties and potential sensing mechanisms.

Here, the main aspects of the design and the sensing mechanism of chemoresistive gas sensors will be discussed in order to explain the reasons for which the research activity have been planned in a specific way, but also for having comparison terms in case possible electric transport phenomena occur.

3.2.1 Introduction to gas sensors

A gas sensor is composed of a receptor and a transducer. The former is provided with a material or a materials system which, on interacting with a target gas, either induces a change in its own properties (work function, dielectric constant, electrode potential, mass, etc.) or emits heat or light. The transducer is a device to transform such an effect into an electrical signal (sensor response). The construction is determined by the transducer used, with the receptor appearing to be implanted within it. From this perspective, a gas sensor can be defined as a sensor in which in a semiconductor material is used as a receptor and/or transducer. Oxide semiconductors can work as both a receptor and a transducer (mostly in the form of a resistor) owing to their chemical and physical stability in hostile environments at elevated temperatures [9].

Not only the selection of a proper oxide semiconductor is important but also the methods and conditions for fabricating sensor devices exert profound influences on gas sensing properties through changes in donor density, crystallite size, contacting geometry between crystals, packing density (or porosity), packing thickness. In order to facilitate the understandings, we have proposed to assume that the sensing properties are determined by three main factors (see Figure 3.13), that is, receptor function, transducer function, and utility factor [10]. The first factor is concerned with how each constituent crystal responds to the surrounding atmosphere containing oxygen and target gases (intraparticle issue). It is unanimous that oxygen is adsorbed on the crystals as negatively charged species, accompanied by the formation of a depletion layer inside the crystals. The target gases disturb the equilibrium through being adsorbed competitively or reacting with the adsorbed oxygen. The foreign substances like sensitizers dispersed on the crystals are assumed to affect these processes anyhow. The second factor is concerned with how the response of each particle is transformed into that of the whole device, and apparently this is related with the mechanism

of electron transport between adjacent crystals (inter-particle issue). For a long time a double Schottky barrier model, discussed later, which assumes migration transport of electrons over the barrier as shown, has been advocated for this process without critical check. The third one is concerned with the attenuation of the response due to the effect of diffusion and reaction of reactive target gases through the pores of the assembly of crystals (assembly issue).
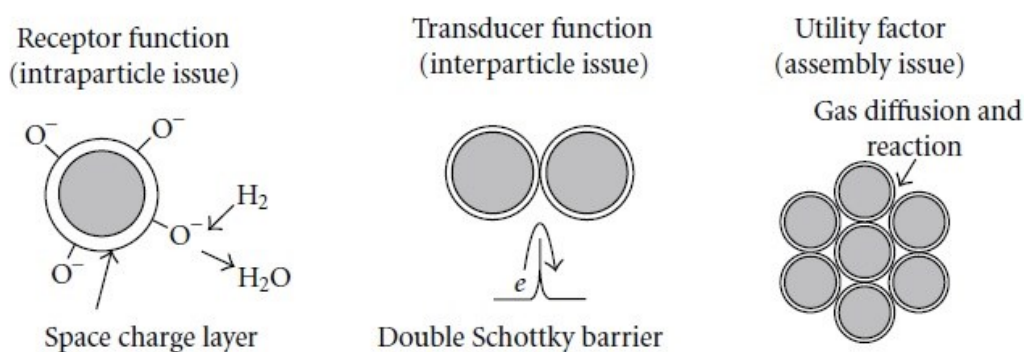
Figure 3.14. Three factors determining the response of semiconductor gas sensors [10].

The above scheme has explained rather well qualitative nature of semiconductor gas sensors in several respects. However, it has failed to give quantitative understandings and, most importantly, to give new insights leading to innovations of this group of sensors. There should have been some serious defaults included in the scheme, particularly regarding the receptor and transducer functions. Several years ago, thin film devices fabricated from hydrothermally prepared colloidal suspensions of SnO_2 by a spin-coating technique showed temperature—almost independent resistances in air in the temperature range 150–400 °C. Such thermal behavior of resistances is hardly consistent with the double Schottky barrier model, discussed later. Instead, tunneling transport of electrons across the contacts (or gaps) between adjacent crystals is strongly suggested. In addition, this transport mechanism has made much easier the theoretical modeling of receptor and transducer functions recently carried out, because the constituent crystals can now be treated independently from each other. As revealed during this process, depletion in small crystals easily goes beyond conventional one (regional depletion) to enter new type one (volume depletion) [10].

3.2.2 Chemoresistive gas sensors

Chemoresistive solid state sensors are devices capable to convert a chemical-physical quantity (as for example the gas concentration) into an electric signal. The operating principle of chemoresistive solid state sensors is based on two different phenomena: the change in the surface conductance and the variation of the bulk (the internal volume of the sensitive material which constitutes the sensor) conductance. In solid-state metal oxides, widely studied from Sensor Group of Ferrara, the difference in electronegativity of a metal atom from oxygen changes the polarity of the electron distribution of bond orbitals, thus modulating the physical properties of the solid, including conductivity. The high electronegativity of oxygen renders this atom as negatively polarized, although there is a class of oxides where the metal-to-oxygen bonds weak enough to allow a reversible chemical redox reaction at the surface with a gaseous species. From the solid-state standpoint, this last occurrence forms a series of energy levels within the energy band-gap at the surface, which are filled up by electrons up to the Fermi level, depleting the volume of the solid neighbouring the surface of electrons. The interaction of gases with the sensing film occurs mainly at the surface, so

polycrystalline materials are recommended to magnify the extension of the surface exposed for reaction [11, 12].

The mechanism of electron transport between neighboring crystals is directly related with the transducer function of sensors. There are probably three representative models, as schematically drawn in Figure 3.14 (left). Spherical crystals (uniform in size), connected with neighbors through a contact or a neck, are assumed to be depleted of electrons in the outer region only. Double Schottky barrier model (a) is a traditional one (Figure 3.14, right). It assumes that electrons are transported from nondepleted (core) region of one sphere to that of another by migration beyond a barrier in between. The barrier height not only determines the conductance of the contacting part but also gives rise to the activation energy of conduction on changing temperature.
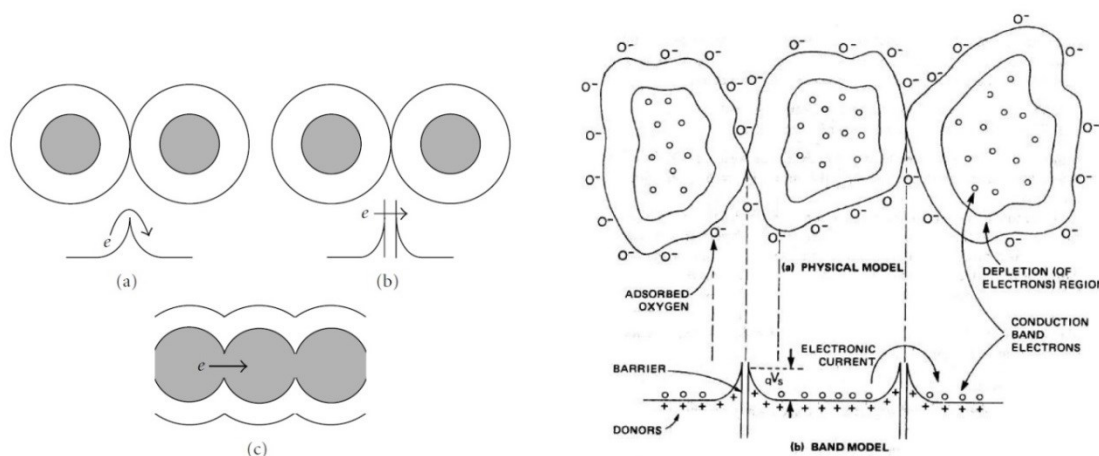
Figure 3.14. Models for electron transport between adjacent crystals (on the left) [11], and physical-band Schottky model (on the right).

Tunneling transport model (b) assumes that electrons located at the periphery of one sphere are transported to that of another by tunneling through a small gap (typically 0–0.1 nm) in between. The conductance is proportional to the density of electrons at the periphery, which is determined by the surface barrier height. On changing temperature, no activation energy is associated with the conductance provided that the barrier height is kept the same. Neck (or conduction channel) model (c) assumes that electrons migrate through a conduction channel which is formed by connecting the core regions of neighboring spheres. The channel width is narrowed at the neck parts so that the conductance is determined by the geometric relation between neck size and depletion depth [10].

In this work, the process usually yielding chemoresistive gas sensors has been used to create possible sensing devices based on ECS powders as functional materials. This process, showed in Figure 3.15, starts from nanopowders synthesis and characterizations, thus screen-printable pastes are prepared and controlling their rheology they are deposited onto commercial alumina substrates. Generally, films based on metal oxides semiconductors are subject to thermal treatments to reach the stability, morphological and structural characterizations are carried out before and after these treatments in order to identify possible variations. However, in the case of ECSs, due to their thermal behaviour, it has been necessary to review the stabilization process. The last step is the device packaging that allows to interface sensors with experimental setup for electrical characterization and tests in gas atmosphere.

The techniques used for characterizations (morphological, structural, thermal, electrical) will be explained in the next paragraph 3.3.
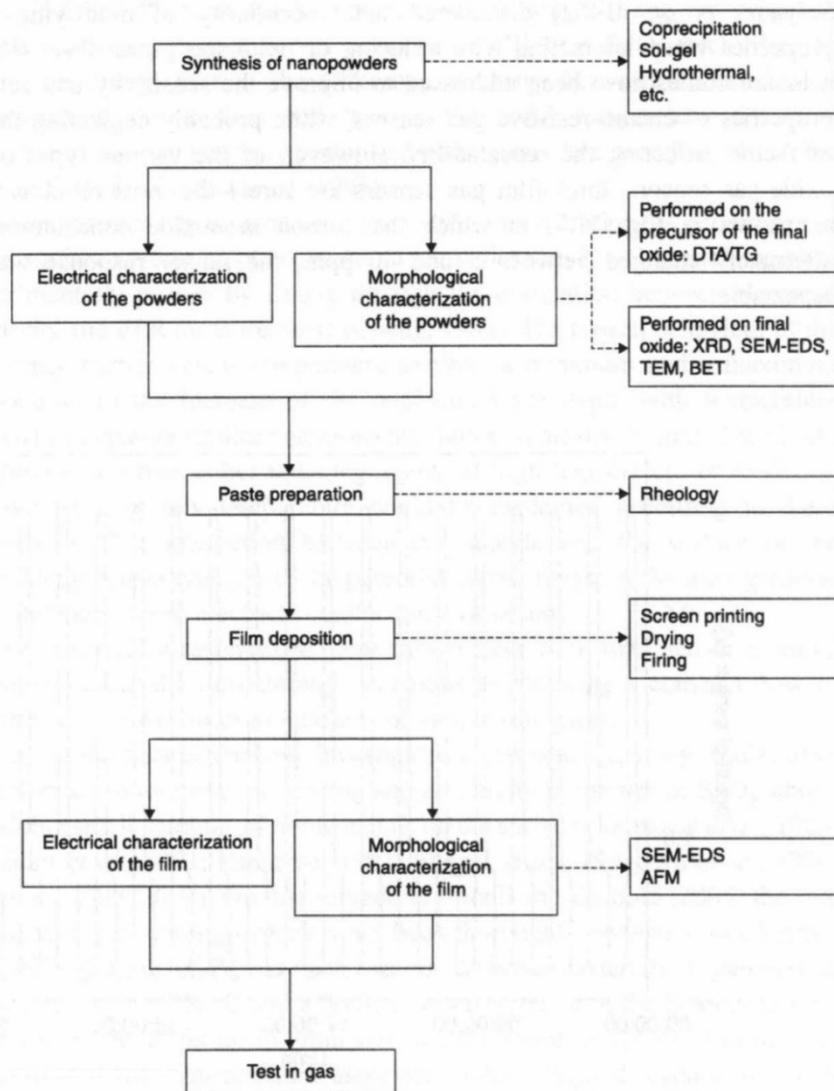
Figure 3.15. Flow chart of the process yielding thick-film for gas sensing devices starting from engineered nanopowders [11].

Gas sensors have a great impact in many areas, such as environmental monitoring, domestic safety, public security, automotive applications, air conditioning in airplanes, spacecrafts and houses, food quality, sensor networks, medical diagnosis, etc. [13-18].

In these fields chemoresistive gas sensors are widely used thanks to their several advantageous characteristics, such as:
- o good sensitivity even at low gas concentration;
- o discrete reliability and repeatability of the measurement;
- o small dimensions;
- o excellent cost-performance ratio;
- o ease of automation.

But, chemoresistive gas sensors based on semiconductor metal oxide are generally operated at elevated temperatures (100–400 °C) in order to accelerate chemical reactions between metal oxide surface and target gas molecules. Due to the thermo-activated

chemical reactions involved in detection mechanisms of these gas sensors, working temperature is a critical parameter, as it influences sensor response, response time, selectivity, power consumption and even sensor structure [19]. Working at a high temperature implies expensive sensor architecture, difficulties in maintaining stable sensor response and a high-power consumption.

Room temperature operation is an issue for intrinsic safety of sensors working in harsh or industrial environment, moreover it is interesting to reduce power consumption and consequently the size of associated electronics. Nowadays, solid-state devices have evolved rapidly improving the quality and decreasing the processing and operating costs. For the majority of metal-oxide semiconductors, the variation of film's electrical resistance induced by bulk/surface charge transfer is promoted by using high temperatures. Despite the significant performances of these devices, thermal-activation entails high power consumption, lower durability and safety risk in presence of flammable gases. Photo-activation mechanism represents a precious alternative to achieve room temperature gas sensing.

In recent years, there have been reports of gas sensors based on ultra-violet (UV) activated metal oxide semiconductors [19-21]. Illuminating these sensors with UV light is a feasible alternative to activate chemical reactions at metal oxide surface without the necessity of heating. It was suggested that UV light affects gas sensor performance through the following ways: (1) UV light leads to dissociation of target gas and chemical surface adsorbed species; (2) UV light increases density of free electron–hole pairs and thus facilitate carrier generation. These physico-chemical phenomena allow gas sensing at room temperature and implantation of these UV activated metal oxide gas sensors in different applications, such as portable devices or low power consumption applications. This particular interest of controlling chemical properties by the presence of electromagnetic radiation has been extended also to non-oxides semiconductors, such as cadmium sulfide. There is a wealth of surface-dependent phenomena for which the enhancement of the chemical properties of semiconductors exposed under electromagnetic radiation has important consequences such as heterogeneous photocatalysis, chemoresistivity, and chemiluminescence. [22, 23].

3.2.3 Sensing films preparation and deposition techniques

The techniques for film preparation can be grouped into two categories depending either on the method used for material synthesis, i.e. whether physical or chemical, or on the fashion used for film deposition, that is, thick film or thin film technology [11]. But mainly it has to consider if the material is soluble or not soluble. The scheme in Figure 3.16 presents deposition and patterning techniques for solution and not processable materials.

Figure 3.16. Deposition and patterning techniques.

For this research activity the basis of screen printing technology has been combined with drop coating. In fact, although ECS powders were used to produce printable pastes, they were not deposited by screen printing technique, even if resulted suitable for it. This because the powders quantities were not sufficient for this deposition method with which the solution of the active material is squeezed through a screen mask onto the substrate surface. Drop coating consists in application of a thin cover to a sample by depositing consecutive drops of a solution on its surface, and allowing the solvent to evaporate. ECSs resulted soluble processable so it was possible to use drop coating that is an easier method than screen printing and allows to avoid waste of material.
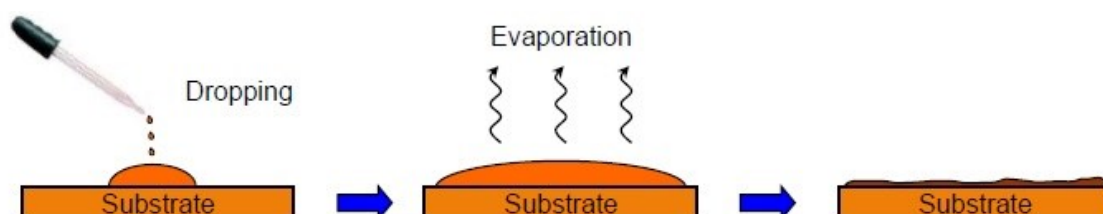
Figure 3.17. Representation of drop coating process.

The disadvantages of drop coating deposition are the limitations in large area coverage, the hardness in thickness control with a consequent poor uniformity. But these limits can be ridded out by using a combination of solvents and heating of the substrate to speed up the evaporation process and/or improve film morphology.

Thick films are fabricated from printable pastes of functional materials in the form of powder, inorganic additives, and organic binders. The structure of the paste easily changes with time, temperature and shear stress. Moreover, the pastes for screen-printing must be thixotropic: during the printing processing, the viscosity of the paste must decrease under an applied shear stress and increase when the stress is removed. The viscosity of the paste depend on the loading in powder, resin and solvents percentage. Resin dissolved in the solvents yield the organic vehicle, whose viscosity affects that of the paste. The most common formulation for scree-printable paste is listed in Table 3.4; specific paste compositions are highly proprietary [11].

Each screen printing paste is essentially composed of three main constituents:

• the *functional material*, which determines the electrical properties of the film;

• the alloying element commonly called "*glass frit*", introduced to give the sensitive layer the capability to adhere to the substrate and the right degree of intergranular cohesion during heat treatment;

• the appropriate *organic vehicle*, necessary to produce a suspension homogeneous and with a viscosity suitable for screen printing.

Despite the preparation of printing pastes it may appear at first sight very simple, it is necessary to point out the complexity of the system by set up for the execution of the entire manufacturing process, due not only the high number of compounds used, but above all to the need of obtain functional layers from those deposited.

Table 3.4. Components in scree-printable paste for gas sensors with oxide semiconductors as functional material.

	Action	Component
	Functional material (nanopowder)	• Metal • Metal oxide (pure, loaded) • Solid solution or mixed oxide
	Powder sintering aid	• Glass frit (e.g. lead borosilicate)
Organic vehicle	Organic wetting agent with low volatility	• Terpineol • Butyl Carbitol or other glycol ethers
	Binder with high molecular weight (resin)	• Ethylcellulose • Acrylic resins • Polyvinylpyrrolidone
	Surfactant	• Lauric acid or other saturated fatty acids
	Catalyst	• Noble metals (e.g. Pt, Pd, Au, Ag)

Rheology of the paste		
	Parameter	Range
	Share rate (s^{-1})	100–1000
	Viscosity (mPa)	70 000–15 000

3.2.4 Sensor substrates and packaging

Substrates used for gas sensors have the dual task of mechanical support for the sensitive layer and of electric insulator between the functional part and circuit elements.

The more used substrate is Al_2O_3 (alumina), because of its good thermal stability and resistance to corrosion and use, its excellent dielectric properties and low cost. Alumina powder is obtained from Bauxite (the principal font of aluminum existent in nature). It is ground together with other oxides (SiO_2, NaO, MgO) in order to obtain a substrate with the desired chemical-physical characteristics. Grinding is effected in a mill with blades to ensure a good mixing level. Then, the obtained compound undergoes two treatments at different pressures depending on the desired thickness (later or less than 1mm). Then, after imposing a form to the substrate, it is exposed to firing for 12-24 hours; this thermal treatment is composed by two principal steps: pretreatment and sintering. The modulation of temperatures and of total firing times is the key to optimize physical-chemical characteristics of materials.

On upper alumina support interdigitated gold electrodes are deposited, whereas on the bottom side there is a platinum heating coil covered by dielectric layer (see Figure 3.17). The alumina substrate is pre-cut in square modules of 2.54 mm side by using of laser.
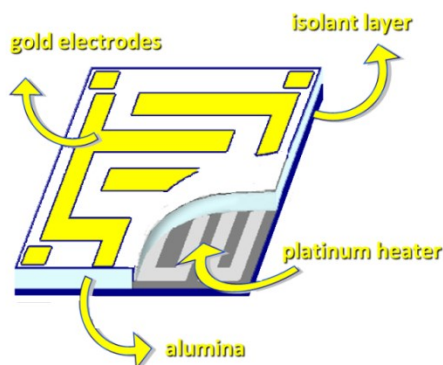
Figure 3.17. Illustration of alumina support for sensors.

The substrate should not play an active role in the sensing activity, moreover a certain compatibility between the sensitive layer and the support must subsist, in order not to create tensions as a result of thermal expansion. Then, substrates have to be characterized from a smooth and uniform surface and from the lowest number possible of visible surface defects. Furthermore the substrate materials must have a chemical and physical compatibility with the materials with which they are in contact.

The sensor must be assembled by means of a technique named bonding, which consists in the connection of the sensor to a support, using four pins. These pins are welded, by thermo-compression, to the heater and to the contacts of the plate on which the film is deposited. This connection, powered by golden wires (99:99%) with a diameter of 0.06 mm, is carried out via the apparatus shown in Figure 3.18.
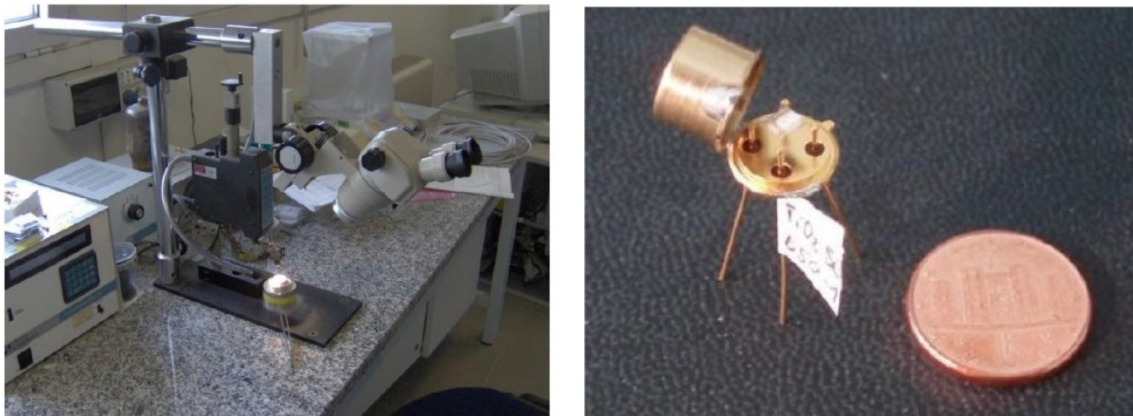
Figure 3.18. Instrument for the packaging (on the left), and example of gas sensor produced at Sensors Laboratory of Ferrara (on the right).

3.3 Investigation techniques and experimental setup

3.3.1 Morphological characterizations

Optical Microscopy

The investigations on sample deposited on microscope glass slides and silicon supports were carried out with the stero-optical microscope Leica EZ4. This microscope is equipped with an integrated digital camera, which conveniently connected to a PC allows processing of images acquired by LAS EZ software. The microscope allows to obtain images in both the transmitted light than in reflected light. In particular, in reflected light incidence angle on the sample can be varied: thanks to a series of LEDs connected in the inner part of the arm.

About the deposition on glass each sample has been acquired in three modes:
- transmitted light indicated by the abbreviation "N * A";
- reflected light with high plus low incidence angle indicated by the abbreviation "N * B";
- reflected light with a low incidence angle indicated by the abbreviation "N * C".
- reflected light with high incidence angle indicated with the symbol "N * D" for the samples at 35X magnification.

For each sample, images were acquired at three different magnifications: 10X and 25X, and in different cases even 35X.

Transmitted light N*A   Reflected light with high plus   Reflected light with low   Reflected light with high
                          low incidence angle N*B   incidence angle N*C   incidence angle N*D
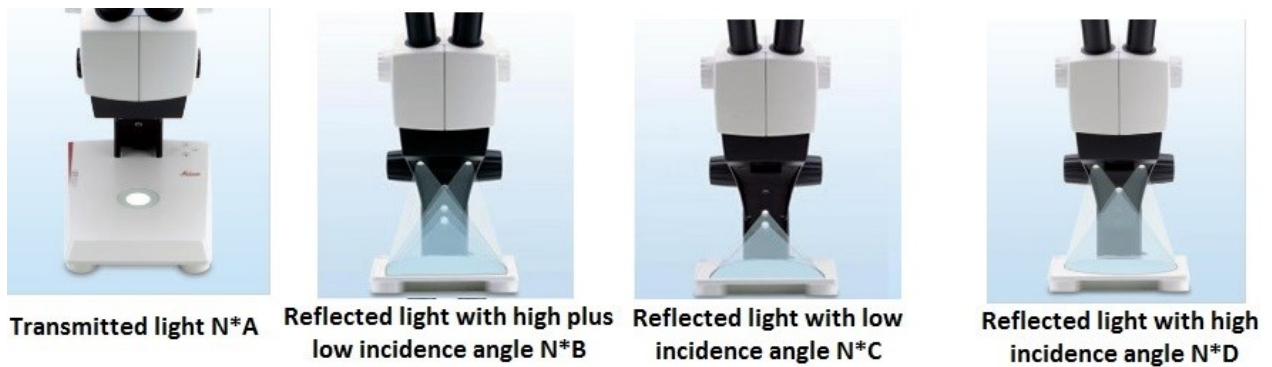
Figure 3.19: Optical microscope configurations used for morphological characterizations.

Regarding the deposition on silicon (necessary for SEM analysis), samples transmitted light are obviously omitted. Since these pictures were useful to facilitate the acquisition of the SEM images, the magnifications used were 10X, 25X for some depositions, while for the others only the magnification 15X was used.

The scale calibration was carried out with a glass decimeter "Wild".

The photos acquired are collect in Appendix A and B at the end of the thesis, each of them is assisted by a comment, with an overall judgment of the quality of the film obtained, such judgment is referred to the possibility of development in research.

SEM-EDX Spectroscopy

The scanning electron microscope exploits a focused beam of primary electrons to hit the sample. The primary beam is not fixed, but it scans the surface of interest: it is controlled in sequence, point by point and line by line, over a small rectangular area of the sample. During the interaction between the primary beam and the atoms of the sample, secondary electrons and other particles are emitted. Secondary electrons are captured by a detector and converted into electrical impulses, which are sent to a monitor in real time. The result is a high resolution black and white image, with high field depth, which is similar to a normal photography. For this reason SEM images are immediately intelligible and easy to understand. The resolving power of a normal electron microscope with tungsten cathode is about 5 nm, but some models can reach 1 nm. The sample is kept under high vacuum (10^{-5} Torr), as the air would prevent the beam emission since secondary electron have low energy. Besides, the sample must be conductive (or metallized), otherwise it could produce electrostatic discharge that would disturb the detection of secondary electrons. Other signals that the sample could emit after the primary beam incidence are: backscattered electrons, X-rays, electron channeling, cathode luminescence, currents induced by the beam and, only for certain samples, transmitted electrons. The sample region from which the interaction signals are emitted is called textitinteraction volume. As regards the microanalysis (EDX spectroscopy), the instrument exploits the X-rays emitted by sample upon the incidence of the accelerated electron beam [24]. These are detected by a special detector that can be a Wave Dispersive spectrometer (WDS) or an Energy Dispersive one (EDS).

The resulting image consists of an X-rays spectrum, from which it is possible to obtain the chemical composition of the analysed material, since every peak of the spectrum corresponds to a precise atomic species. The X-radiation comes from the ionization of the inner orbits of atoms by the incident beam. A primary electron can remove an electron belonging to the K, L orM atomic orbit, loosing the correspondent energy EK, EL or EM. The ionized atom can acquire more stability by going down to a lower energy level or, alternatively, through the occupation of the hole by an outer electron with the emission of an

X-photon. The released energy can be absorbed by another electron, which can jump out of the atom (Auger electron emission). The emitted X-radiation is characteristic of the atom and gives information about its chemical species. However, the electron beam generates not only a characteristic spectrum, but also a continuous one (background radiation), due to the interaction between electrons and the atomic nuclei. Therefore the system must be able to analyze and separate the different energies.

For acquisitions made with the microscope Scanning electron you used a Zeiss SEM EVO 40 at the Center for Electron Microscopy University of Ferrara.
Operating parameters:

- Source LaB6
- Maximum acceleration voltage 30 kV
- Variable pressure chamber (sample non metallic)

Before proceeding with the SEM investigations, each sample was photographed with an optical microscope in order to optimize the collected electron microscope.
Also for photos collected by SEM, in Appendix A and B, it was given a judgment that follows the scheme indicated in the description of the optical microscope.

Figure 3.20. SEM Zeiss EVO 40, located at the Microscopy Center of the University of Ferrara.

3.3.2 Structural characterizations

The X-rays are a range of electromagnetic radiation extremely penetrant, characterized by shorter wavelengths than that of visible light, between 10 nm and 0.01 nm. The phenomenon of diffraction of X-rays by the crystals derives from an interaction between the energy of the incident radiation and the crystalline matter. The technique of X-ray diffraction is based on the coherent elastic scattering: the macroscopic phenomenon of diffraction is generated by the coherent sum of all electromagnetic waves, diffused by the atoms that lie along the same family of lattice planes. This diffusion produces a beam diffracted only in the directions in which the waves, scattered by all the atoms belonging to a same lattice, are in phase coincidence. Certain geometric conditions must be satisfied and can be mathematically expressed in two forms: the equations of Laue and the Bragg's law. The resulting diffraction spectrum, comprising both the positions that the intensity of the effects of diffraction, is a fundamental physical property of the substance, useful not only for its rapid identification, but

also for a full interpretation of its structure. In fact, with this analysis it is possible to understand the size, the shape and the orientation of the primary cell and the position of atoms inside it.

Powders method (XRPD, X-Ray Powder Diffraction)

A powder of a crystalline material contains a high number of crystallites, whose size is of the order of 0.01 nm. Since the population of crystallites is statistically oriented, surely there would be some of them arranged in the correct way to satisfy the Bragg's diffraction condition:

$$\lambda = 2d\sin\theta$$

An experiment of diffraction of X-ray from powders essentially requires: an X-ray source, the sample to be investigated and a detector able to detect the diffracted Xrays (Figure 3.21). The X radiation commonly used is that emitted by copper (whose characteristic wavelength of the K↵ radiation is 1.5418 °A). The end result, developed by the software, is a diffraction spectrum or diffractogram constituted by a series of peaks having different intensity and angular position and relative to the various crystalline phases present in the sample. From it, the following characteristics of the sample can be read: chemical characterization, existing crystalline phases and their percentage compared to the overall crystalline phase, the average size of crystallites. In order to correctly interpretate the diffractogram, a comparison with the reference database of crystalline substances is done.

The collected by XRD were made with Bruker D8 Advance diffractometer, with the following characteristics:

- tube: Cu Kα1, α2; 40kV; 40mA;
- detector: SiLi (SOLX), geometry θ-θ, scan-step 0.02 ° 2θ, scan-time variables for the different samples as a function of the specific needs.

The XRD data were processed using the program Topas® Bruker AXS.

Figure 3.21. XRD Diffractometer Bruker, located at the Physics and Earth Sciences' Department of the University of Ferrara.

The collected XRD on film depositions were performed on sample holder in silicon zero back-ground. As regards ECS powder as provided by ENI, are deposited also on a base of silicon zero back-ground, and then analyzed by XRD.

3.3.3 Thermal characterizations

The thermogravimetric analysis measures in a continuous way the variation of weigth in function of the temperature of a sample that is kept under controlled atmosphere [25]. The analytical result is usually expressed with a thermogram (TG curve) showing the temperature on the abscissa and on the ordinate the change in mass as an absolute value or percentage (curve of thermal decomposition). A thermogravimetric analyzer consists of four main parts: a microbalance, a furnace, a "purge" system to ensure an inert or reactive atmosphere and a computer that handles the control of the instrumental parameters. The oven usually has temperatures between room temperature and 1500 °C, with a heating rate ranging from slightly more than zero up to 200 °C per minute. The gases used for the control of the atmosphere may be nitrogen, argon or air; their aim is to favor the removal of the decomposition gases of the sample, since the saturation of the atmosphere would otherwise hinder the evolution of the sample. To have a reactive atmosphere it is possible, for instance, to feed the system with oxygen, in order to study any oxidation phenomena. Besides, the sample holder should be as inert as possible with regard to the material in analysis, so as not to have adverse reactions that could damage the measure. Another important analysis that can be perfomed with this instrumentation is the Differential Thermal Analysis (DTA). It is a particularly suitable thermal method to study endothermic and exothermic transformations and transitions accompanied by variations of specific heat. The DTA measures the temperature difference that is established between a sample and an inert reference, as the temperature varies over time. In correspondence of a physical-chemical transformation in the sample, a peak is recorded. The investigations were carried out with a thermogravimetric balance Netzsch STA 409 PC Luxx.

Figure 3.22. Thermogravimetric balance Netzsch STA 409 PC Luxx, located at the Physics and Earth Sciences' Department of the University of Ferrara.

Investigations by means of thermogravimetric balance have allowed to determine the following quantities:

• TG, weight variation with increasing temperature (expressed in percentage respect to the weight of the material at the beginning of the measure ~24°C);
• DTG, first derivative of the TG curve, it expresses the rate of change of the weight of the sample investigated, with increasing the temperature, (expressed in mg/min);

• DTA, temperature difference between the sample and the standard. With this quantity it is possible to identify exothermic or endothermic reactions. Since the temperature difference is instrumentally determined by two thermocouples working in opposition, in practice, measuring the change in voltage (microvolts / mg).

The acquisitions were performed in air flow (20 °C/min) in the ramp (10 °C /min), from 25 °C up to a maximum temperature defined as a function of the type of sample, in particular:

i) for powders as provided by ENI has set the maximum temperature equal to 1000 °C (temperature was set considering thermogravimetric analyzes present in the publications made on materials ECS).
ii) for pastes without the temperature was set up to 800 °C (this temperature was set because it was certain that the organic vehicle was already completely eliminated)
iii) for organic vehicle with alumina the maximum temperature was set equal to 800 °C (this temperature was set because it was certain that the organic vehicle was already completely eliminated)
iv) for pastes with glass frit the maximum temperature was set equal to 450 °C (there has been limited at a temperature of 450 °C as the glass frit at a higher temperature would be melted, damaging the sample holder of the thermobalance).

3.3.4 Electrical characterizations

For a preliminary measurement of the film resistance, it was chosen to use a standard multimeter, but as expected the films were too resistant than the resolution of the instrument. Therefore, electrical characterizations were carried out with the use of specific test chambers in which it is possible to perform measurements on single sensor (Figure 3.23 a, b).
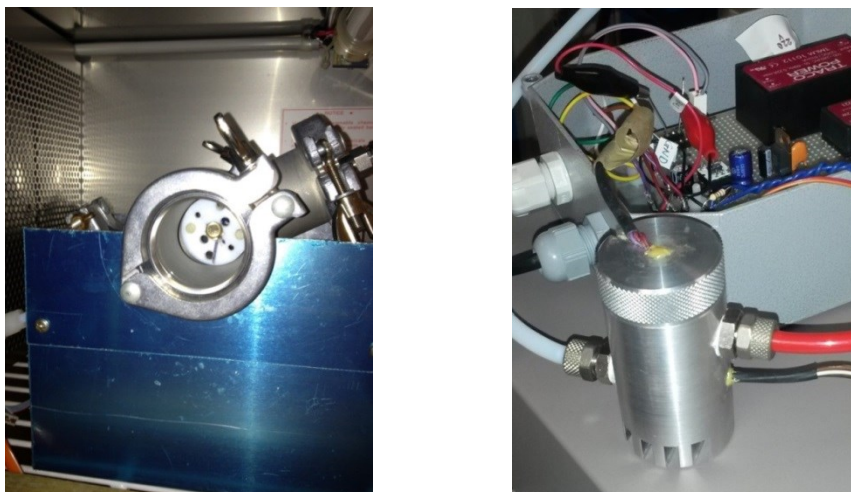
Figure 3.23. Single sensor chambers used for electrical measurements.

In order to evaluate the response of a sensor is necessary to have appropriate instruments, which allow to work in ideal conditions, enabling to carry out repeatable measurements.
The apparatus, showed in Figure 3.24, used consists of:
- flow meters for gas mixing;
- test chamber;
- data acquisition system.

The gas that we want to study are contained in bottles, connected to flow meters that allow to set the flow. This flow is then sent to the measuring chambers, at which are connected through teflon tubes. To know which flow is to be set, the following relation must be used:

$$F = \frac{F_{tot} \times C}{C_{bot}} \qquad (1)$$

where F_{tot} is the total flux in the flow meter (in this case 500 sccm[5]), C is the gas concentration that one wants to send to the chamber and C_{bot} is the gas concentration in the bottle (certified by the supplier).
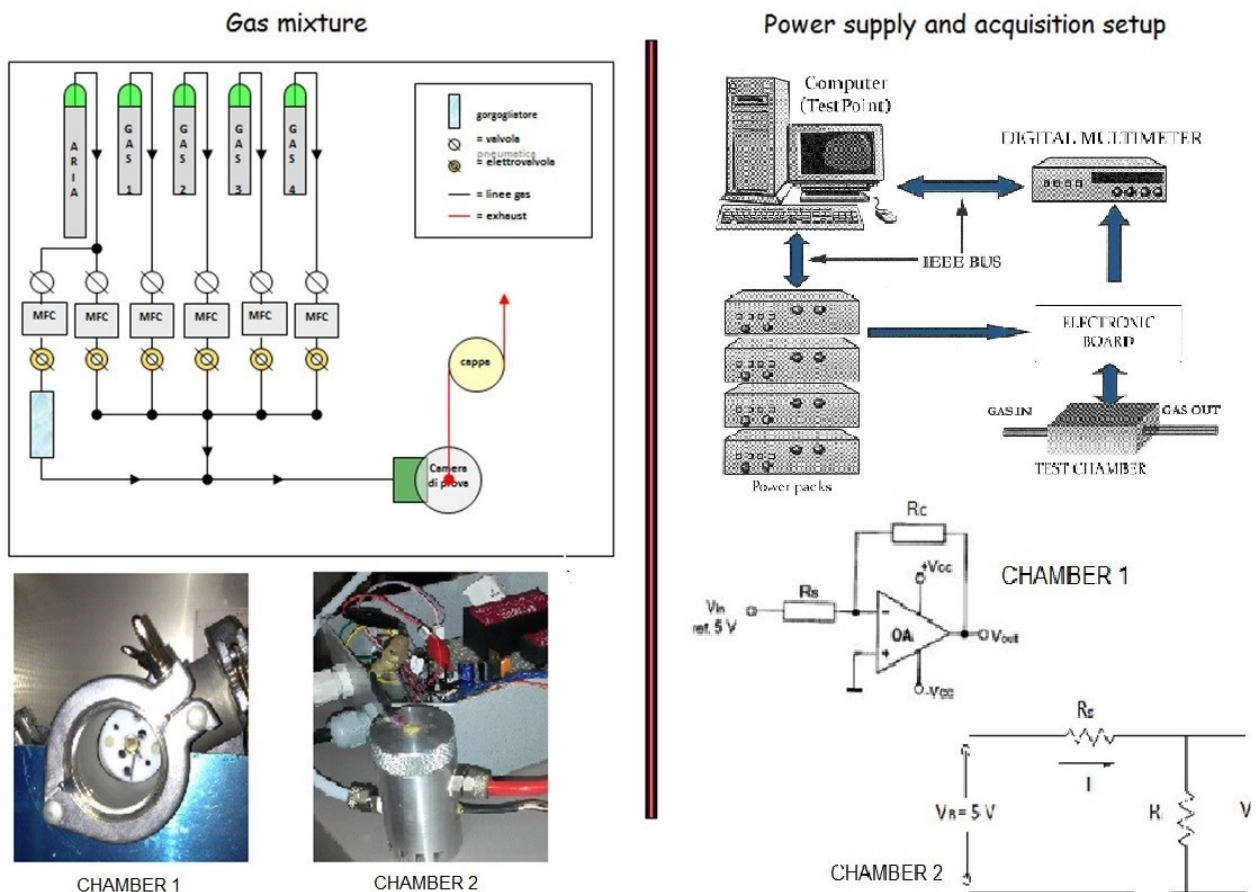
Figure 3.24. Diagram of the experimental setup and the circuits that regulate the acquisition for the two single test rooms.

The measurement chamber is the place in which sensors are positioned. It has a cylindrical shape, it is made of aluminum and hermetically sealed by a cover through bolts. At the center of the chamber there is the gas diffuser, while sensors are positioned circularly around it. In every chamber it is possible to place a humidity sensor and a temperature sensor. Furthermore, it is important to specify that the gas is diffused uniformly inside the chamber in order to solicit sensors at the same time.

Each chamber has inside two commercial sensors for monitoring the temperature and the humidity, respectively. In the following table the values of temperature and Relative Humidity are shown in a range from 100 sccm of dry air to 100 sccm of wet air.

---

[5] Standard Cubic Centimeters per Minute.

Table 3.4. Calibration values of humidity measure in the chambers for an increasing wet flux.

Flux [sccm]	100 dry	90dry + 10wet	80dry + 20wet	70dry + 30wet	60dry + 40wet	50dry + 50wet	40dry + 60wet	30dry + 70wet	20dry + 80wet	10dry + 9wet	100 wet
RH%	5	16	24.1	32.4	40.7	49.2	57.7	66.5	74.5	84.5	94.4
T [°C]	25.7	25.7	25.7	25.7	25.7	25.7	25.7	25.7	25.7	25.7	25.7

In order to detect the changes in conductance of the sensor is necessary to insert it inside a circuit, represented in Figure 3.24 (bottom right).

It can be observed that the chamber 1 is regulated by a circuit whose main component is constituted by an operational amplifier (OA), while the chamber 2 is associated with an electronic device that uses a voltage divider. It is necessary to emphasize the distinction between the two systems because each circuit diagram leads to a different formula for the calculation of the sensor response .

For the chamber 1, the input signal is connected at the negative entrance of the amplifier while the positive one is grounded. At the ends of the sensor resistor R_S and applied load resistor R_c, it has respectively the voltage values V_{in} and V_{out}. Fixing V_{in} equal to -5V , because of the virtual short circuit to the inputs of the OA, the inverting input terminal is at the same potential that the non-inverting input terminal. In this way the sensor is subjected to a constant potential difference of 5 V until the OA works far from saturation. Being the values of V_{in} and R_c known and constant, the output voltage V_{out} is then proportional to the conductance. Then, the expression for sensor conductance G_s results:

$$G_S(1) = \frac{1}{R_S} = -\frac{V_{out}}{R_C \cdot V_{in}} \tag{2}$$

Then, the expression of response assumes a really simple shape, independent from the circuit parameters:

$$\mathrm{Re}\,sponse(1) = \frac{G_{gas} - G_{air}}{G_{air}} = \frac{V_{out}(gas)}{V_{out}(air)} - 1 \tag{3}$$

where G_{gas} is the sensor conductance in presence of target gas, whereas G_{air} in presence of air only.

In the circuit associated to chamber 2, the sensor resistor R_S and applied charge resistor R_c, are connected in series, so they are crossed by the same current the voltage V_{out} measured at the output is linked to the sensor conductance G_s from the formula:

$$G_S(2) = \frac{1}{R_S} = \frac{V_{out}}{R_C \cdot (V_{in} - V_{out})} \tag{4}$$

where V_{in} is the power supply fixed at 5 V.

Also in this case the expression of response assumes a really simple shape, independent from the circuit parameters:

$$\mathrm{Re}\,sponse(2) = \frac{G_{gas}}{G_{air}} = \frac{V_{out}(gas)}{V_{out}(air)} \frac{V_{in} - V_{out}(air)}{V_{in} - V_{out}(gas)} \tag{5}$$

For each test it will be specified electrical system used to measure and the load resistance applied.

This allowed us to make some assumptions of improved suspension and related depositions. First, the introduction of an alternative deposition method: the drop coating is undoubtedly fast and inexpensive, but does not allow the control of the thickness of the deposition; Therefore, since the density of the samples leaves presuppore the possible use of the screen printing technique, after investigating further the effectiveness of the paste in its various formulations it opts for the use of screen printing. This will allow for a greater number of devices that will result therefore reproducible on a large scale and especially characterized by the film thickness controlled.

The acquisition system must manage all phases regarding the sensor electronics (see Figure 3.24). It is made of:
-   <u>Multimeter K2000 (Keitheley)</u> serves to convert all output voltages from analog to digital. Then these values will be sent to the computer. The multimeter has ten input channels and a sensitivity of ten decimal digits.
-   <u>Management and acquisition software</u> consists of a program, in TestPoint, capable of acquiring all the ten input channels of the multimeter (eight gas sensors, a temperature sensor and a humidity sensor), at regular intervals (an acquisition every five seconds). Through this software it is possible to visualize the graphic of the response of sensors and it is possible to control or modify supply voltage values to set sensors at the desired temperature.

Reference

[1] Bellussi G., Carati A., Rizzo C., Diaz Morales U., Zanardi S., Parker W. O., Millini R., Organic-inorganic hybrid silicates and metal-silicate having an ordered structure, WO 2008/017513 A2

[2] Bellussi G., Carati A., Rizzo C., Diaz Morales U., Zanardi S., Parker W. O., Millini R., Organic-inorganic hybrid silicates and metal-silicate having an ordered structure, US 2010/0191009

[3] Bellussi G., Carati A., Millini R., Rizzo C., Zanardi S., Process for preparing organic-inorganic hybrid silicates and metal-silicates with an ordered structure and new hybrid silcates and metal-silicates, WO 2013/098261 A1

[4] Bellussi G., Millini R., Montanari E., Carati A., Rizzo C., Parker Jr. W. O., Cruciani G., de Angelis A., Bonoldi L., Zanardi S., A highly crystalline microporous hybrid organic-inorganic aluminosilicate resembling the AFI-type zeolite, Chem. Commun, 48 (2012) 7356-7358

[5] Zanardi S., Bellussi G., Parker Jr. W. O., Montanari E., Bellettato M., Cruciani G., Carati A., Guidetti S., Rizzo C., Millini R., The role of boric acid in the synthesis of Eni Carbon Silicates, Dalton Trans. 43 (2014) 10617-10627

[6] Bellussi G., Montanari E., Di Paola E., MilliniR., Carati A., Rizzo C., Parker W. O., Gemmi M., Mugnaioli E., Kohl U., Zanardi S., ECS 3: A crystalline hybrid organic-inorganic aluminosilicate with open porosity, Angewandte Chemie International Edition 21 (2012) 666-669

[7] Zanardi S., Parker Jr. W. O., Carati A., Botti G., Montanari E., On the thermal behaviour of the crystalline hybrid organic-inorganic aluminosilicate ECS-3, Microporous and Mesoporous Materials 172 (2013) 200-205

[8] Bellussi G., Carati A., Di Paola E., Millini R., Parker Jr. W. O., Rizzo C., Zanardi S., Crystalline hybrid organic-inorganic alumino-silicates, Microporous and Mesoporous Materials 113 (2008) 252-260

[9] Jaaniso R., Tan O. K.,Semiconductor Gas Sensors, Woodhead Publishing Series in Electronic and Optical Materials, 2013, ISBN-13: 978-0857092366

[10] Yamazoe N., Shimanoe K., Receptor Function and Response of Semiconductor Gas Sensor, Journal of Sensors, 2009 (2009), 1-22

[11] Guidi V., Malagu' C., Carotta M.C., Vendemiati, "Printed films: Materials science and applications in sensors, electronics and photonics" B. in WOODHEAD PUBLISHING SERIES IN ELECTRONIC AND OPTICAL MATERIALS (2012) pp. 278-334

[12] Madou M. J., Morrison S. R., Chemical Sensing with Solid State Devices, 1989 Academic, New York

[13] Kortidisa I., Moschovis K., Mahmoude F.A., Kiriakidis G., Structural analysis of aerosol spray pyrolysis ZnO films exhibiting ultra low ozone detection limits at room temperature, Thin Solid Films 518 (2009) 1208–1213

[14] Guidi V., Carotta M.C., Fabbri B., Gherardi S., Giberti A., Malagù C., Array of sensors for detection of gaseous malodors in organic decomposition products, Sensors and Actuators B 174 (2012) 349– 354

[15] Giberti A., Carotta M.C., Fabbri B., Gherardi S., Guidi V., Malagù C., High-sensitivity detection of acetaldehyde, Sensors and Actuators B 174 (2012) 402– 405

[16] Fabbri B., Gherardi S., Giberti A., Guidi V., Malagù C., Sensing of gaseous malodors characteristic of landfills and waste treatment plants, JOURNAL OF SENSORS AND SENSOR SYSTEMS 3, 61–67, 2014

[17] Carotta M.C., Cervi A., Giberti A., Guidi V., Malagù C., Martinelli G., Puzzovio D., Ethanol interference in light alkane sensing by metal-oxide solid solutions, Sensors and Actuators B 136 (2009) 405–409

[18] Malagu' C., Fabbri B., Gherardi S., Giberti A., Guidi V., Landini N., Zonta G., Chemoresistive gas sensors for detection of colorectal cancer biomarkers, Sensors 2014, 14, 18982-18992

[19] Zhang C., Boudiba A., De Marco P.,. Snyders R, Olivier M.-G., Debliquy M., Room temperature responses of visible-light illuminated WO3 sensors to NO_2 in sub-ppm range, Sens. Actuators B 181 (2013) 395-401

[20] Liu L., Li X., Dutta P.K., Wang J., Room temperature impedance spectroscopy-based sensing od formaldehyde with porous TiO2 under UV illumination, Sens. Actuators B 185 (2013) 1-9

[21] Comini E., Cristalli A., Faglia G., Sberveglieri G., Light enhanced gas sensing properties of indium oxide and tin dioxide sensors, Sens. Actuators B 65 (2000) 260-263.

[22] Giberti A., Fabbri B., Gaiardo A., Guidi V., Malagù C., Resonant photoactivation of cadmium sulfide and its effect on the surface chemical activity, Applied Physics Letters 104 (2014) 222102

[23] Giberti A., Casotti D., Cruciani G., Fabbri B., Gaiardo A., Guidi V., Malagù C., Zonta G., Gherardi S., Electrical conductivity of CdS films for gas sensing: Selectivity properties to alcoholic chains, Sensors and Actuators B 207 (2014) 504-510

[24] Goldstein J.I. et al., Scanning electron microscopy and x-ray microanalysis, Springer (2003)

[25] Coats A.W., Redfern J.P., Thermogravimetric Analysis: A Review, Analyst 88 (1963) 906924

Chapter 4
Gas sensors based on Eni Carbon Silicates

The objective of the collaborative project between Eni and the Physics and Earth Science Department of the University of Ferrara, from which the results of this thesis, was to investigate the possibility of using the ECS powders as functional materials for the deposition of films by standard techniques in order to study the possible use of these materials in sensing field.

The production of films and the electrical characterization were carried out by sensors group, managed by Prof. Vincenzo Guidi, while the morphological, structural and thermal characterizations were performed by group supervised by Prof. Giuseppe Cruciani.

4.1 Part I: Preliminary tests

The powders delivered by Eni for the realization of the project were six: ECS 4 and 14 (precursor BTEB), ECS 5 and 9 (precursor BTEBP), ECS 12 and 13 (precursor BTENaph). Undoubtedly, the material on which Eni has provided more information is ECS 14 and this is the reason for which it was the first selected for the empirical tests of solubility. In fact, it was considered that the crystalline state and the "plate" morphology that characterize the ECS 14 were basic properties in order to use the powder as a functional material and to investigate possible electrical conduction behaviour. Furthermore, the channels formed by the benzene rings, main components of the molecule, should allow a facilitated diffusion of the analytes that represents a fundamental property for the possible use in the sensing field. The information about heat treatments on ECS 14 resulted fundamental: XRD analysis, performed by Eni's researchers, on ECS 14 to 200 ° C for 1 hour of permanence (Figure 4.1) showed a degradation of the material, then it was chosen to carry out the various steps required for the realization of the sensitive film at room temperature.
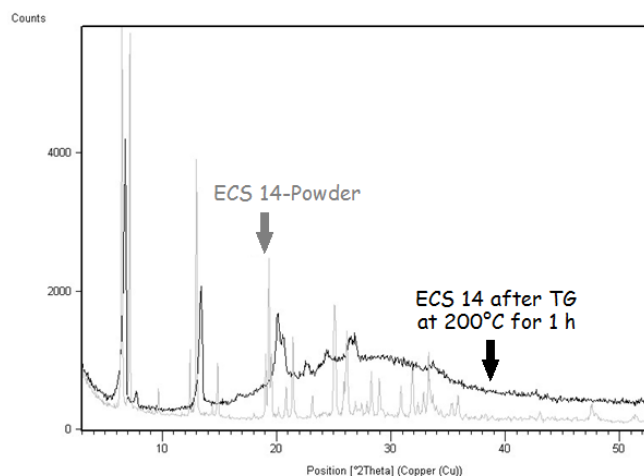
Figure 4.1. XRD analysis on ECS 14 powder before and after heat treatments.

The study of the films made with ECS powders can be divided into two steps. In the first level films deposited on quartz glass substrates were investigated by optical microscope (transmitted light and reflected). The indications obtained in this first phase have allowed to determine the most suitable solvents for the realization of the suspension, and as a consequence of being able to switch to the second phase of the study. Then, the suspensions were carried out with solvents which have provided interesting results in the first phase study and films were deposited also on monocrystalline silicon supports. In this case the investigations were carried out by optical microscope in reflected light, SEM and X-rays diffraction (grazing incidence geometry and θ-θ).

The parameters took into account in these analysis are the following:

i) effectiveness of the solvents in getting a good dispersion of the materials;

ii) continuity of thin films;

iii) adhesion of thin films to the support;

iv) influence of the solvent used on the crystalline structure (only for XRD).

4.1.1 Combination of powders and simple solvents

4.1.1.1 Solubility tests and film depositions

The novelty of these materials required a highly empirical approach. Working at room temperature, several solvents were studied as function of their polarity (Figure 4.2) in order to bring the ECS 14 powder in solution. Once it was evaluated the solutions texture the deposition of quartz glass was carried by means drop coating, then the homogeneity and the adhesion of the films to the supports were assessed.

Relative Polarity	Compound Formula	Group	Representative Solvent Compounds
Nonpolar	R - H	Alkanes	Petroleum ethers, ligroin, hexanes
	Ar - H	Aromatics	Toluene, benzene
	R - O - R	Ethers	Diethyl ether
	R - X	Alkyl halides	Tetrachloromethane, chloroform
	R - COOR	Esters	Ethyl acetate
	R - CO - R	Aldehydes and ketones	Acetone, methyl ethyl ketone
	R - NH$_2$	Amines	Pyridine, triethylamine
	R - OH	Alcohols	Methanol, ethanol, isopropanol, butanol
	R - COHN$_2$	Amides	Dimethylformamide
	R - COOH	Carboxylic acids	Ethanoic acid
Polar	H - OH	Water	Water

Figure 4.2. Solvent polarity chart.

Specifically, the solvents selected have been five: water, ethanol, acetone, chlorobenzene and toluene. The concentration of the solutions is equal to 5 mg / ml; after manual agitation manual, prepared samples were placed in a sonic bath for ten minutes. At the sight none of the solutions appeared transparent and then dissolved, but all of them were all suspended differing in the amount of bottom body present.

In particular, the resulting solutions by using polar solvents (water, ethanol and acetone) were characterized by a smaller amount of precipitated solute than solutions obtained with apolar solvents (toluene and chlorobenzene), in which the bottom body was significant. Subsequently through drop coating (<200 µl) solutions were deposited on substrates of quartz glass (diameter 12.7 mm and thickness of 1.5 mm) and the solvent evaporated at room temperature. Once it was established that the ECS 14 is more akin to polar solvents, it was decided to decrease powder/ethanol ratio, since the sample prepared by using ethanol resulted more transparent than that with acetone and water. Then, it was mixed by means of a magnetic stirrer, the remains on the bottom was not completely dispersed but it was still lower than the undiluted solution with ethanol. Even for this sample a film was deposited by drop coating on quartz at room temperature.

Other four solvents, polar and apolar, were tested: acetic acid diluted to 40% (from glacial acetic acid to 99.9%), methanol, acetonitrile and dichloromethane. The solution with methanol appeared similar to that with ethanol (in fact it is a polar solvent), and then with little remains on the bottom, but more transparent. The solution with dichloromethane is precipitated as in the case of toluene (that it is apolar) although more clear. The solution with acetonitrile was as white as that in water, but with more remains. Finally the solution with acetic acid 40% resulted transparent. It was necessary to determine whether or not the latter solvent degrade the structure of the ECS 14 molecule or whether it was just an excessive dilution. Only for solution with acetic acid a films was deposited by drop coating at room temperature, since it is found to be the most transparent with absence of remains on the bottom.

The following table summarizes all the solutions prepared as preliminary tests and a brief description of the same samples is reported:

Table 4.1. Solutions prepared with ECS 14 powder in the first level of preliminary tests.

Powder	mg	Solvent	ml	Solutions
ECS 14	2.6	WATER	0.5	White and totally suspended
	2.5	ACETIC ACID 40%	0.5	Totally transparent
	2.5	METHANOL	0.5	Similar to ethanol but more transparent
	2.5	ETHANOL	0.5	Suspended with less precipitate than in chlorobenzene
	2.5	DILUTED ETHANOL	0.5	Disperse with little precipitate
	2.5	ACETONITRILE	0.5	Water-like but with precipitate
	2.7	ACETONE	0.5	Suspended with little precipitate
	2.7	DICHLOROMETHANE	0.5	As toluene but clearer
	2.7	CHLOROBENZENE	0.5	Less precipitate than in toluene
	2.5	TOLUENE	0.5	High amount of precipitate

Therefore, the samples deposited on quartz glass by means of drop coating, in order of decreasing polarity of the solvent, are five: water, acetic acid, ethanol, dilute ethanol and acetone. The deposited films resulted to be well adherent to the substrate even in the moment in which they were handled for the following measurements of characterization. By means of an optical microscope, some images of the films deposited onto quartz glasses were acquired and some of them are shown in Figure 4.3, while the complete collection, carried out by Dr. Casotti, is reported in Appendix A (Tables A1-A7).

(a)   *(b)*   *(c)*

(d)   *(e)*
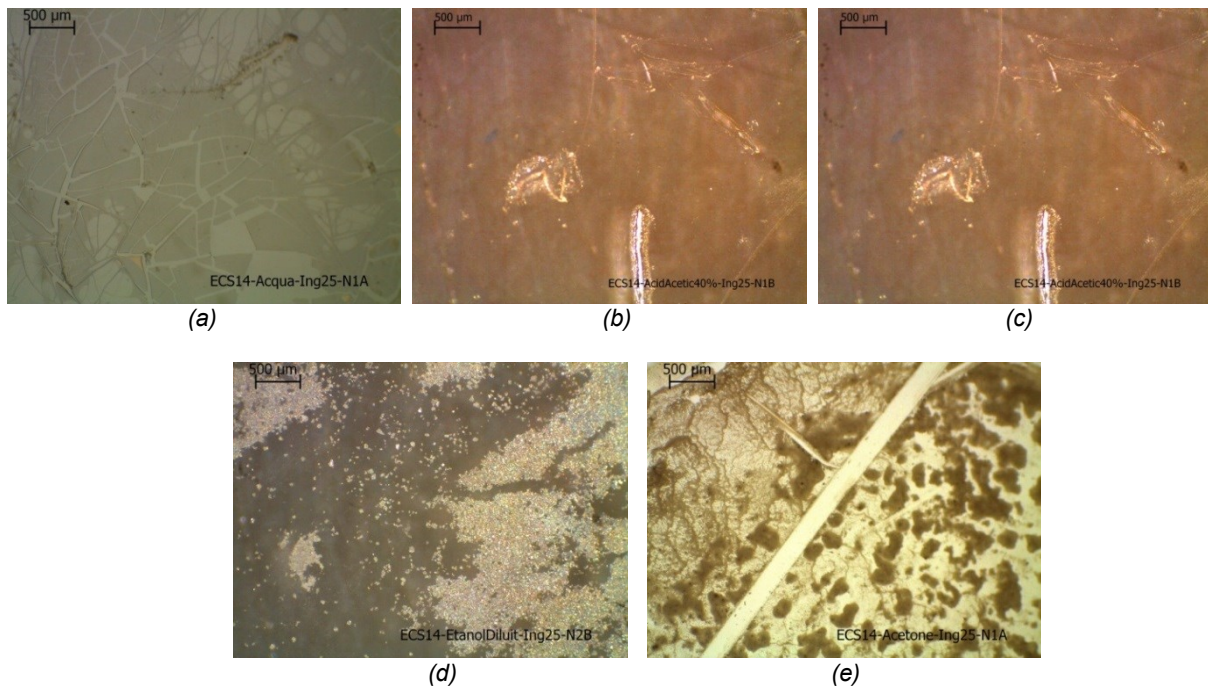
Figure 4.3. Films deposited by drop coating onto quartz glasses and formed by solutions of ECS 14 and a) water; b) acetic acid 40%; c) ethanol; d) diluted ethanol, and e) acetone.

One can observe that the water-based film seems crystallized, the one in acetic acid 40% is transparent, the one in ethanol presents agglomerates of functional material while the diluted sample appears opaque and uniform, and finally the sample containing acetone appears uneven and inconsistent.

4.1.1.2 Powders and films characterizations

The morphological and structural characterizations of the films had the objective of investigating aspects that are considered significant for the applicability of the materials in the design of gas sensors. These can be summarized as following:

i) Effect of solvents in getting a good dispersion of ECS materials. A good dispersion of the powders by the solvents supports the absence or in any case a low presence of agglomerates in the films deposited on a rigid support, thus allows to achieve a uniform film with uniform physical characteristics.

ii) Continuity and uniformity of the films deposited on rigid media. The continuity of the rigid substrates coating involves a film without cracking, this aspect is one of the most common problems in the films production. Uniformity refers to film thickness. The presence of cracks induces a physical discontinuity in the film and consequently the impossibility of current conduction or however an increase of the resistivity in the same film in function of the degree of cracking.

iii) Adhesion of thin films to the rigid support. This is an essential feature in sensors design sensor in order to ensure a good physical-mechanical strength of the film itself in addition to allow the current conduction with the electrodes in the support, and to guarantee the operation of the sensor.

iv) Inalterability of the ECS crystalline structure by the solvent used. The alterability of the crystalline phase or however of the microstructure of the powders used by the solvent used in the production of the dispersion would compromise the possibility to attribute film properties to the crystalline structure and / or microstructure of the original powders.

Morphological charcaterization: Optical Microscopy

In the first level of investigation films obtained from suspensions of ECS 14 have been made for different type of solvent, the degree of dilution of the solvent (acetic acid), powder / solvent (ethanol). The following summary table indicates the samples made according to the type of solvent:

Table 4.2. Results of optical investigations on solutions prepared with ECS 14 and polar solvents in the first level of preliminary tests.

Solvent	Optical Microscopy investigation
Water	i) do not appear aggregates ii) uniform film but very strong presence of fractures create mutually separate scales. Different thicknesses at the edges (darker areas) iii) the film is coated onto, the edges of the flakes in some cases appear raised by support
Acetic acid 5%	i) do not appear aggregates ii) the film thickness is uniform and continuous, the presence fractures of the edges of the deposition that create flakes mutually separated, iii) the film is coated onto, the edge of the deposition is consists of scales that appear not adherent to the support
Acetic acid 40%	i) do not appear aggregates ii) the film thickness uniform and continuous, the edge of the deposition decreases the thickness iii) the film is well bonded to the substrate, in this regard was made a test of scratching with a steel tip
Ethanol - concentrate	i) zones appear aggregates ii) the film does not appear uniform thickness, probably by affect the continuity of the film iii) the film is bonded to the support
Ethanol – diluted 1	i) in general do not appear aggregates, some area at the edges of the film with the presence of aggregates or different thickness compared to the rest of the film (circled in red) ii) the surface is covered in areas, probably due to the low amount of deposited material, however, the areas covered appear smooth and continuous. The area with the presence of aggregates (and circled in red) highlights of cracks iii) the film is bonded to the support
Ethanol - diluted 2	i) the presence of aggregates or still areas of thickness different than the rest of the film (circled in red) ii) the surface is not coated evenly (by attributable to the aggregates), but continuous. iii) the film is bonded to the support
Acetone	i) strong presence of agglomerates ii) the film does not appear uniformly thick (lighter areas and darker areas), but continuous. iii) the film is well-adherent

From the table one can see that the observations by optical microscope for deposition obtained with "ethanol - diluted 1" are generally positive, while observations regard deposition obtained with the suspension "ethanol - diluted 2" give a negative judgment for the presence of agglomerated and non-uniformity in the coating of the support. Both suspensions with ethanol are made with a low and similar powder / solvent ratio, from this one can take a significant indication regarding the importance of working on the methodology of the suspension production and the powder / solvent ratio.

Structural characterization:

- *Absorbance and photoluminescence*

Optical analysis may result useful to investigate if the emission properties of the substance vary as a function of the solvent used, and also one can determine if the material is degraded or modified by the type of solvent. On five samples containing ECS 14 absorption and photoluminescence measurements were carried out in air conditions. The absorption was measured with a spectrofluorometer and the photoluminescence was measured using a laser with a wavelength of 325 nm and a detector PMA (Photonic Multichannel Analyzer).
The absorption measurements (Figure 4.4) have yielded useful results for three of the five samples tested: a solution in water, acetic acid, and diluted ethanol. The absorption peak was detected at around 290 nm.
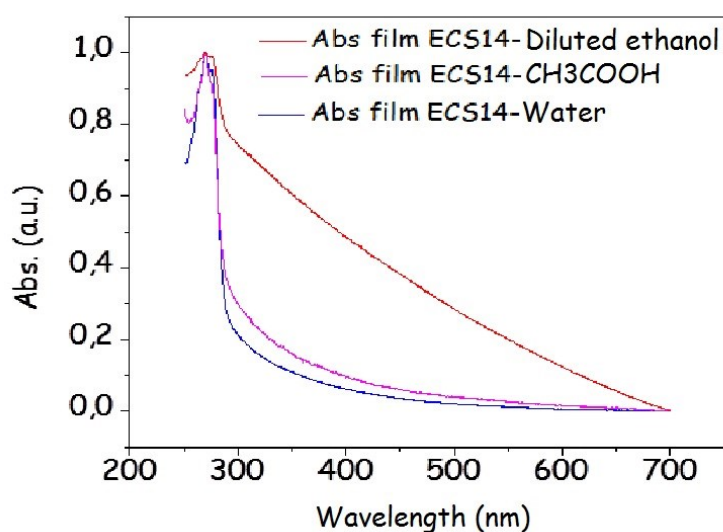
Figure 4.4. Absorption spectra related to films of ECS 14 in solution with dilute ethanol (red), acetic acid 40% (pink), and water (blue) deposited by means of drop coating on quartz glass supports.

The photoluminescence was carried out both on films and on powders the ECS 14 (Figure 4.5); the emission peak of the films is quite comparable to that of the powders for all the solvents used except for the water. It could mean that only with water, the material is degraded or interacts with the solvent, while in other cases the films seem to maintain the same optical properties of the powder Precisely emissions more similar to the powder PL measurement are those in diluted ethanol and in acetone, while the acetic acid and ethanol hold an intermediate position.
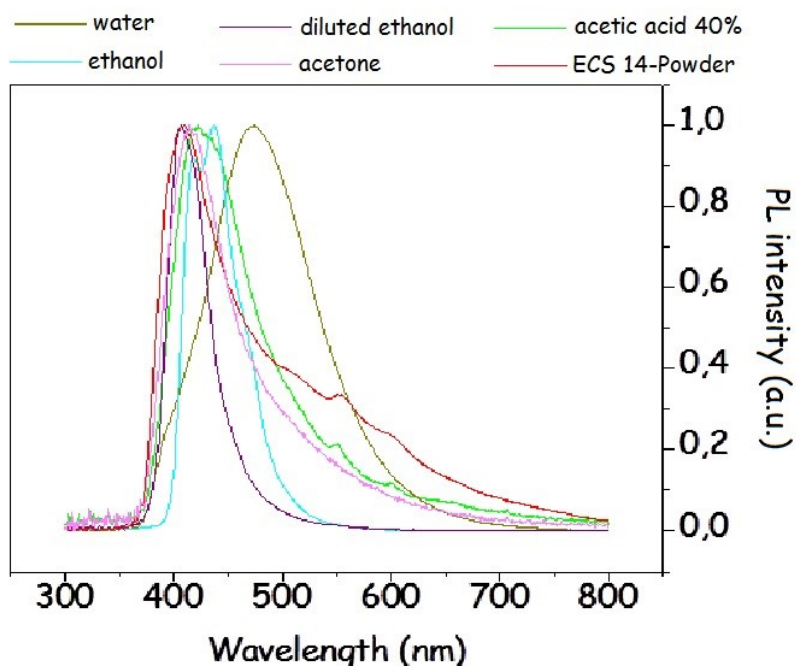
Figure 4.5. Emission spectra related to ECS 14 powder (red) and films deposited by means of drop coating on quartz glass supports starting from solutions of water (olive green), dilute ethanol (violet), acetic acid 40% (green), concentrate ethanol (light blue), and acetone (lilac).

- *X-ray diffraction*

By way of completeness the results of XRD collected with grazing incidence realized on films containing ECS 14 are also reported despite not having given a positive contribution to the study, because the amorphous material (glass) of which the supports were made has generated a loud noise in the diffractogram.

The diffraction patterns obtained from different samples are dominated by the diffusion of the glass. Therefore, it is possible to conclude that the grazing incidence setting for suspension of ECS-14 deposited onto quartz glass supports is not to be taken into account for future investigations, except for a comparison with the results obtained in θ-θ geometry.
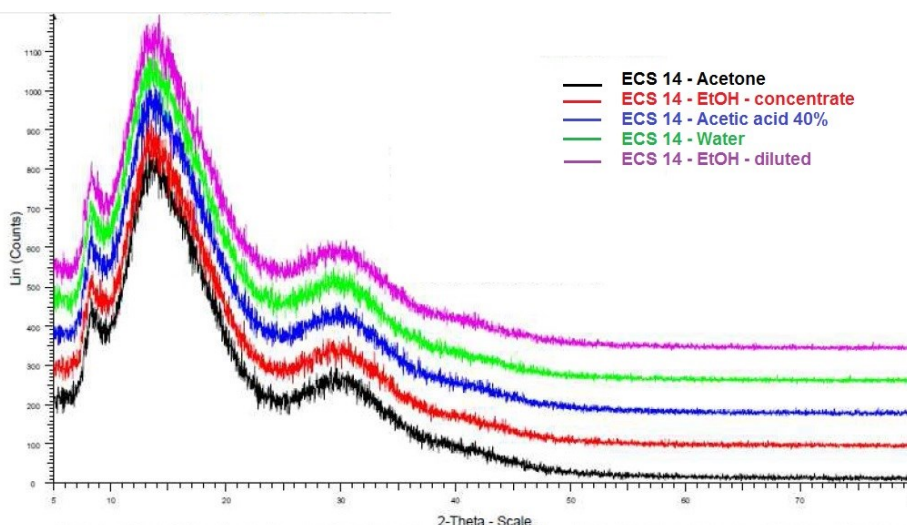
Figure 4.6. Diffraction patterns obtained by grazing incidence setting on films containing ECS 14 powder and polar solvents produced in the first level of solubility tests.

4.1.2 Polar solvents investigation

4.1.2.1 Solubility tests and film depositions

<u>Study of the solvents selected for solutions with ECS 14</u>

Based on the preliminary tests carried out it was decided to deepen the study of film technology of by using ECS 14 and polar solvents, in particular ethanol and acetic acid. In fact, the samples prepared using these two solvents resulted the most uniform from the point of view of the deposition by optical microscope analysis. Furthermore, investigations of absorption and photoluminescence performed on depositions and powder as it provided consistent information; for which it was assumed that ethanol and acetic acid did not affect the functional material. Then, four new solutions were produced:

Table 4.3. Solutions prepared with ECS-14 powder and polar solvents in the second level of preliminary tests.

Powder	mg	Solvent	ml	Support
ECS 14	2.5	ACETIC ACID 40%	0.5	QUARTZ GLASS SILICON ALUMINA
	2.3	ACETIC ACID 10%	0.5	
	2.3	ACETIC ACID 5%	0.5	
	1.7	DILUTED ETHANOL	0.5	

By means of an optical microscope images were acquired some of the films deposited on quartz glass, except for the deposition of the solution of ECS 14 in acetic acid 10% which unfortunately has been damaged during the work. Then, by way of completeness, it is preferred to show optimal microscope photos and SEM images obtained with depositions on silicon substrates. The complete collection, carried out by Dr. Casotti, is reported in Appendix A (Tables A8-A11). Images of depositions on glass are not reported because it is considered redundant with respect to the first analysis explained in the previous paragraph.

(a)   *(b)*
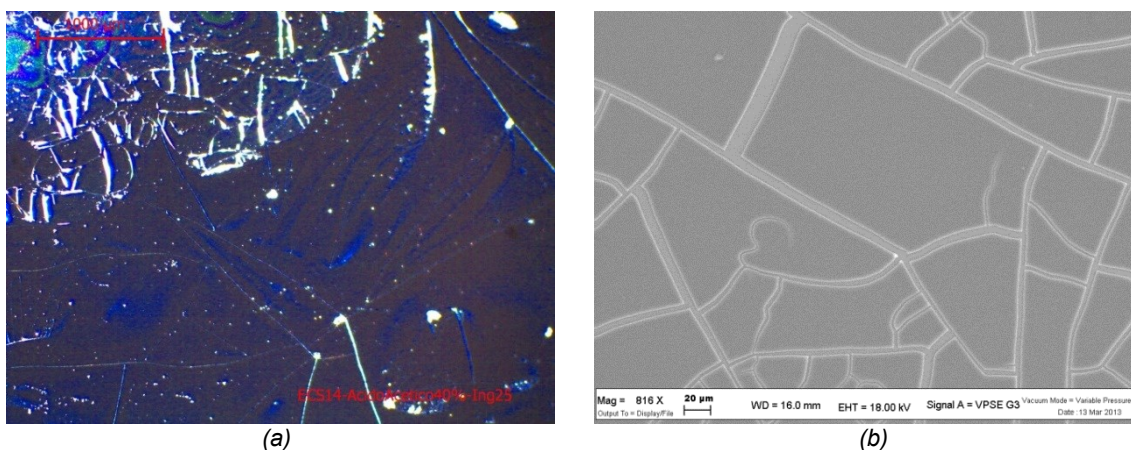
Figure 4.7. (a) Optical microscope photo of the film containing ECS-14 and acetic acid 40% deposited on silicon by drop coating and (b) SEM image of the film.

(a)	(b)
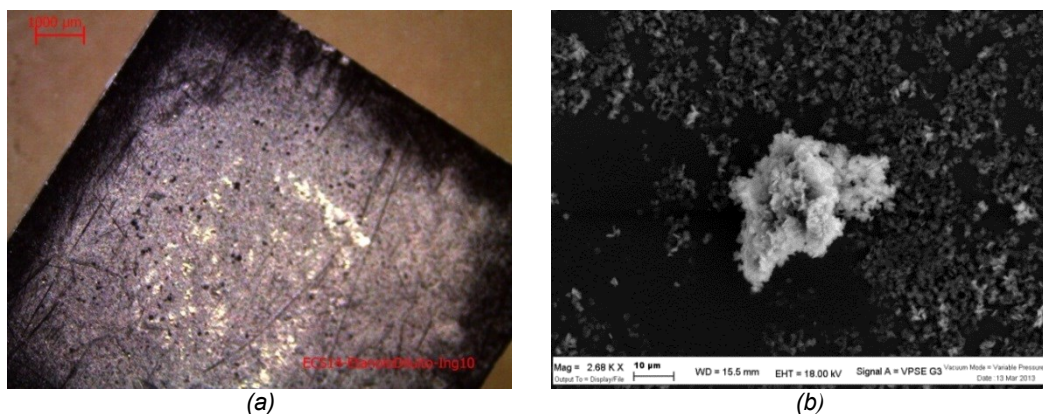
Figure 4.8. (a) Optical microscope photo of the film containing ECS-14 and diluted ethanol deposited on silicon by drop coating and (b) SEM image of the film.

It may be observed again that the samples in acetic acid are transparent and appear crystallized, as occurred with the water during the first level of preliminary tests. Instead deposition with diluted ethanol is characterized by significant clusters of ECS 14 that were not present in the preliminary deposition, resulted dull and uniform.

A more detailed analysis of this morphological characterization will be presented in the next section towards a comparison with structural information by XRD investigation.

Study of the solvents selected for solutions with ECS 5

Based on the results obtained with ECS 14 it was chosen to study another material. The choice fell on ECS 5 as characterized by the same morphology of the ECS 14, i.e. crystalline material formed by small "plates". Then two new solutions were prepared:

Table 4.4. Solutions prepared with ECS-5 powder and polar solvents in the second level of preliminary tests.

Powder	mg	Solvente	ml	Support
ECS 5	2.5	ACETIC ACID 40%	0.5	QUARTZ GLASS SILICON ALUMINA
	1.7	DILUTED ETHANOL	0.5	

Optical microscope and SEM images obtained with depositions on silicon substrates are reported below. The complete collection, carried out by Dr. Casotti, is reported in Appendix A (Tables A12-A15).

(a)	(b)
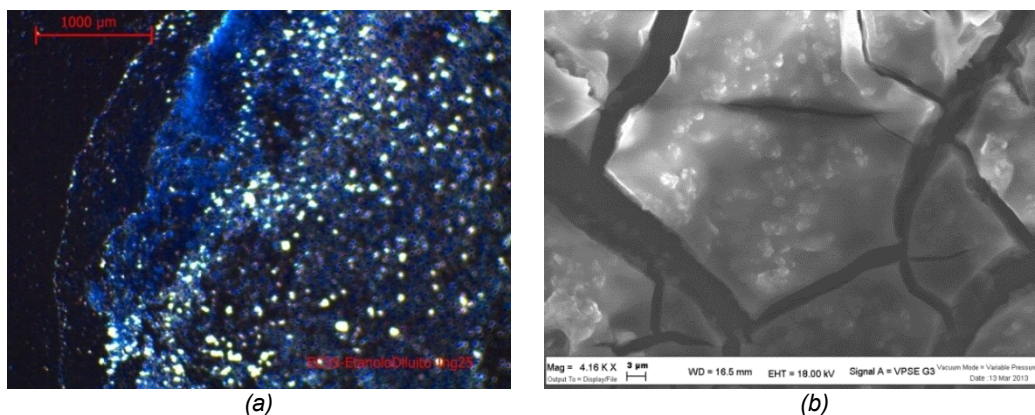
Figure 4.9. (a) Optical microscope photo of the film containing ECS-5 and acetic acid 40% deposited on silicon by drop coating and (b) SEM image of the film.
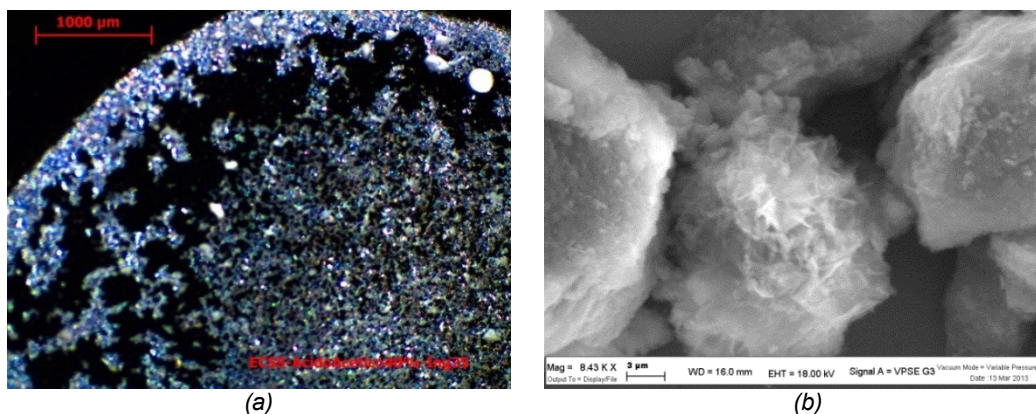
Figure 4.10. (a) Optical microscope photo of the film containing ECS-5 and diluted ethanol deposited on silicon by drop coating and (b) SEM image of the film.

Contrary to what occurred for ECS 14, using ECS 5 deposition with acetic acid 40% is more "gritty" of that in diluted ethanol that appears almost transparent. A more detailed analysis of this morphological characterization will be presented in the next section towards a comparison with structural information by XRD investigation.

4.1.2.2 Powders and films characterizations

The first level of investigation had indicated that the solvents that appear better in achieving the films are acetic acid in different percentages and ethanol (with low ratio powder / ethanol). With these considerations, it was also proceeded with the deposition of suspension on monocrystalline silicon substrates. This choice offers some advantages:

a) XRD: since support is not amorphous (glass-like) the relative noise in diffraction patterns is eliminated or at least reduced, as even the silicon substrates require plexiglas sideburns to be loaded on the diffractometer;

b) SEM: the depositions on conductive supports allow to collect excellent SEM images also in not high vacuum conditions.

To facilitate the investigation by SEM it was decided to implement in advance photos by optical microscope in reflected light.

a) ECS 14 films

Structural charcaterization: XRD diffraction

Below XRD collections of the depositions containing ECS-14 and, as solvents, acetic acid 5% and diluted ethanol (low ratio powder / solvent) are presented. For both depositions were made collections with θ-θ geometry and grazing incidence. A comparison with XRPD powder provided by ENI were also presented.

The investigation was not carried out on the depositions obtained with suspensions containing acetic acid 10%, and 40% acetic acid, since the SEM images gave indications of poor presence of crystals for these depositions, while the crystals of ECS-14 are well visible in the deposition obtained by suspension containing ethanol. Therefore, it is reasonable to assume that the acetic acid affects the crystal structure, consequently the deposition obtained by the suspension at lower acetic acid content should be the one containing more residues of crystal structures, remarkable with X-ray diffractometry,. As a result of depositions obtained with suspensions containing acetic acid, the survey was carried out only on the film containing acetic acid 5%.
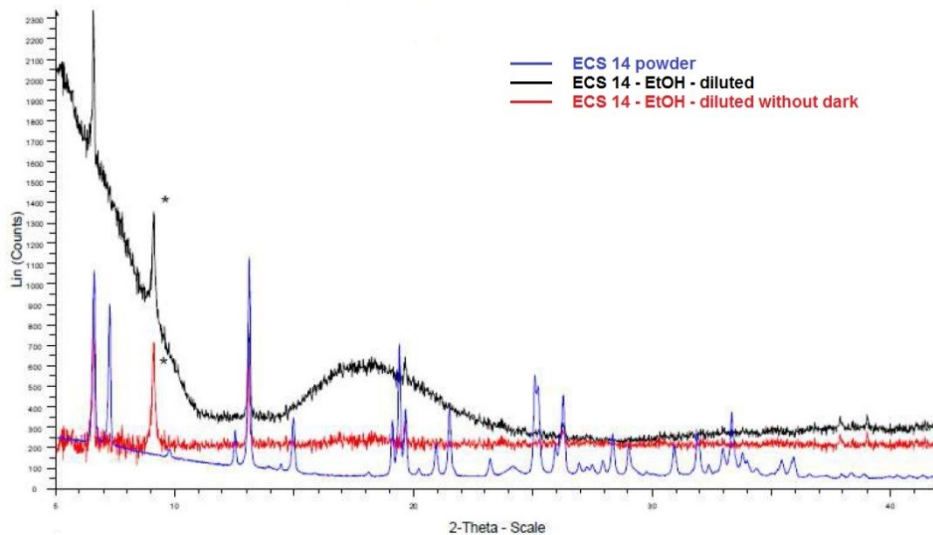
Figure 4.11. Diffraction patterns obtained by geometria θ-θ setting both on ECS 14 powder and on films containing ECS 14 and diluted ethanol produced in the second level of solubility tests (*spurious peak due to the support).

The XRD patterns show the comparison between the powder XRD provided by ENI (blue) and the XRD of the deposition obtained with the suspension containing powder and diluted ethanol (black). The same curve that has been stolen the dark with the EVA program is shown in red. This background is mainly due to diffusion phenomena of the plexiglas support on which silicon substrate was placed.

The data obtained from the XRD collection about the deposition with ethanol were used to derive the cell parameter *c* and the thickness of the crystals in the same direction (Figure 4.11). From literature, it is known that ECS 14 crystallizes in the hexagonal space group P6/mcc, with crystalline structure shown in previous chapter. It suggests that the *c*-axis is normal to the basal plane of the crystals.
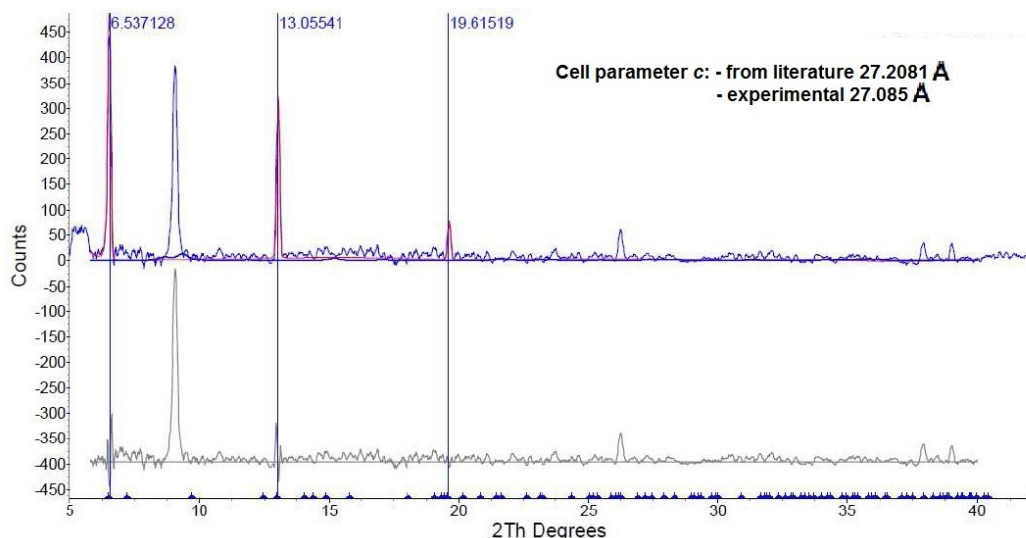
Figure 4.12. Determination of cell parameter from diffraction patterns (geometry θ-θ setting) on films containing ECS 14 and diluted ethanol produced in the second level of solubility tests.

The analysis of the diffractogram was developed with the Program Topas® of Bruker. It is well known that in a diffractogram the width of a diffraction peak is inversely proportional to the size of the crystal in the orthogonal direction to the lattice plane corresponding to this

reflection, purged the effects of enlargement instrumental (see Figure 3.2). In this case, after their identification, the basal reflections peaks were individually fitted (using function FP "fundamental parameters" implemented into TOPAS). This function allows to determine accurately the enlargement of the peak, since it calculates instrumental effects of enlargement and then the dimensions determined in the [001] direction are accurate. It was determined a crystallites thickness of about 90 (19) nm; this is comparable with that derived from the images published for the ECS-14.

The parameter of cell c was determined from the 2θ position of the peaks (002), (004) and (006). By calculations, it was determined that c is equal to 27.085Å, while data in the literature for ECS-14 indicates c = 27.2081 Å. These values appear to be very close, so it can be concluded that the powder ECS 14 has maintained its crystalline structure in the deposition with ethanol. The presence of only basal reflections compared to other diffractions confirms what it was also observed in the SEM images, this means the crystallites are almost totally iso-oriented with the base resting the silicon support.

For comparison, the collected XRD setting θ-θ (red) and grazing incidence (black) obtained from the deposition of the suspension ECS 14 are shown below, as well as the pattern of the powder provided by ENI (blue).
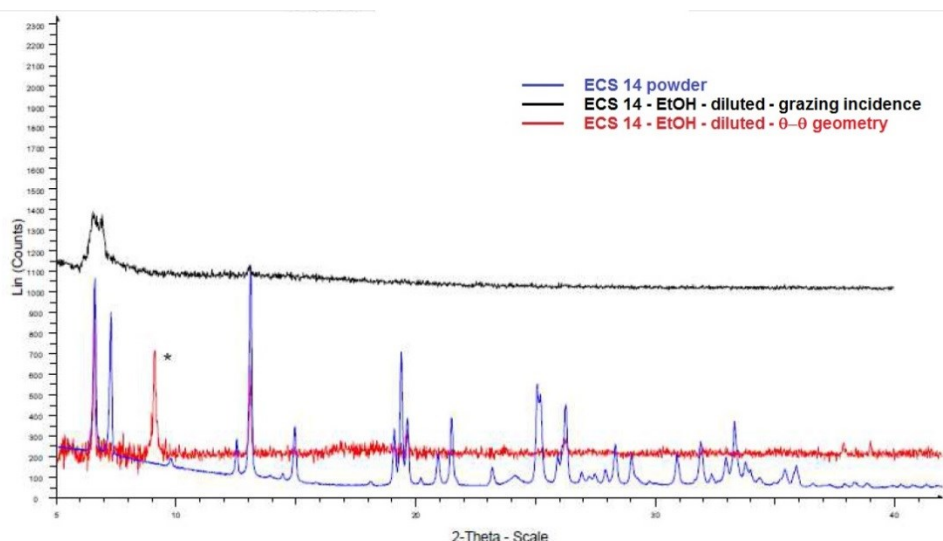
Figure 4.13. Diffraction patterns on ECS 14 powder (blue) and on films containing ECS 14 and diluted ethanol obtained by geometry θ-θ setting (red), by grazing incidence (black), (*spurious peak due to the support).

The comparison suggests that the grazing incidence setting is less effective for film iso-oriented as in the case of ECS 14 than θ-θ geometry.

The following pattern represents a comparison of the between XRD on deposition obtained by suspension containing acetic acid 5%, measured by θ-θ geometry (black), and the XRD pattern of the ECS 14 powder (blue) provided by ENI.
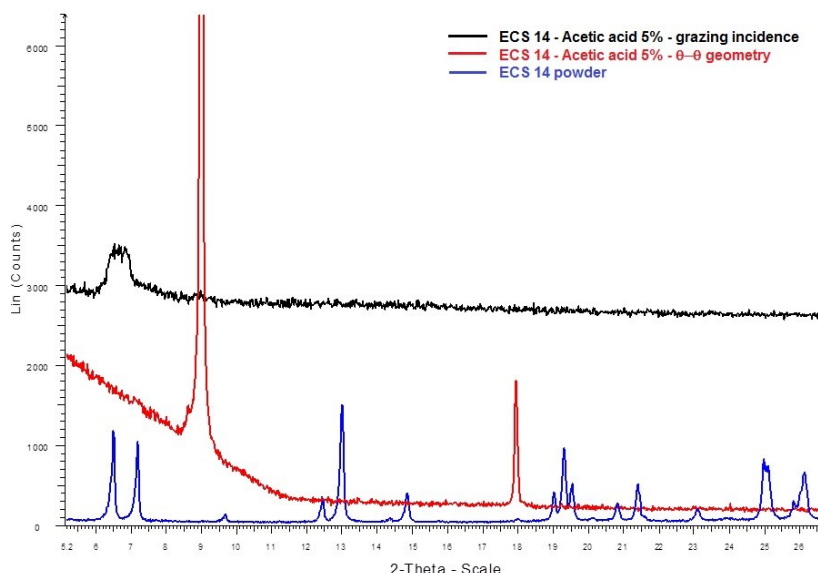
Figure 4.14. Diffraction patterns of ECS 14 powder (blue) and of films containing ECS 14 and acetic acid 5% obtained by geometry θ-θ setting (red), by grazing incidence (black).

It is noted that, except two peaks attributable to the substrate, there were no peaks attributable to the ECS 14 structure, then it must be assumed that the crystallinity of the material has been removed during treatment with acetic acid. This observation is confirmed also by grazing incidence measure.

Morphological charcaterization: Optical Microscopy and SEM

In the second level of investigation films obtained from suspensions of ECS 14 have been made for different type of solvent, the degree of dilution of the solvent (acetic acid), powder / solvent (ethanol). The following summary table indicates the samples made according to the type of solvent:

Table 4.5. Results of optical, SEM, ans XRD investigations on solutions prepared with ECS 14 and polar solvents in the second level of preliminary tests.

Solvent	Optical Microscopy, SEM	XRD
Acetic acid 5%	i) one can appreciate some massive aggregate, perhaps crystalline. Likely caused transformation due to acetic acid ii) the thickness film is uniform, it is confirmed the presence of fractures at the edges, it can be seen of fractures also in the inner part of the deposition iii) the film is well bonded on silicon substrate, the edge of the deposition is made from flakes that do not appear not adherent to the support	The crystallinity has been removed, probably acetic acid has destroyed crystal structure.

Acetic acid 10%	i) one can appreciate some massive aggregate, perhaps crystalline. Likely caused transformation due to acetic acid ii) the thickness film is uniform, it is confirmed the presence of fractures whose create flakes iii) the flakes are bonded to the silicon substrate, except at the edge	Not done
Acetic acid 40%	i) from higher magnification images one can notice a small massive aggregate, perhaps crystalline mass which is in the film. Likely caused transformation due to acetic acid ii) the film is highly fractured and tends to create flakes, whose appear to be of uniform thickness. At the edge of the deposition flakes appear larger than the inner part iii) it can be appreciated flakes both at the edge, that do not appear adherent to the silicon substrate, and inside of the deposition where appear raised from the support	Not done
Diluted ethanol	i) it can be appreciated the presence of aggregates ii) in the film will one can appreciate the single crystals, which tend to be arranged along the basal plane parallel to the support, then there is a tendency to create a continuity in the coating of the support, which however it is not complete (little material). The thickness tends to be uniform, apart from the presence of aggregates that modify such uniformity iii) the single crystals appear well bonded to silicon support	The crystallinity is evident, it can be appreciated an iso-orientation of crystals of ECS 14: basal plan parallel to the plane of the support, it was possible determine the thickness of such crystals of about 90 nm, and size of the cell parameter *c* are comparable with those reported in the literature for the powder

One can conclude that the suspensions obtained with ethanol diluted give best results:

- maintain the crystal structure,
- the crystals are arranged with the c-axis normal to the support
- good disaggregation
- good coverage
- to improve the formulation and test the adhesion on different types of support.

The structural stability of the ECS 14 in the films obtained with acetic acid is compromised.

b) ECS 5 films

Structural charcaterization: XRD diffraction

Regarding the powder ESC-5 were realized suspensions with solvents which have given encouraging results with the ECS-14powder, then acetic acid and ethanol were used.

Below XRD collections of the depositions of ECS-5 made from suspensions containing solvents such as acetic acid 5% and diluted ethanol are presented. For both depositions collections with θ-θ geometry (diffraction patterns: black and green) and grazing incidence (diffractograms: brown and fuchsia) were made. A comparisons with ECS-5 powder XRPD provided by ENI (diffractogram: blue) is also shown.

In the pattern obtained by θ-θ geometry on film containing ECS-5 and aceti acid 40%(green diffractogram), one can observe peaks, these do not correspond to those of the ECS-5 powder diffractogram; this would suggest the presence of a crystalline phase with a different structure from that of the ECS-5. In the same diffractogram, there are two more intense peaks between 18-20 ° 2θ, maybe attributable to the support. The same peaks, with less intensity, were also highlighted in the collection carried out on the same samples with grazing incidence geometry (fuchsia diffractogram).

In the depositions made with the dispersions of ECS-5 in diluted ethanol, there are no peaks interesting, probably the crystal structure was destroyed by ethanol, or the material deposited is too small to obtain an appreciable signal. Other peaks are attributable to the support.
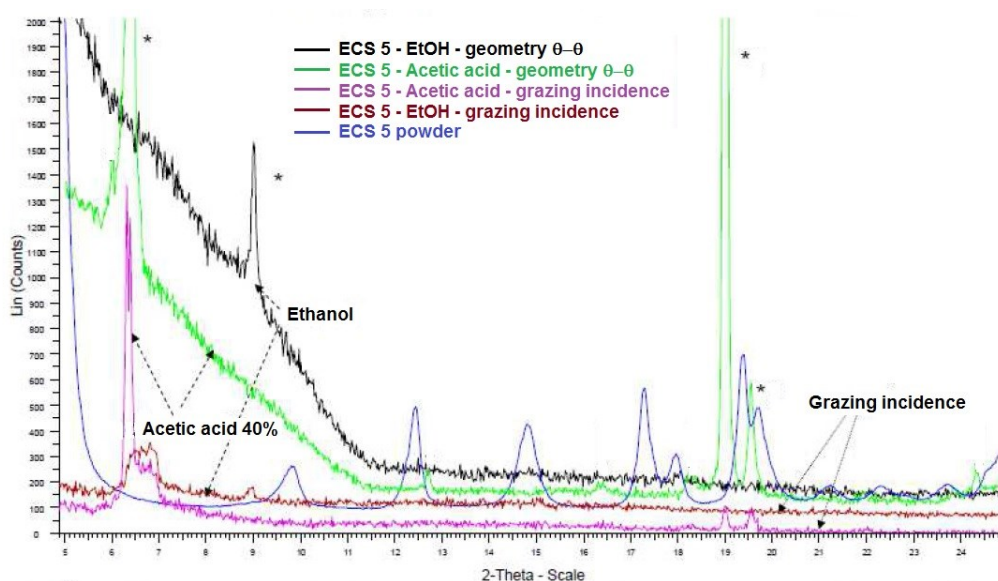
*Figure 4.15. Diffraction patterns of ECS 5 powder (blue); films containing ECS 5 and acetic acid 5% obtained both by grazing incidence (fuchsia) and θ-θ geometry (green); films containing ECS 5 and diluted ethanol obtained both by grazing incidence (red) and θ-θ geometry (black); (*spurious peak due to the support).*

The direct comparison of the diffractograms about films containig ECS14 and ECS-5 (Figure 4.16), both deposited on silicon substrates and obtained by a suspension with ethanol, points out that in the case of the ECS-14 the crystal structure is maintained, while this does not happen for the ECS-5.
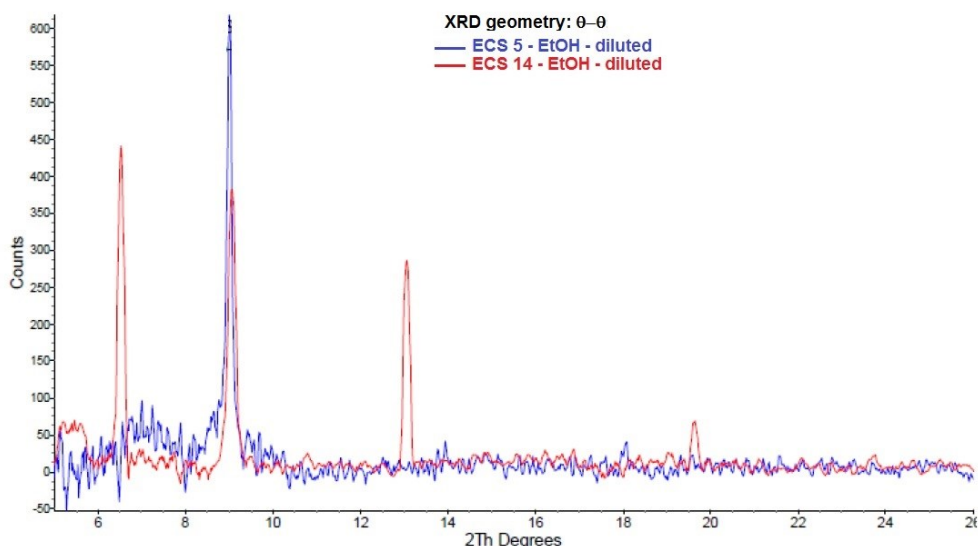
Figure 4.16. Diffraction patterns of films containing ECS 14 and diluted ethanol (red) and ECS 5 and diluted ethanol (blue) obtained both by θ-θ geometry.

As noted above, in the cases of deposition of ECS-5 with acetic acid, it is observed in the pattern the presence of diffraction peaks due perhaps to a phase recrystallized after dissolution in acetic acid. Instead, in the case of the ECS-14 there is no degree of crystallinity.

Morphological charcaterization: Optical Microscopy and SEM

It is reported below a summary table showing the suspensions used to perform the deposition on glass and silicon substrates, and corresponding observations regarding the optical microscope (transmitted and reflected light), SEM and XRD investigations.

Table 4.6. Results of optical, SEM, and XRD investigations on solutions prepared with ECS 5 and polar solvents in the second level of preliminary tests.

Solvente	*Optical microscope*	*SEM*	*XRD*
Acetico acid 40%	i) presence of agglomerates ii) the film is not characterized by uniform thickness and surface appears irregular, but continues. iii) the film looks well adherent	i) strong presence of agglomerates ii) the deposition appears divided into two zones: a central zone and a marginal zone that acts as a crown to the first, the film is not continuous between the two areas (missing material), SEM images reveal presence of a fractured mass, which incorporates aggregates / crystals iii) the material appears bonded to the silicon support	indications of crystallinity, even if the original structure is not maintained

110

Diluted Ethanol	i) strong presence of agglomerates ii) aggregates are distributed on the surface which does not appear to be continued iii) the "film" is substantially made from aggregates that appear adherent to the substrate	i) strong presence of agglomerates ii) crystalline aggregates are distributed on the surface, but there is not a continuous surface iii) aggregates appear adherent to the substrate	indications of crystallinity loss

Suspensions obtained with acetic acid show a coverage characterized by fractures and incorporated crystals. The crystal structure seems to be more sensitive to dissolution or changes caused by the solvent.

4.1.2.3 Electrical measurements

Despite the electrical characterization was one of the purposes of the second part of the research activity, it was considered that it was appropriate to verify whether depositions made so far could be used as a sensitive film, then assessing the possible electrical conductance. Therefore, as previously mentioned, the samples were also deposited on alumina substrates (2.54 mm x 2.54 mm) used in the Sensors Laboratory for designing of gas sensing devices. These substrates are composed of a platinum heater, an alumina layer, and gold interdigitated electrodes (see Figure 3.17). The following images show the films depositions on alumina both with ECS 14 (Figure 4.17) and ECS 5 (Figure 4.18).

(a)   *(b)*   *(c)*   *(d)*
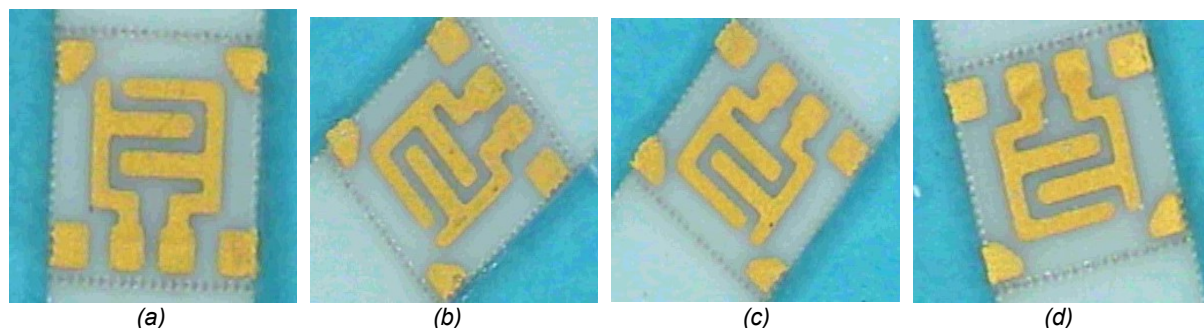
Figure 4.17. Films deposited by means of drop coating on alumina substrates (2.54 mm x 2.54 mm), and containing ECS-14 dispersed in a) acetic acid 40%; b) acetic acid10%; c) acetic acid5%, and d) diluted ethanol.

(a)   *(b)*
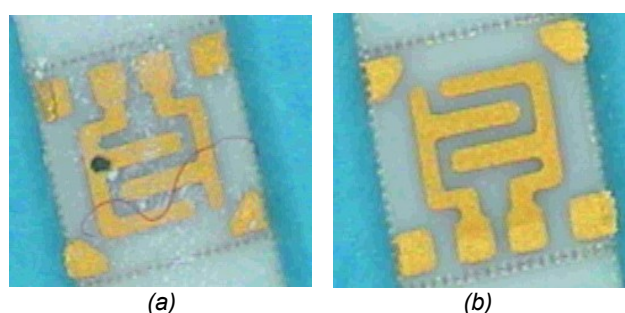
Figure 4.18: Films deposited by means of drop coating on alumina substrates (2.54 mm x 2.54 mm), and containing ECS-5 dispersed in a) acetic acid 40%; b) diluted ethanol.

Using thermo-compression technique the alumina substrates, on which six different films were deposited, were bonded with gold wire (diameter 0.06 mm) in order to connect

interdigitated electrodes on the substrate to an appropriate support for electrical conductance measurements (Figure 4.19).

For a preliminary measurement of the films resistance it was chosen to use a standard multimeter, but as expected the films were too resistant than the resolution of the instrument. Then, proceeded with the use of a dedicated test chamber in which it is possible to carried out measurements on a single device (Figure 3.23).

As described in the previous chapter, the experimental setup is based on standard electronics, sensors are placed in the test chamber in which it is possible to introduce different gases. The composition of the gas mixtures is selected through a pneumatic system mainly composed of mass flowmeters.
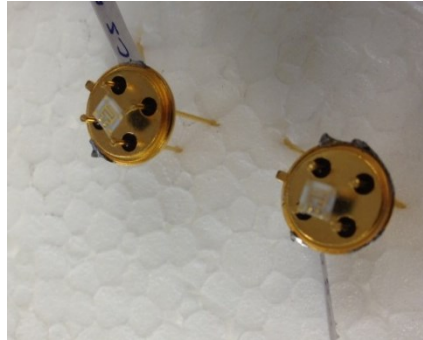
Figure 4.19. Sensors manufactured using alumina substrates covered with films containing ECS 14 and ECS 5.

The experience of the Sensors Laboratory of the University of Ferrara is based on metal-oxide semiconductors that require high temperatures in order to operate in optimal conditions. This heat is supplied through the resistor present in the substrate to which a voltage is applied. Through the power and current measurement, one can acquire the values of resistance and temperature of the device tested. The contacts interdigitated present in the alumina substrate are connected to a circuit that uses an operational amplifier circuit supplied with a constant voltage of 5 V.

The measurements were performed at a temperature of 25 ° C with a load resistor R_f of 1 GΩ in dry conditions. The following plots represent voltage measures acquired for films containing diluted ethanol and both ECS 14 (Figure 4.20) and ECS 5 (Fig 4.21).
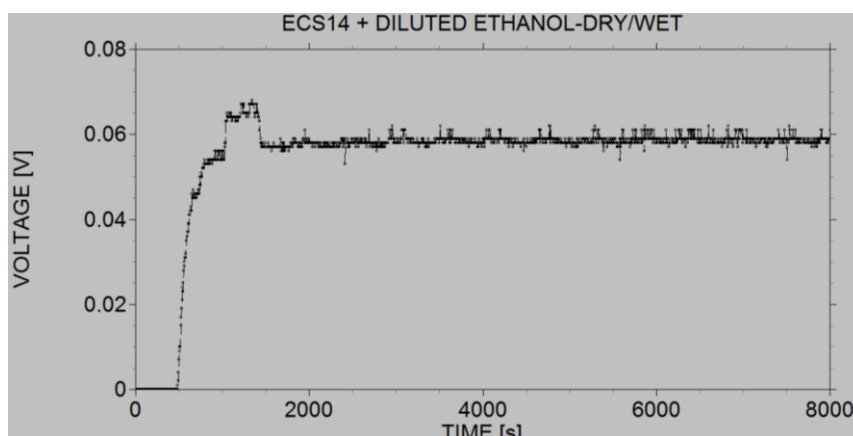
Figure 4.20. Output voltage measured with sensitive film composed of ECS-14 and diluted ethanol.

As one can observe from the graphs, the acquired signal is stable and evaluable in both measures. The SEM investigation has allowed to understand the lack of significance of the

measured signals with films based on acetic acid and at the same time has been found useful in order to improve the film-based ethanol.
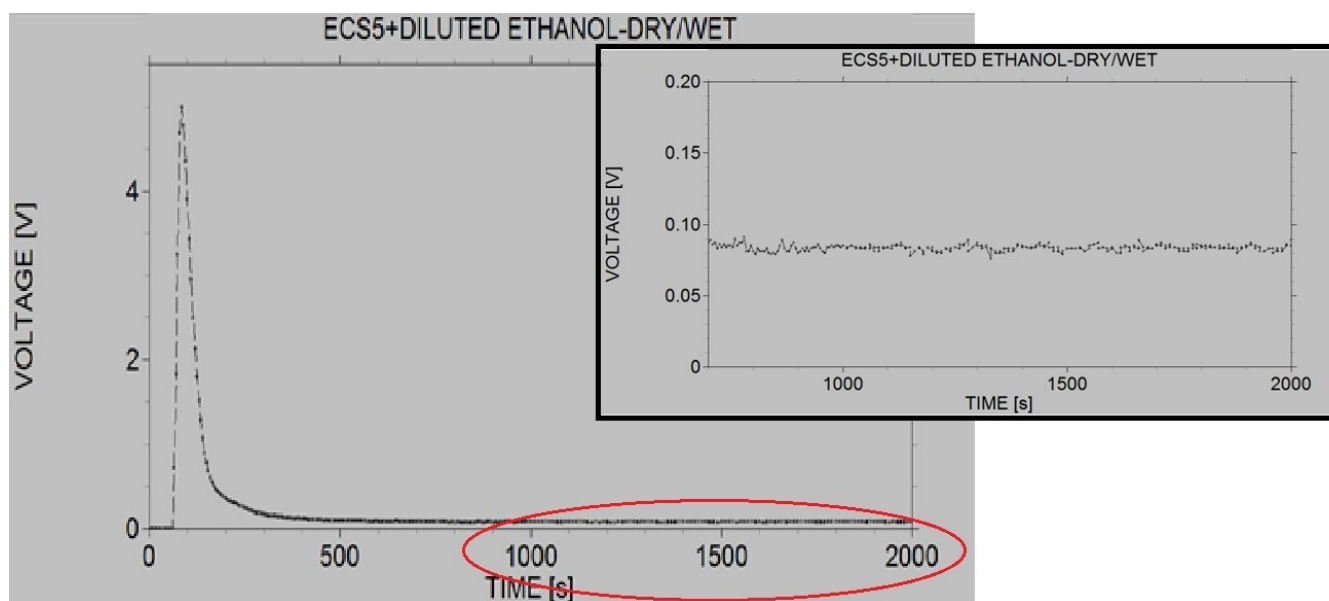
Figure 4.21. Output voltage measured with sensitive film composed of ECS-5 and diluted ethanol.

Conclusions

The tests carried out on ECS 14 and ECS 5 have led to satisfactory results, since it has been possible to deposite and handle at room temperature the films resulted adherent to the substrate. The morphological characterization above allows to draw important conclusions, useful to direct research in the second phase of this project.

The analysis by optical absorption measurements and photoluminescence allowed a preliminary assessment of the possible degradation operated by the solvents used in the dust ECS 14.

The SEM images show that there are a cracking phenomenon in films based on acetic acid, a phenomenon that decreases with the decrease of the percentage concentration of the solvent. The distance between the "clods" in the films with ECS 14 and acetic acid 40% and 10% is significant, whereas with for acetic acid 5%deposition is uniform, but there is no trace of the powder. Instead for ECS 5 with acetic acid 40%, despite the presence of cracking, the agglomerations of functional material are evident. The cracking and the powder dissolving in acetic acid are most likely the cause of the absence of electrical activity in the devices tested.

As regards the film-based dilute ethanol, the deposition is more uniform in the case of ECS 14 compared to ECS 5. In both samples, however, agglomerates of functional material are evident and the crystal structure of the powder is well distinguished. This explains the electrical transport properties recorded for devices made with these two films.

The subsequent XRD investigations have highlighted the "aggressiveness" of acetic acid, which seems to completely dissolve the powder. Therefore, the ethanol is found to be the best candidate for the production of films containing ECS materials.

The preliminary electrical measurements proved fundamental since they have shown the ability to generate electrical activity in the films, and then to use the ECS materials for the production of sensing films.

The next steps related to production of based-diluted ethanol samples both with ECS 14 and ECS 5. It will also increase the concentration of the functional material compared to the

113

previous samples, so as to obtain films more compact and to assess whether the presence of a major quantity of ECS material could affect the electrical signal measured.

On the basis of results obtained by ECS 14 and ECS 5 it was also decided to study ECS 13 by means of the same method, because it has proven very efficient from a optical point of view. The spectrometry study has been developed through collaboration with Prof. Alberto Quaranta (University of Trento).

4.2 Part II: ECS powders as sensing functional materials

The activities carried out during the first phase of the project has allowed to verify the possibility of preparing sensing devices starting from ECS powders.

It was shown that by means of drop coating technique at room temperature one can achieve handle and electrically active films in which the optical and structural properties of ECS 14 phase are maintained. Thus, since it has been achieved not only the purposes set for the preliminary study (filmability), but it was also verified the possibility of preparing the operating devices, it was decided to continue the activity both by applying to other phases ECS the method qualified in the first investigations and by expanding deposition, processing and characterization techniques.

The SEM analysis had shown the need to increase the concentration of the functional material with respect to the solvent, but also to subject the solutions to specific treatments in order to make the depositions more homogeneous and uniform. It was chosen to give priority to the optimization of the device with active layer of ECS 14 (precursor BTEB) and ECS 13 (precursor BTENaph) proved very efficient in the optical response.

During the preliminary phase, the research was focused on the powder ECS 14 as it represented the material on which Eni had provided more informations. It was considered that the crystalline state and the "plate" morphology which characterize the ECS were basic properties in order to use the powder as a functional material to the electrical conduction. Moreover, channels (7.5 Å x 9 Å) in the inorganic layer formed by facing benzene rings, main components of the molecule, should allow an easy diffusion of analytes, fundamental property for possible use in sensing field.

As the ECS 14, also ECS 13 is characterized by a crystalline state and "plate "morphology ". But the channels conformation (3.8 Å x 5.2 Å) results different because they are formed by perpendicular and not facing benzene rings, which are then orthogonal to the layers (Figure 3.12).

On the basis of the informations obtained by means of thermogravimetric analysis about ECS 14, it was chosen to continue operating at room temperature in order to produce and deposit sensing films, as in the first phase of activity.

Furthermore, since the ECS powders are hybrid materials, it was decided to develop a device with active layer obtained by the deposition of the zeolite Y, rich in aluminum, and each of organo-silane precursor in order to have references about the behavior both of inorganic and inorganic components, forming the hybrid material.

The investigations can be divided into two large families, definable as a function of the vehicle type used for making the suspensions:

    A. solvents,
    B. organic vehicles

Compared to the investigations carried out in the first phase of the study, in which solvents were used as dispersing vehicles; in the second phase, in addition to solvents organic

vehicles, generally used in the sensing field for the production of screen printing pastes oxide semiconductor based, were also used as the dispersing medium.

The implementation of screen printing paste components as dispersing medium, could represent an advantage for a contingent industrialization phase in future.

The study of the two types of dispersing vehicles were developed in parallel. This working method has not only allowed a comparison of the effectiveness of the dispersants used, in order to determine step by step which road looked better, but also in particular allowed to implement the features of different dispersants. The specific properties of individual solvents such as effectiveness dispersive/disaggregating on the powders and the ability to give continuity to the film would acquire greater value when combined in a single deposition. For this purpose, dispersions were produced with a mix of solvents. This technical solution has proved particularly effective in achieving a significant quality improvement of the films produced. In particular, given the effectiveness of the ethanol in the dispersion of the ECS powders, it was decided to add it to the organic vehicle to improve its properties and subsequently new texts with acetone have revealed disintegranting significant capacity of this solvent on the powders ECS, initially discarded.

As regards ECS materials used, it must specify that has expanded the range with respect to the investigations carried out in the first research phase in which they studied only two powders, ECS 14 and ECS 5. Therefore, in this context powders ECS 4, 5, 9, 12, 13 and 14 have been used, although studies have focused particularly on the materials ECS 13 and 14 because considered more attractive by ENI, and also because during the development of the project they have better growth prospects than other materials.

As noted above, the research activity was divided according to two courses of study based on the components used to bring the ECS powder in suspension, each path was in turn articulated in function of the investigated aspects:

A. Solvents investigation
1. Depositions with high powder/ethanolo ratio
2. Solubility tests
3. Role of ethanol and acetone

B. ECS as functional materials for screen printing paste preparation
4. Pasta
   a. Complete formulation
   b. Formulation without organic vehicle
   c. Formulation without glass frit

Finally, given the results obtained with the electrical conductivity measurements, it was necessary to understand the contribution of organic and inorganic components of ECS hybrid material.

4.2.1 Solvents investigation

4.2.1.1 Depositions with high powder/ethanol ratio

The encouraging results obtained in the first phase of activity through the use of ethanol as a solvent towards the necessity to improve the continuity of the film led to decide for an increasing of powder/solvent ratio for the production of new depositions.

In fact, the concentration of the samples prepared during the preliminary study was of 2.5 mg of powder in 0.5 ml of ethanol, it was decided to produce suspensions of 10 mg in 0.01 ml.

The following table shows the actual quantities used for each ECS material as well as specific treatments performed.

Table 4.7. ECS powder and ethanol quantities used for sample preparation with high powder/solvent ratio.

Powder	mg	Solvent	ml	Treatments
ECS 4	10.8	Ethanol	0.01	
ECS 5	11	Ethanol	0.01	TWO CYCLES OF ULTRASOUND:
ECS 9	10.1	Ethanol	0.01	15 MINUTES AT 80 °C FOR EACH CYCLE
ECS 12	10.1	Ethanol	0.01	
ECS 13	10.2	Ethanol	0.01	300 W POWER
ECS 14	11.2	Ethanol	0.01	

The solutions were deposited onto microscopy glass slides (20*20 mm^2) by means of the drop coating and dried under a hood at room temperature. Investigations by optical microscope, carried out by Dr. Casotti, are shown in Appendix B table B1, in which some fundamental aspects for the characterization have been taken into account for the samples gradually prepared during the second phase of activity. The images taken at the Laboratory Sensors were necessary for a preliminary analysis of the samples investigated, in order to be able to address the continuation of the study, but they are not presented here.

At a first analysis, one can say that the depositions are linked by the presence of agglomerates and, although there is not a uniform thickness, they are characterized by the presence of a film which gives continuity to the deposition itself. Moreover, all films were coated on the glass support.
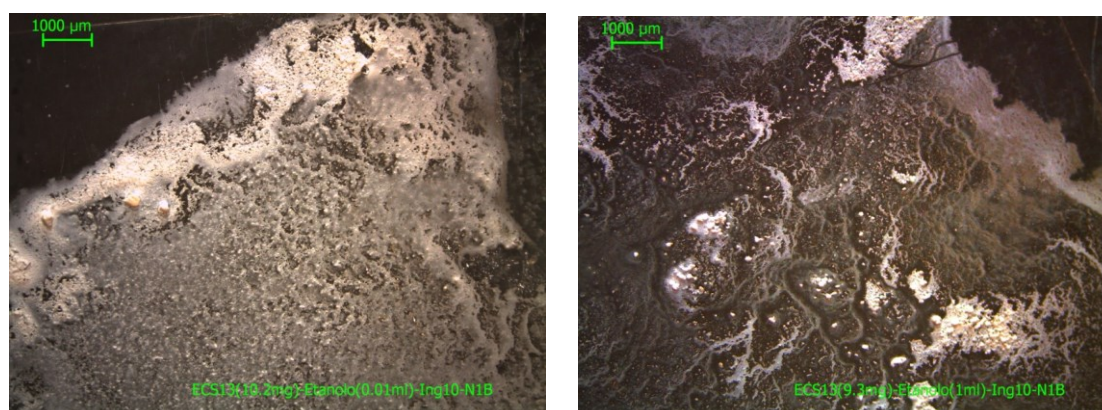
*Figure 4.22. Images obtained in reflected light setting with optical microscope (magnification 10) on a) **high** and b) **low** ECS-13/ethanol ratio film deposited by means of drop coating on microscope slide.*

The deposition of high powder/ethanol ratio carried out in the second phase of activity (Figure 4.22 a) has a greater continuity than low ratio prepared in the first phase during preliminary study (Fig. 4.22 b). However, it is observed the inability of ethanol to breakdown, to which successively it has been provided both through the use of specific treatments and by the addition to the suspension of other components.

4.2.1.2 Solubility tests

The results obtained during the first phase of activity regarding the study of solubility were satisfactory and it was opted for the expansion of this study to all six powders delivered by ENI using different solvents, polar and nonpolar. The goal was not only to confirm the results obtained in the preliminary phase, but also their compatibility with those related to powders not yet tested so far.

Table 4.8. ECS powders and solvents quantities used for sample preparation.

Powder	mg	Solvent	ml	Treatments
ESC 14	10	Ethanol	0.5	
	4.8	Benzene	0.25	
	5.2	Acetone	0.25	
	5.4	Chloroform	0.25	
ECS 4	3.2	Ethanol	0.25	
	5.4	Benzene	0.25	
	4.9	Acetone	0.25	
	5	Chloroform	0.25	
ECS 5	10.3	Ethanol	0.5	
	4.7	Benzene	0.25	
	5	Acetone	0.25	TWO CYCLES OF ULTRASOUND:
	4.9	Toluene	0.25	
ECS 9	5.2	Ethanol	0.25	1. 20 MINUTES AT 300 W and 20 °C
	4.9	Benzene	0.25	2. 20 MINUTES AT 300 W and 50 °C
	4.8	Acetone	0.25	
	4.8	Toluene	0.25	
ECS 12	4.6	Ethanol	0.25	
	4.3	Benzene	0.25	
	4.6	Acetone	0.25	
	4.6	Toluene	0.25	
ECS 13	9.3	Ethanol	1	
	2.3	Benzene	0.25	
	6	Acetone	0.25	
	4.7	Toluene	0.25	

The solutions were deposited onto microscopy glass slides (20*20 mm^2) by means of the drop coating and dried under a hood at room temperature.
Further investigations by optical microscope, carried out by Dr. Casotti, are shown in Appendix B table B2; two of those images regard the same solutions containing ECS 14 powder and ethanol, but the two films were deposited in two different moments.
During the first half of the activity had already been tested toluene with ECS 14 powder and the resulting solution showed a significant remains on the bottom, so that for both ECS 14 and 4 (having the same precursor, BTEB) was prepared a solution with chloroform instead of the one with toluene. The other powders were instead tested with toluene for completeness with respect to the preliminary tests.
The decision of testing again polar and nonpolar solvents was make primarily to verify the results initially obtained and, in addition, the assessment on the dispersion degree of the solutions and the study by optical microscope on the depositions have confirmed that all six powders are allied to polar solvents.

Regard the depositions analysis, it has to refer to the morphological and structural characterizations performed by the group of prof. Cruciani. The images taken at the Laboratory Sensors were necessary for a preliminary analysis of the samples investigated, in order to be able to address the continuation of the study, but they are not presented here.

Looking at the picture above, it can be concluded that the depositions are characterized by the presence of agglomerates, which however has not been possible to determine whether this is a set of particles or aggregates. The film deposited for the most part present a wide particle size distribution. The depositions containing nonpolar solvents such as benzene, toluene and chloroform are not characterized by uniform thickness and continuity and do not present thin films. On the contrary, the depositions containing polar solvents, acetone and ethanol, although not present a uniform thickness, however are characterized by the presence of a film which gives continuity to the deposition itself. All films were coated on the glass support.

For the sensors optimization is important to the ability of solvents to confer uniformity to the films and to disaggregate powder clusters to obtain a narrow particle size distribution curve moved to fine particles.

Therefore, it was necessary to prepare new samples using solvents and techniques that would allow to make more effective disaggregation.

About this aspect, the choice to retest acetone was convenient: in fact, despite until that moment ethanol (Figure 4.23 a) has been proved suitable for the production of sufficiently continuous films, it seems that acetone (Figure 4.23 b) may confer greater disaggregation.
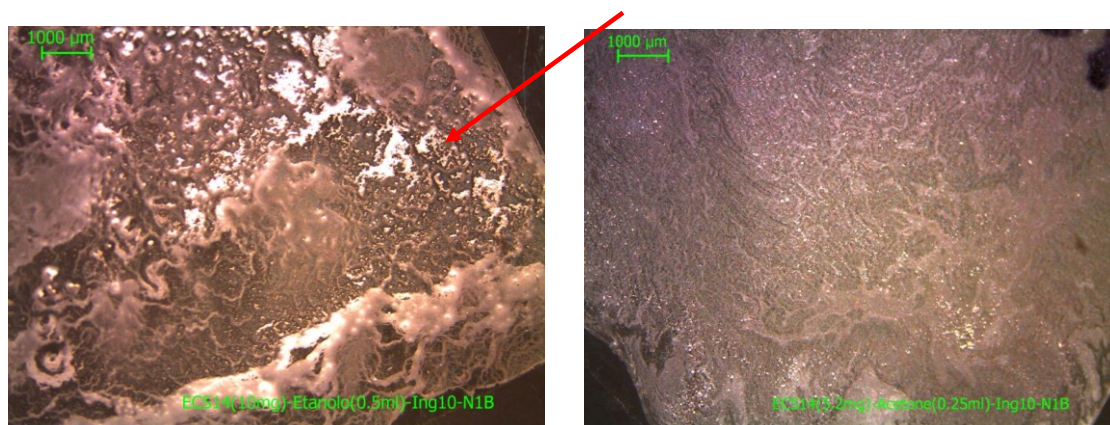
*Figure 4.23. Images obtained in reflected light setting with optical microscope (magnification 10) on a) ECS-14/**ethanol** and b) ECS-14/**acetone** film deposited by means of drop coating on microscope slide [red arrows indicate particle agglomerates].*

The next step was to create a suspensions containing both ethanol and acetone so to verify if the union of the two solvents in a single sample confer it, respectively, the continuity of the film given by ethanol and the dissagregation by acetone.

4.2.1.3 Role of ethanol and acetone

On the basis of the results obtained in the previous tests, the preparation of the suspensions and relative depositions was carried out in two steps in order to study, in addition to the combined action of more solvents (ethanol and acetone), also the effect of a ultrasonic treatment with higher power (600 W instead of 300 W) on ECS powder suspensions both with single solvent and with combination of ethanol and acetone.

I. Samples containing ECS powder and single solvent

Table 4.9. ECS powders and solvents quantities used for sample preparation

Powder	mg	Solvent	ml	Treatments
ECS 14	50.3	Ethanol	0.01	ONE ULTRASOUND CYCLE: 60 MINUTES AT 50 °C AND POWER 600 W
	49.7	Acetone	0.01	
ECS 13	50.1	Ethanol	0.01	
	49.2	Acetone	0.01	

It must specify that samples prepared in this step were placed in direct contact with the ultrasonic bath, while the samples described in the previous paragraphs were placed in a glass becker immersed in the ultrasonic bath. This explains the use, for the samples in question, of a lower temperature during the treatment (50 ° C instead of 80 ° C).

The solutions were deposited onto glass slides for microscopy 20 * 20 mm^2 by means of the drop coating, except for the sample containing ECS 14 and acetone whose density had not allowed the deposition through pasteur pipette, after all the study of a deposition by means of spatula would result not very productive. Below images made by optical microscope Sensors Laboratory are shown.

(a) (b) (c)
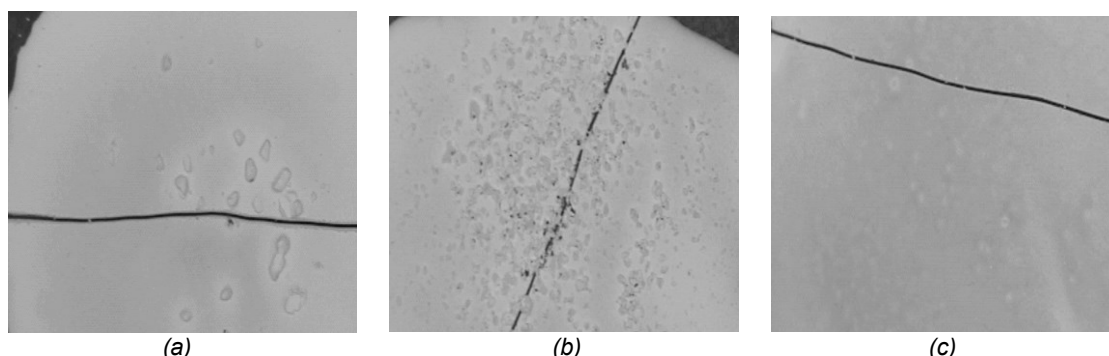
*Figure 4.24. Depositions on microscope slides of solutions containing **ethanol** and a) ECS 14, b) ECS 13, and c) **acetone** and ECS 13.*

Looking at the images in Figure 4.24 one can formulate two main considerations:
- acetone has disaggregating action than ethanol which instead has an covering action, probably surface active;
- the use of double power ultrasound, compared to the treatments performed in the samples described in the first two points of the research, had permitted to deposit films characterized by a minor presence of agglomerates than the depositions described in the first two points, despite the amount of ECS material was even five times higher than samples made in step 1 in the suspension with high powder / ethanol ratio.

II. Samples containing ECS powder and a combination of ethanol and acetone

Table 4.10. ECS powders and solvents quantities used for sample preparation

Powder	mg	Solvent	ml	Solvent	ml	Treatments
ECS 14	50.3	Ethanol	0.01	Ethanol	0.01	ONE ULTRASOUND CYCLE: 60 MINUTES AT 50 °C AND POWER 600 W
	49.7	Acetone	0.01	Acetone	0.01	
ECS 13	50.1	Ethanol	0.01	Ethanol	0.01	
	49.2	Acetone	0.01	Acetone	0.01	

The solutions were deposited by means of the drop coating on microscope slides 20 * 20 mm^2 and on silicon substrates for the analysis by optical microscope (see table B3), for XRD and SEM (see table B4) investigations, and on alumina 2.54 * 2.54 mm^2 for the realization of sensing devices.

Below images made by optical microscope Sensors Laboratory (alumina) are shown.

(a)   (b)
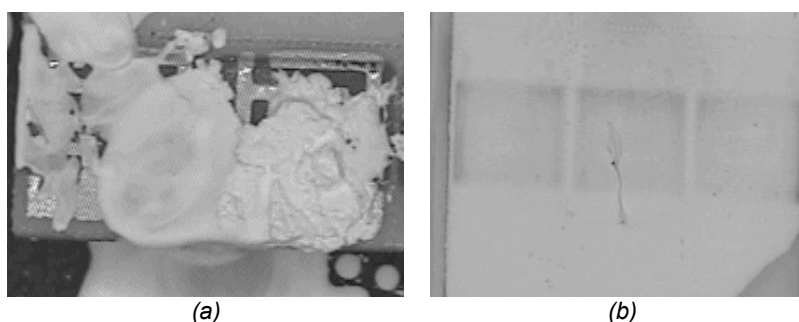
*Figure 4.27. Films deposited on alumina starting from solutions of a) **ECS 14** and **ethanol-acetone,** b) **ECS 14** and **acetone-ethanol**.*

(a)   (b)
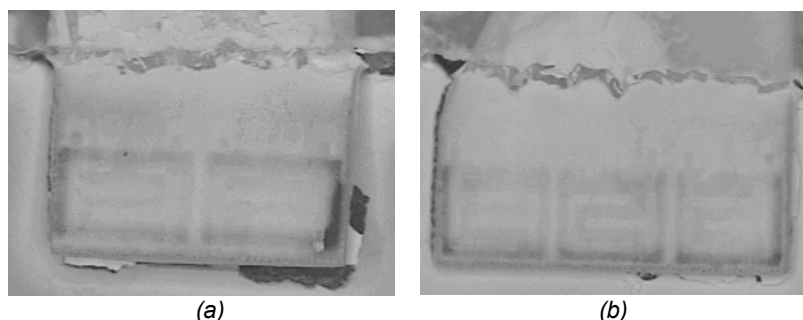
*Figure 4.28. Films deposited on alumina starting from solutions of a) **ECS 13** con **ethanol- acetone** b) **ECS 13** and **acetone-ethanol**.*

Comparing the depositions with single solvent in Figure 4.26 with those in Figure 4.27-28 related to the solvents mix one can observe that the combined action of ethanol and acetone, together with the use of a second cycle of high power ultrasound, allowed to break up the agglomerates which persisted in the single solvent deposition.

The order in which solvents are used does not appear crucial: only in the deposition of ECS 14 with ethanol-acetone on alumina (Fig. 4.27 a) there are still some clumping.

It could be concluded that it is necessary to treat the suspension containing ECS powder using high power ultrasound because they allow a greater particles disaggregation, whose structure is not modified as deduced from XRD investigations conducted by the group of Prof. Cruciani and discussed forward.

Furthermore, the combined action of ethanol and acetone allows the elimination of aggregates / agglomerates in the suspension. As regards the order of use would be required further investigation for each of the six powders delivered by ENI.

4.2.1.4 Morphological characterizations

Depositions with high powder/ethanol ratio: optical microscopy

As evidenced by the analysis presented in table B1 (Appendix B), there was a lack of disagglomeration / disaggregation ECS powders. This aspect induces to hypothesize a low proportion of fine material, since the material remains aggregated, consequently there is not a good coating. However, for the materials ECS 13 and 14 one can observe a better coating than the other powders ECS, this suggests that ethanol is particularly effective to make films containing the materials ECS 13 and 14. The latter consideration is in line with the request for ENI to focus the investigation on these two materials.

Solubility tests: optical microscopy

From analysis of table B2 presented in Appendix B, it is noted that generally the depositions, which produce quality films have been constituted by polar solvents (ethanol and acetone), while the depositions with nonpolar solvents (benzene, toluene and chloroform) are problematic.

It can observe in many cases depositions are characterized of a thin film. It is a continuous semitransparent film of not certain origin. The thin film differs from the film (as referred to in the comments), because the latter is covering, opaque or semi-opaque.

Even in this case solvents, which tend to generate such a thin film, are polar solvents, in line with the results obtained in the first activity phase. The polar solvents tend to give a continuity, even if the disagglomeration and disaggregation occurs in several cases, however only in part.

So far, polar solvents have not generated continuous films, only in some cases seems to be present a thin film that is often continuous. The thickness of films is not always uniform, since the presence of aggregates and / or agglomerates alters their uniformity. Anyway, the films appear coated on the surface.

The decision to re-test acetone, which at first had been discarded, resulted appropriate because it gave interesting indications to its use to obtain useful films for gas sensing design.

In particular for ECS 14, there have been obtained the best results using acetone and ethanol: acetone gave good disintegrants / disagglomeranting properties, while ethanol of well-coverage.

These issues have prompted the idea of creating a new set of experiments about the combination of ethanol and acetone in a unique solution, as will be shown later that have produced very good results.

Role of ethanol and acetone: optical microscopy and SEM

The comparison between the deposition obtained with the powders ECS 13 and 14 realized with a single solvent, ethanol and acetone, in this step and the depositions obtained with the same powders and solvents made in the previous two steps, indicating a better success of the latter depositions produced. This improvement is most likely due to the increase of ultrasonic power.

As regards the deposition obtained with the mix of solvents, it can be seen not only a general improvement of the depositions compared to those of steps 1 and 2, but also to those obtained in step 3 with single solvent.

In particular, both for the ECS 14 and ECS 13, depositions obtained by adding acetone starting from suspensions made from the powder in ethanol seem to be the best.

Observations of the SEM images about the depositions made both with ECS 13 and 14 powder dispersed in a mixture of solvents indicate a substantial similarity of the surfaces, characterized by aggregates and cracks, even if depositions containing ECS14 are individual particles clearly visible.

Based on the characteristics at high magnification (SEM) of the depositions surfaces, it can be observed that for the same powder they are similar, then it could seems that the succession of the solvents used for the realization of the suspension do not have importance. Instead, a lower magnification (optical microscope), one can notice some differences compared to the characteristics of surface quality of the depositions.

Therefore, it can be concluded that only at low magnification, it is possible to appreciate the importance of the sequence in the addition of solvents for the realization of " mixed suspensions " in order to obtain a deposition of higher quality.

4.2.1.5 Structural characterizations

Role of ethanol and acetone: optical microscopy and SEM

XRD collections were carried out on the following samples:
- pure powder ECS 13 and 14 as provided by ENI;
- deposition obtained with powders suspended in ethanol to which was added to the suspension of acetone;
- depositing powder obtained by ECS powders suspended in acetone to which was added to the suspension in the ethanol.

Below the investigations carried out by XRD on the depositions made using suspensions created with the mixture of solvents, and the material ECS 13 as provided by ENI, as well as the comparison between the diffraction patterns (in order to optimize the comparison, the dark was subtracted).

The relative comparison of the ECS 13 powder diffractogram with the diffraction patterns of the depositions on a monocrystalline silicon support (zero back-ground) obtained by the suspension of the two solvents and ECS 13 shows a maintenance of the powder crystallinity (only a bit structural variations). But it also does not show a particular crystallites iso-orientation.

In particular, there was an increase in intensity of the peak at 7-8 ° 2-Theta, the diffractograms obtained from films of mixed solutions than the pure powder. This peak is not known to belong to the ECS 13 structure, then it is probably due to contamination or a residue of the synthesis.
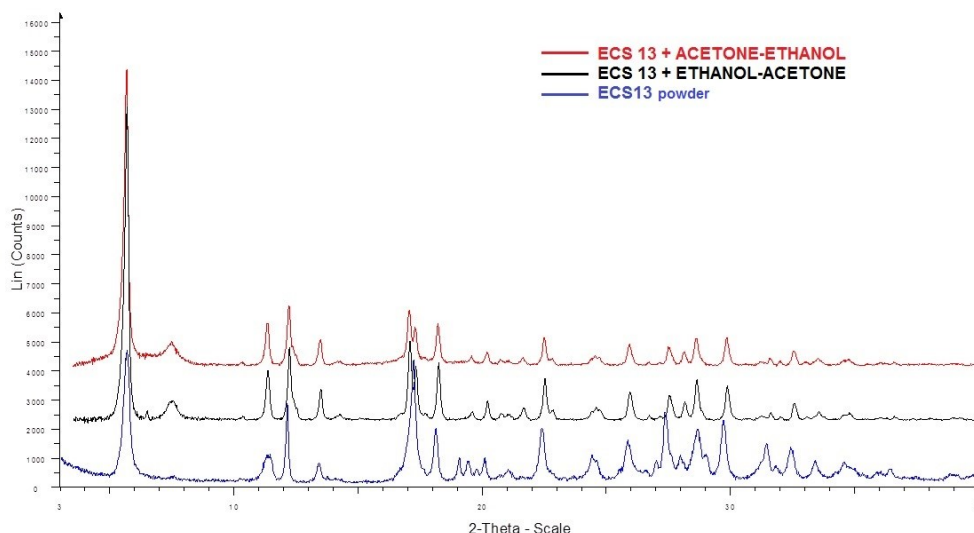
Figure 4.29. Diffraction patterns of films containing ECS 13 and acetone with adding of ethanol (red), ECS 13 and ethanol with adding of acetone (black) and ECS 13 pure powder (blue).

An increase was also present in the peak between 12-13 ° 2-Theta, diffraction patterns obtained from films of mixed solutions compared to powder as it is. At 17 ° 2-Theta it has the splitting of the peak compared to single peak present in the diffraction patterns obtained from the pure powder. In the area between 19-20° 2-Theta there is the disappearance of two peaks in the diffraction patterns obtained from films of mixed solutions compared to ECS 13 powder. In the area between 27- 28 ° 2-Theta one can notice a decrease in the intensity of a couple of peaks (one in particular) with respect to the pure powder.

In general it can be said that the increase of intensity of the peaks is attributable to an increase in the crystallinity of the material, while the disappearance of the peaks is attributable to a slight structural modification of the material.

Below the investigations carried out by XRD on the depositions made using suspensions created with the mixture of solvents, and the material ECS 14 as provided by ENI, as well as the comparison between the diffraction patterns (in order to optimize the comparison, the dark was subtracted).
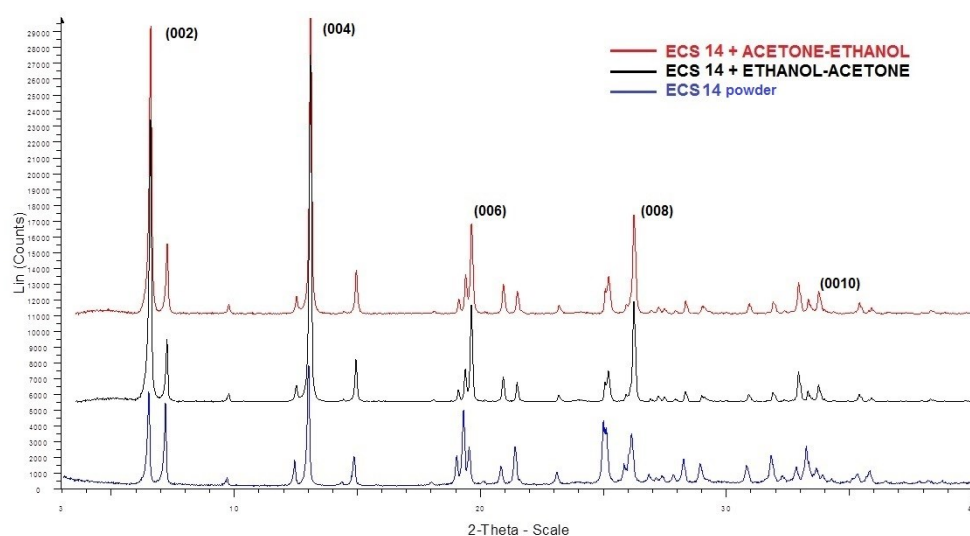
Figure 4.30. Diffraction patterns of films containing ECS 14 and acetone with adding of ethanol (red), ECS 14 and ethanol with adding of acetone (black) and ECS 14 pure powder (blue).

123

The relative comparison of the powder diffractogram with the diffraction patterns of the depositions on a monocrystalline silicon support (zero back-ground) obtained by the suspension of the two solvents and ECS 14 shows the maintenance of crystallinity (structural stability) of the ECS 14 powder. There was also a significant iso-orientation of the crystallites on the plane (001). This aspect is evidenced by the peaks intensity ratio of the basal reflections (indicated in the Figure 4.30) with respect to the corresponding basal peaks of the pure powder. One can note that the peaks mentioned above are relatively more intense in depositions obtained from mixed solvents samples compared to pure powder.

Conclusions

The preparation of suspensions for ECS 13 and 14 powders obtained by a mixture of solvents (ethanol, acetone) had given an improvement of the depositions (observed at low magnification: optical microscope), compared to the deposition obtained with a suspension consisting of a single solvent. At higher magnifications (SEM) there are no terms of comparison with depositions made with a single solvent but in all depositions it is possible to observe the presence of fractures. Moreover, the depositions obtained with the same powder seem highlight substantial differences (SEM images). It was also seen that a probable structural alteration and an increase in crystallinity for ECS 13 powder occur. On the other hand, the depositions carried out with ECS 14 powder and appears significant crystallites iso-orientation.

Another important aspect is the beneficial effect for the optimization of the depositions (disagglomeration / disaggregation) of the ECS powders produced by using relatively high power ultrasound.

Finally, the XRD investigations have allowed to establish that in the deposition obtained with the ECS 13 powder dispersed in the solvents mixture there are structural variations and an estimated increase in the crystallinity, while the depositions obtained with ECS powder 14 dispersed in the solvents mixture maintain stable the crystalline structure and there is a relevant crystals iso-orientation.

4.2.2 ECS as functional materials for screen printing paste preparation

On the basis of previous experience of the Sensors group about metal- oxides semiconductors as sensing films, it was decided to use the powders ECS as functional material in the process refined for the production of printing pastes for thick film.

The paste is produced by combining three main components:

- the functional material, generally a powder nanometer, which dominates the electrical properties of the film and sensing;
- the glass frit, a vitreous compound that has the task to promote adhesion between the particles and the layer to the substrate after heat treatment;
- the organic vehicle, composed of a polymer / resin added to a volatile solvent which act respectively by the provisional bonding of the powders and as a regulator of the viscosity of the dough, giving it the characteristic of printability.

Depending on the use of the thick film may be absent and the frit may be added, in a very low percentage by weight catalysts and other additives.

The research on the preparation of pastes powders ECS was divided into three steps:

a) use of the complete formulation containing functional material, frit and organic vehicle;
b) elimination of the organic from the total formrulation;
c) elimination of the frit from the total formulation.

The choice of developing the activity according to this path will be motivated in the step by step description of the experimental procedure to each passage.

4.2.2.1 Study of paste component's contributions

a) COMPLETE FORMULATION

In anticipation of making a greater number of depositions for the same sample, it was chosen to use quantities of ECS powder exceed the suspension up to here described. The ECS powders were brought into solution by adding glass frit and organic vehicle.

Table 4.11. Quantity of ECS powders used in the preparation of pastes.

Powder	ECS 14	ECS 4	ECS 5	ECS 9	ECS 12	ECS 13
mg	199	103.1	104	101.6	103.3	106.5

According to the following steps, several statements were made:
I.   the samples were not subjected to ultrasonic treatment but simply manually mixed and deposited on <u>microscope slides</u> (for the optical microscope investigation) by drop coating. The samples deposited on glass were subsequently heated to 100 ° C for 30 minutes, except for ECS 9 and 12 heated at 50 ° C for 3 hours (because were prepared subsequently to the other samples);
II. to the samples described above it was added 25 microliters of absolute ethanol except for ECS 14, for which 50 microliters were used since the amount of powder employed was double than that used for the other ECSs. It was not performed any specific treatment, the samples were hand blended and deposited onto <u>slides for microscopy</u> (for optical microscope investigation), <u>silicon</u> (for SEM, XRD, thermal analysis) and on <u>alumina supports</u> (for electrical characterization) through drop coating.

Investigations by optical microscope and SEM, carried out by Dr. Casotti, are shown in table B5 and B6 Appendix B respectively. Deposition on alumina substrates are showed in tables B10-B16.The images taken at the Laboratory Sensors were necessary for a preliminary analysis of the samples investigated, in order to be able to address the continuation of the study, but they are not presented here.

From the images in table B6 it can be observed that the addition of ethanol allowed to confer greater continuity to the films, characteristic already investigated in the previous paragraph. However, the images also show the persistence of agglomerates, for which it was necessary to investigate further the suspension to identify "unwanted" components and/or appropriate techniques that confer uniformity to the films.
Therefore, it was decided to investigate the action of each component of the complete formulation of the paste in order to understand if the formation of agglomerates depended on one rather than the other: first the glass frit (point b) and then the organic vehicle (point c). It was also used different treatments, ultrasound in the first case (point b) and magnetic stirring in the second (point c), in order to evaluate the effect of each on the two suspension.
The action of the acetone as disaggregating agent and of high power ultrasound had not taken into account in the study of the powder ECS as a functional material for the paste, since their effects were identified retrospectively compared to the execution time of the samples described above.

b) FORMULATION BASED ON GLASS FRIT

As mentioned in the comments on the depositions made by using the complete paste formulation (functional material, glass frit and organic vehicle), it was required a thorough investigation on the action of each component to see if the formation of agglomerates depended on one rather than from 'other.

In this part it will be described the procedure by which the samples were prepared by using ECS powder and frit, then eliminating the organic vehicle from the complete formulation. Since this is only a test of disaggregation, it was not considered necessary to use all six ECS powders, so it was chosen to use only ECS 14 and 13, indicated by ENI as materials to be favored in the study of possible sensing phenomena. The amount of powder used was reduced by half compared to the suspensions described in point a (complete formulation), in order to avoid unnecessary wastage of material.

Table 4.12. Amount of ECS powder used in the paste formulation with the elimination of the organic system.

Powder	ECS 14	ECS 13
mg	50.2	50.5
Frit [mg]	1.2	1.2
Ethanol [ml]	0.05	0.05

The ECS powders were put into solution by adding glass frit and ethanol, the latter had played only the function of solvent considering the solid consistency both of the functional material and frit, so it was necessary employ a larger amount of ethanol in order to obtain a suspension density was that to allow the deposition by means of the drop coating.

The suspensions were treated using two cycles of ultrasound, for 15 minutes each one, with power of 300 W and bath heated at 80 ° C. The test tubes containing the suspensions were not put directly in contact with the bath, but were put in a becker in turn immersed in the bath.

The two solutions were deposited on microscope slides by drop coating. The disaggregating action of the acetone and of high power ultrasound had not taken into account in the study, since it had been identified retrospectively compared to the execution time of the samples in question.

On the contrary of samples prepared following complete paste formulation for which the paste were made by manually mixing the three components, one can observe that in the preparation of these suspensions ultrasound were used.

Looking at the pictures in Table B7 (Appendix B) one can see that the films are not uniform and present again considerable size agglomerations. Consequently, it was not considered convenient to achieve the sensing devices starting from suspensions made.

Then, it has opted for the elimination of the frit from the paste mixture: in fact the evidence just discussed, when compared with the depositions made using the complete paste formulation, leaving to assume that the formation of agglomerates is caused by the presence of glassy oxides given their more compact consistency than that of the ECS powder. Moreover, the glass frit requires very high melting temperatures to actually become functional in the sintering of the powder, but these temperatures cannot be reached by the ECS materials since it would be degraded.

c) FORMULATION BASED ON ORGANIC VEHICLE

Based on the considerations developed in the previous paragraphs, it was decided to produce solutions containing ECS powders and organic vehicle without glass frit.

Furthermore, it was used a double percentage of the organic vehicle compared to the complete paste formulation described in section a.

In anticipation of making a greater number of depositions starting from the same solution, it was chosen to use significant quantities of ECS powders than test carried out with the use of the glass frit.

Table 4.13. Amount of ECS powders used in the formulation of the paste with elimination of glass frit.

Powder	ECS 14	ECS 4	ECS 5	ECS 9	ECS 12	ECS 13
mg	102.8	102.8	102.8	102.8	102.8	102.8

According to the following steps, several statements were made:

I. after being subjected to two cycles of ultrasonic each of one hour and 300 W of power and immersed in the bath at 50 ° C, the sample were deposited on <u>glass slides for microscopy</u> through the use of the spatula and on <u>alumina supports</u> by capillarity using pasteur pipettes. The suspensions were too dense to be filed by drop coating. Then, it was decided to operate on the composition of "pasta" keeping the same type of treatment;

II. 10 microliters of absolute ethanol were added to the samples described above which were subjected to magnetic stirring for about 12 hours. This choice was dictated by the fact that the preliminary analysis performed with the optical microscope on the samples described in the previous point of this section showed a reduction of the agglomerates with respect to the deposition produced with formulations described in points a and b, even if had not been complete eliminated. Therefore, it was decided to use another different treatment as well as the addition of ethanol which already proved to be a useful solvent. Then, the suspensions were deposited on <u>microscope slides, silicon and on alumina supports</u> by drop coating, except the samples containing ECS 9 and 12 deposited on a glass slide and silicon by means of spatula and on alumina by capillarity of the pasteur pipette because of the density of the suspension.

The images presented in Table B8 and B9 were made by Dr. Casotti, respectively through optical microscope and SEM analysis. Deposition on alumina substrates are showed in tables B10-B16.

Images related to the depositions on glass about suspensions containing ECS powder and organic vehicle treated with ultrasound show the persistence of agglomerates, even if in smaller quantities and size compared to the samples containing also glass frit and not treated with ultrasound, presented in point a. However, it can be seen that the addition of ethanol gave a greater continuity to the film, characteristic already investigated in the course of the research, instead the introduction of magnetic agitation such as disaggregating treatment had conferred greater uniformity to the films considerably reducing the quantity and size of the agglomerates.

The disaggregating action of the acetone and of high power ultrasound had not been taken into account in the study of the ECS powder as a functional material for the paste, since it had been identified retrospectively compared to the execution time of the samples.

The depositions containing ECS 14 and 13 are resulted more uniform than those containing other ECS powders. A more in-depth analysis about the characteristics of the depositions will be discussed in the next section and in Appendix B, thanks to chacterizations performed by group of Prof. Cruciani.

From the study of suspensions in complete paste formulation was revealed the need to identify "unwanted" components and/or appropriate techniques that would give continuity and consistency to the film.

The targeted choices made during the research development had led to define a suitable formulation to obtain suspensions whose density allows to suppose the possible use of the screen printing technique. Neverless the films obtained by formulation described above have characteristics of adhesion, continuity and uniformity necessary for the realization of sensing devices. It is desirable further investigations concerning the action of acetone on the paste formulation without glass frit and the comparison of this effect with that obtained with magnetic stirring treatment.

4.2.2.2 Morphological characterizations

Complete paste formulation

The comparison between films (tables B5 and B6 in Appendix B) obtained using ECS powders as functional material in complete paste formulation with and without the addition of ethanol shows an inability of the solvent to operate as disagglomeration/disaggregation agent; although one can observe an improvement of the deposition obtained by ECS 13 in which ethanol was present, compared to that without ethanol.

In general, observing the SEM images show in table B6 one can note a common presence of coarse elements and a poor granulometric selection, but also the presence of fractures for various depositions. Only for the depositions containing powders ECS 13 and 14, you can highlight a good size selection.

Formulation based on glass frit

Analyzing optical microscopy images (table B7 in Appendix B), it is evident the still presence coarse elements, in fact there was not a disagglomeration. Therefore, it is confirmed that the glass frit has a negative effect on the disaggregation/disagglomeration, despite in the preparation of these samples ultrasound are also used to achieve this purpose.

The next step was to understand what would happen by removing the glass frit in the preparation of the suspension, replacing it with organic vehicle.

Furthermore, the elimination of the glass frit is also linked to the requirements of heat treatments at high temperature during the processing, but it is known that high temperature are closed to ECS powders due to their crystallographic stability.

Formulation based on organic vehicle

By optical microscopy images analysis (table B8 in Appendix B), it appears that the depositions obtained with ECS powders dispersed in organic vehicle without glass frit and with the addition of ethanol give depositions far better than those without ethanol. The presence of ethanol improves the continuity, consistency and in such way also disaggregation.

From SEM observations for the depositions obtained from suspensions of powders ECS added to organic vehicle (not frit) and ethanol (table B9 in Appendix B) can be seen the presence of cracks as common feature, and only for the depositions ECS 13 and 14 has a good selection of the particles. This aspect also appeared in photos by optical microscopy. Moreover, by the same picture can be seen that the particles tend to aggregate reducing the

surface porosity of the system. On the contrary for ECS 13 and especially for ECS 14 powder there is a significant surface porosity, since the particles that tend more to aggregation than to agglomeration. This aspect in the sensors operating process could prove very useful, since an "open" and diffused porosity could allow exponentially to increase the sensitive area of the ECS layer, improving the sensitivity of the sensor.

Considering the results obtained from studies carried out in the previous steps, one can concluded that however ethanol has a positive effect in the disagglomeration / disaggregazione of ECS materials dispersed in organic vehicle. The action of this solvent is strongly opposed by the presence of glass frit, then with the ECS materials is to avoid the use of the latter as a component for the production of suspensions, both with solvents and with organic vehicle, but it is recommended the addition of ethanol.

4.2.2.3 Structural characterizations

Comparison between patterns on paste-based films containing ECS 13 and ECS 14

XRD collections about depositions on silicon supports produced by using ECS 13 dispersed in organic vehicle with glass frit and ethanol, ECS 13 powder dispersed in organic vehicle without glass frit and with ethanol and its comparison with the ECS 13 powder as provided by ENI (in order to optimize the comparison, the background has been subtracted).
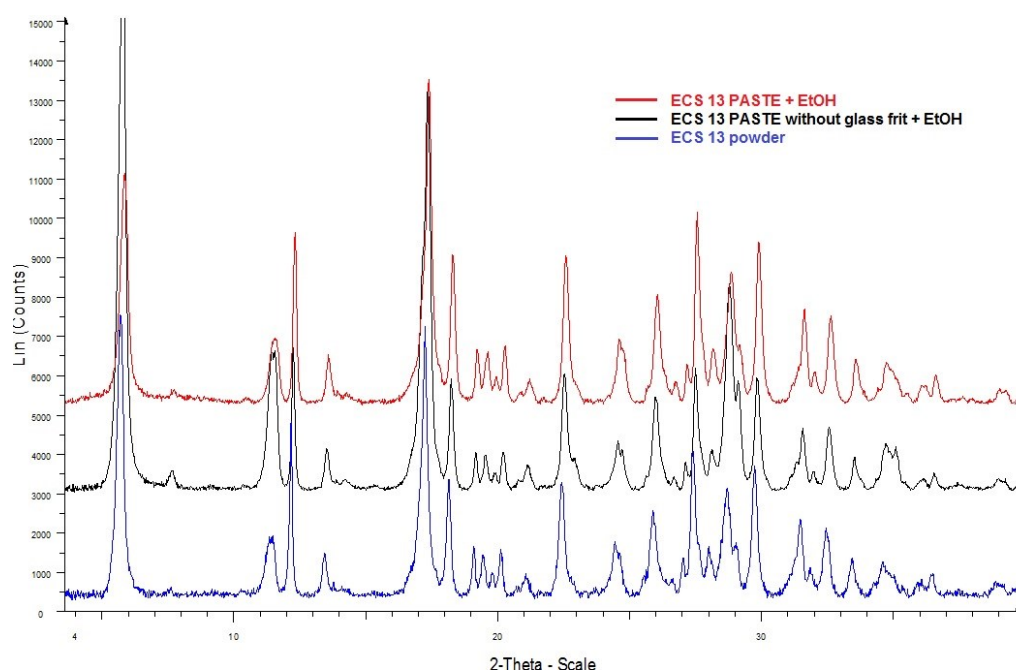
Figure 4.31. Diffraction patterns of films containing ECS 13 in complete paste formulation with ethanol (red), ECS 13 in formulation based on organic vehicle with ethanol (black), and ECS 13 pure powder (blue).

The comparison of the three diffractograms, it appears that the ECS 13 material present in the two different formulations (with and without frit) with added ethanol highlights the structural stability crystalline. It is not observed an appreciable crystals iso-orientation, but it is evident the increase in the intensity of the peak between 7-8 ° 2-Theta deposition compared to powder as it is. This peak is not due to the structure of 'ECS 13, but rather to a contamination or the presence of residues of synthesis.

XRD collections about depositions on silicon supports produced by using ECS 14 dispersed in organic vehicle with glass frit and ethanol, ECS 14 powder dispersed in organic vehicle without glass frit and with ethanol and its comparison with the ECS 14 powder as provided by ENI (in order to optimize the comparison, the background has been subtracted).
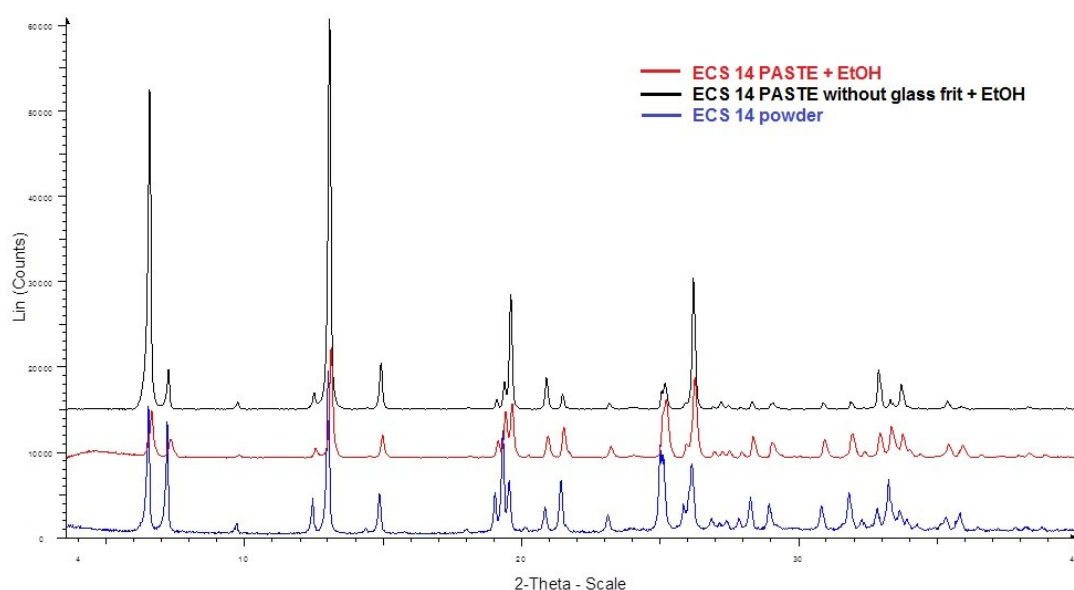
Figure 4.32. Diffraction patterns of films containing ECS 14 in complete paste formulation with ethanol (red), ECS 14 in formulation based on organic vehicle with ethanol (black), and ECS 14 pure powder (blue).

From the comparison of the three diffractograms, it appears that the crystallinity of the ECS 14 powder which is present in two pastes (with and without frit) with ethanol is maintained. Figure 4.32 indicates the stability of the crystal structure and a significant iso-orientation of the powder dispersed in organic vehicle with ethanol and without glass frit.

XRD investigations have established that the ECS 13 and 14 powders dispersed in organic vehicle with glass frit not suffer degradation of the crystal structure. Also the addition of ethanol does not affect the crystal structure. The comparison of the pure powder diffractogram with those of pastes containing ECS 14 shows the maintenance of the structural stability of the powder and a heightened degree of crystallites orientation on the plane (001).

4.2.2.4 Thermal characterizations

The acquisitions were performed under air flow (20°C/min) in ramp (10°C/min), from 25 °C up to a maximum temperature depending on the type of sample. Investigations by means of thermogravimetric balance have allowed to determine the following samples:

- powders as well as provided by ENI has set the maximum temperature equal to 1000 ° C (this limited temperature was set considering thermogravimetric analyzes present in the publications made on materials ECS);
- the organic vehicle with alumina, setting the maximum temperature equal to 800 ° C (so with this temperature as it was certain that the organic vehicle was already completely eliminated);
- powders in complete paste formulation, setting the maximum temperature equal to 450 ° C (there has been limited at a temperature of 450 ° C as the frit at a higher temperature would be melted, damaging the sample holder of the thermobalance);

- powders in paste formulation without glass frit, setting the temperature up to 800 ° C (so with this temperature it was certain that the organic vehicle was already completely eliminated).

In this analysis was considered useful to include not only the respective pure powders as supplied by ENI (ECS 13 and 14), and the relative two samples based on paste formulation, but also the "organic vehicle", which is the other key component for achieving the pastes.

The addition of alumina in the organic vehicle for the realization of measurements in thermogravimetry was necessary to achieve depositions, which contained the component in suspension with the characteristic of being inert to a thermogravimetric analysis. The aim was to obtain a material with the paste which was actually deposited and dried in the hood, in such a way as to achieve a more reliable comparison with the depositions formed by organic vehicle and ECS powders, they also deposited and then analyzed in thermogravimetry. Once realized the suspensions were deposited on glass (type glass window), then dried under a hood. Once dry the depositions have been scraped away, producing fragments "gummy". These fragments were well chopped and analyzed by thermogravimetric balance.

The powders as provided by ENI, were analyzed without any kind of treatment.

Thermal investigations on ECS 13 samples

Figures 4.33 and 4.34 show the direct comparison between TG, DTG and DTA curves obtained by thermal investigations on ECS 13 samples:

i)   ECS 13 pure powder,
ii) deposition containing organic vehicle and alumina,
iii) deposition containing ECS 13 powder dispersed complete paste formulation with addition of ethanol,
iv) deposition containing ECS 13 dispersed in organic vehicle with ethanol and without glass frit.
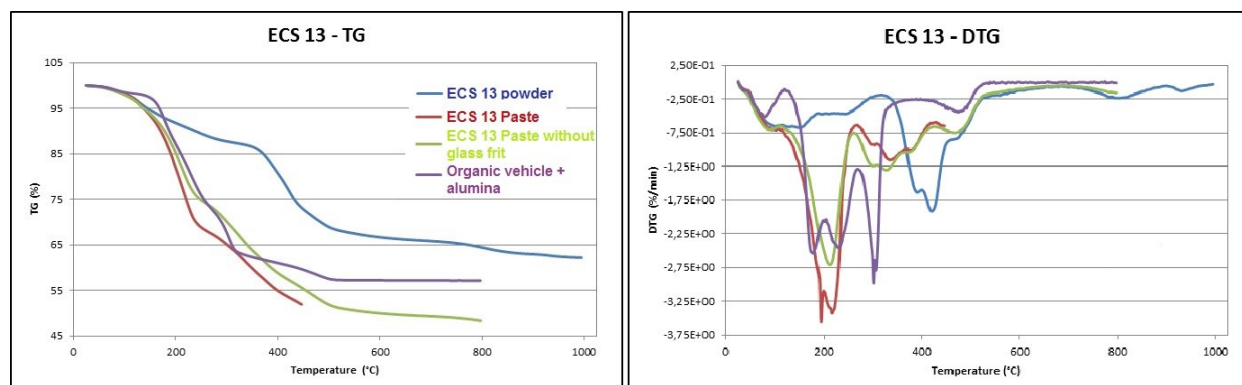
Figure 4.33. Comparison of TG and DTG curves among samples containing ECS 13 pure powder (blue), ECS 13 in complete paste formulation (red), ECS 13 in paste formulation without glass frit and with ethanol (green), and organic vehicle in addition with alumina.

Table 4.14. Analysis of TG and DTG curves among samples containing ECS 13.

Sample	ECS13 – TG e DTG
Powder	The weight loss increasing the temperature can be divided in three zones: 80 – 380 °C, 380 – 490 °C, and 490 – 1000 °C. These are connected to the loss of the organic and inorganic ECS 13 material.

131

Organic vehicle + alumina	The weight loss increasing the temperature can be divided in three zones: 40 – 170 °C (loss of more volatile organic compounds), 170 - 310 °C, 310 – 500 °C, and 500 – 800 °C (in this zone there is not weight loss anymore, probably the organic vehicle was eliminated).
Paste + EtOH	The weight loss increasing the temperature can be divided in two zones: 80 – 230 °C (the curve at low temperatures is characterized by a very sweet trend, then the weight loss increases in a sudden way), and 230 - 450 °C.
Paste without glass frit + EtOH	The weight loss increasing the temperature can be divided in three zones: 80 – 250 °C (the curve at low temperatures is characterized by a very sweet trend, then the weight loss increases in a sudden way), 250 – 500°C, and 500 – 800° C.

The TG curves of the powders dispersed in organic vehicle with and without glass frit have a comparable trend. The curve obtained with the organic vehicle added to alumina has a weight loss almost comparable to the pastes containing also ECS powder at least up to about 300 ° C. Instead, the ECS 13 powder shows a weight loss is similar to the other three curves only up to about 150 ° C, then the loss in weight of the latter is lower than the others. Therefore, it must be concluded that the loss in weight of the pastes are mainly attributable to organic vehicle.
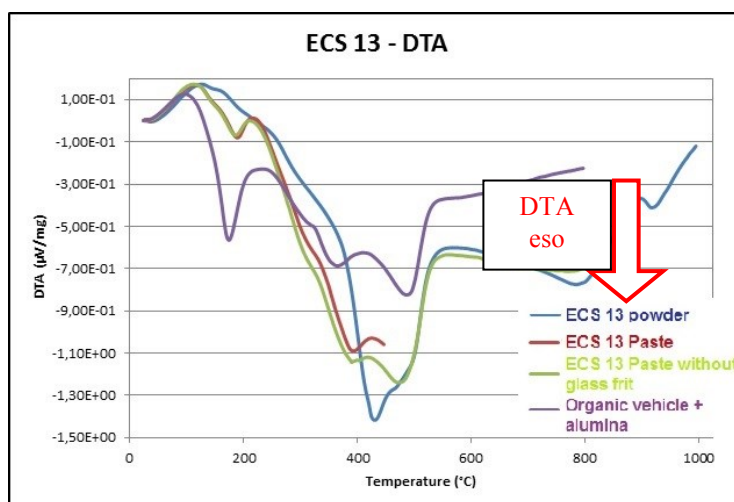
Figure 4.34. Comparison of DTA curves among samples containing ECS 13 pure powder (blue), ECS 13 in complete paste formulation (red), ECS 13 in paste formulation without glass frit and with ethanol (green), and organic vehicle in addition with alumina.

Table 4.15. Analysis of DTA curves among samples containing ECS 13.

Sample	ECS13 - DTA
Powder	The weight loss increasing the temperature can be divided in four zones: 100 – 380 °C (one can observe a thermic peak with maximum at 120 °C, due to a water loss), 380 – 490 °C (characterized by an asimmetric esothermic peak with maximum at 410 °C, due to combustion of organic component and gas emission), 520 – 1000 °C, 520 – 800 °C (there is a slight decline followed, after 800 ° C, by an increase in the yield curve. In practice, it has a new exothermic peak, connecting it to the combustion reactions and gas emission).
Organic vehicle + alumina	The weight loss increasing the temperature can be divided in four zones: 40 – 150 °C (area characterized by an endothermic peak attributable to the elimination of the most volatile of the organic), 150 – 310 °C (one can

	observe an exothermic peak attributable to an oxidation reaction, followed by an endothermic peak, attributable to the elimination of substances which are less volatile than the first area,), 310° – 500° C (two exothermic peaks always referable to oxidation reactions, and an endothermic peak attributable to the gasification of low volatile substances), and 500 – 800°C.
Paste + EtOH	The weight loss increasing the temperature can be divided in three zones: 80 – a 160 °C (there is an endothermic peak with maximum around 120 °C to be connected with the water emission), 160 – 240 °C (it has an exothermic peak with maximum around 190 °C, to be connected with combustion reactions and gas emission), and 190 °C – 450° C (it has a curve trend which indicates an exothermic peak is not complete, probably linked to a second combustion reaction and gas emission).
Paste without glass frit + EtOH	The weight loss increasing the temperature can be divided in four zones: 80 – a 150° C (there is an endothermic peak with maximum around 120 °C to be connected with the water emission), 150 – ad 250 °C (it has an exothermic peak with maximum around 200 °C, to be connected with combustion reactions and gas emission), 250 – 550 °C (it has a curve trend which indicates an very wide exothermic peak, consisting of the superposition of two peaks. This double peak is probably due to a second series of combustion reactions and emission gas), and 550 – 800 °C (there is a plateau, index of organic substances oxidizable depletion).

Thermal investigations on ECS 14 samples

Figures 4.35 and 4.36 show the direct comparison between TG, DTG and DTA curves obtained by thermal investigations on ECS 14 samples:

i) ECS 14 pure powder,
ii) deposition containing organic vehicle and alumina,
iii) deposition containing ECS 14 powder dispersed complete paste formulation with addition of ethanol,
iv) deposition containing ECS 14 dispersed in organic vehicle with ethanol and without glass frit.
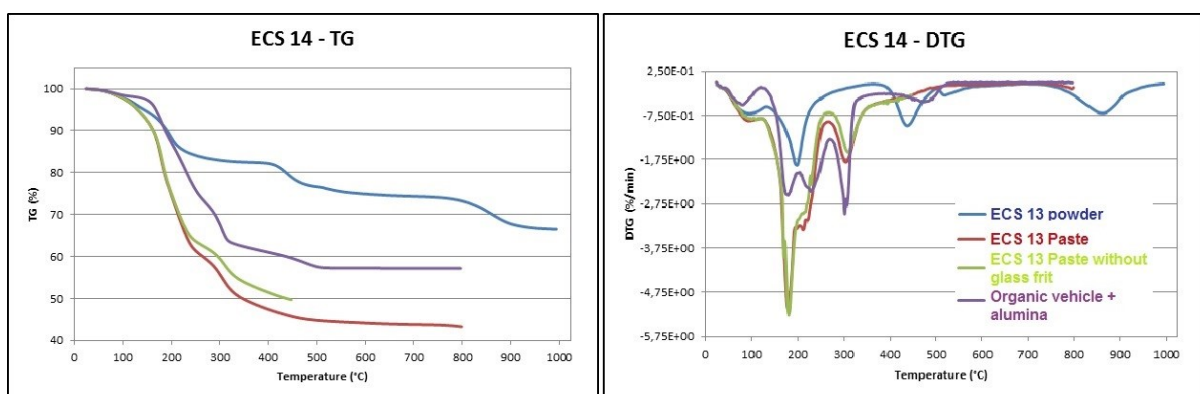
Figure 4.35: Comparison of TG and DTG curves among samples containing ECS 14 pure powder (blue), ECS 14 in complete paste formulation (red), ECS 14 in paste formulation without glass frit and with ethanol (green), and organic vehicle in addition with alumina.

Table 4.16. Analysis of TG and DTG curves among samples containing ECS 14.

Sample	ECS14 – TG e DTG
Powder	The weight loss increasing the temperature can be divided in three zones: 80 – 200 °C (there is a weight loss followed by a plateau up to 400 °C), 400 – 490 °C (there is a second weight loss followed by a plateau up to 780 °C), and 780 – 920 °C (there is a third weight loss followed by a plateau up to 1000 °C). These areas are to be connected to the loss of the organic and inorganic ECS 14material.
Organic vehicle + alumina	The weight loss increasing the temperature can be divided in four zones: 40 – 170 °C (loss of the most volatile of the organic vehicle), 170 – 310 °C, 310 – 500 °C, and 500 – 800 °C (in this area, there are no more weight loss, obviously the organic vehicle was completely lost).
Paste + EtOH	The weight loss increasing the temperature can be divided in three zones: 80° – 230° C (the curve at low temperatures is characterized by a very soft trend, then the weight loss increases in a sudden way), and 230 – 450 °C (there is a weight loss with a minor slope than the previous section).
Paste without glass frit + EtOH	The weight loss increasing the temperature can be divided in two zones 60 – 330 °C, and 330° a 800° C (there is a plateau). These traits are to be connected to the loss of the organic vehicle.

The comparison of the curves TG regard powders dispersed in organic vehicle with and without glass frit indicate a similar trend. While the curve obtained with the organic vehicle added to alumina has a weight loss close to the first two up to 150 ° C, beyond this temperature is observed a shift of the weight loss of the latter to temperatures high, with respect to the other curves. The ECS 14 powder indicates a weight loss which is maintained close to the three curves mentioned above only up to about 150 ° C, then the loss of the pure powder is lower than the other three samples. Therefore, it must be concluded that the loss in weight of paste during heat treatment are mainly attributable to organic vehicle.
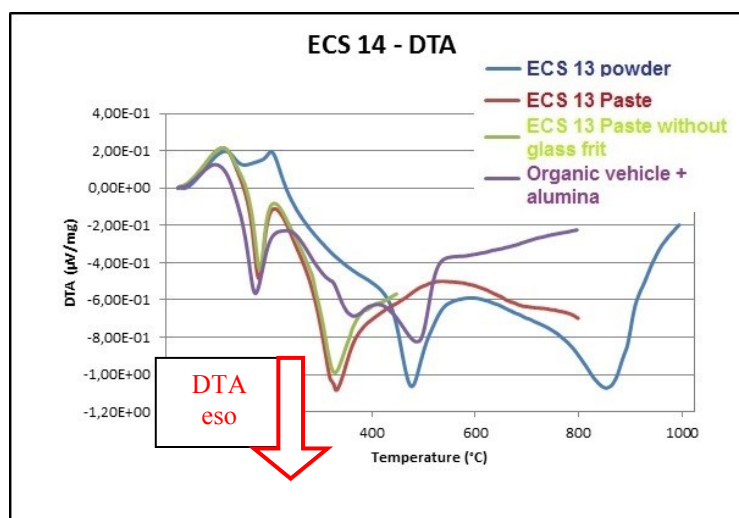
Figure 4.36. Comparison of DTA curves among samples containing ECS 14 pure powder (blue), ECS 14 in complete paste formulation (red), ECS 14 in paste formulation without glass frit and with ethanol (green), and organic vehicle in addition with alumina.

Table 4.17. Analysis of DTA curves among samples containing ECS 14.

Sample	ECS14 - DTA
Powder	The weight loss increasing the temperature can be divided in three zones: 50 – 230 °C (there is a double endothermic peak with maximum around 160 and 210 °C, connected with the loss of water), 230 –560 °C (there is an exothermic peak with maximum around 470 °C, connected with a combustion phenomenon of the organic material component and gas emission), and 560 1000 °C (from 560 to 780 °C there is a slight decline, followed from 780 ° up to 1000 ° C, by new exothermic peak with maximum at around 870 ° C, connected always to the combustion reactions and emission of gases).
Organic vehicle + alumina	The weight loss increasing the temperature can be divided in four zones 40 – 150 °C (characterized by an endothermic peak attributable to the elimination of the most volatile part of the organic vehicle), 150 – 310 °C (observed an exothermic peak attributable to an oxidation reaction, followed by an endothermic peak, attributable to the elimination of substances which are less volatile than the first zone), 310 – 500 °C (observed two exothermic peaks always referable to oxidation reactions, and an endothermic peak attributable to the gasification of low volatile substances), and 500 – 800 °C.
Paste + EtOH	The weight loss increasing the temperature can be divided in three zones: 60 – 140 °C (there is an endothermic peak with maximum around 120 °C connected with the water emission), 140 – 210 °C (there is an exothermic peak with maximum around 180 °C, connected to the combustion reactions and gas emission), and 210 – 450 °C (it has a curve trend which indicates an exothermic peak around 320 °C, probably due to a second combustion reaction and gas emission).
Paste without glass frit + EtOH	The weight loss increasing the temperature can be divided in four zones: 50 – 170° C (shows an endothermic peak with asymmetric maximum around 150 °C, connected with the water loss), 170 – 230° C (shows an exothermic peak with maximum around 190 °C connected with a combustion phenomenon of the material organic component and gas emission), 230 – 500° C (highlights a new exothermic peak with maximum at 330 ° C, always connected with combustion reactions and gas emission), and 500 – 800 °C.

Conclusions

The investigations TG/DTA show that powder weight losses in mixtures of ECS 13 and 14 with organic vehicle and glass frit occur at lower temperatures or comparable to those of the pure powders. Investigations have shown that ethanol added to the complete paste formulation did not give a substantial improvement to the realization of the depositions. Considering this aspect it was necessary to understand which component, between glass frit and organic vehicle has played the negative role. It was also found that the crystalline structure of the ECS 13 and 14 materials in the suspensions obtained with organic vehicle and ethanol, without glass frit, did not undergo modifications.

The thermal investigations carried out on samples containing ECS 13 and 14powders added to organic vehicle without the glass frit show weight losses at lower temperatures or comparable to those of the pure powders, as for the complete paste formulation. The investigations have revealed that ethanol added to the paste obtained by using ECS powders, organic vehicle without the addition of glass frit gave a substantial improvement to the realization of the depositions. Considering this aspect it was understood that the

presence of glass frit in paste affect cleanly disaggregation/disagglomeration of ECS powders.

It was also found that the crystalline structure of the materials ECS 13 and 14 in the suspensions obtained with organic vehicle and ethanol (without the addition of frit) do not undergo changes. It also appears a certain degree of preferential orientation for the crystals of ECS 14powder.

4.2.3 Study of organic and inorganic components used for ECSs synthesis

Based on the results obtained from measurements of electrical conductivity, discussed in the next section, it was necessary to evaluate the response specificity of the hybrid ECS materials compared both to the inorganic component, testing a sensor prepared with the active layer consisting of zeolite Y, and to the organic component, testing a sensor prepared with the active layer consists of the precursor ECS materials, after checking the filmability.

Regard the inorganic component it was used two different Y zeolites as functional material: the first USY Zeolite HSZ 360 HUA (TOSOH) serie, called Y(1) zeolite, is characterized by an effective ratio Si/Al equal to 13.8 does not contain sodium (delivered by Prof. Cruciani), the second USY zeolite HSZ 320 NAA (TOSOH) serie, called Y(2) zeolite, differs from the first beacuse it also contains 15% sodium by weight (delivered by ENI) [1]. For the preparation of the suspensions were used about 100 mg of zeolite Y in the paste formulation without glass frit but with the addition of ethanol. The suspension was easily filmable as regards the Y(1) zeolite [glass, alumina], whereas it was most difficult the deposition of the Y(2) zeolite because of the density and the significant presence of agglomerates, despite the treatments performed on the suspension. The images about deposition on glass and alumina are showed in table B10 and B17 of Appendix B, respectively.

Regarding the organic component precursors delivered by ENI (about 100 mg), 1.4-bis (trimethoxy-silyl-ethyl-benzene), BTEB, and 2.6-bis- (tri-ethoxy-silyl-naphthalene), BTNaph have been used as functional material in the paste formulation without glass frit but with the addition of ethanol. The suspensions were easily filmable [glass, alumina], but had not dried even after several days in the hood, so it was not possible to make and test devices with the active layer consisting of the organic component.

4.2.3.1 Morphological and structural characterizations

As requested by ENI was produced a paste whose crystalline component consists of HY zeolite in order to verify the possible conductivity of such material in the form of deposition.

Analysis of the deposition containing zeolites by optical microscopy (see Table B10 in Appendix B) has highlighted the absence of agglomerates and film appears continuous and characterized by an uniform thickness. For Y(1), some cracking in the central zone of the deposition make continuity not perfect, as shown below.

Figure 4.37. Film obtained by using Y(1) zeolite dispersed in organic vehicle and ethanol.

To check the structural integrity of the zeolite deposited compared to the same form of powder, it is reported here below a comparison between the diffraction patterns.
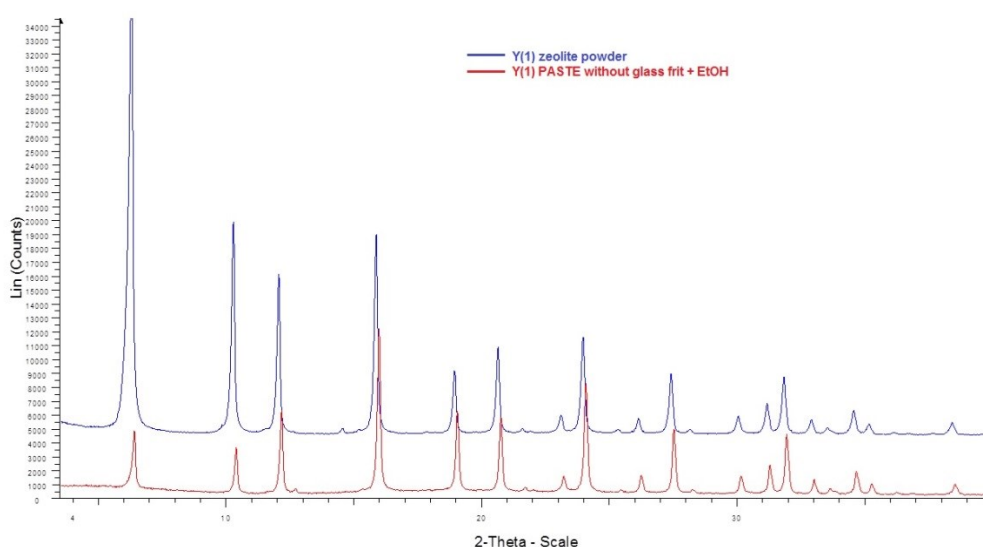
Figure 4.38. Diffraction patterns of films containing Y(1) zeolite in formulation based on organic vehicle with ethanol (red), and pure zeolite powder (blue).

The comparison clearly indicates that the zeolite deposited in the form of paste maintains its structural integrity. The shift of the peaks is due to the different sample holder used for the two collections: for the pure zeolite powder it was used an aluminum holder with side door loading, while the deposition of zeolite in paste was carried out on a silicon zero back-ground support. The different ratios of the peak intensity are also due to the different method of measurement used: the strong intensity decreasing of the first two peaks is due to the fact that the deposition of the paste does not completely cover the area illuminated by the incident X-rays beam in the lower measure angle (grazing incidence, larger illuminated area) with a net effect of the volume sampled reducing in low angle than at a high angle.

4.2.4 Electrical characterizations

4.2.4.1 Complete paste formulation

Among devices prepared using six different powders ECS as functional material in the complete paste formulation, showed in tables B11-15 in Appendix B, only that based on ECS 14 has been tested since the depositions with ECS 4, 9 and 12 were too thick so the bonding

137

process would cause the film disintegration, instead depositions based on ECS 5 and 13 were damaged during the bonding.

This allowed to make some assumptions to improve suspensions and related depositions. First of all, the introduction of an alternative deposition method: the drop coating is undoubtedly fast and inexpensive, but does not allow the control of the deposition thickness. Then, since the density of the samples suggests the possible use of the screen printing technique, after investigating further the effectiveness of the paste in its various formulations it will be desirable the introduction of screen printing. This will allow to produce a greater number of devices that will result reproducible on a large scale and especially characterized by a controlled film thickness.

The ECS 14 in the complete paste formulation with the addition of ethanol was tested in chamber 1 with CO, methane, hydrogen sulfide, acetaldehyde, ammonia and humidity.

Figure 4.39. Photo of the device made of ECS 14 powder in complete paste formulation with the addition of ethanol.

Below the graphs relating humidity measurements, signals in the presence of the other gases tested gave negligible results.
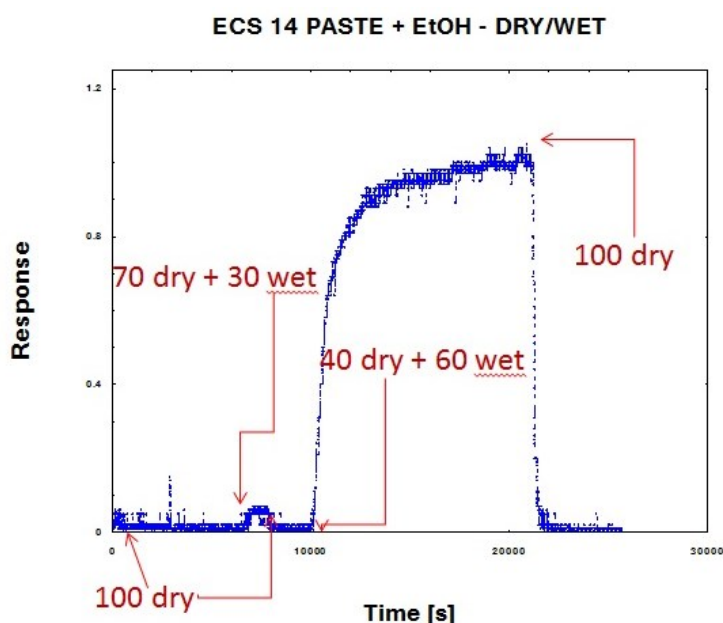
Figure 4.40. Response of sensor produced with ECS 14-PASTE+ETHANOL in DRY/WET conditions.

Figure 4.40 shows the response of the device based on ECS 14 powder in the complete paste formulation tested with two different combinations of dry/wet air. The measurement was performed using a load resistance R_c equal to 470 MΩ and operating at room temperature, since heat treatment could degrade the film.

It can be observed that starting from a flow of 100 cc /min of dry air a slight raising of the signal occurs in correspondence of the combination of 70 cc/min dry and 30 cc/min wet and a significant increase for the combination 40 cc/min dry and 60 wet[6]. The signal appears clean and iy is essential to highlight the speed with which it returns to the base line when a total dry flow is restored.

The device has resulted to be sensitive to humidity and characterized by an extremely fast and reversible response obtained at room temperature.

On the basis of the peculiarities of the measure just discussed, it was assumed that it was possible to obtain a device calibration in humidity.

Below humidity calibration performed by steps of 10 cc/min, starting from a completely dry flow arriving at a totally wet flow.

(a)

Figure 4.41a shows the zoom of humidity calibration in the range from 100 cc/min dry to 40 cc/min dry - 60 cc/min wet. It can be observed that the combination of 90 cc/min dry with 10 cc/min wet has not been shown since it was not possible to distinguish an increase in the signal with respect to noise fluctuation. There was a not linear abrupt increase of the response and then an higher film conductance, in correspondence of wet air flow increase with respect to dry. It is important to highlight that in the moment in which it has gone from a combined flow of 60 cc/min dry and 40 cc/min wet at a completely dry flow, the signal not only has returned to the initial base line, but also the slope of the curve appears significant.

The response of the sensor shows consisting values starting from the combination 30 cc/min dry and 70 cc/min wet (response equal to 1.5), as shown in the graph of full calibration in Figure 4.41b. The increase of the curve coincides with the different combinations of flux

---

[6] A flow of wet air equal to 100 cc/min at room temperature corresponds roughly to 95% of humidity, while a dry air flow equal to 100 cc/min corresponds to about 5% humidity.

applied, until reaching the saturation value (response equal to 50) given by the electronic system in correspondence of a totally wet flow applied. In any case, it is significant that the switch from totally wet to totally dry flow produces a sudden return of the curve at the base line.

Then, the conditions emerged with the preliminary humidity test (Fig. 4:40) have been confirmed by the calibration obtained later (Fig. 4:41 a, b).

ECS 14 PASTE+ EtOH DRY/WET CALIBRATION

(b)
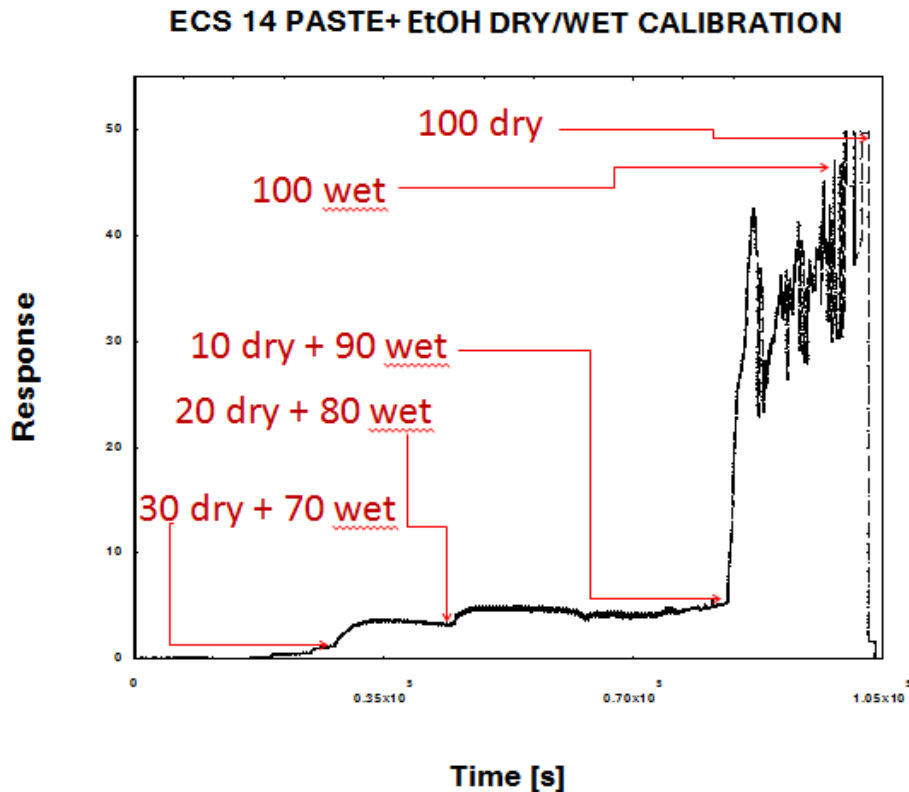
Figure 4:41. Humidity calibration of sensor based on ECS 14-PASTE + ETHANOL a) in the range 100% dry ÷ 40% dry, b) in the range of 30 dry% ÷ 100% wet.

4.2.4.2 Formulation without glass frit

Among sensors prepared using the six different ECS powders as functional material in the paste formulation without glass frit, were tested ECS 14, 4, 9 and 13. The depositions with ECS 12 were too thick and the bonding process would cause the film disintegration. On the contrary devices ECS 5 based did not show enough material to cover the alumina substrate. This situation had also emerged with the first devices analyzed in the previous section. It was already highlighted the need to improve the suspension and the relative depositions perhaps through the introduction of an alternative deposition method such as screen printing technique.

1) The ECS 14 in paste formulation without glass frit was tested in chamber 1 with methane, acetaldehyde, ammonia and humidity.
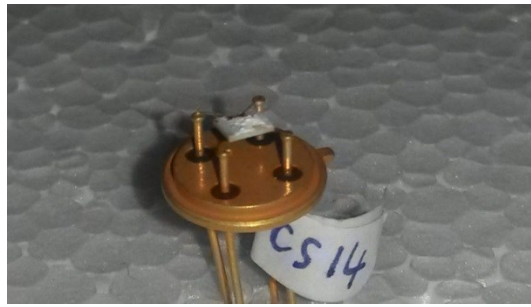
Figure 4.42. Photo of the device made of ECS 14 powder in paste formulation without glass frit.

Below only the graphs relating humidity measures are shown, because signals in the presence of the other gases are negligible results.
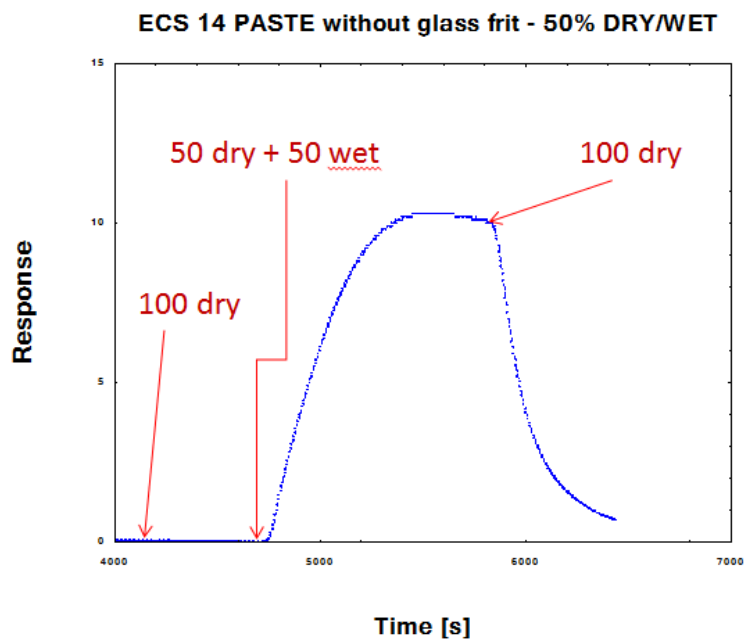
Figure 4.43. Response of sensor produced with ECS 14-PASTE without glass frit in DRY/WET conditions.

The graph in Figure 4.43 shows the response of the device ECS 14 powder based in the paste formulation without glass frit in a combination of dry/wet air. The measurement was performed using a load resistance R_c equal to 47 MΩ and operating at room temperature.

It can be observed that starting from a flow of 100 cc/min of dry air, a significant and well defined response occurs in correspondence of the combination of 50 cc/min dry and 50 cc/min wet. The signal also appears cleaner than that obtained in a first measurement with the device made with the complete paste formulation. It is important to highlight the speed with which the curve returns to the base line when a total dry flow has been restored.

The device resulted to be sensitive to humidity and characterized by an extremely fast and reversible response obtained at room temperature.

On the basis of the peculiarities of the just discussed measure, it was assumed that it was possible to obtain a humidity calibration of the sensor.

Below is humidity calibration performed by steps of 10 cc/min, starting from a completely dry flow arriving at a totally wet flow.

Figure 4.44 a shows the humidity calibration in the range of 100 cc/min dry to 60 cc/min dry - 40 cc/min wet. It can be observed that the combination of 90 cc/min dry with 10 cc/min wet

has not been shown since it was not possible to distinguish an increase in the signal with respect to noise fluctuation. There was a not linear abrupt increase of the response and then an higher film conductance, in correspondence of wet air flow increase with respect to dry.

ECS 14 PASTE without glass frit - DRY/WET CALIBRATION (1)

80 dry + 20 wet

70 dry + 30 wet

60 dry + 40 wet

100 dry

Response

Time [s]

(a)

ECS 14 PASTE without glass frit - DRY/WET CALIBRATION (2)

60 dry + 40 wet

50 dry + 50 wet

40 dry + 60 wet

30 dry + 70 wet

20 dry + 80 wet

100 dry

Response

Time [s]

(b)

142
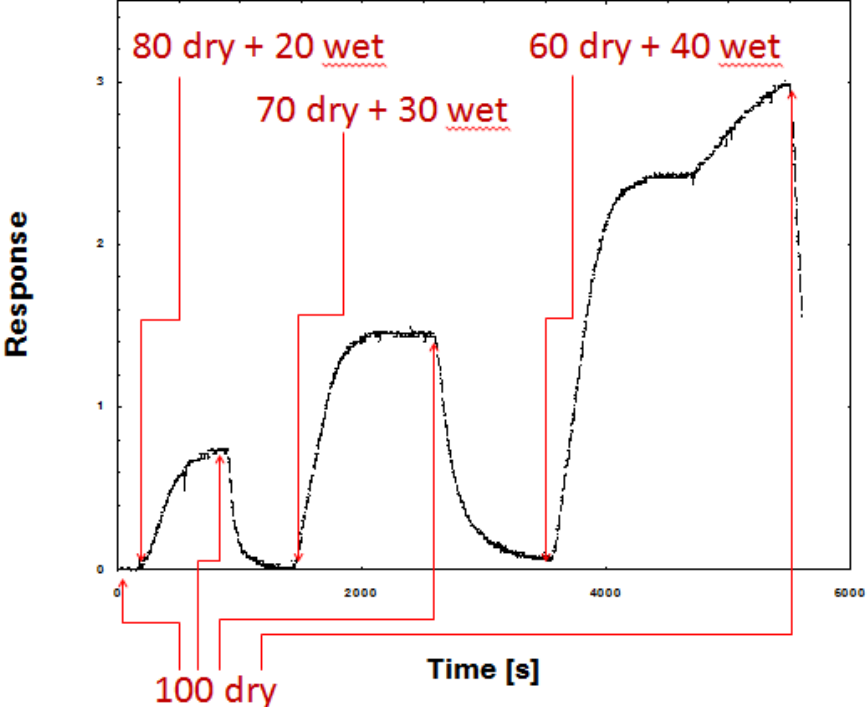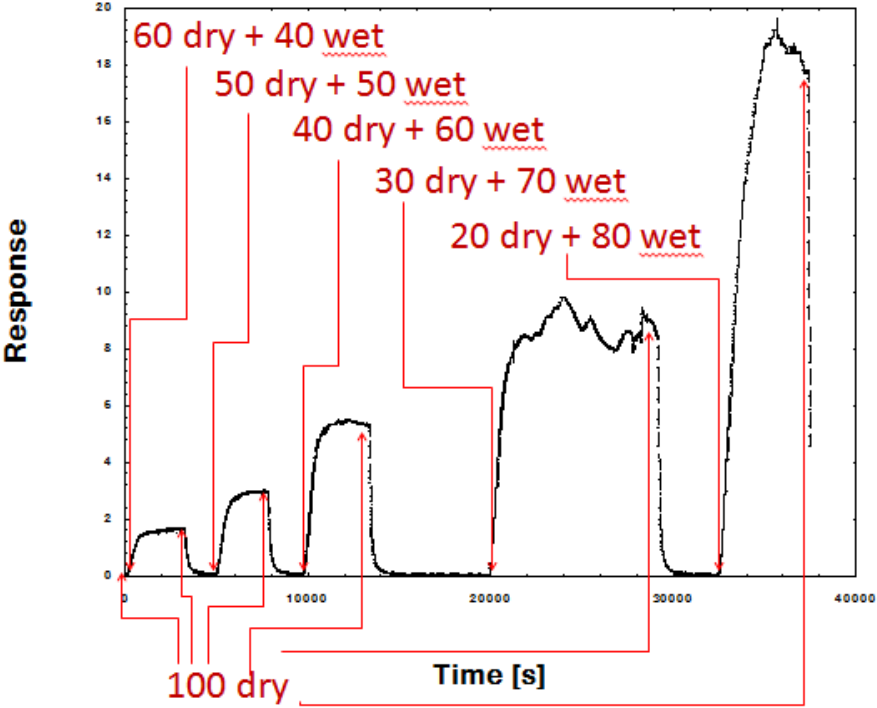
One can observe that after each combined dry/wet flux it has been wanted to verify the reversibility of the device by sending a totally dry flux: one can easily see that not only the signal is returned to the initial base line, but the slope of the curve is also significant .

The response of the sensor starts to assume consisting values from the combination 70 cc/min dry and 30 cc/min wet (response equal to 1.5), as shown in Figure 4.44 a, value which for ECS 14 in the complete paste formulation with added of ethanol was reached in correspondence of the combination inverse dry/wet, that is 30 cc/min dry and 70 cc/min wet. The increase of the curve coincides with the different combinations of flux applied, until reaching a response equal to 25 (see Figure 4.44 c) corresponding to a totally wet flow. In any case it is noted that the switch from totally wet to totally dry flow generates a sudden return of the curve at the base line.

The conditions emerged from the humidity test (Figure 4.43) were then confirmed by the calibration subsequently obtained (Figure 4.44, b, c).

It is important to emphasize the greater response stability of the film based on ECS 14 in the paste formulation without glass frit than that obtained with sensor based on the complete paste formulation with addition of ethanol.

ECS 14 PASTE without glass frit - DRY/WET CALIBRATION (3)
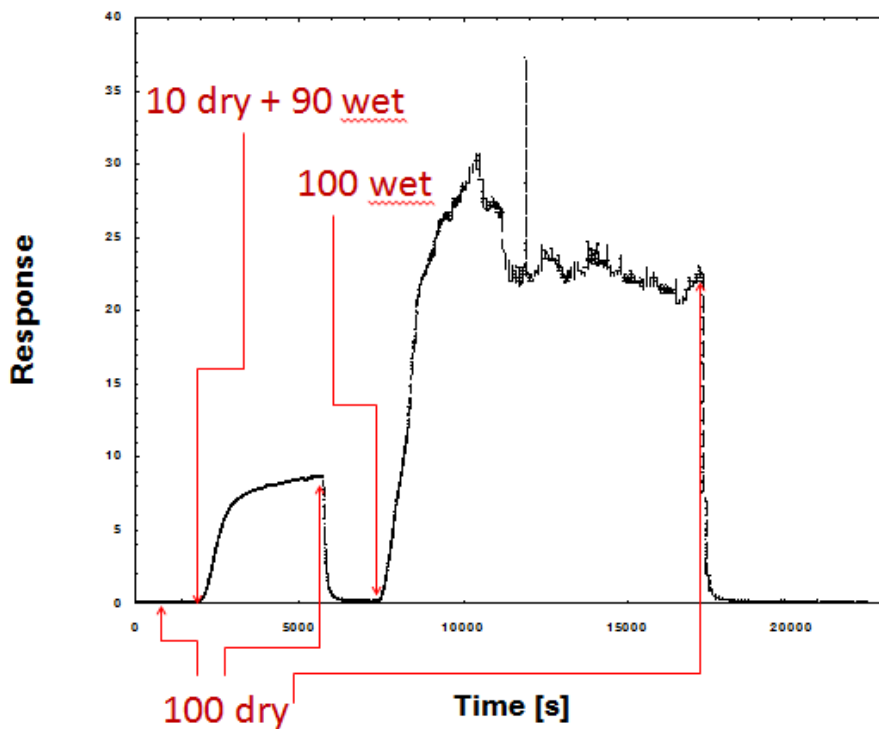
(c)

Figure 4.44. Humidity calibration of sensor based on ECS 14-PASTE without glass frit a) in the range 100% dry ÷ 60% dry, b) in the range of 60 dry% ÷ 20% dry, and c) in the range 10% dry ÷ 100% wet.

2) The ESC 4 in the paste formulation without glass frit was tested in chamber 2 with ethanol, toluene, benzene, acetone and humidity.
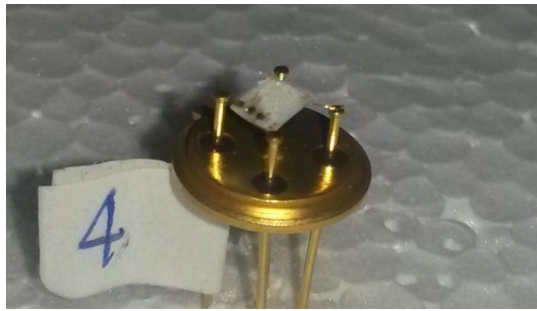
Figure 4.45. Photo of the device made of ECS 4 powder in paste formulation without glass frit.

Below the measures carried out testing benzene (C_6H_6) and humidity are shown, signals in the presence of the other gases gave negligible results.
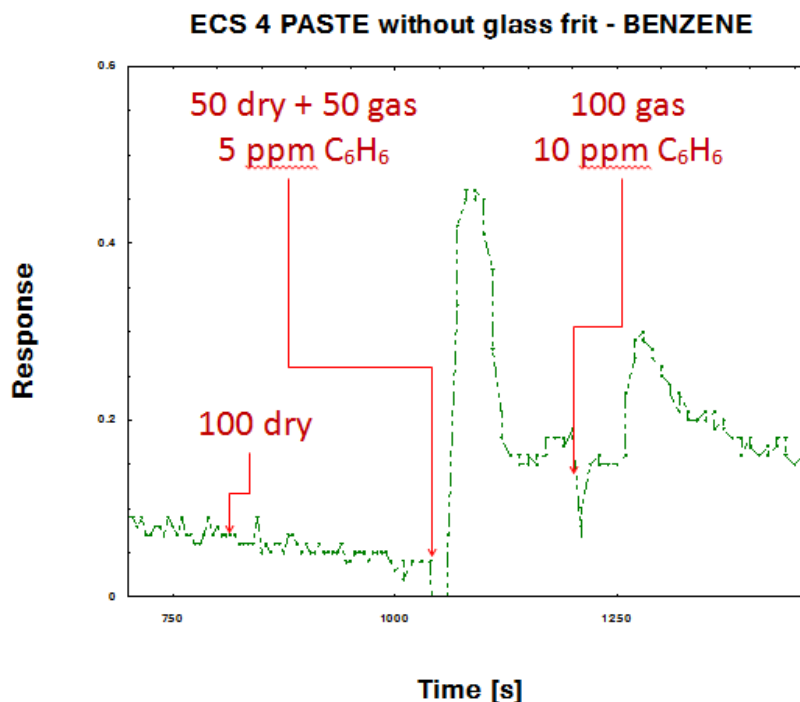
Figure 4.46. Response to BENZENE of sensor produced with ECS 4-PASTE without glass frit in DRY conditions.

The measure with benzene was performed using a load resistance R_c equal to 1 GΩ and operating at room temperature.

It can be observed that starting from a flow of 100 cc/min of dry air and passing to the combination 50 cc/min dry and 50 cc/min of benzene, the response results fast, even if the variation of conductance in the presence of the gas, after reaching a peak, is stabilized at a value slightly above the base line refers to the totally dry flow, so the response value results low. Subsequently, in correspondence of a totally flow of benzene, the device has undergone a slight variation of conductance then return to the stabilization value obtained in the previous measure at 50% dry/benzene. This latter phenomenon would require a depth on the basis of a measurement cycle.

The device should be subjected to further testing with benzene at room temperature.

The measurement with humidity was also performed using a load resistance R_c equal to 1 GΩ and operating at room temperature.

It can be observed that starting from a flow of 100 cc/min of dry air, a well-defined response is obtained in correspondence to the combination 50 cc/min dry and 50 cc/min wet. It is

important to highlight the rapidity of the response, even if the variation of conductance in the presence of moist air, after reaching a peak, is stabilized at a value slightly above the base line refers to the totally dry flow, so the response is low.

Later, in correspondence of a wet flow the device has undergone a slight change in conductance and then return to the stabilization value obtained in the previous measure 50% dry/wet. This latter phenomenon would require a depth on the basis of a measurement cycle. The device should be subjected to a further round of measures with humid air at room temperature.
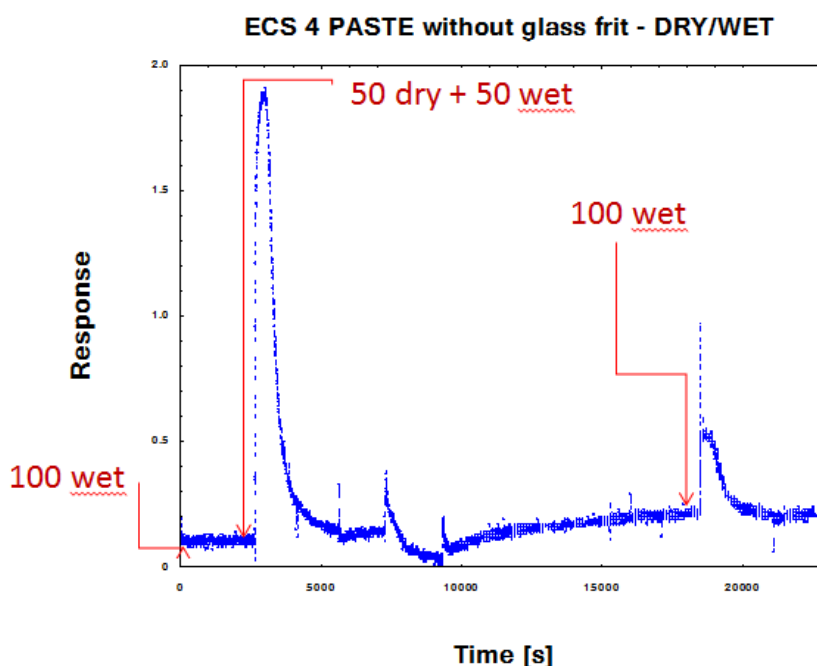
Figure 4.47. Response of sensor produced with ECS 4-PASTE without glass frit in DRY/WET conditions.

3) The ESC 9 in the paste formulation without glass frit was tested in chamber 2 with ethanol, toluene, benzene, acetaldehyde, hydrogen sulfide and humidity.

Figure 4.48. Photo of the device made of ECS 9 powder in paste formulation without glass frit.

Below only humidity measure is shown, because signals in the presence of other gases resulted negligible.

The measurement was performed using a load resistance R_c equal to 1 GΩ and operating at room temperature.

It can be observed that starting from a flow of 100 cc/min of dry air a well-defined response has been obtained in correspondence to the combination of 50 cc/min dry and 50 cc/min wet.

It is important to highlight the velocity with which the curve returns to the base line when a total dry flow is restored.
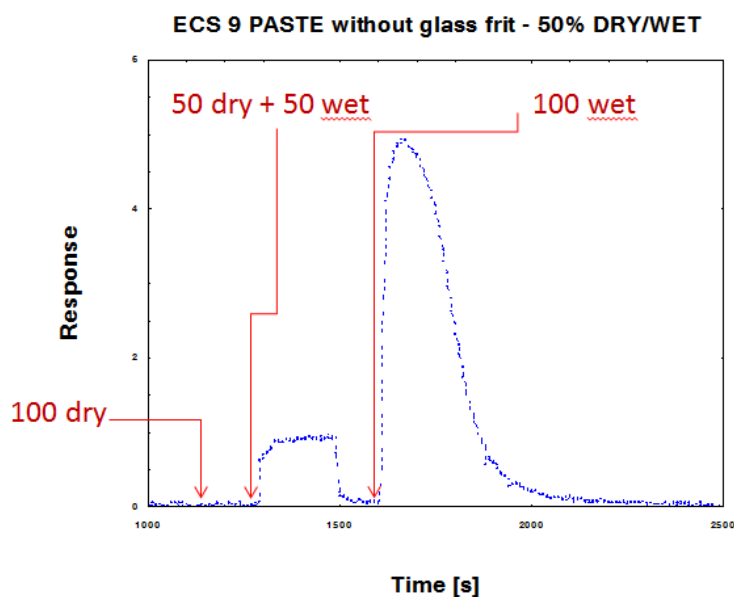
Figure 4.49. Response of sensor produced with ECS 9-PASTE without glass frit in DRY/WET conditions.

Subsequently, in correspondence of a totally wet flow, the device has responded quickly and then return to the base line, even if the dry flow was not restored yet. This latter phenomenon would require a depth on the basis of a measurement cycle.

The device resulted to be sensitive to humidity and characterized by an extremely and reversible fast response obtained at room temperature.

Based on the characteristics of the measures just discussed, it is assumed that it is possible to obtain a calibration humidity in the device in question and that it is necessary to perform a wider series of tests on this type of film.

4) The ESC 13 in paste formulation without glass frit was tested in chamber 2 with acetaldehyde and humidity, but signals resulted negligible.

Figure 4.50. Photo of the device made of ECS 13 powder in paste formulation without glass frit.

4.2.4.3 Formulation without glass frit with addition of ethanol

Among devices prepared using the six different powders ECS as functional material in the paste formulation without glass frit with addition of ethanol were tested ECS 14, 12 and 13. The depositions with ECS 5 and 9 were too thick for bonding process which would have caused the cracking of the film, instead the depositions with ECS 4 were damaged during the bonding.

146

1) The ECS 14 in the paste formulation without glass frit with addition of ethanol was tested in the chamber 2 with acetone, benzene, toluene, ethanol and humidity.

Figure 4.51: Photo of the device made of ECS 14 powder in paste formulation without glass frit and with addition of ethanol.

Below the measures with benzene (C_6H_6) and humidity are shown, whereas signals in presence of other gases resulted negligible.

The measurement was performed using a load resistance R_c equal to 1 GΩ and operating at room temperature.

It can be observed that starting from a flow of 100 cc/min of dry air and passing to the combination 50 cc/min dry and 50 cc/min of benzene a fast response occurs, even if the variation of conductance in the presence of the gas, after reaching a peak, is stabilized at a value slightly above the base line refers to the totally dry flow, so the answer is low. Subsequently, in correspondence of a totally benzene flow, the device has undergone a slight variation of conductance then return to a stabilization value even lower than the response in the presence of a totally dry flow. After, the dry flow has been restored and then applied again the combination 50 cc/min dry and 50 cc/min of benzene: the response of the device is low, and it can be observed that the stabilization value is the same achieved with the total flow of benzene. These developments need of further investigation on the basis of a measurement cycle.

The device should then be subjected to further testing with benzene at room temperature.

The measurement was performed using a load resistance R_c equal to 100 MΩ and operating at room temperature, since heat treatment could degrade the film.

It can be observed that starting from a flow of 100 cc/min of dry air a well-defined response occurs in correspondence to the combination of 50 cc in dry and 50 cc/min wet. It is important to highlight the rapidity of response and its stabilization, even if the variation of conductance in the presence of humidity is low. Subsequently, in correspondence of a totally wet flow the device has undergone a further increase in conductance stabilizing it quickly and returning equally rapidly to the value of the base line at the moment in which a completely dry flow has been restored.

ECS 14 PASTE without glass frit + EtOH - BENZENE
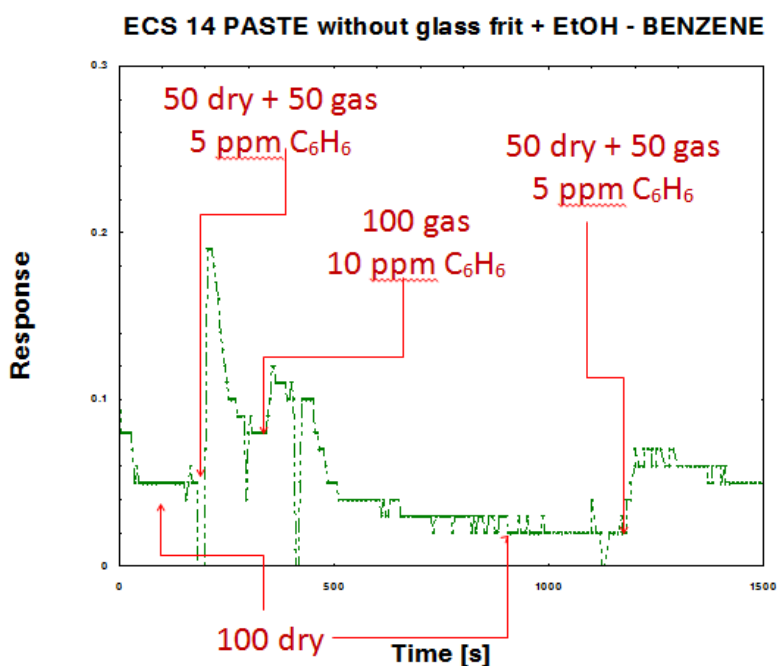
Figure 4.52. Response of sensor produced with ECS 14-PASTE without glass frit and addition of ethanol tested with BENZENE in dry conditions.

Other responses obtained at room temperature using the same device tested with the combination of 50% dry/wet, and 100% wet flow are quite similar to those obtained in measurement showed in Figure 4:52 analyzed previously. Therefore, it is necessary to test in more detail the device that, from the point of view of the deposition, resulted to be the more continuous and uniform film, among those made.

ECS 14 PASTE without glass frit + EtOH - DRY/WET
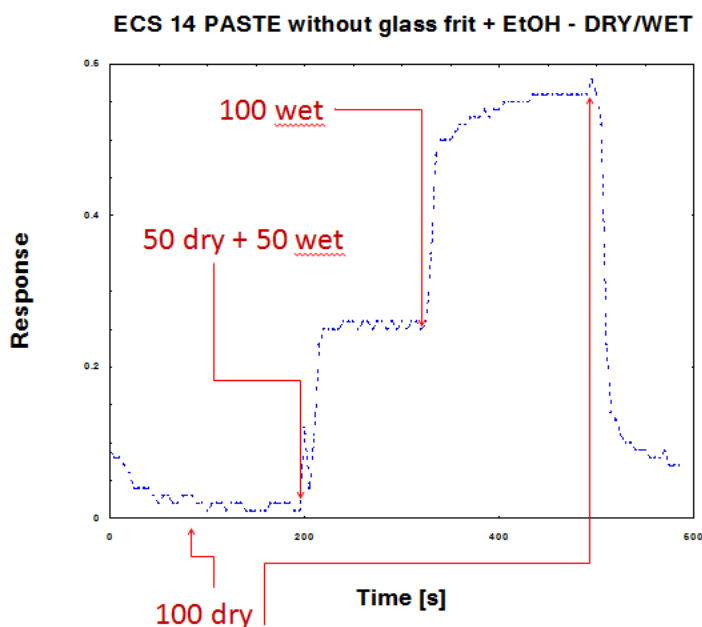
Figure 4.53. Response of sensor produced with ECS 14-PASTE without glass frit and addition of ethanol in DRY/WET conditions.

2) The ECS 12 in the paste formulation without glass frit and with addition of ethanol was tested in the chamber 2 with acetone, benzene, toluene and ethanol. The signals measured in the presence of the gases gave negligible results.

Figure 4.54: Photo of the device made of ECS 12 powder in paste formulation without glass frit and with addition of ethanol.

3) The ECS 13 in the paste formulation without glass frit and with addition of ethanol was tested in the chamber 1 with benzene, toluene, ethanol, acetaldehyde, hydrogen sulfide, CO, ammonia and humidity.

Figure 4.54. Photo of the device made of ECS 13 powder in paste formulation without glass frit and with addition of ethanol.

Below only measures with acetaldehyde (CH_3CHO) are presented, because signals measured in the presence of other gases gave negligible results.
The measurement was performed using a load resistance R_c equal to 1 GΩ and operating at room temperature.

In Figure 4.55 it can be observed that starting from a dry air flow of 100 cc/min a well-defined response already occurs in correspondence of the combination of 90 cc/min dry and 10 cc/min acetaldehyde (equivalent to 10 ppm of gas). First of all, it is important to note the negativity of the response, typical of oxidazing reaction, while measures analyzed so far have a positive response corresponding to a reducing reaction. Furthermore it must be emphasized the rapidity of the response and its stabilization, even if the variation of conductance in the presence of the gas is low. It is fundamental to specify that the response of a signal is a positive defined value, in this case it is intentionally submitted a response characterized by negative values to put greater emphasis on the characteristics detected in the measurements carried out in anticipation of comparison with other tests which will be presented hereinafter.

Then, other two measures were carried out combining dry air and gas: it is observed that, for the both mixture 80 cc/min dry and 20 cc/min acetaldehyde (equivalent to 20 ppm concentration), and 50 cc/min dry and 50 cc/min acetaldehyde (equivalent to 50 ppm concentration), the change in conductance and the answer assume the same value of the first combination dry/gas sent before (10 ppm). So it seems that the device with the combination 90 cc/min dry and 10 cc/min acetaldehyde already reaches a kind of saturation

value. The response of the device has returned quickly to baseline line every time a completely dry flow has been restored.

The device device should be subjected to a further round of measures with acetaldehyde at room temperature.
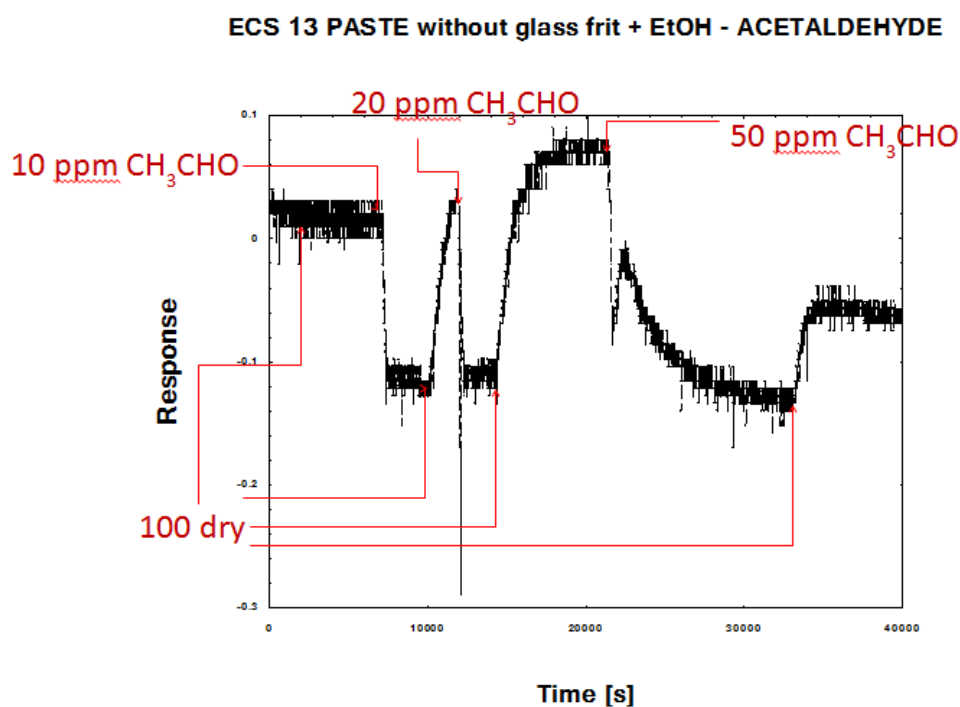
Figure 4.55. Response of sensor produced with ECS 13-PASTE without glass frit and addition of ethanol tested with ACETALDEHYDE in dry conditions.

The graphs shown in Figures 4.56 and 4.57 show the measurements carried out using the same device in tests of acetaldehyde combined with a mixture of dry and wet air.

From the comparison of these two measures with the response showed in Figure 4.54, one can observe that the signals obtained with the addition of water to the mixture in both cases are characterized by a positive response, thereby reducing, in contrast both with the previous measures with gas and complete dry flow, and only with dry/wet flow. The latter, although they had returned a response equal to half of the tests with acetaldehyde and for this reason not presented in this report since considered negligible, however indicated an output voltage decrease and then a conductance decrease.

Instead, when comparing the responses obtained in the two measurements showed in Figure 4.56 and 4.57 similar values are observed, then it appears independent to fix aceltaldeide concentration rather than humidity. This is to mean that it is the presence of humidity to generate a change in the reaction and consequently in the performance of response.

Therefore, it is necessary to test in more detail the device that, from the point of view of the deposition, presents continuous and uniform film as much as that achieved by ECS 14 in the same formulation.
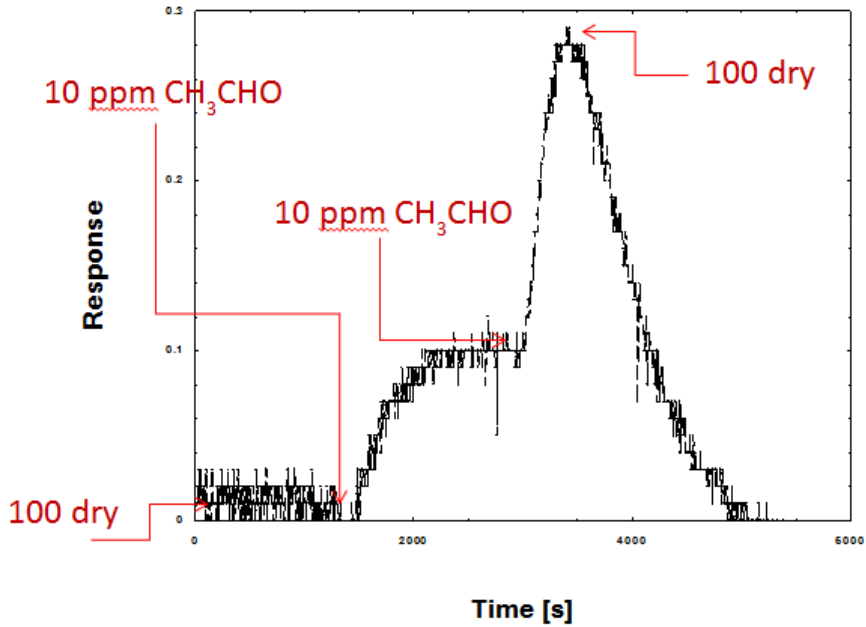
Figure 4.56. Response of sensor produced with ECS 13-PASTE without glass frit and addition of ethanol tested with fixed ACETALDEHYDE concentration (10 ppm) in increasing DRY/WET conditions.
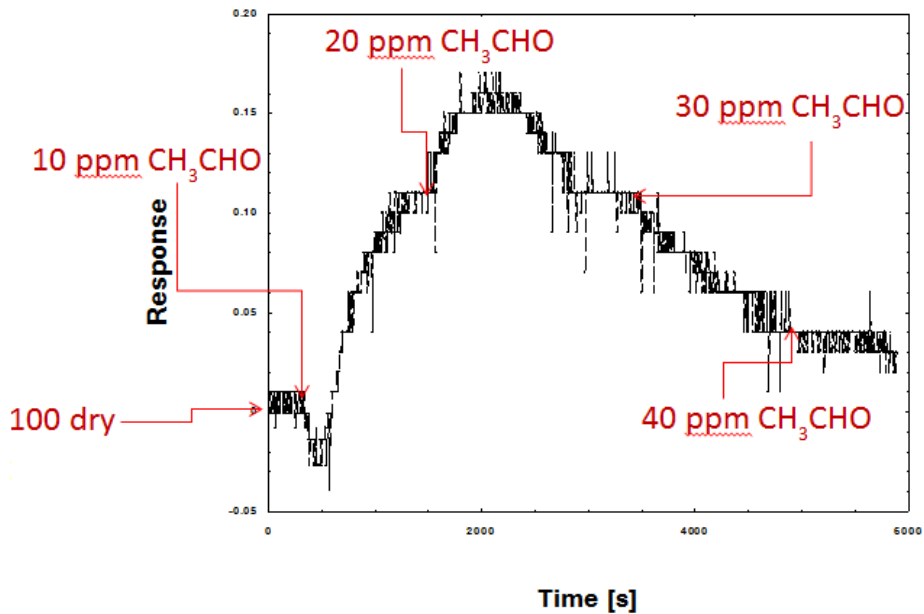
Figure 4.57. Response of sensor produced with ECS 13-PASTE without glass frit and addition of ethanol tested with increasing ACETALDEHYDE concentration in fixed DRY/WET conditions.

4.2.4.4 Study of inorganic component

1) The Zeolite Y(1) in paste formulation without glass frit and with addition of ethanol was tested in the chamber 1 with benzene, acetaldehyde and humidity, but there were no signals variations.
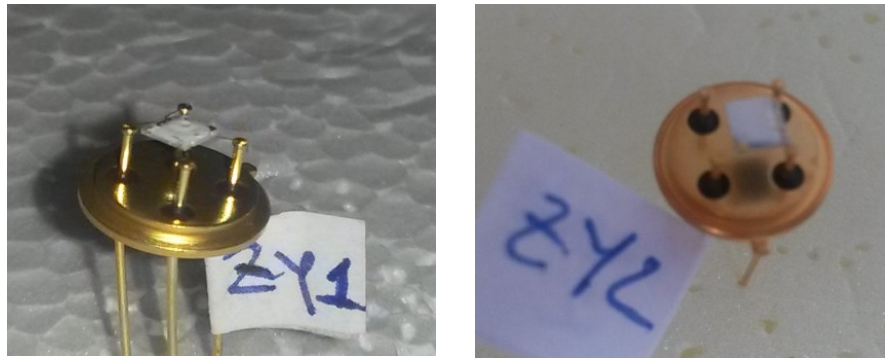
Figure 4.58. Photo of the device made of Y(1) and Y (2) zeolite powders in paste formulation without glass frit and with addition of ethanol.

2) Despite being produced two suspensions using the same formulation employed for Y(1), only with the second deposition it was not possible to provide a device based on Zeolite Y(2). In fact the first deposition on alumina produced, despite the permanence in the hood for several days at room temperature, had a gelatinous consistency, for which it was not possible to produce devices.
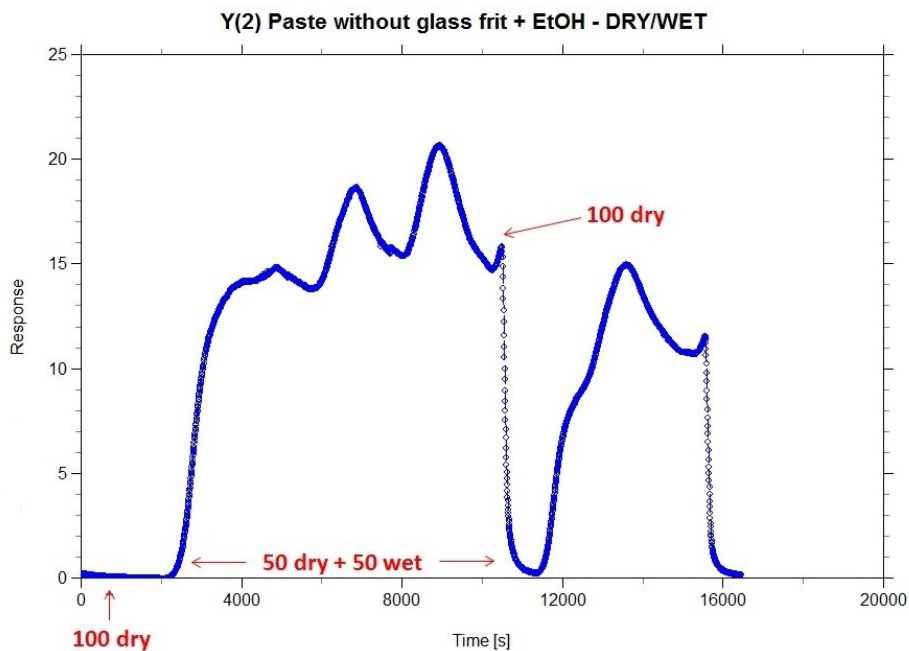
Figure 4.59. Response of sensor produced with Y(2) zeolite PASTE without glass frit+ETHANOL in DRY/WET conditions.

The graph in Figure 4.59 shows the response of the device Y(2) powder based in the paste formulation without glass frit and addition of ethanol in a combination of dry/wet air. The measurement was performed in chamber 1 using a load resistance R_c equal to 47 MΩ and operating at room temperature.

It can be observed that starting from a flow of 100 cc/min of dry air a significant response occurs in correspondence of the combination of 50 cc/min dry and 50 cc/min wet, but it is not stable and it seems affect by a periodical variation. The response time is higher than that of sensor based on ECS 14, whereas the recovery time is similar. Instead the response value is a little bit less than sensor based on ECS 14 prepared with the same composition.

Below in Figure 4.60 humidity calibration performed by steps of 10 cc/min is showed, starting from a completely dry flow arriving at a totally wet flow.
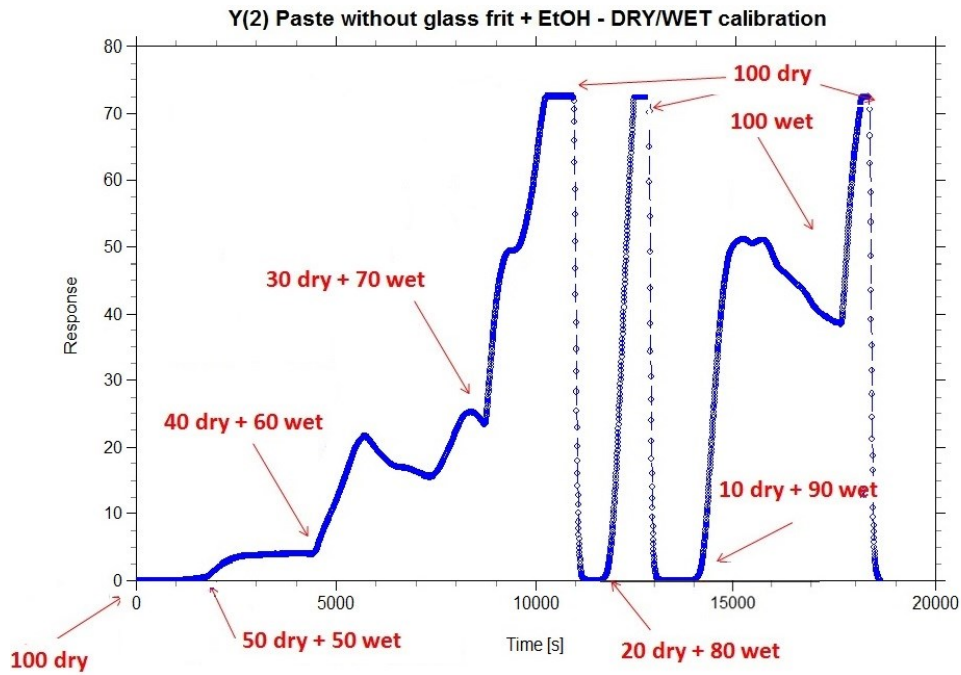
Figure 4.60. Humidity calibration of sensor based on Y(2) zeolite PASTE without glass frit + ETHANOL in the range 100% dry ÷ 100% wet.

In the range from 100% dry to 50 cc/min dry-50 cc/min wet no variation in voltage out was observed. The response corresponding to 50-50 dry/wet is three times lower than the first measurements in the same conditions. For the range 40 cc/min dry-60 cc/min wet the signal is not stable, then for 30 cc/min dry-70 cc/min wet the signal saturates. The same for 100 cc/min wet, while for 10 cc/min dry combined with 90 cc/min wet the sensor gives an high response but absolutely instable.

So, it was chosen to test the repeatability and stability of this sensor prepared by using the inorganic component implemented in ECS powders discovered by Eni.
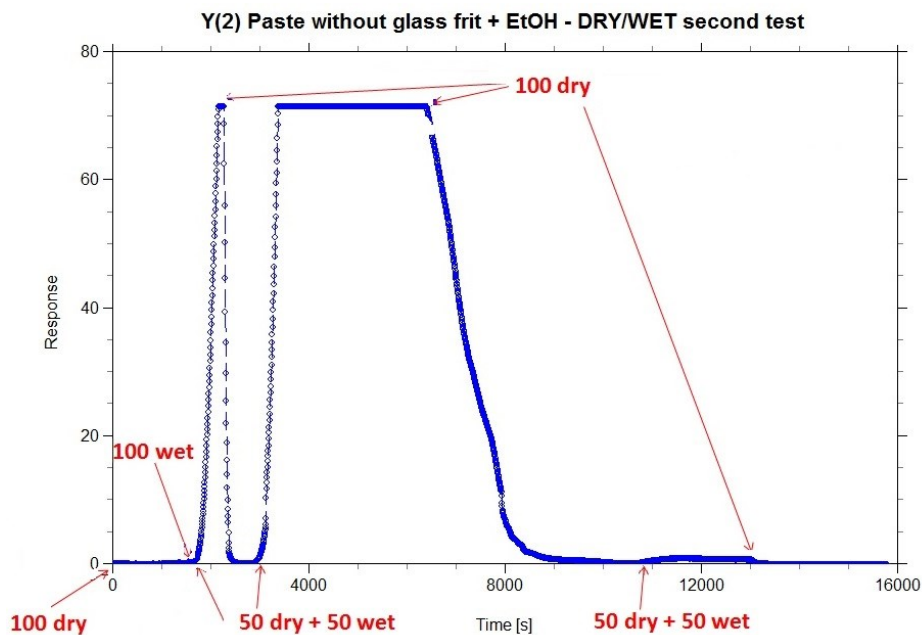
Figure 4.61. Response of sensor produced with Y(2) zeolite PASTE without glass frit + ETHANOL tested in DRY/WET conditions to verify repeatability and stability.

Comparing the three responses at 50 cc/min dry and 50 cc/min wet, with the previous two measurements acquired in the same conditions it is the absence of repeatability and the signal stability seems artificial and depending on a sort of a water saturation inside the zeolite molecule.

4.3 Gas performances: results discussion and interpretation of sensign mechanism

In the following table corresponding to the three films made with each type of material ECS shows the gas tested and their respective results.

Table 4.18. Gas tested and their respective responses obtained by electrical conductivity measurements.

ECS	FORMULATION	GASES	RESPONSE
14	a	CO, METHAN, HYDROGEN SULFIDE, AMMONIA, ACETALDEHYDE, BENZENE, HUMIDITY	HUMIDITY
	b	METHAN, AMMONIA, ACETALDEHYDE, BENZENE, HUMIDITY	HUMIDITY
	c	ACETONE, TOLUENE, ETHANOL, BENZENE, HUMIDITY	BENZENE and HUMIDITY
4	a	*	*
	b	ACETONE, TOLUENE, ETHANOL, BENZENE, HUMIDITY	BENZENE and HUMIDITY
	c	X	*
5	a	X	*
	b	X	*
	c	X	*
9	a	*	*
	b	HYDROGEN SULFIDE, TOLUENE, ETHANOL, ACETALDEHYDE, BENZENE, HUMIDITY	HUMIDITY
	c	*	*
12	a	*	*
	b	*	*
	c	ACETONE, TOLUENE, ETHANOL, BENZENE	NO
13	a	X	*
	b	UMIDITA', ACETALDEHYDE	NO
	c	CO, HYDROGEN SULFIDE, AMMONIA, TOLUENE, ETHANOL, ACETALDEHYDE,BENZENE, HUMIDITY	ACETALDEHYDE
Y (1)	c	ACETALDEHYDE, BENZENE, HUMIDITY	NO
Y (2)	c	HUMIDITY	HUMIDITY

Legend: ***** device not yet tested
X damaged device
NO: no signal
a = COMPLETE PASTE FORMULATION WITH ETHANOL (powder + glass frit + organic vehicle + ethanol)
b = PASTE without glass frit (powder + organic vehicle)
c = PASTE without glass frit and with ethanol (powder + organic vehicle + ethanol)

154

4.3.1 Humidity: comparison between ECS 14 and zeolite based sensors

The most significant results have been obtained with humidity, testing sensors based on ECS 14 powder both in complete and without glass frit paste formulation. The conductance, resistance and response values referred to these measurements are reported in Table 4.19 as function of increasing relative humidity.

Table 4.19. Conductance, resistance and response values obtained in humidity conditions by electrical conductivity measurements with sensors based on ECS 14 in formulation with and without glass frit, and Y(2) in formulation without glass frit.

RH %	ECS 14 Paste + EtOH			ECS 14 Paste without glass frit			Y(2) Paste without glass frit + EtOH		
	G [µs]	R [MΩ]	Response	G [µs]	R [MΩ]	Response	G [µs]	R [MΩ]	Response
5	0,21	4,81	0	1,45	0,69	0	1,45	0,69	0
16	0,21	4,81	0	1,45	0,69	0	1,45	0,69	0
24,1	0,21	4,75	0,01	2,51	0,40	0,74	1,45	0,69	0
32,4	0,22	4,65	0,03	3,55	0,28	1,46	1,53	0,65	0,06
40,7	0,22	4,56	0,05	3,64	0,28	1,52	2,15	0,47	0,49
49,2	0,24	4,16	0,16	5,60	0,18	2,87	7,36	0,14	4,09
57,7	0,31	3,20	0,50	9,04	0,11	5,25	32,5	0,03	21,5
66,5	0,96	1,05	3,59	13,7	0,07	8,47	106	0,01	72,5
74,5	1,17	6	4,60	27,4	0,04	17,9	106	0,01	72,5
84,5	1,20	0,84	4,76	12,3	0,08	7,51	75,2	0,01	50,9
94,4	10,6	0,09	50,1	30,9	0,03	20,4	106	0,01	72,5

In the previous table the results related to sensor based on Y(2) zeolite in paste formulation without glass frit are also reported. Indeed, once obtained such significant response in humidity conditions with ECS 14, a device based only on zeolite used in ECS synthesis was created in order to understand the role of organic and inorganic parts in electrical conduction of the powder.

It is evident that sensor based on ECS 14 in formulation without glass frit has higher performances than complete paste formulation even if the response increase shows an anomalous behavior in correspondence of 84.5 % RH. For what concerns the sensor based on zeolite the response to a complete wet flux is almost three times higher than ECS 14 sensor prepared with the same paste formulation, even if the conductance and response curves showed in Figure 4.62 present the same trend as function of %RH. But one can observe that up to 49.2 % RH the response of zeolite is almost negligible, so it seems there is an activation threshold.
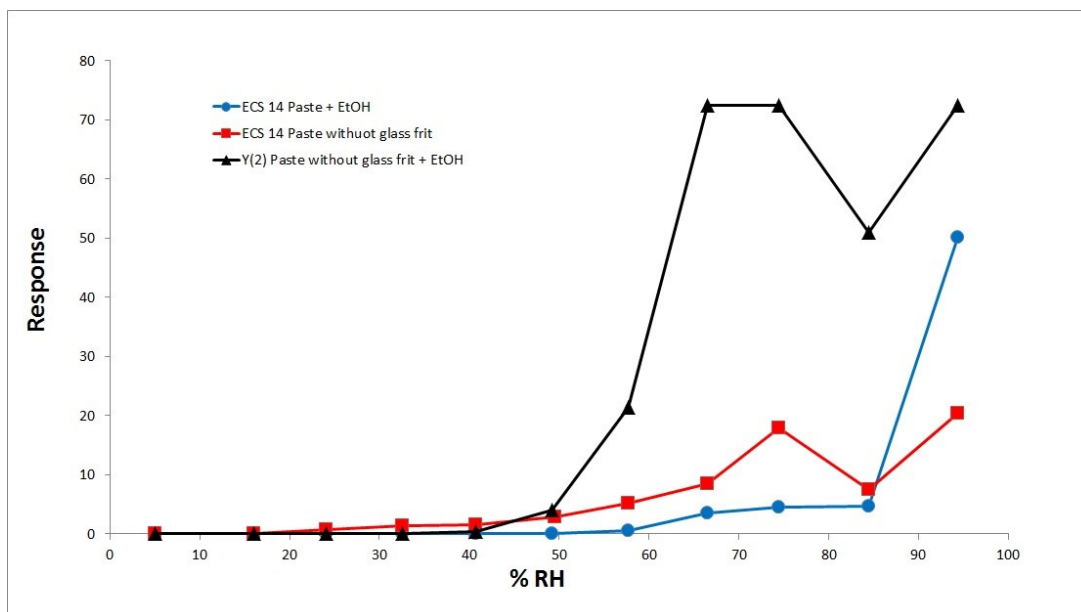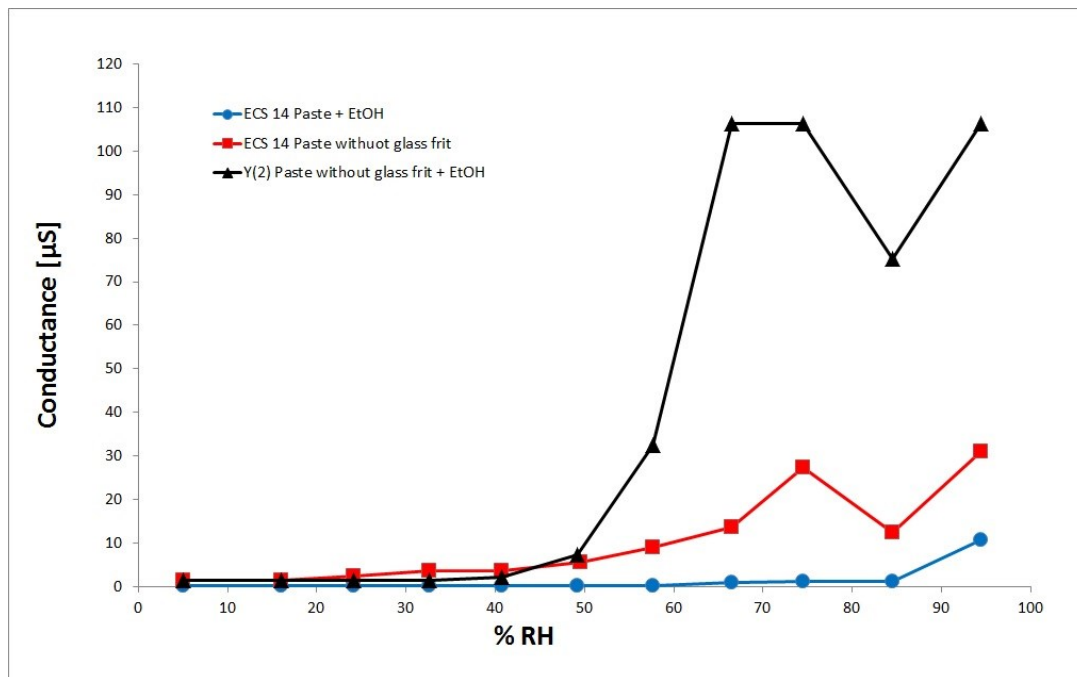
Figure 4.62. Conductance (up) and response (bottom) curves of ECS 14-based sensors as function of humidity concentration in case of complete paste formulation with addition of ethanol (blue), composition without glass frit with addition of ethanol (red), and response of Y(2) zeolite in formulation without glass frit and addition of ethanol (black).

4.3.2 Interpretation of ECS 14 sensing mechanism

Before to determine the role of inorganic and organic components, it was necessary to understand if the conductance variations depend on an interaction of water molecules with possible superficial absorbed oxygen atoms or with ECS's channels. To investigate this aspect two method were useful: tests with Gas Chromatography technique or measurements in nitrogen atmosphere. The former allows to determine possible chemical interaction between gas injected and sensing film; in this case if water and molecular oxygen came out, an absorption of superficial oxygen atoms could be occur. Instead, studying possible conductance variations by measurement in air and in nitrogen atmospheres it is

possible to determine if N_2 take away oxygen atoms on the film surface. It resulted more convenient to use the second method, so sensors based on ECS 14 powder and Y(2) zeolite in paste formulation without glass frit were tested in air and nitrogen condition with injection of wet air for humidity measurements.

Sensor based on zeolite did not show any signal variations in the switch both from dry air to nitrogen conditions and from nitrogen to wet air condition.
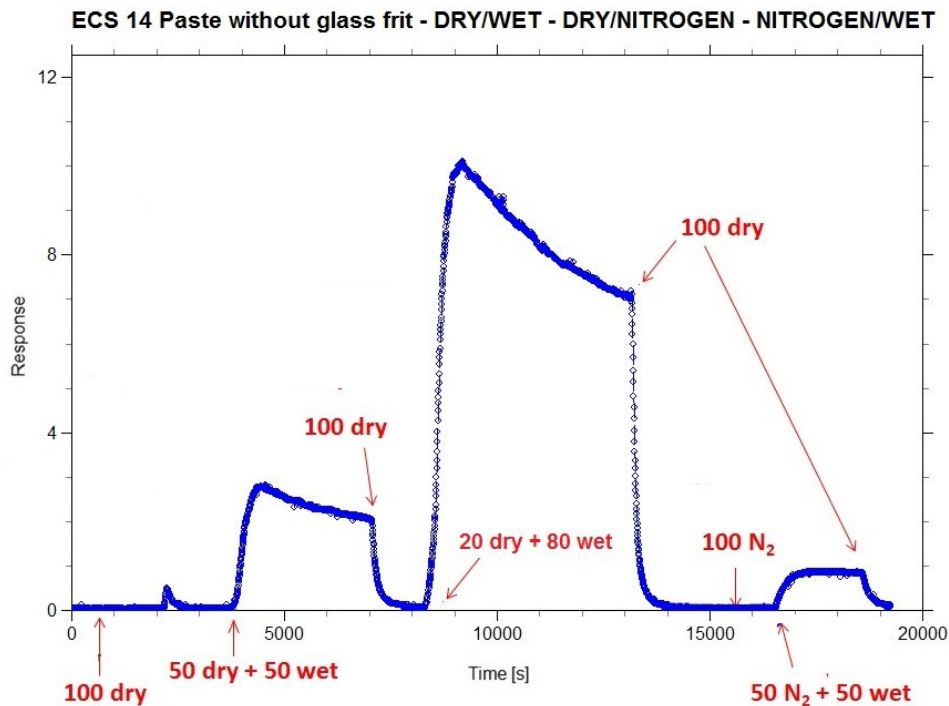
Figure 4.63. Response of sensor based on ECS 14 in paste formulation without glass frit tested in dry/wet and nitrogen/wet conditions.

Figure 4.63 confirms the stability and a discrete repeatability of sensor based on ECS 14. It can be observed absence of conductance variation switching from completely dry air to nitrogen conditions; only a low variations is registered injecting about 50% of relative humidity.

So it can be concluded that sensing mechanism depends on interaction between water molecules and ECS's channels, and superficial absorption gives a negligible contribution.

At this point, two fundamental factors have to be considered: first the respective dimensions of water molecule and ECS 14 channels, second the high electronegativity of water.

The ECS 14 has channels of 7.5x9 Å, while water is a planar molecule 0.59 Å high and 1.5 Å large so it can pass both in the main and in the secondary channels, which are almost three times smaller than the former. Since oxygen has a higher electronegativity, the summit of the molecule hosts a partial negative charge (δ-), while the ends entail partial positive charge (δ+); then the best candidate inside the ECS 14 structure is the sodium (0.93), which has about four times less electronegativity than oxygen atom (3.44). As shown in Figure 4.64, when water molecules meet sodium atom form an hydration layer with a preferential orientation and a limited freedom of movement. Then, most likely one can suppose that water molecules enters in the secondary channels of ECS 14 with oxygen atoms oriented towards sodium (yellow balls). So the latter, introduced in the synthesis by sodium aluminate ($NaAlO_2$) and sodium hydroxide (NaOH), is unarguably the receptor function.
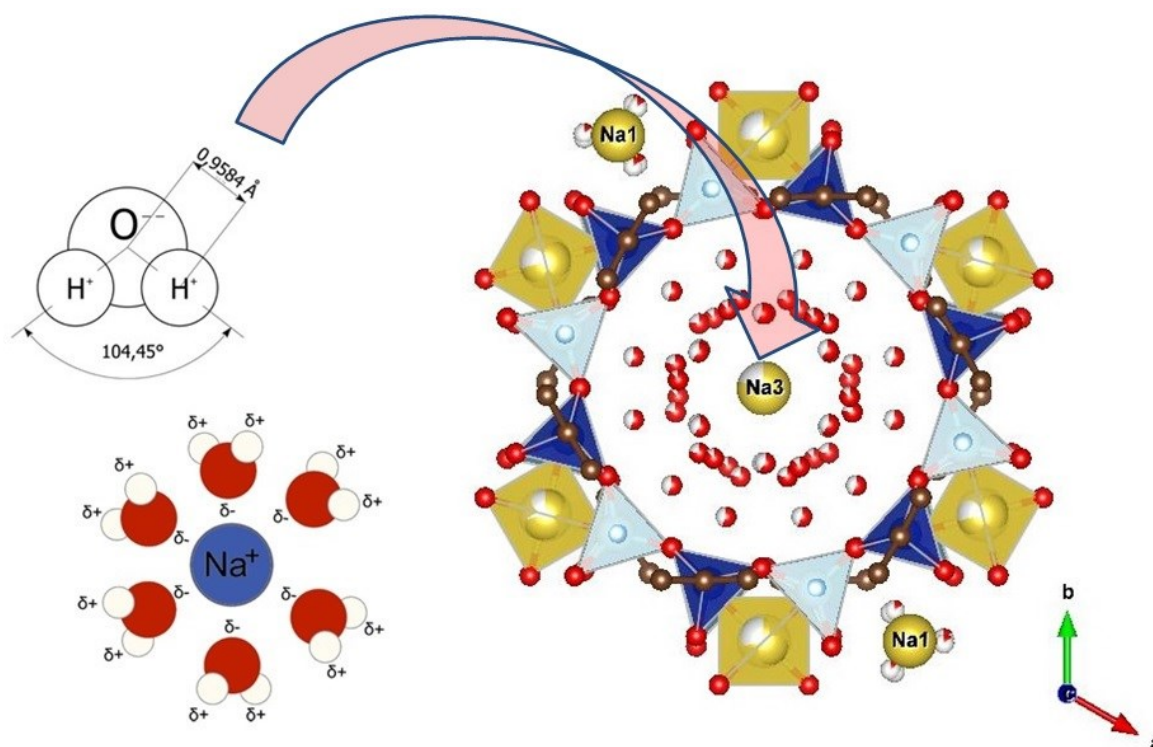
Figure 4.64. Schematic representation of interaction water-ECS 14.

In the light of these hypothesis and also of the fact that an electrical activity with zeolite containing sodium was registered, it has to investigate its role in sensing mechanism of ECS powders. Referring to sensors performances in humidity conditions discussed before, it is clear that the presence of inorganic component for the sensing mechanism is important, but it is not exclusive. Indeed, even if Y zeolite contributes to humidity detection, the measurements with sensor based on pure inorganic component show a lack of stability and repeatability, then it is difficult to control such device. Then, it is convenient to deep the interaction of this zeolite with water starting from a brief introduction to zeolites.

4.3.2.1 Receptor function: Hydrophilic zeolites

It is known that zeolites are microporous aluminosilicate minerals, commonly used as commercial adsorbents and catalysts; their porous structure can accommodate a wide variety of cations, such as Na^+, K^+, Ca^{2+}, Mg^{2+} and others. These positive ions are rather loosely held and can readily be exchanged for others in a contact solution. The term zeolite means "boiling stone", from the Greek ζέω (zéō), meaning "to boil" and λίθος (líthos), meaning "stone"; it was originally coined because upon rapidly heating the material, it produced large amounts of steam from water that had been adsorbed by the material. Zeolites are the aluminosilicate members of the family of microporous solids known as "molecular sieves." The term molecular sieve refers to a particular property of these materials, i.e., the ability to selectively sort molecules based primarily on a size exclusion process. This is due to a very regular pore structure of molecular dimensions. The maximum size of the molecular or ionic species that can enter the pores of a zeolite is controlled by the dimensions of the channels.

Recently, it has been demonstrated that in presence of sodium and temperatures USY zeolites may undergo framework destruction by scission of ≡Si−O−Si≡ bridges and, as framework is destructed, the material retains a lower number of water molecule; it loses microporosity and the average pore size increases. Moreover, the amount of sorbed water decreases with sodium load what could be related to reduction in zeolite's crystallinity, as

one expects more water to be retained by materials with more cavities. Average pore size is almost constant at loads below 15%, but this quantity increases in samples with higher loads [2]. Anyway, Y zeolites containing sodium have demonstrated to adsorb substantially more water than others without sodium. This is shown in Figure 4.65, which illustrates the water adsorption at room temperature of aluminium deficient US-Y type zeolites, CBV-780 and CBV-901, and CBV-100 which is an NA-Y zeolite (commercial zeolites manufactured by Zeolyst International) [3].
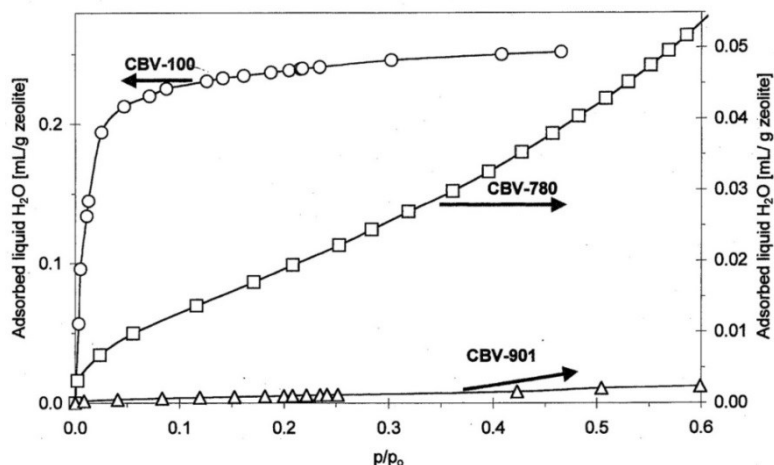
Figure 4.65. Adsorption of water on hydrophilic (CBV-100) and hydrophobic (CBV-780 and CBV-901) zeolites at room temperature [3].

Specific experiments and relative simulations of water adsorption on hydrophilic zeolite (CBV-100) are presented in Figure 4.66. The curve obtained with simulation at 200°C suggests that water largely adsorbs on the external surface at elevated temperatures even on this hydrophilic zeolite. It is not clear whether the adsorbent-adsorbate interaction is too weak to hold the physorbed water molecules in the micropores at higher temperatures or diffusion control prevents a micropore condensation (Langmuir isotherm) [3].

This difference in water adsorption between zeolites with and without sodium confirms the results obtained with sensors based on Y(1) and Y(2) zeolites in paste formulation without glass frit and addition of ethanol. Therefore, aslo the role of receptor function of inorganic part in ECS 14 humidity detection is confirmed. In any case, since it has demonstrated that Y(2) zeolite alone is not sufficient to repeat performances obtained with sensor based on ECS 14, it has to determine the possible role of organic part.
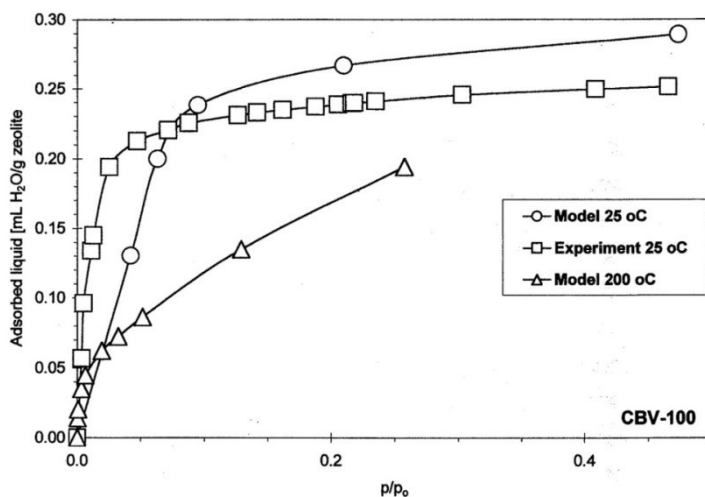
Figure 4.66. Experimental and simulated adsorption isotherms of H_2O on hydrophilic zeolite (CBV-100) [3].

4.3.2.2 Water detection: more information by optical characterizations

To understand the sensing mechanism of ECS 14 in presence of steam it results useful to compare optical measurements performed for a parallel project indeed on optical properties of ECS materials by Prof. Alberto Quaranta (University of Trento).
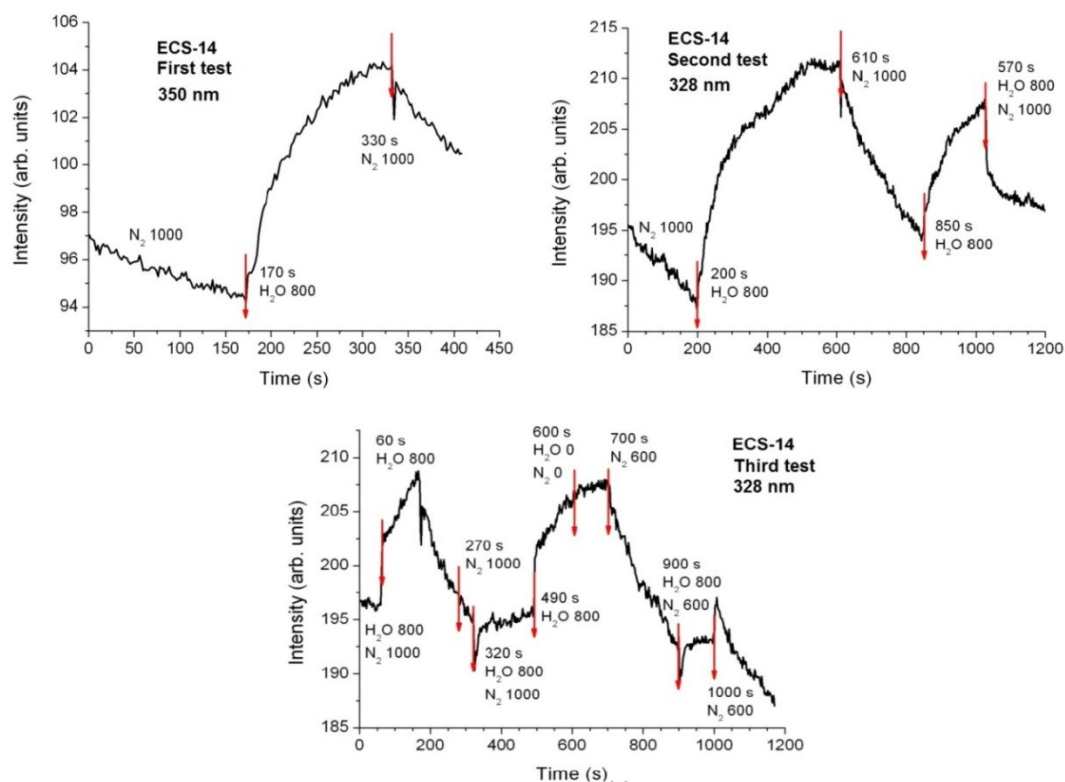
Figure 4.67. Optical measurements on ECS 14 tested with steam.

Tests in N_2/steam conditions were performed with an experimental setup similar to that used in this work for electrical characterizations, replacing the gas test chamber with an optical spectrometer containing an appropriate analysis chamber.

Results of three different proves, in Figure 4.67, show a decrease in N_2 atmosphere and an increase in steam conditions for ECS 14 emissions, at 290 nm (isolated rings) and 350 nm. Then, the ECS 14 emission decrease for dehydration and increase for rehydration. The significant decrease of isolated species emission could be associated with a major quenching due to a stronger interaction corresponding to dehydration.

A similar phenomenon was observed also for ECS 17, another material synthetized wth the same precursor of ECS 14. ECS 17 is the first aluminosilicate built from only the three-ring secondary building unit. This new material shows intriguing reversible collapsibility upon dehydration/rehydration. Mild thermal treatment under vacuum causes its crystalline structure to collapse due to facile elimination of the water molecules around the cations. Successive exposure to ambient atmospheric moisture gives back the hydrated crystalline form [4].

Aromatic ECS hybrids are optically active in absorption and emission and suitable for applications such as wavelength converters and antenna systems, where they could be employed as donors [5-6]. While the presence of the organic component introduces interesting optical properties, it makes hybrid materials less thermally stable than their totally inorganic counterparts.
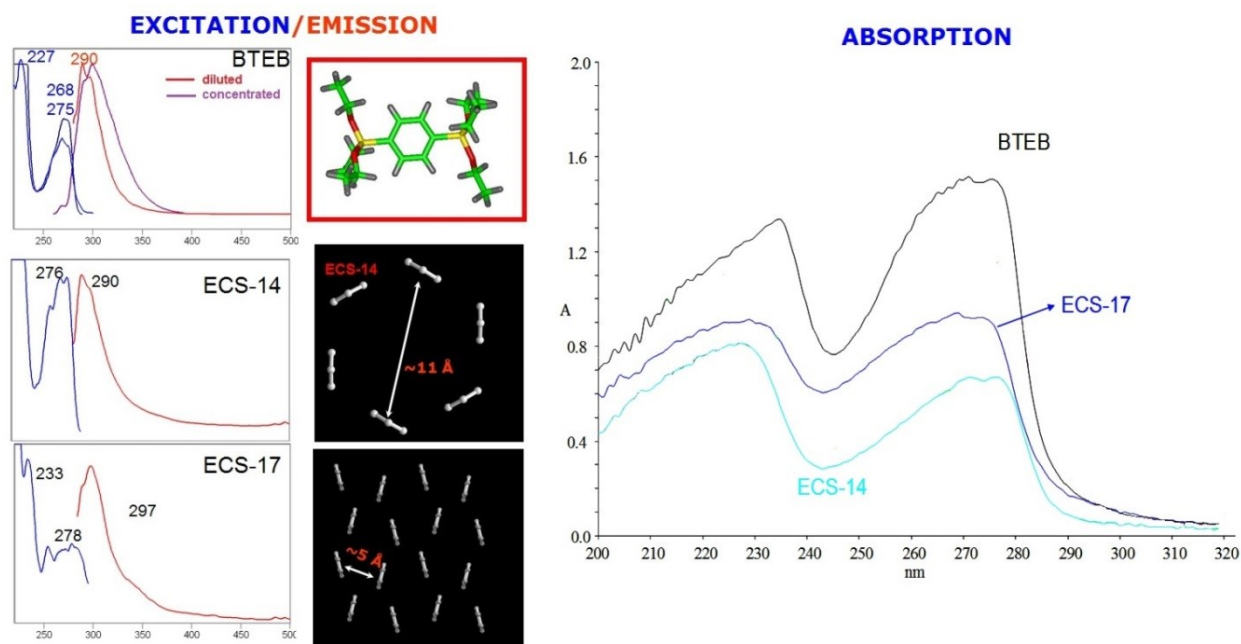
Figure 4.68. Optical spectra of precursor BTEB, ECS 14 and ECS 17 powders.

The optical properties of the hybrid solids, showed in Figure 4.68, are determined by the organic component (monomeric and excimeric emission of BTEB at 297 and $\approx$ 330 nm respectively).

ECS-14 emits at almost the same wavelength as the precursor, at variance with ECS 17, whose emission band is red-shifted signalling an electronic interaction that does not occur in ECS 14 in agreement with the different configuration of aromatic rings. Despite the close packing the emission of the rings is not significantly quenched.

Absorption and emission vary, pointing to diverse structural arrangement of the aromatic units and increasing interaction (lower distance) at higher red shift (ECS 14 $\leq$ ECS 17).

The same analysis were carried out applying a treatment overnight under vacuum (10^{-3} mbar) at 70 °C, in order to investigate the effect of dehydration/rehydration on ECS 17 and ECS 14.

Concerning the electronic transitions in ECS 17, both absorption and emission are red-shifted with dehydration under vacuum over the 25−70 °C range. Absorption positions for ECS 17 shift from 227 and 268.5 nm to 231 and 273.5 nm. These evidences points to an increased interaction among aromatic units in the dehydrated material. This could result from one or more factors: (i) changes in the ring's chemical environment; (ii) reduced distance between rings; and (iii) increased coplanarity between rings. This finding is in agreement with the structural changes demonstrated for ECS 17 in Ref. [4]. Moreover, in emission, the fluorescence intensity of monomeric species shifts from 292 nm to 298.7 and decreases in intensity, while the intensity of the shoulder at 340 nm due to excimers increases somewhat (Figure 4.69 a). For ECS 14, no shifts are shown but there is an intensity increase corresponding to dehydration. Instead, the emission shows the same behavior described for ECS 17, but for ECS 14 the recovery with rehydration is not complete, as observed with ECS 17 exposed to the same treatment but at room temperature. (Figure 4.69 b).
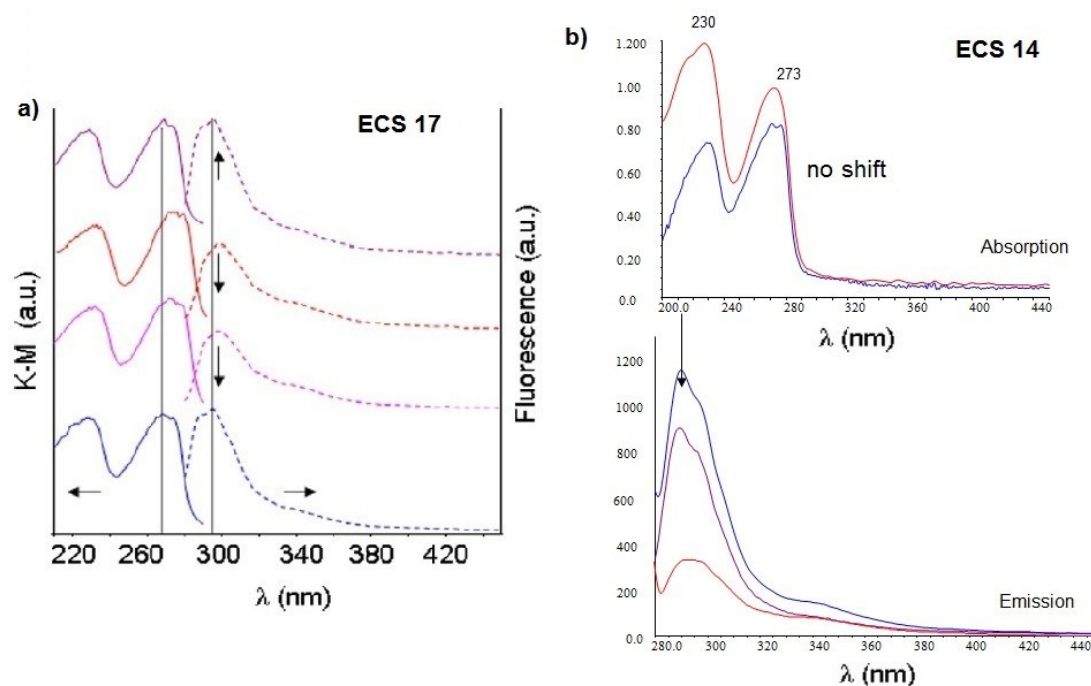
Figure 4.69. Optical spectra of a) ECS 17 as-synthesized (blue), after dehydration overnight under vacuum at 25 °C (pink) and at 70 °C (red), and after re-equilibration under ambient humidity (purple).
Continuous line = normalized absorption spectra reported in Kubelka−Munk function; dotted line = fluorescence emission at λexc= 270 nm [4]; b) ECS 14 as-synthesized (blue), after dehydration overnight under vacuum at 25 °C (pink) and at 70 °C (red), and after re-equilibration under ambient humidity (purple).

Also absorption spectra in the NIR region were collected to monitor changes in vibrational properties caused by the hydration state of ECS 17 and 14. These spectra are compared with the spectra for the pure BTEB precursor and a Na−Y zeolite (HSZ-320NAA Tosoh) in Figure 4.69. The vibrational absorption bands arise from:

- silanols bonding water molecules, giving rise to a broad band near 6800 cm^{-1} (first overtone of OH groups) with two resolved components maxima at 6980 and 6740 cm^{-1}, similarly to silanols in Y zeolite interacting with H_2O or other OH groups,
- physisorbed water with a strong band centered at 5177 cm^{-1},
- organic compounds giving a weak band at 5909 cm^{-1} due to the first overtone of C−H groups,
- organic (with C−H and C−C combination) and inorganic (with O−H overtone) components in the complex 4200−4700 cm^{-1} region, with peaks at 4517 and 4416 cm^{-1}.

In Figure 4.70, the effect of dehydration/rehydration is reported as well, showing that treatment overnight under vacuum (10^{-3} mbar) at 70 °C effectively dehydrated the sample, removing the signal at 5177 cm^{-1} due to physisorbed water. The OH signals sharpened and shifted to higher energy (new maximum at 7193 cm^{-1}) in the position attributed to isolated silanols in inorganic matrixes and in hydrophobic BTEB. The benzene absorptions around 5900 and 4500 cm^{-1} were not affected by dehydration.

Optical and vibrational properties confirmed that physisorbed water is easily removed from ECS 17 and ECS 14. The effects of rehydration, under ambient conditions, on the vibrational and electronic properties are reported in Figures 4.69 and 4.70. The OH absorption, physisorbed water signal, electronic absorption, and emission were restored as for the as-synthesized sample [4].
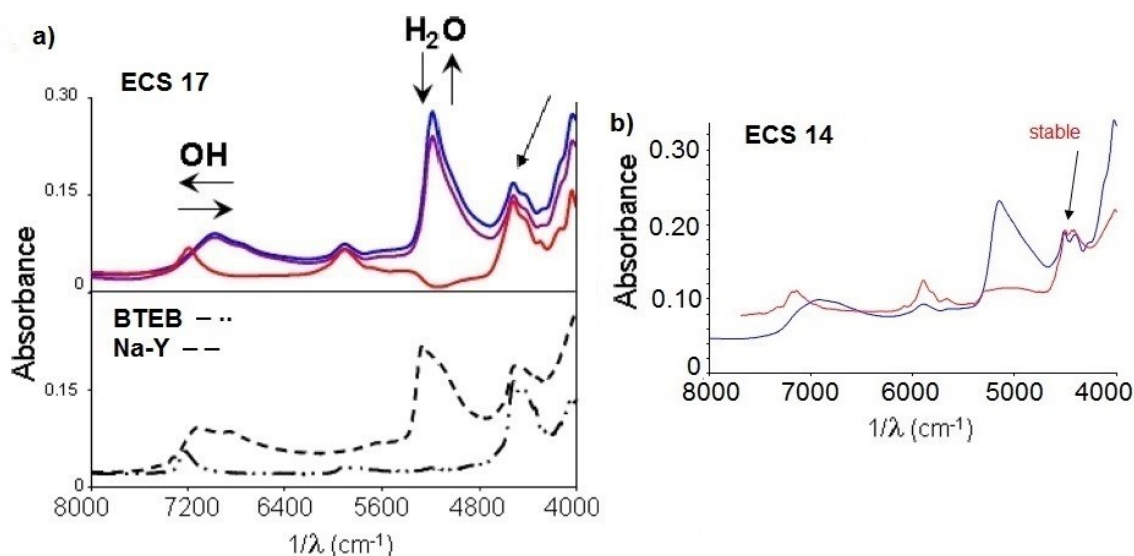
Figure 4.70. a) Top: NIR spectra of ECS 17 as-synthesized (blue), after dehydration overnight under vacuum at 70 °C (red), and after reequilibration under ambient conditions (purple). Bottom: NIR spectra of the BTEB precursor and Na−Y zeolite. b) NIR spectra of ECS 14 as-synthesized (blue), after dehydration overnight under vacuum at 70 °C (red).

In Ref [4] it was concluded that drying under vacuum, or simply dehydration, caused the structural collapse triggered by the loss of hydration water molecules around the cations. Rehydration completely reversed the collapse. Equating the hybrid structure of ECS 17 to an inorganic zeolite and following the classification schemes of the zeolite thermal behavior [7], we can conclude that the ECS 17 framework is "collapsible" following the Baur classification [8]. Because the collapse is fully reversible, it is classified as category 2 (completely reversible dehydration accompanied by a large framework distortion and decrease in unit cell volume) [9]. The optical properties of "collapsed" ECS 17 differed from the as-synthesized form by red shifts in both absorption and emission spectra. Partial quenching of monomeric emission fluorescence agrees with the increased ring interaction for the dehydrated structure [4].

On one hand, since ECS 14 does not show red shift in hydration conditions, no stronger rings interaction occurs with respect to ECS 17. On the other side, the intensity decrease in hydration might be associated to a slight collapse as for ECS 17. But, it is significant to highlight the stability of ECS 14 at low energy, whereas ECS 17 suffers of partial decrease. Moreover, the peak at 5909 cm^{-1}, belonging only to organic compound, is maintained in the transition hydration/rehydration. This suggests that, while in hydration the ECS 17 collapse is slightly wide, for ECS 14 the organic part play an anchoring role for the structure, as a bridge between hydration and rehydration structure configurations. This "bridge" could be the transduction element in humidity sensing mechanism.

4.3.2.3 Transduction function: holes or electrons for electrical transport?

In the brief discussion about gas sensors presented in Chapter 3, it arises they are composed of two main elements: a receptor and a transducer. Until now, the investigation about humidity sensing by ECS 14-based sensor has identified sodium atoms as receptor, belonging to inorganic component, which induces a change in its own properties interacting with the target gas. But a detailed analysis on humidity measurements with sensors based on ECS 14 and on the Y zeolite used in its synthesis as inorganic component revealed that, despite zeolite showed a significant conductance variation at room temperature, the

response was not stable and repeatable. Moreover, for zeolite-based sensor it seemed necessary an humidity threshold to activate the detection. Then, thinking about the high performances of ECS 14-based sensor, it is clear that the sensing mechanism depends not only on inorganic component, but also on the organic part that seems fundamental to govern the properties changes induced by zeolite, and then to confer the mentioned features. Therefore the organic component acts as transducer, transforming the effect of interaction between sodium and water molecule into an electrical signal (sensor response).

Analyzing ECS 14 structure, it could be possible to investigate the different mechanism that might occur by interaction of the hybrid material with water molecules.
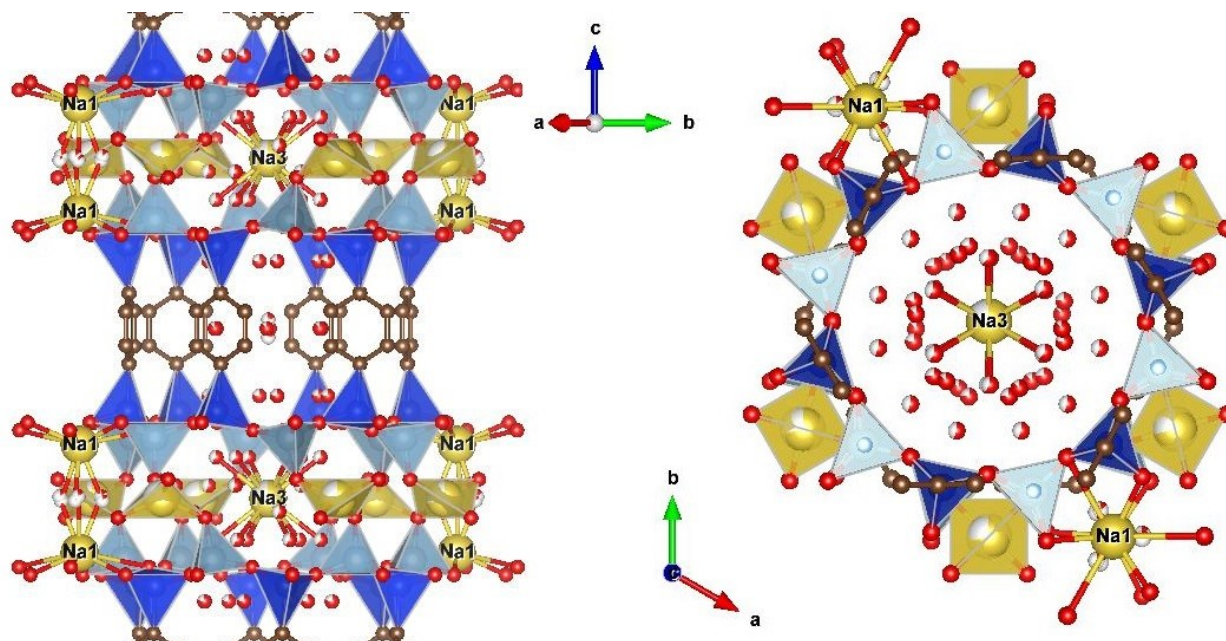
Figure 4.71. Detailed representation of ECS 14 structure: [SiO$_3$C] tetrahedral in light blue, [AlO$_4$] in blue, phenylene rings in brown, oxygen atoms in red, sodium in yellow. H$_2$O molecules can be distinguish by H atoms in white [images granted by Prof. Cruciani].

Considering sodium atoms in ECS 14 (Figure 4.71), one can observe the presence of three sites which have different structural roles:

- o **Na(1)**, with occupancy of 100%, coordinates oxygen atoms belonging to SiO$_4$ and AlO$_4$ scaffolds, but also H$_2$O sites with low occupancy;
- o **Na(2)**, indicated by a yellow tetrahedral, has occupancy of ~70% and completes the scaffolds connection coordinating 4 oxygen atoms belonging to AlO$_4$ and being highly underbonded;
- o **Na(3)**, with occupancy of ~80%, is placed in the cavity center and it is totally solvated by 12 water molecules

The distances of Na(1)-O and Na(3)-O from water molecules are between 2.3 and 2.7 Å, but Na(1) has other three bonds 3.2 Å long.

The residual H$_2$O molecules are placed at 3.5 Å from sodium atoms, then they form H-bonds and/or weak interaction creating a complex network.

It is not easy to associate the conductance increase acquired by electrical measurements with interactions of water and ECS 14 structure, and a possible comparison with metal-oxides semiconductors, that recorded a conductance increase when interact with reducing gases, does not result useful because they are governed by band structure.

So, it has to be identified the cause of conductance increase in ECS 14. Now, considering the kind of interaction between water and the three "Na types", some consideration regard to possible effect on ECS 14 structure are proposed.

Starting from Na(1), that coordinates base oxygen atoms belonging to SiO_4 tetrahedral, one might suppose that these oxygen atoms undergo a variation in charge contribution due to H_2O absorption. The apical oxygen atoms of the tetrahedral should convey of this change and then to transfer it to benzene rings, borne by the same apical oxygen atoms, which could generate a negative carrier flux through their electronic cloud. Benzene is characterized by carbon atoms sp^2 hybridized, they form a planar six-membered ring: each carbon has a p orbital available for overlap with p orbitals of its neighboring carbons. If we consider favorable overlap of these p orbitals all around the ring, the result is the model shown in Figure 4.72 [10].
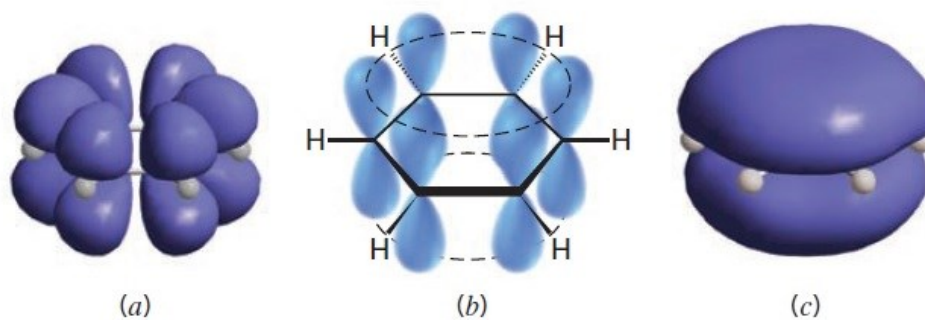
Figure 4.72. (a) Six sp^2-hybridized carbon atoms joined in a ring (each carbon also bears a hydrogen atom). Each carbon has a p orbital with lobes above and below the plane of the ring. (b) A stylized depiction of the p orbitals in (a). (c) Overlap of the p orbitals around the ring results in a molecular orbital encompassing the top and bottom faces of the ring [10].

A similar situation may occur for Na(3), placed in the center of the larger channel and solvated by 12 H_2O atoms, even if the solvation shell of Na(3) is rather distant from organic layer. So it might think that the perturbation involves the second or the third shell. Anyway, the respective dimensions of water molecule and main channel create a more favorable condition for interaction between Na and water.

Considering Na(2), bonded with four oxygen atoms of AlO_4 tetrahedral, it is possible that its interaction with water molecules generates an hole transport due to the oxygen vacancies typical of alumina. This effect might be added with a charge defect due to an overall content of ~14 Na atoms per unit cell, far below the content necessary for compensating the charge of the 24 Al atoms present in the unit cell [5].

These considerations are only suppositions because a more deepened study has to be carried out. In particular simulation about dislocation of electronic density and FTIR analysis in operando mode would give some useful information to explain the possible conduction mechanism.

How the organic component operates as transducer is difficult to determine and reach more investigations. Anyway, considering the state of art regard electrical properties of other organic-inorganic materials such as the amorphous precursors PMOs, and other complex system as hybrid perovskites [11-13].

4.3.3 Comparison between ECS 14-based and well-known humidity sensors

A brief comparison between ECS 14-based and other types of humidity sensors is presented, in order to verify if the performances of new hybrid sensors could be considered of high level.

It was chosen devices operating at room temperature tested with different humidity concentration, so to replay the measurements conditions used for ECS 14.

The sensors chosen were composed of manganese oxides and poly(o-anisidine) composites.

Figure 4.73 a shows typical responses of three sensors based on different manganese oxides. These oxides gave resistive type elements which reduced d.c. resistance on exposure to humidity at room temperature.
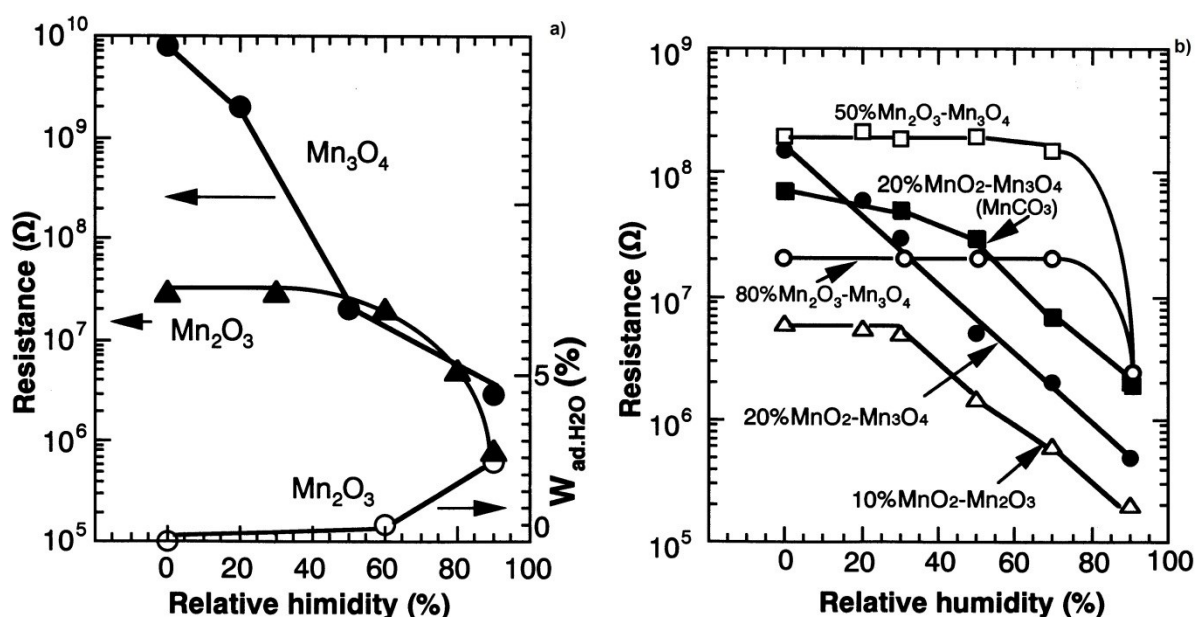
Figure 4.73. a) The d.c. resistance and reversible water content for an element using Mn_2O_3 (calcined at 600°C) and Mn_3O_4 (calcined at 1000°C) as a function of relative humidity. b) Relative humidity dependence of d.c. resistance for various elements using hybrid systems [14].

The resistance of the element using MnO_2 or Mn_3O_4 decreased slightly or drastically, respectively, with increasing RH. On the other hand, the one using Mn_2O_3 was sensitive to humidity only in the high RH range above 60%. The humidity sensing behavior was strongly dependent on the oxides, reflecting the differences in microstructure.

The sensor elements using MnO_2, Mn_2O_3 and Mn_3O_4 as a single phase have limitations in humidity sensing performance due to the microstructures and/or resistances of the respective oxides. The use of a mixture of these oxides (hybrid system) was found to be effective for optimizing humidity sensing performances (Figure 4.73 b).

A satisfactory humidity sensing performance can be achieved by the use of a mixture 20%MnO_2–Mn_3O_4 [14].
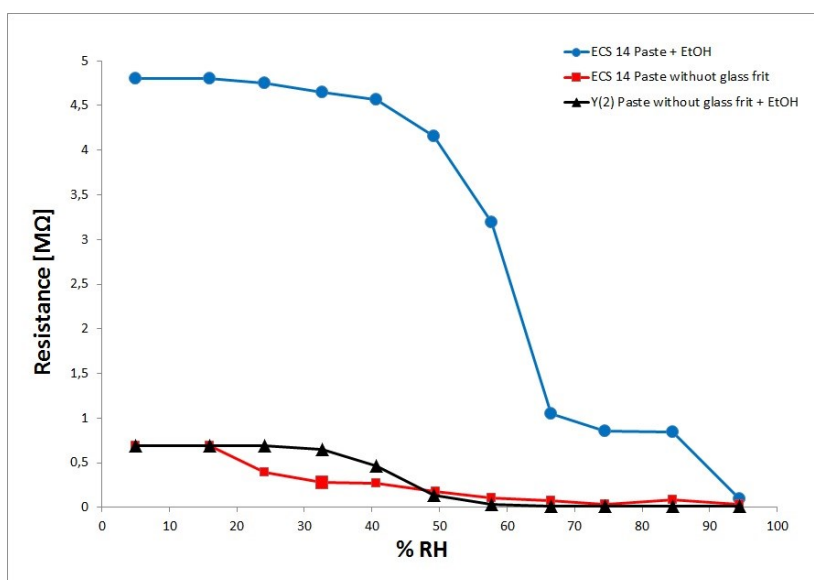
Figure 4.74. Resistance curves of ECS 14-based sensors as function of humidity concentration in case of complete paste formulation with addition of ethanol (blue), composition without glass frit with addition of ethanol (red), and response of Y(2) zeolite in formulation without glass frit and addition of ethanol (black).

By the comparison of manganese oxides as single phase and also as hybrid system with resistance values obtained with sensors based on ECS 14 in complete and without glass frit paste formulation, one can observe that the behavior of sensor in complete paste formulation is similar to 50%MnO_3–Mn_3O_4. Instead, sensor based on formulation without glass frit shows a slighter decrease, the same for zeolite. Regarding the values obtained, it can be asserted that at room temperature ECS 14-based humidity sensors has a similar resistance variation to chemoresistive metal-oxides sensors, even if not so high as for mixture 20%MnO_2–Mn_3O_4.

A comparison with pure organic and organic/metal oxide composites tested in humidity at room temperature is also proposed. It has been demonstrated that electrical conductivity of polymers and its derivatives strongly depends on the redox state, doping level and moisture content. This property provides a possibility of using these polymers as a humidity sensing materials. Recently, polymer/inorganic composites have been considered for their improved properties compared with those of pure conducting polymers and inorganic materials [15].
Figure 4.75 shows resistance variations of poly(o-anisidine) (POA) and poly(o-anisidine)/WO_3 (POA/WO_3) composites with two different WO_3 weight percents.
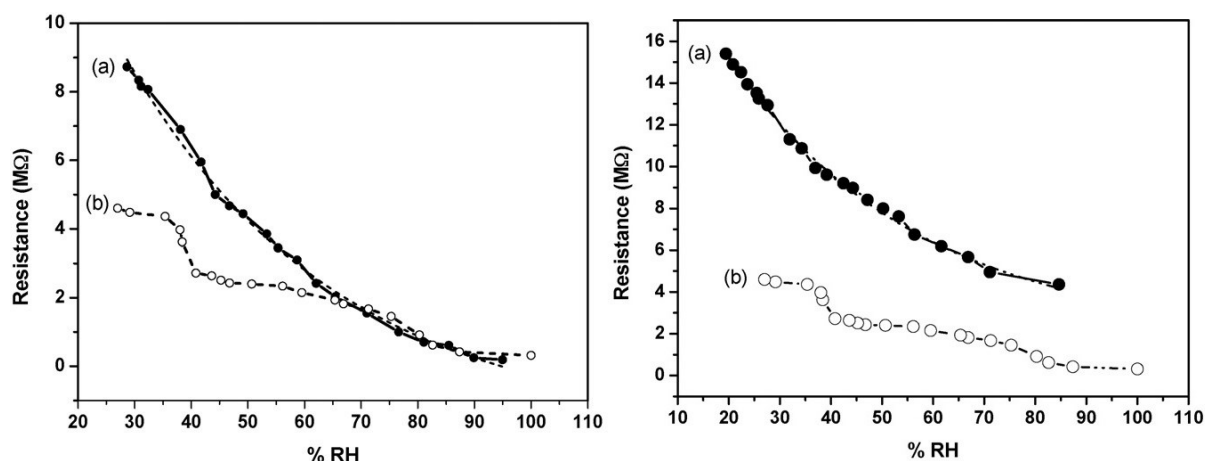
Figure 4.74. Variation of resistance as function of relative humidity for ((a-left) POAWO10, (a-right) POAWO30 composites, and (b) POA [15].

167

It is seen that the resistance decreases with an increase in RH for POA as well as for all the composites. Then, when the wt% of WO_3 in the composite is increased form 10% to 30%, the variation in resistance is qualitatively similar to that of POAWO10. The resistance value of the composites are higher than that of pure POA, due to hygroscopic property of the oxide.

It is observed that the humidity sensing properties of POA/WO_3 composites are better than those of the pure POA [15].

It can be observe that the resistance trend of ECS 14-based sensor showed in Figure 4.73 is similar to that of POA in Figure 4.74, but the variation for relative humidity increase is higher, as for POAWO10-30.
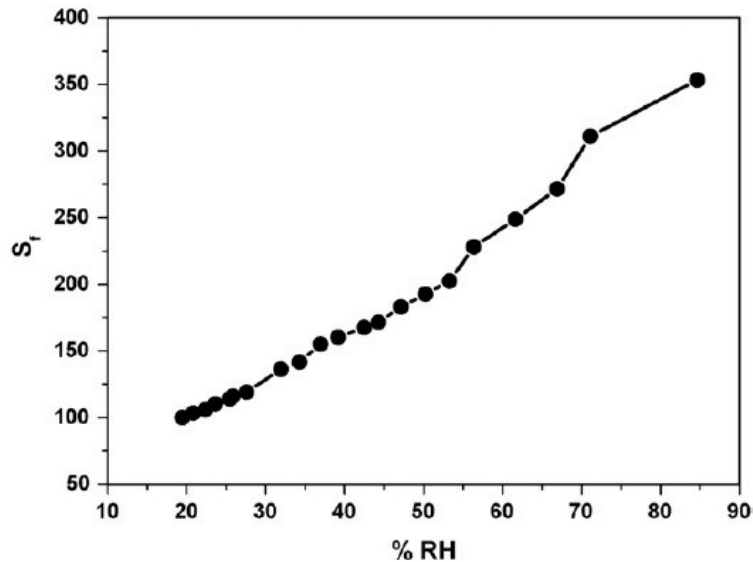
Figure 4.76. Variation of percentage response factor S_f with change in relative humidity (%) for POAWO30 composite [15].

Comparing the percentage response for POAWO30 in Figure 4.76 with response of ECS 14-based sensors in Figure 4.62, one can conclude that ECS sensors shows better response than organic/metal oxide sensor.

Concluding, the performances of ECS 14-based sensor is comparable with commercial humidity sensors based on metal-oxides semiconductors, and it is more sensitive than other hybrid devices.

Reference

[1] http://www.tosoh.com/our-products/advanced-materials/zeolites-for-catalysts

[2] Sandoval-Díaz L.-E., Palomeque-Forero L.-A., Trujillo C. A. , Towards understanding sodium effect on USY zeolite, Applied Catalysis A: General 393 (2011) 171–177

[3] Halasz I., Kim S., Marcus B., Hydrophilic and hydrophobic adsorption on Y zeolites, Molecular Physics 100 (2002) 3123-3132

[4] M. Bellettato, L. Bonoldi, G. Cruciani, C, Flego, S. Guidetti, R. Millini, E. Montanari, W. O'Neil Parker Jr., S. Zanardi, Flexible structure of a thermally stable hybrid aluminosilicate built with only the three-ring unit, J. Phys. Chem. C 118 (2014) 7458-7467

[5] Bellussi G., Millini R., Montanari E., Carati A., Rizzo C., Parker W. O., Jr., Cruciani G., De Angelis A., Bonoldi L., Zanardi S., A Highly Crystalline Microporous Hybrid Organic−Inorganic Aluminosilicate Resembling the AFI-type Zeolite. Chem. Commun. 2012, 48, 7356−7358.

[6] Bellussi, G., Bonoldi, L., Carati, A., Montanari, L., Rizzo, C., Zanardi S., Fusco, R. Wavelength Converter. Italian Patent MI2010A001926, October 21, 2010

[7] Cruciani, G. Zeolites Upon Heating: Factors Governing Their Thermal Stability and Structural Changes. J. Phys. Chem. Solids 2006, 67, 1973−1994

[8] Baur, W. H. Self-limiting Distortion by Antirotating Hinges is the Principle of Flexible but Noncollapsible Frameworks. J. Solid State Chem. 1992, 97, 243−247

[9] Alberti, A.; Vezzalini, G. Topological Changes in Dehydrated Zeolites: Breaking of T-O-T Oxygen Bridges. In Proceedings of the Sixth International Zeolite Conference; Olson, D., Bisio, A., Eds.; Butterworth: Guildford, U.K., 1984; pp 834−841

[10] Graham Solomons T.W., Fryhle C.B., Organic Chemistry, 10th ed., John Wiley & Sons, USA, 2011

[11] Mizoshita N., Ikai M., Tani T., Inagaki S., Hole-Transporting Periodic Mesostructured Organosilica, Journal of American Chemistry Society 131 (2009) 14225–14227

[12] Mizoshita N., Yamanaka K., Hiroto S., Shinokubo H., Tani T., Inagaki S., Energy and Electron Transfer from Fluorescent Mesostructured Organosilica Framework to Guest Dyes, Langmuir 28 (2012) 3987−3994

[13] Xing G., Mathews N., Sun S., Sien Lim S., Ming Lam Y., Grätzel M., Mhaisalkar S., Chien Sum T., Long-Range Balanced Electron and Hole-Transport Lengths in Organic-Inorganic $CH_3NH_3PbI_3$, 342 (2013) 344-347

[14] Chao-Nan Xu, Kazuhide Miyazaki, Tadahiko Watanabe, Humidity sensors using manganese oxides, Sensors and Actuators B 46 (1998) 87–96

[15] Dewyani Patil, You-Kyong Seo, Young Kyu Hwang, Jong-San Chang, Pradip Patil, Humidity sensing properties of poly(o-anisidine)/WO_3 composites, Sensors and Actuators B 128 (2008) 374–382

Conclusions

This PhD thesis, result of a collaboration between the Department of Physics and Earth Sciences of the University of Ferrara and ENI Spa, was intended to characterize ECS materials and identify a possible use in the sensing field.

The studies carried out not only represented a material characterization in the strict sense, but rather the development of methods useful to obtain functional films for the design of sensitive devices.

For this purpose, the research was organized following two main ways:

i) films obtained with solvents,

ii) films obtained with screen printable composition.

Both research ways have been proven effective and several improvements and developments have emerged. The work has been focused in particular on the powders ECS 13 and 14 because they are considered most interesting from ENI, but also because during the preliminary tests they gave the best results for the production of films.

Regard to the first part of the research, the solubility tests and the subsequent deepening with polar solvents made with powders 14 ECS and ECS 5 have led to satisfactory results, since it has been possible to deposit and handle at room temperature the films that were well adherent to the substrate.

Regarding the films obtained with solvents in the first phase of research it can be concluded:

- polar and apolar solvents were tested to obtain suspensions containing ECS powders (ECS 14 and 5), and the relative deposition: among the polar solvents tested, acetone and ethanol gave the most interesting results;
- optical analysis by absorption and photoluminescence measurements allowed a preliminary assessment of possible degradation operated by the solvents used with ECS 14;
- the subsequent SEM investigation highlighted "aggressiveness" of acetic acid, which seems to completely dissolve the powder;
- ethanol was found to be the best candidate for the production of films containing ECS materials, even if the amount of powder used were found to be low;
- preliminary electrical measurements have proved fundamental since they have shown the ability to generate electrical activity in the films, and to use the ECS materials for the production of sensing films.

Therefore, it was proceeded to increase the concentration of the functional material compared to the selected solvent, so as to obtain films more compact and to assess whether the presence of a greater quantity of ECS material might affect the electrical signal measured. Furthermore, on the basis of results obtained with ECS 14 and ECS 5, it was decided to study also ECS 13 by means of the same method, because it was proven very efficient from the optical point of view.

About the films obtained with solvents in the second phase of research:

- acetone showed disintegrating properties, while the ethanol showed covering properties;

- exploiting these characteristics, films were obtained from the combination of the two solvents, in order to implement each other properties mentioned above. These tests were made with powders ECS 13 and ECS 14, getting good quality films;
- tests with solvents have also underlined the importance of the preparation method, in order to obtain a good diaggregation/disagglomeration of ECS powders with simple solvent used (ethanol or acetone). In particular it was seen that the preparation of the suspensions is particularly effective only with relatively high power ultrasound.

Regard the films obtained with screen printable technology in the second phase of research:

- for each ECS powder three different suspensions were produced starting from the composition used in the production of screen printing pastes generally employed for sensors based on metal oxides semiconductor. This method of deposition would have the advantage of controlling the thickness of the films in the process of industrialization of the product, with numerous advantages on operational specifications of the same. The three different suspensions allowed to study the role of each component used in the formulation of screen printing paste and it was concluded that the optimal composition is obtained by using ECS powder and organic vehicle, eliminating the glass frit;
- from this study it was also arised that the addition of ethanol to organic vehicle (implementation suggested by studies on films made with solvents), greatly improves the ability disaggregating/disagglomeranting allowing to obtain good quality films;
- in this regard the removal of glass frit was a winning choice as this component has proved unsuitable, because it tends to counteract the action of ethanol over to require high temperatures in order to facilitate their glue action both between the components of paste and between it and the substrate;
- regards the quality of the film, on depositions that have given good results or at least encouraging, it was arised by X-ray diffractometry that the crystalline structure of the materials (in the specific cases ECS 13 and 14) had maintained stable: the crystalline structure can be considered the same of the starting powders;
- the thermal stability of the depositions obtained with pastes composition based on organic vehicle was tested. These tests arised that the films can be used at relatively low maximum temperatures, since they are degraded when subjected to relatively high temperatures: in fact, both the organic vehicle part of the film itself and the structure of ECS crystals are modified when used at temperatures higher than 100 °C; as it is known from published articles about and by the thermal tests performed;
- electrical conductivity measurements were performed on the devices made using the formulation of the screen printing paste. It was identified a selectivity to humidity by the ECS 14 such as to allow the calibration of two devices. Generally, it is not possible to get responses such significant at room temperature, so the devices results really innovative with respect to the technologies currently on the market;
- anyway it is important to highlight that tests on devices based on ECS 14 and ECS 4 with benzene vapors, and with ECS 13 in the presence of acetaldehyde registered no negligible responses. These gases are of considerable interest because their emissions are monitored in various fields: from air and water quality to that of the food, from medical pathologies to industrial processes;
- finally it was studied individually the inorganic component used in the synthesis of ECS powders in order to assess whether the electrical activity, shown by the film

containing ECS powders, depended only on the inorganic part or not, but tests in gas showed no conductance variations in the zeolite-based film.

The use of the knowledge of the sensor group of the University of Ferrara on the production of printing pastes for thick film turned out to be essential: in-depth study about the interaction of ECS powder with each component used in the paste has identified an optimal formulation in which the functional material is the ECS powder. This formulation combined with the use of solvents and specific treatments, such as ultrasound and magnetic stirring, has proven successful in order to realize well adherent, continuous and uniform films characterized by a density such as to let assume the possible use of the screen printing technique which deposition. This would allow the production of a significantly larger number of devices characterized by faster times and lower costs than actual commercial sensors.

Then, the ECS powders are innovative functional materials for the design of electrically active films by means of simple deposition technique, so that they can be processed in selective devices, operating at room temperature, then at minimum consumption.

The electrical properties revealed suggest the use of the ECSs as functional materials for the construction of sensors suitable to for gaseous analytes detection. The operation of such devices is reminiscent of the chemoresistive transduction model, for which there is a change in the conductivity of the material as a result of surface chemical reactions with the analyte. Good quality chemoresistive sensors require speed, selectivity and reversibility of the response, since they have to report rapidly and with high sensitivity the appearance/disappearance of chemical species in the atmosphere, and they can be distinguished them.

The metal oxides semiconductors (ZnO, SnO$_2$, WO$_3$, TiO$_2$,...), extensively studied for sensing applications, have been shown to possess suitable properties of charge transport and high surface reactivity such as to place them at the first place between the materials used for the production of commercial sensing devices. The chemoresistive sensors operation is constrained to the thermo-activation at high working temperatures. The need to supply sensors based on metal oxides semiconductors represents a limit for their portability, since the battery and the electronics associated with it playing a disadvantageous role from the point of view of size and consumption, nevertheless safety in situations that involve explosive gases.

The sensors prepared with ECSs showed an electrical response characterized by speed and reversibility already at room temperature, completely innovative properties in the field of gas sensors. ECSs-based sensors also showed a dependence of the response from changes in analyte concentration in the atmosphere, an aspect which makes them extremely interesting from the application point of view, since it can produce independent sensors by the heating circuitry resulting more functional for portable equipment. Nevertheless, the response of the ECS proved selective, crucial factor in the preparation of complex sensors matrices.

Therefore, the sensors obtained by the ECS hybrids have the property of speed, reversibility and selectivity of extremely interesting electrical response that makes them competitive with respect to systems currently in use. The technological advantage of room temperature operating and the selectivity are added to the novelty of the application of ECSs as active materials in sensors for gas. In fact, so far hybrid materials obtained starting from the same precursors showed mainly optical and catalysis properties, as documented in chapter 2. The specific structural features of ECSs seem to combine the stability, characteristic of the inorganic component, with high quality sensing properties of organic materials [S. Wang et al. Organic / inorganic hybrid sensors: A review, Sensor and Actuators B 182 (2013) 467-481].

Regarding the state of art, relying on our knowledge, only occasionally electrical transport properties in hybrid materials derived from the same precursors have been reported in the literature [N. Mizoshita et al., Hole Transporting periodic mesostructured organosilica, J. Am. Chem. Soc. 131, 14225 (2009)]. The only contribution inherent sensing applications was presented by the Inagaki group, who discovered the PMO. In any case the measurements carried out with benzene were obtained by photo-activating the material with a LED [Yuliarto B., Kumai Y., S. Inagaki, H. Zhou, Enhanced benzene selectivity of mesoporous silica SPV sensors by incorporating phenylene groups in the silica framework, Sensors and Actuators B 138 (2009) 417-421].

Appendix A

The objective of film characterization was the investigation of aspects considered significant for the applicability of the materials in the design of sensors.

The aspects taken into account can be summarized as:
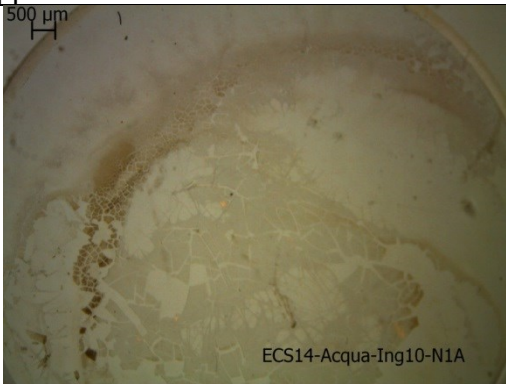
i) _Effectiveness of solvents in getting a good dispersion_ of ECS 14 and ECS 5. A good dispersion of the powders by the solvents induces the absence or almost low presence of agglomerates in the films obtained on a rigid support, thus achieves films with uniform physical characteristics.

ii) _Continuity and uniformity of the films obtained on rigid support._ The continuity of the coating involves a film without cracking, this aspect is one of the most common problems in the production of the films. The uniformity refers to the thickness of the film. The presence of cracks induces a physical discontinuity in the film and consequently the impossibility of current conduction or in any case an increase of the resistivity in the same film as function of the cracking degree.

iii) _Adhesion of thin films to the rigid support._ The adhesion of thin film to the rigid support of the sensor is a fundamental feature to ensure a good physical-mechanical strength of the film itself in addition to allowing the current conduction through the interdigitated electrodes on the substrate and then to guarantee the operation of the sensor.

Combination of powders and simple solvents

Table A1. Deposition on glass containing ECS 14 and water.

ECS 14 – Water
Magnification: 10X and 25X transmitted light: "N * A" reflected light high + low angle: "N * B" low angle light reflected: "N * C" **Observations:** i) do not appear aggregates ii) uniform film but very strong presence of fractures that create separate scales; different thicknesses at the edges (darker areas) iii): the film is adherent, the edges of the flakes in some cases appear raised from the support
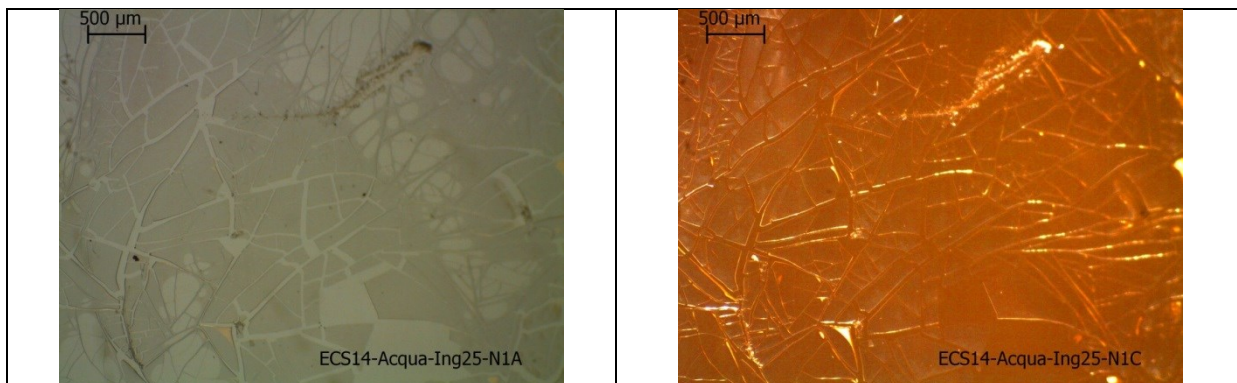
Table A2. Deposition on glass containing ECS 14 and acetone.
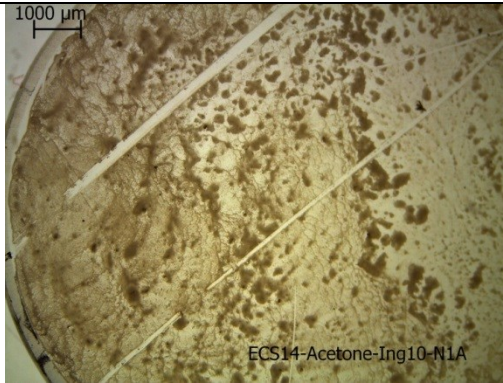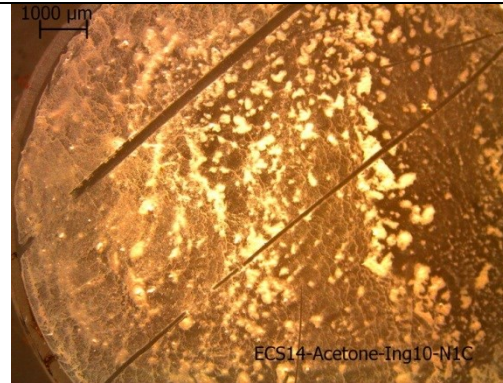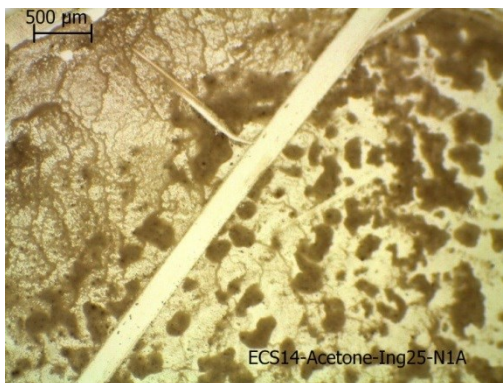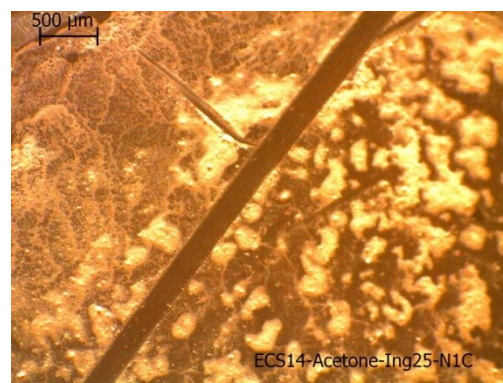
ECS 14 – Acetone

Magnification: 10X and 25X
transmitted light: "N * A"
reflected light high + low angle: "N * B"
low angle light reflected: "N * C"

Observations:

i) strong presence of agglomerates
ii) the film does not appear uniformly thick (lighter areas and darker areas), but continuous.
iii) the film is well-adherent

Table A.3: Deposition on glass containing ECS 14 and acetic acid 5%.
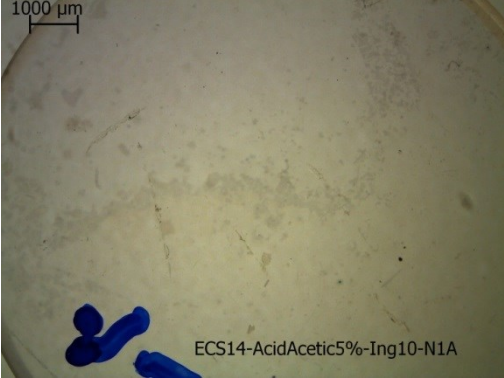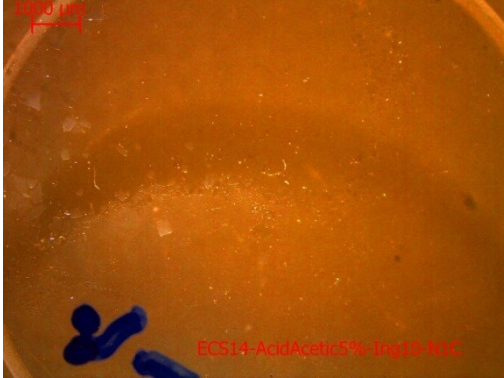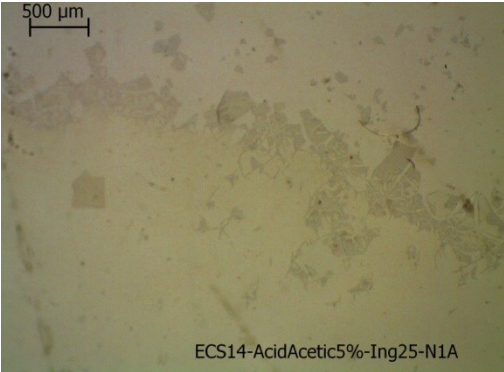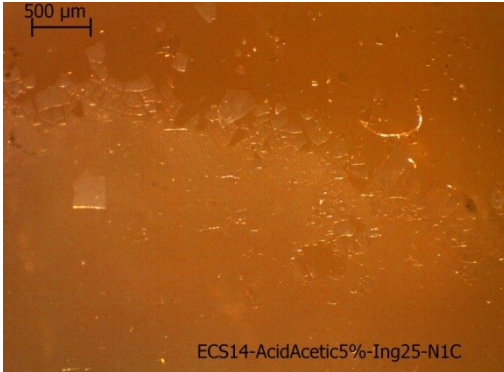
ECS 14 – Acetic acid 5%

Magnification: 10X and 25X
transmitted light: "N * A"
reflected light high + low angle: "N * B"
low angle light reflected: "N * C"
Observations:
i) do not appear aggregates
ii) the film thickness is uniform and continuous, the presence of fractures at the edges of the deposition create separate flakes
iii) the film appears adherent, the edge of the deposition is made from flakes that appear not adherent to the support

Table A4. Deposition on glass containing ECS 14 and acetic acid 40%.

ECS 14 – Acetic acid 40%

Magnification: 10X and 25X
transmitted light: "N * A"
reflected light high + low angle: "N * B"
low angle light reflected: "N * C"
Observations:
i) do not appear aggregates
ii) the film thickness is uniform and continuous, at the edge of the deposition the thickness decreases
iii) the film is well bonded to the substrate, regard this it was made a scratch proof with a tip steel
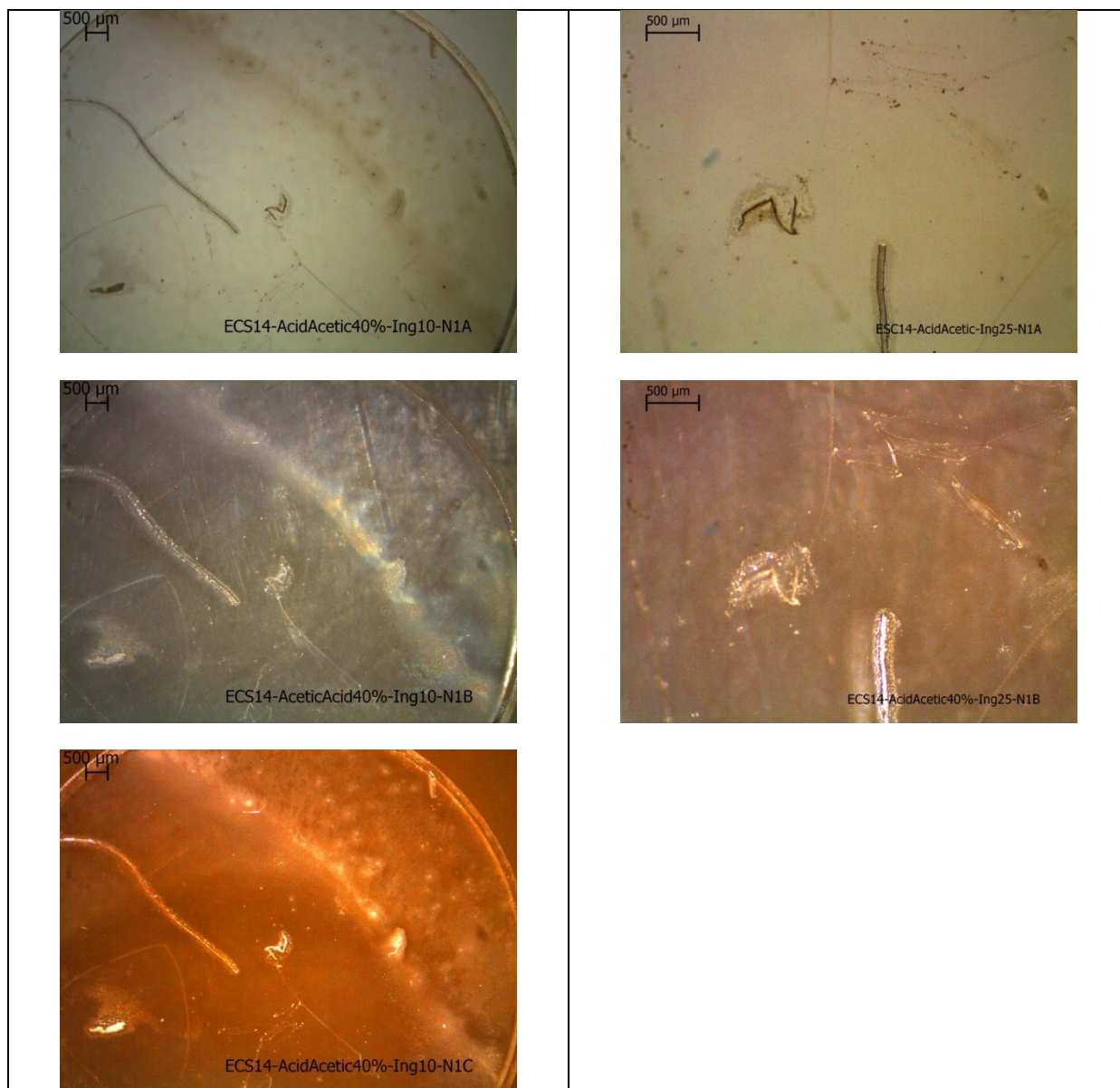
Table A5. Deposition on glass containing ECS 14 and not diluted ethanol.

ECS 14 – Not diluted Ethanol

Magnification: 10X and 25X
transmitted light: "N * A"
reflected light high + low angle: "N * B"
low angle light reflected: "N * C"
Observations:
i) there are zones characterized by aggregates
ii) the film does not present uniform thickness, likely this affects the continuity of the film
iii) the film is bonded to the support
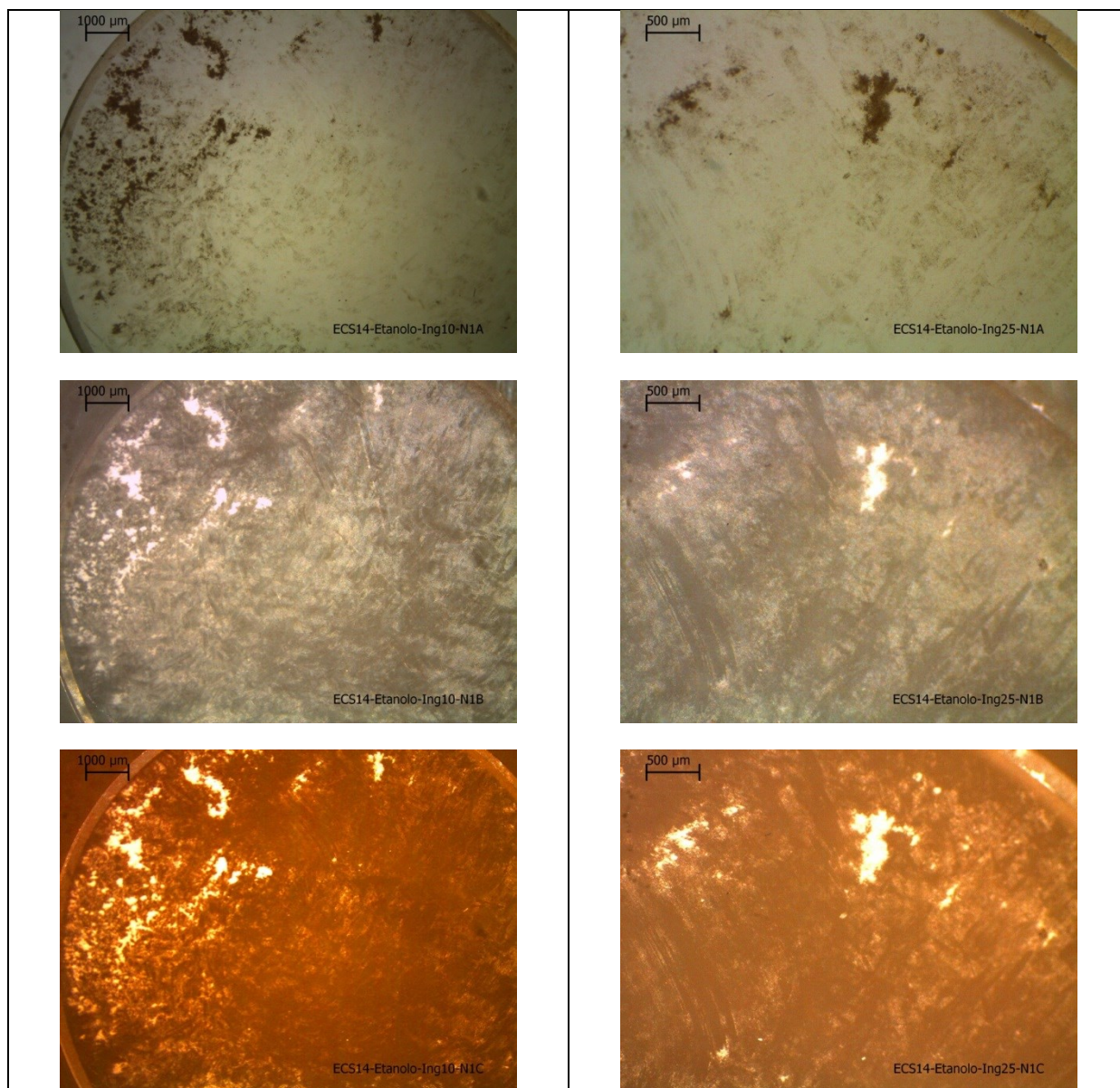
Table A6. Deposition on glass containing ECS 14 and diluted ethanol (sample 1).

ECS 14 – Diluted Ethanol –1

Magnification: 10X and 25X
transmitted light: "N * A"
reflected light high + low angle: "N * B"
low angle light reflected: "N * C"

Observations:

i) in general aggregates do not appear, some area at the edges of the film shows the presence of aggregates or different thickness with respect to the rest of the film

ii) the surface is covered in areas, probably due to the low amount of material deposited, however, the areas covered appear smooth and continuous. The area with the presence of aggregates shows the cracks

iii) the film is bonded to the support
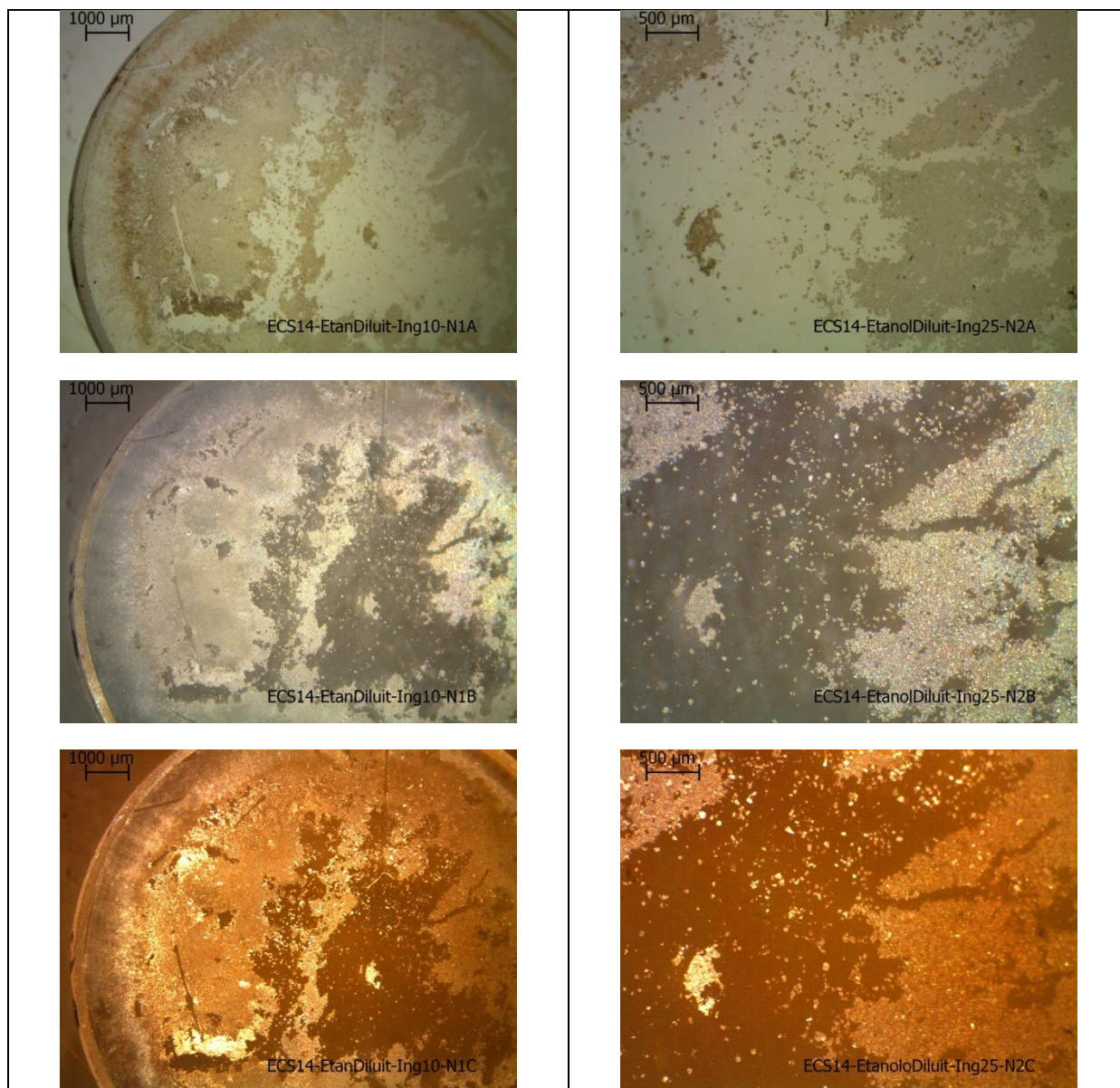
Table A7. Deposition on glass containing ECS 14 and diluted ethanol (sample 2).

ECS 14 – Diluted Ethanol – 2

Magnification: 10X and 25X
transmitted light: "N * A"
reflected light high + low angle: "N * B"
low angle light reflected: "N * C"
Observations:
i) the presence of aggregates or still areas of different thickness with respect to the rest of the film
ii) the surface is not coated in a uniform way (due to the aggregates), but continuous.
iii) the film is bonded to the support

ECS14-EtanoloDiluito/2-Ing10-N1A

ECS14-EtanoloDiluit/2-Ing25-N1A

ECS14-EtanoloDiluito/2-Ing10-N1B

ECS14-EtanoloDiluit/2-Ing25-N1B

ECS14-EtanoloDiluito/2-Ing25-N1C

ECS14-EtanoloDiluito/2-Ing25-N1C
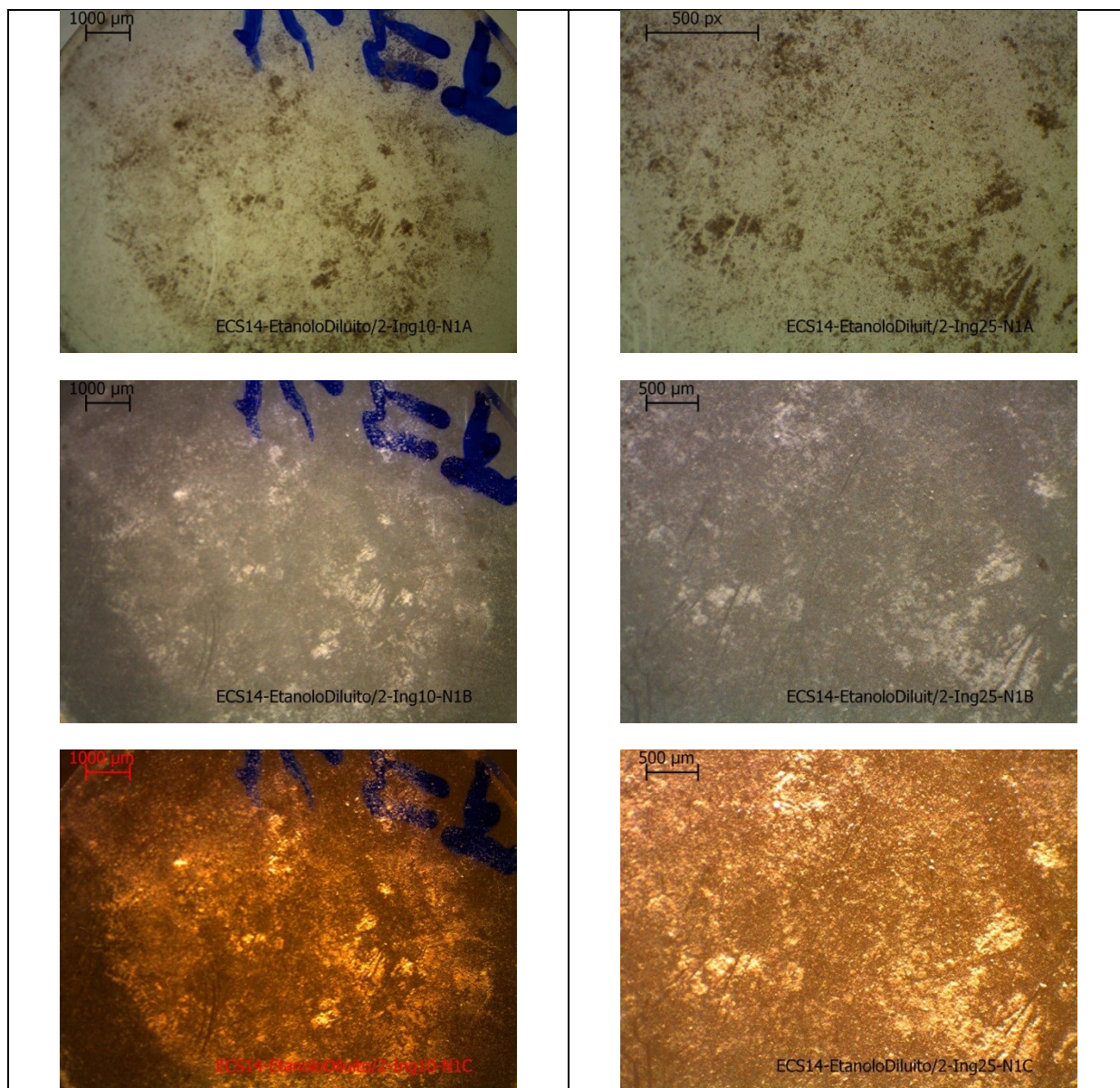
Polar solvents investigation

Table A8. Deposition on glass containing ECS 14 and acetic acid 5%.

ECS 14 – Acetic acid 5%

Magnification of optical microscope: 10X and 25X in reflected light
Observations:
i) in the mass that constitutes the film one can appreciate some aggregates, perhaps crystalline. Likely this modification is due to acetic acid
ii) the film has uniform thickness, it is confirmed the presence of fractures at the edges, other fractures can been noted also in the inner part of the deposition
iii) the film is adherent, the edge of the deposition is made from flakes that appear not adherent to the support
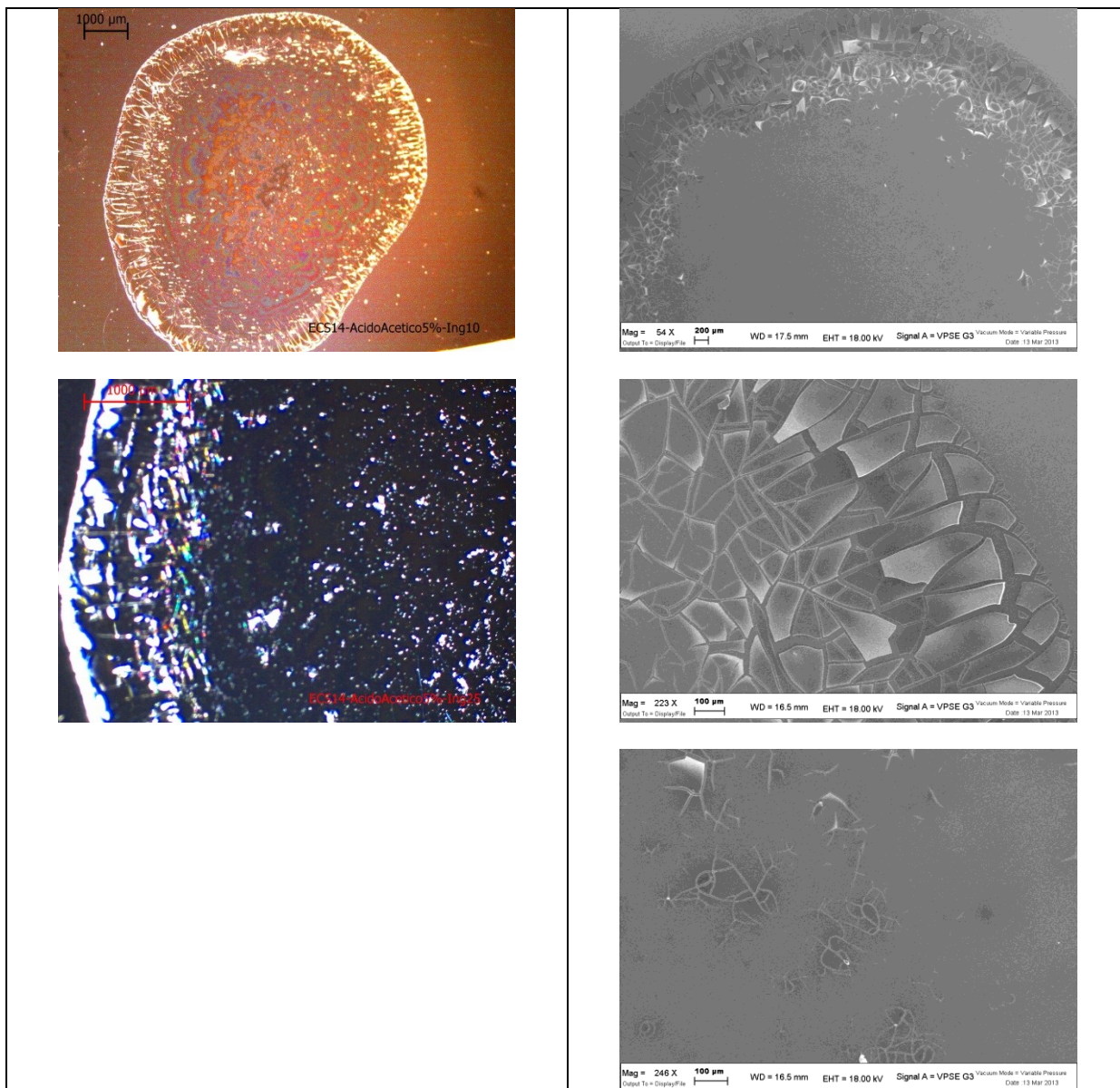
Table A9. Deposition on silicon containing ECS 14 and acetic acid 10%.

ECS 14 – Acetic acid 10%

Magnification optical microscope: 10X and 25X in reflected light
Observations:
i) in the mass that constitutes the film one can appreciate aggregates, perhaps crystalline. Likely this modification is due to acetic acid
ii) the film has uniform thickness, the presence of fractures tends to form flakes
iii) the flakes appear adherent, apart from the edges of the themselves that seem unstuck from the support
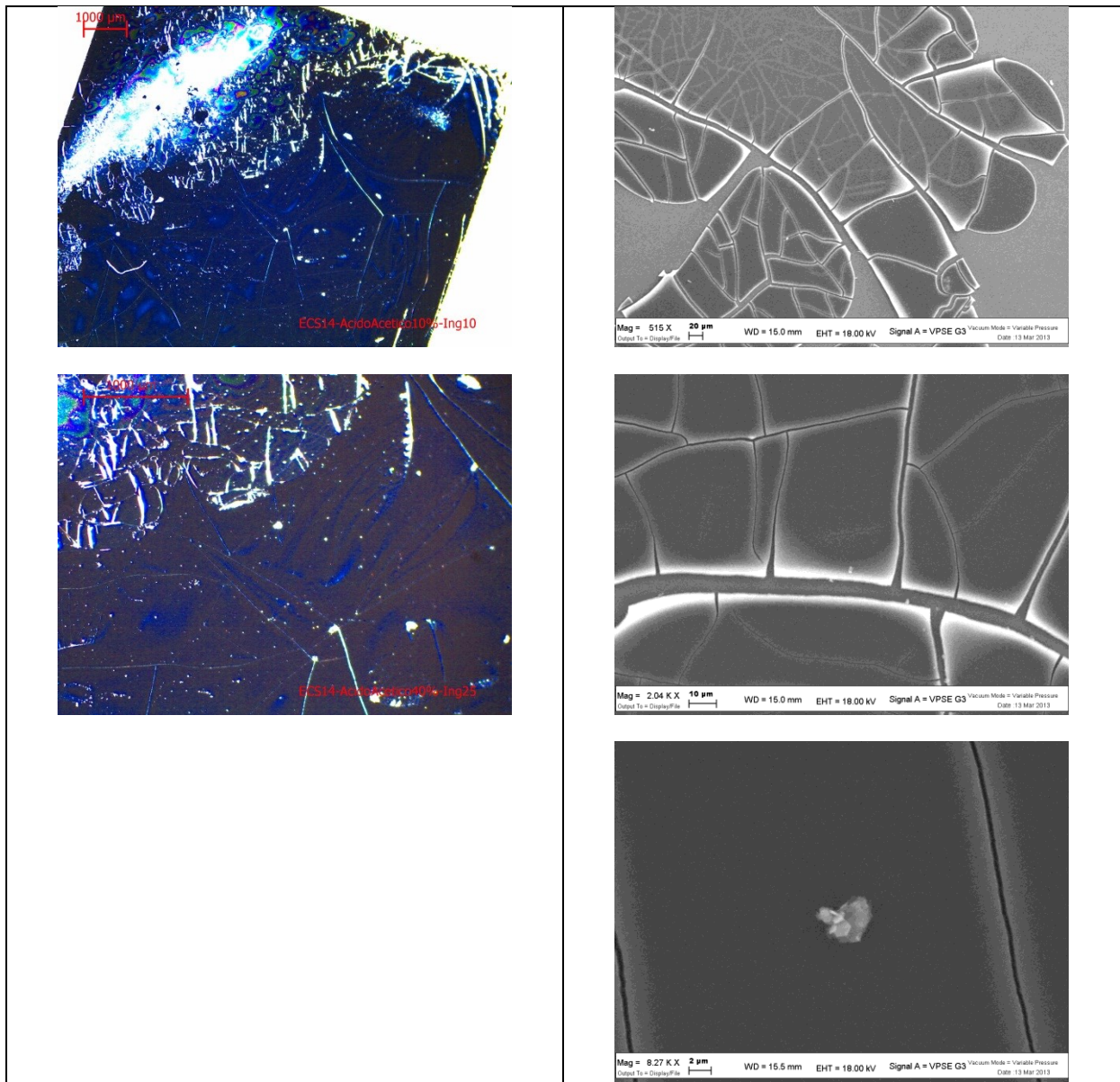
Table A10. Deposition on silicon containing ECS 14 and acetic acid 40%.

ECS 14 – Acetic acid 40%

Magnification optical microscope: 10X and 25X in reflected light
Observations:
i) at higher magnification one can notice a small aggregate, perhaps crystalline, likely due to acetic acid
ii) the film appears to be strongly fractured and tends to form flakes, these seem to have uniform thickness. At the edge of the deposition flakes appear larger than in the inner part
iii) one can appreciate scales at the edge that appear not adherent to the substrate, while the flakes inside the deposition appear with raised edges from the support
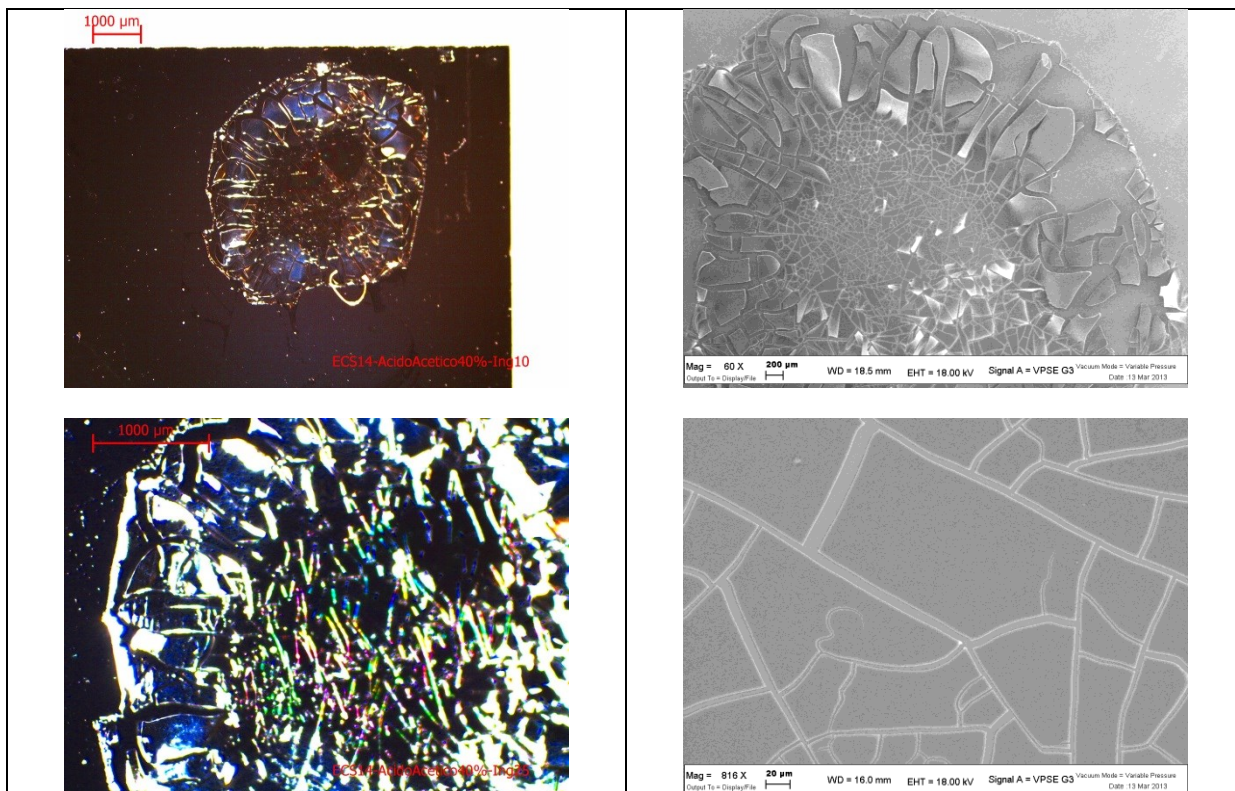
Table A11. Deposition on silicon containing ECS 14 and diluted ethanol.

ECS 14 – Diluted Ethanol

Magnification optical microscope: 10X and 25X in reflected light
Observations:
i) good dispersion of the materials despite the presence of aggregates
ii) in the film one can appreciate the single crystals, which tend to be arranged with the basal plane parallel to the support, then there is a trend to create a continuous coating on the support, which however is not complete (not sufficient quantity of material). The thickness tends to be uniform, apart from the presence of aggregates that modify such uniformity
iii) the single crystals appear adherent to the silicon substrate
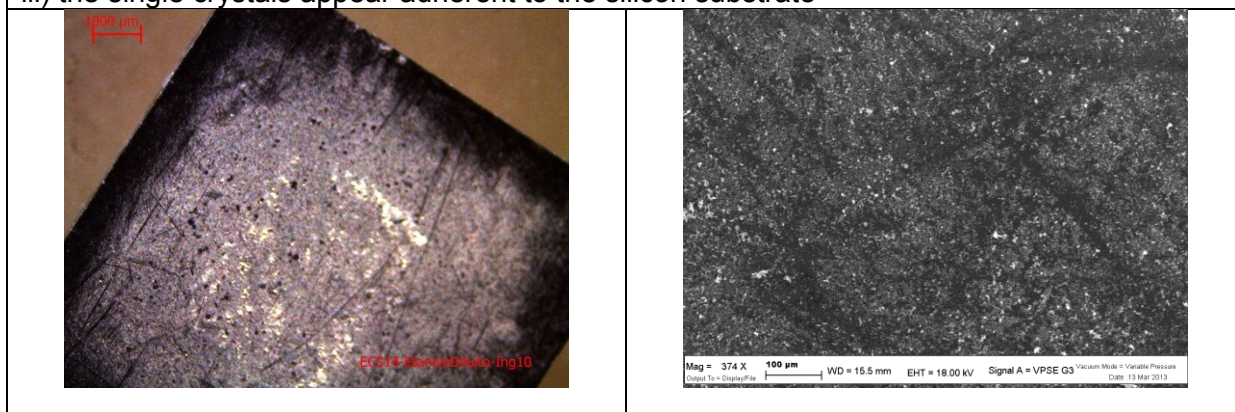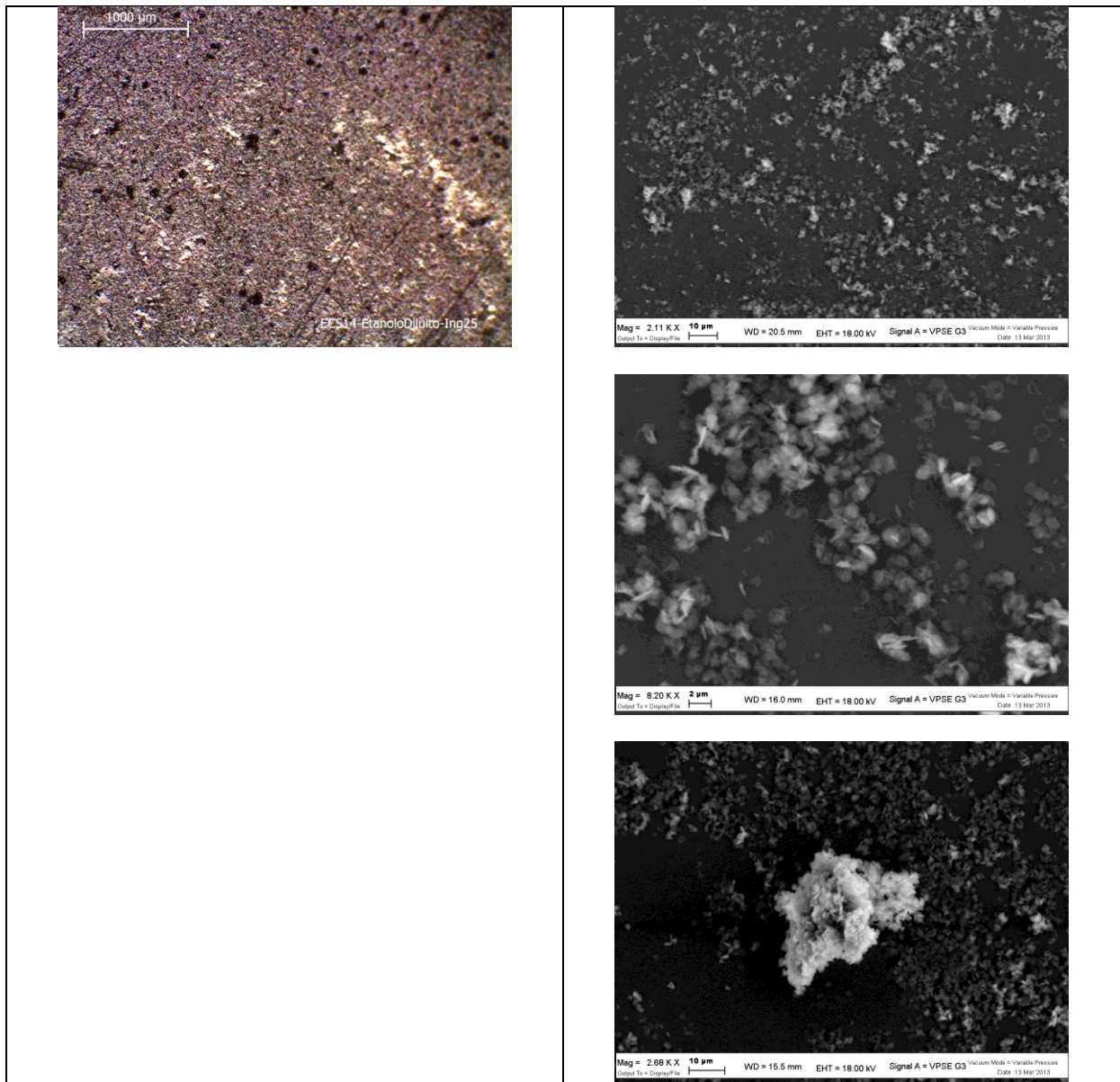
Table A12. Deposition on glass containing ECS 5 and acetic acid 40%.

ECS 5 – Acetic acid 40%

Magnification: 10X and 25X
transmitted light: "N * A"
reflected light high + low angle: "N * B"
low angle light reflected: "N * C"
Observations:
i) presence of agglomerates
ii) the film does not appear uniform thickness and the surface is irregular, but continuous
iii) the film is well-adherent
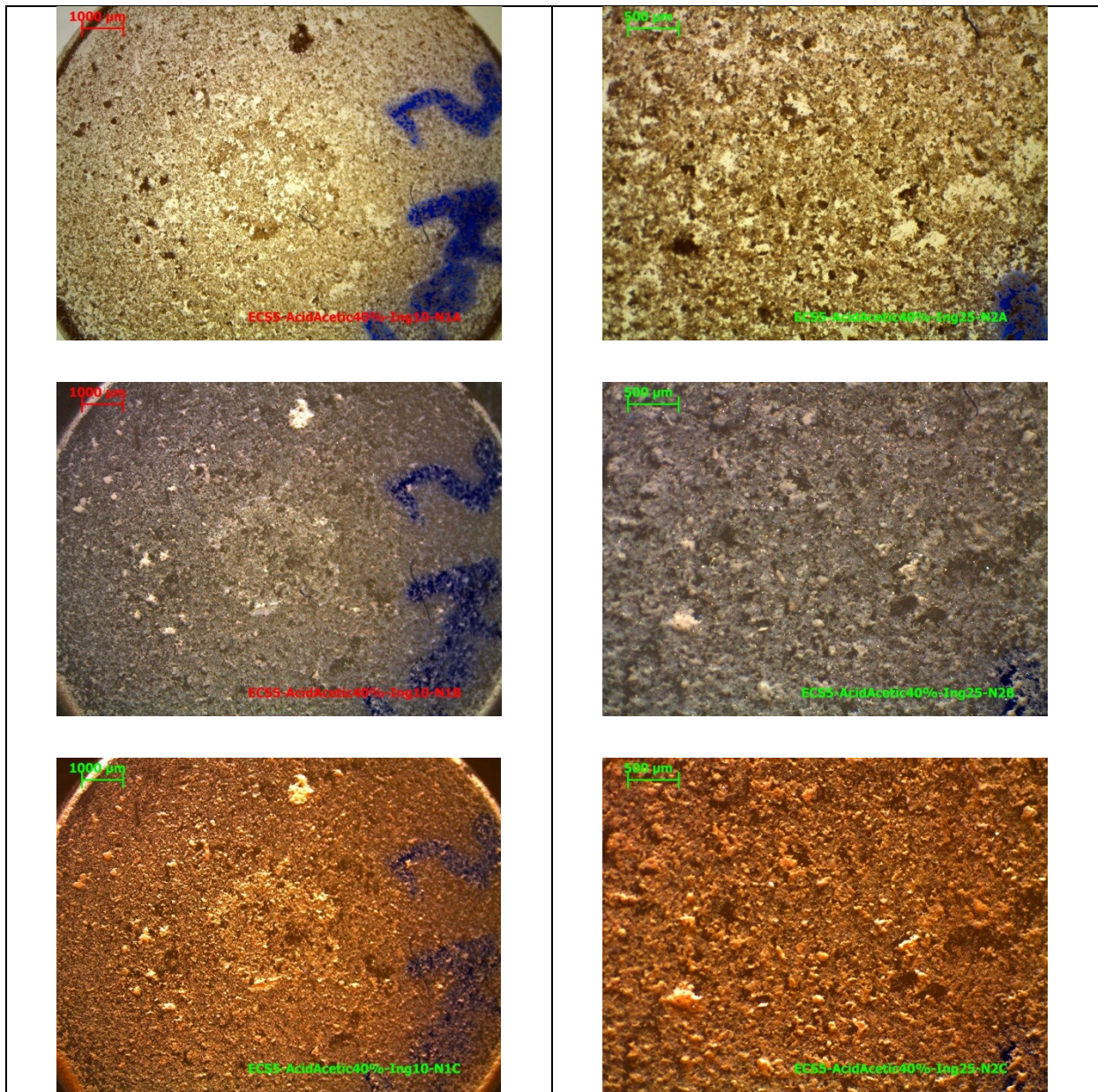
Table A13. Deposition on glass containing ECS 5 and diluted ethanol.

ECS 5 – Diluted Ethanol

Magnification: 10X and 25X
transmitted light: "N * A"
reflected light high + low angle: "N * B"
low angle light reflected: "N * C"
Observations:
i) strong presence of aggregates
ii) aggregates distributed on the surface that do not appear continuously.
iii) the film is substantially constituted by aggregates that appear adherent
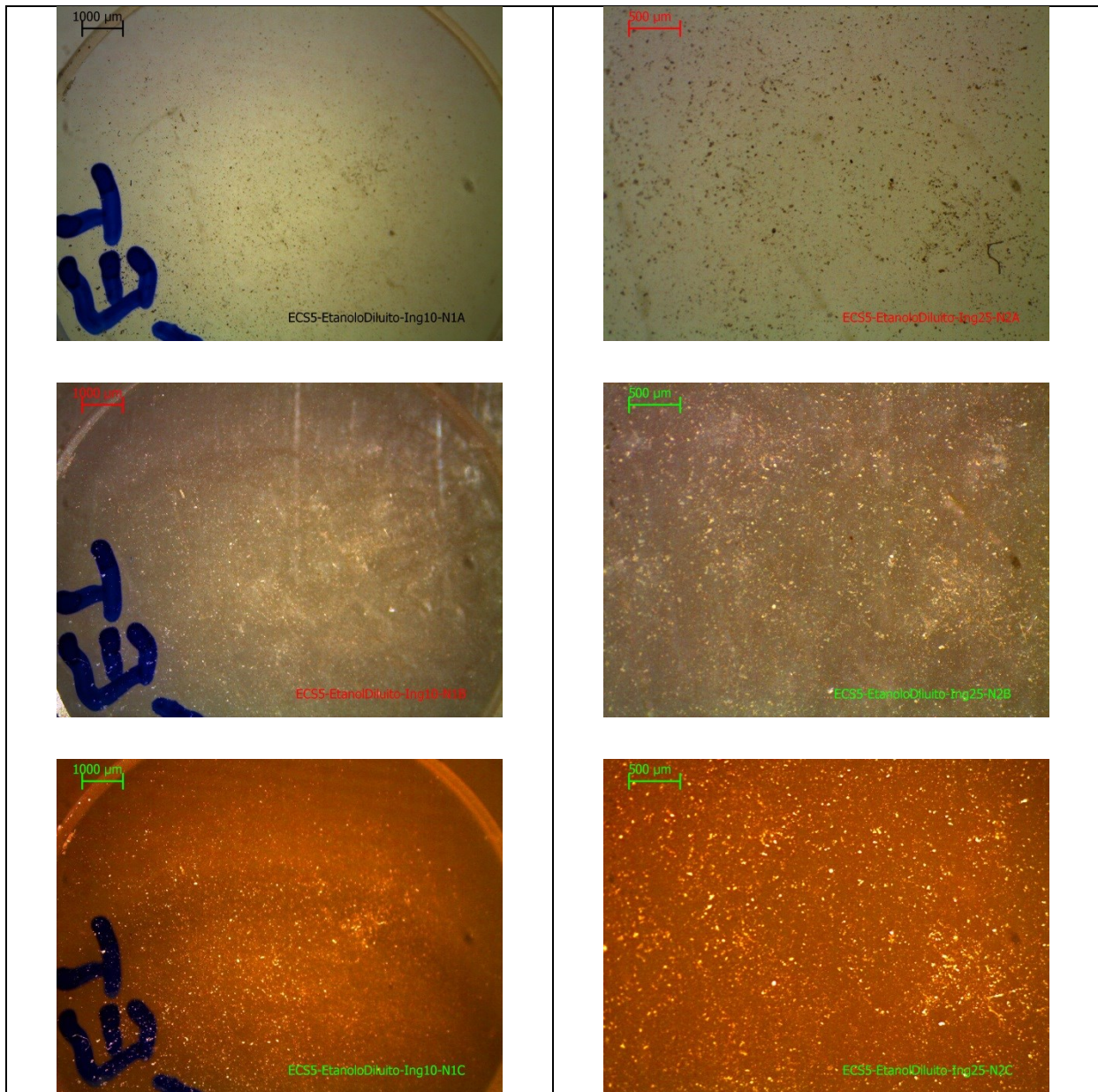
Table A14. Deposition on silicon containing ECS 5 and acetic acid 40%.

ECS 5 – Acetic acid 40%

Magnification optical microscope: 10X and 25X
Observations:
i) the strong presence of agglomerates
ii) the deposition is divided into two zones: a central and a peripheral zone which acts as a crown to the first, the film is not continuous between the two zones (missing material), the SEM photos show the presence of fractured mass that incorporates aggregates/crystals
iii) the material is bonded to the silicon support
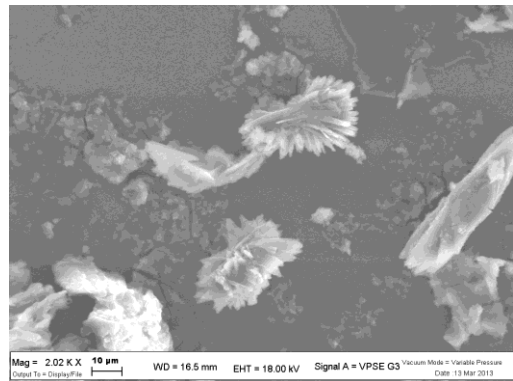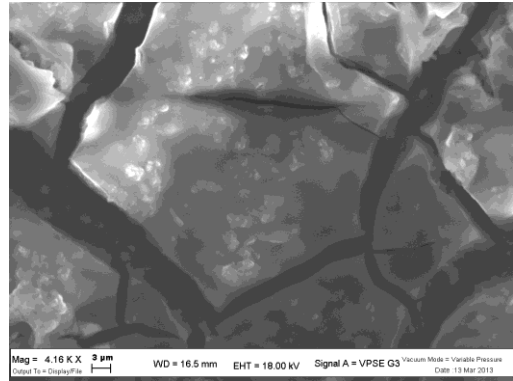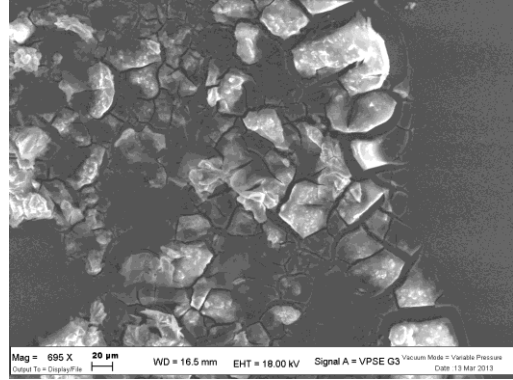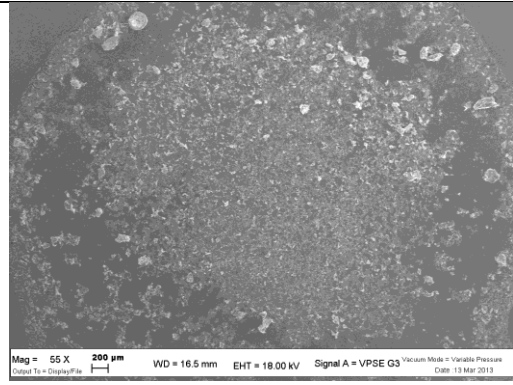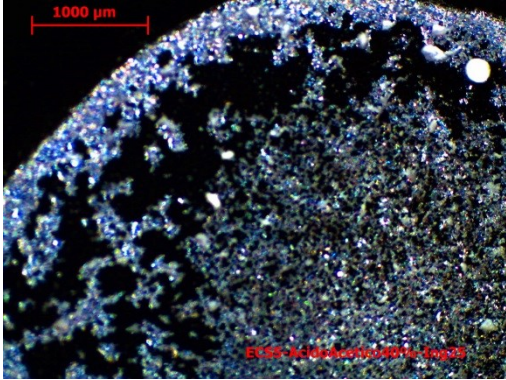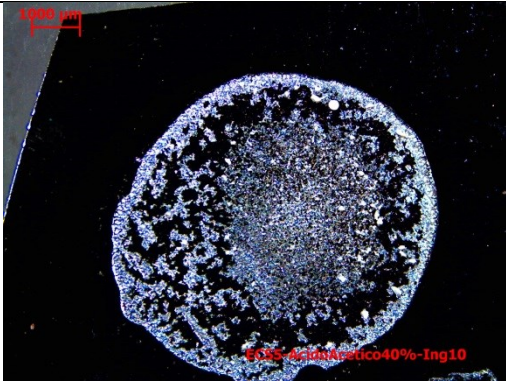
Table A15. Deposition on silicon containing ECS 14 and diluted ethanol.

ECS 14 – Diluted Ethanol

Magnification optical microscope: 10X and 25X
Observations:
i) strong presence of aggregates
ii) crystalline aggregates are distributed on the surface; there isn't a continuous surface
iii) the aggregates appear adherent to the silicon substrate
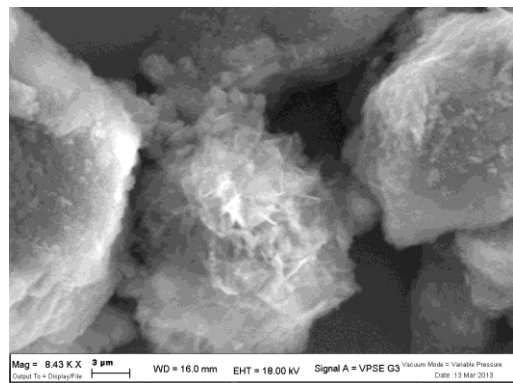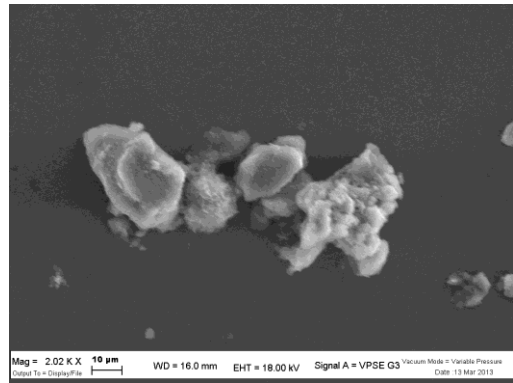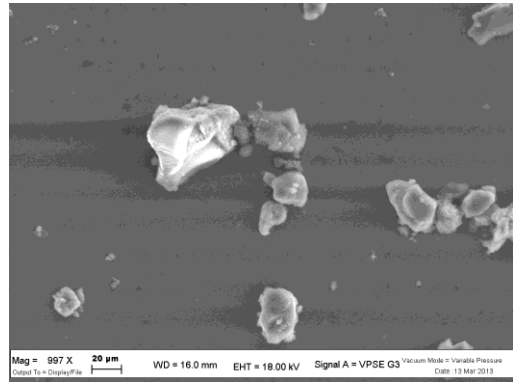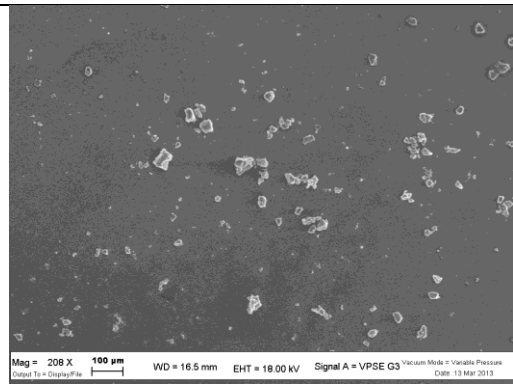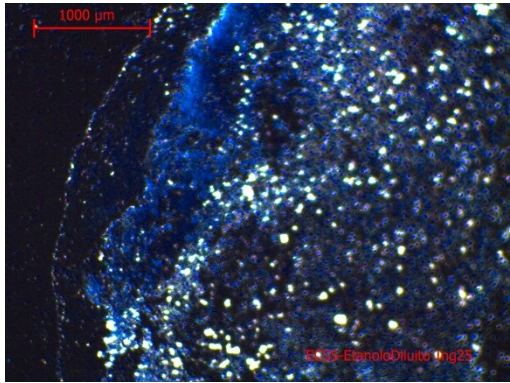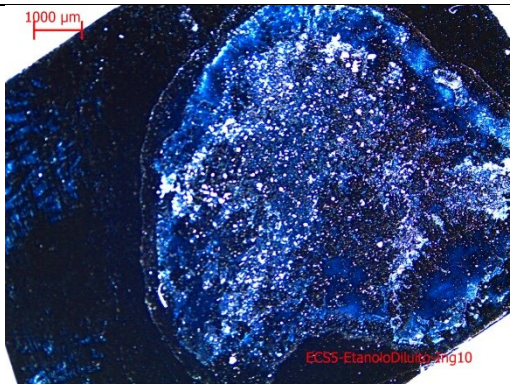
Appendix B

The objective of films characterization was to investigate significant aspects in order to define the quality of a deposition, then the applicability of dispersants vehicles (solvents and organic vehicle) added to ECS materials in sensors production. Following, the issues considered during the optical microscope and SEM investigations are listed. For each aspect investigated is also described the technique used for the analysis.

i) The efficacy of the organic vehicle and/or solvent/s for obtaining a good dispersion of ECS powders: a good dispersion of the powders by the organic vehicle and/or the solvent/s induces an absence or however a low presence of agglomerates and also of aggregates[7] in the films. The latter aspect is closely connected with the particle size distribution. Thus, it is possible to achieve a film with uniform physical characteristics.

ii) Continuity and uniformity of the films obtained on rigid supports.
The continuity of rigid substrates coating involves a film without cracks or holes. This aspect is one of the most common problems in the realization of the films. The uniformity refers to the thickness of the film[8]. The physical presence of discontinuities, such as cracks or holes in the film, causes the impossibility of current conduction or in any case an increase of the resistivity in the same film as a function of the degree of discontinuity.

iii) Adhesion of thin films to the rigid support.
The adhesion of the thin film to the rigid support of the sensor is an indispensable feature to ensure a good physical-mechanical strength of the film itself, in addition to allowing the passage of current from film to interdigitated electrodes, then to ensure the operation of the sensor. This analysis was carried out by observing whether or not there was a detachment of the film from the support on which it was deposited by droap coating.

---
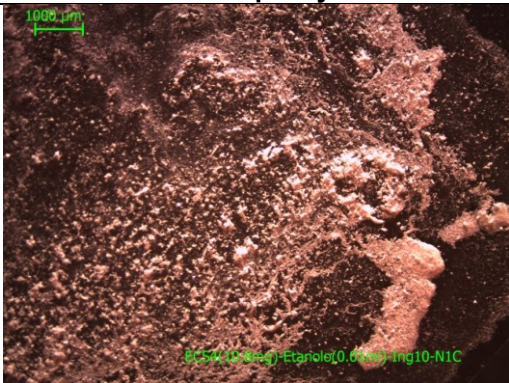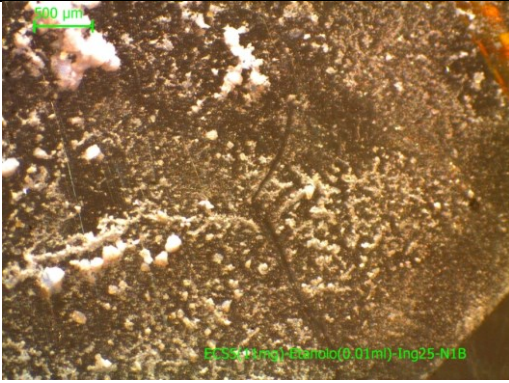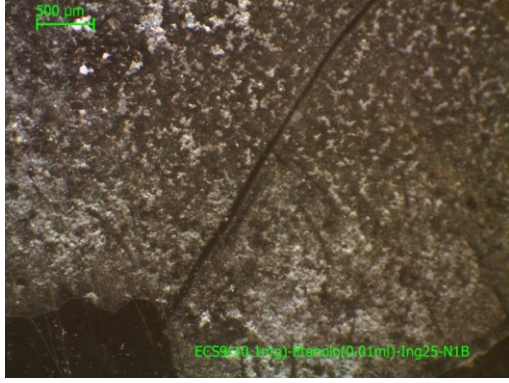
[7] **Particle**: a minute piece of matter with defined physical boundaries; **aggregate**: a particle composed melted particles or strongly bound, **agglomeration**: a set of particles or aggregates with weak bonds in which the resulting external surface is similar to the sum of the surfaces of the single components. For images analysis obtained by optical microscope the terms particle and aggregate are used with the same meaning because it cannot distinguish from each other. While, in case of SEM investigations the same meaning is given to the terms aggregates and agglomeration.
Particle size distribution: dimensions of the aggregates (and/or particles) compared to the volume (or weight)percentage. **Well selected**: the presence of aggregates and/or particles with dimensions close, **on average selected**: the presence of aggregates and/or particles with average size similar, **little selected**: the presence of aggregates and / or particles with different size relatively. The determination of the granulometric sorting or uniformity in this context is rather difficult, therefore it will give a qualitative indication of the presence of aggregates and/or particles of different size but not a quantitative indication. For the optimization of sensors is important to allow the disaggregation of obtaining a particle size distribution curve close (well-selected) and moved out of fine particles. SEM analysis about particle size distribution is referred to the particles, since the distinction between particles and aggregates is easier (which it is not possible by optical microscope), unless otherwise noted.
[8] **Film**: a continuous opaque or semi-opache surface which is made of particles of variable size, the color of this surface is a function of the film thickness and the type of settings given to the microscope, **thin film**: a continuous semi-transparent surface of uncertain origin.

Solvents investigations

Table B1: Depositions with high powder/ethanol ratio

Powder	mg	Solvent	ml	Film quality
ECS 4	10.8	Ethanol	0.01	presence of agglomerates, particles on average selected, presence of veins which give continuity
ECS 5	11	Ethanol	0.01	strong presence of agglomerates, particles little selected, continuity due to veins consist of small particles
ECS 9	10.1	Ethanol	0.01	presence of agglomerates, particles poorly selected, the presence of a background film gives continuity
ECS 12	10.1	Ethanol	0.01	presence of agglomerates, particles from on average to
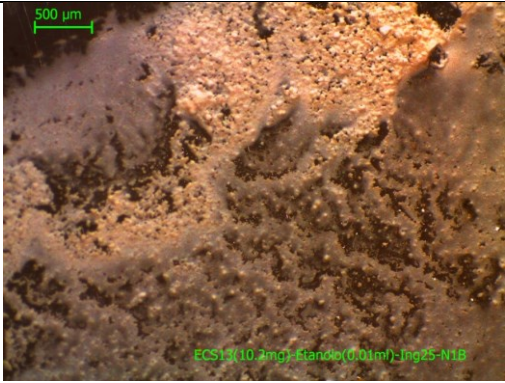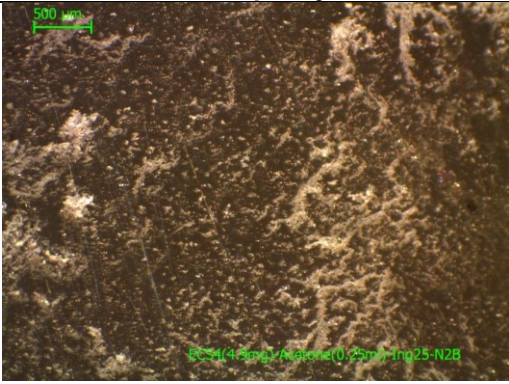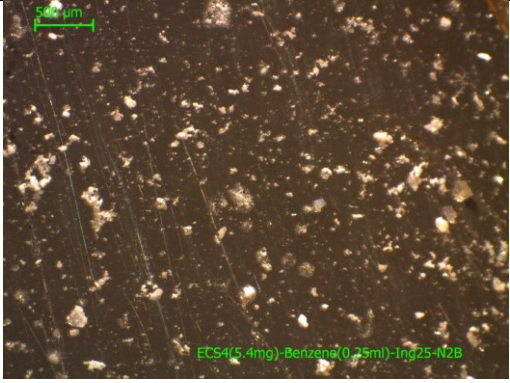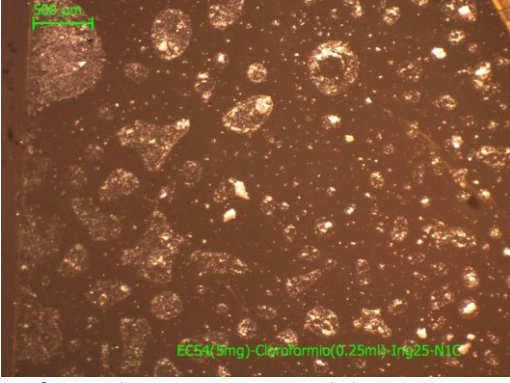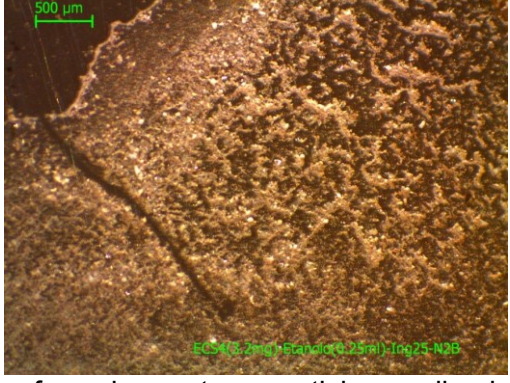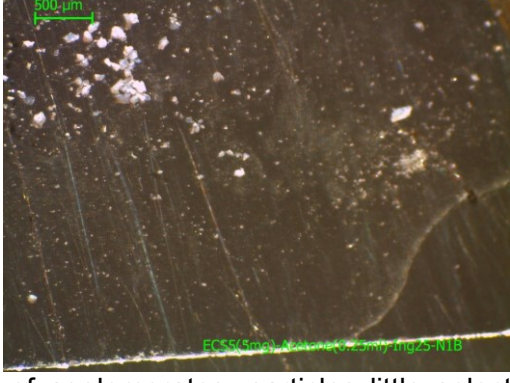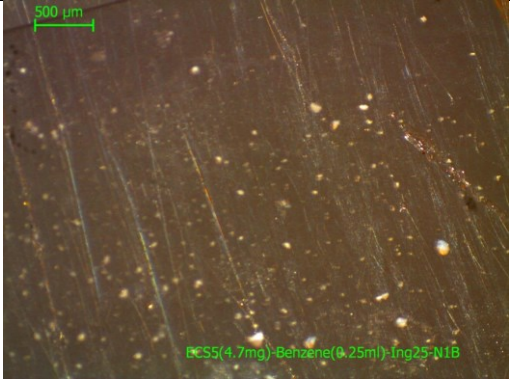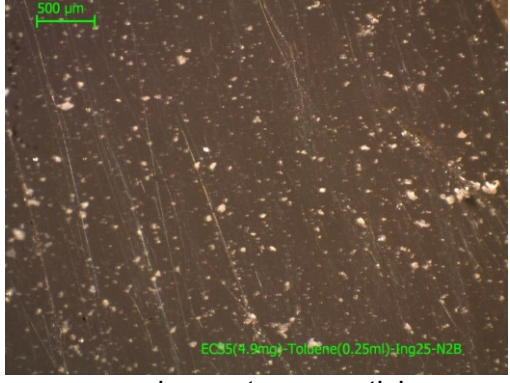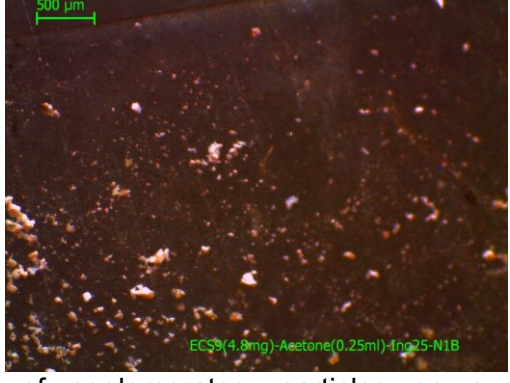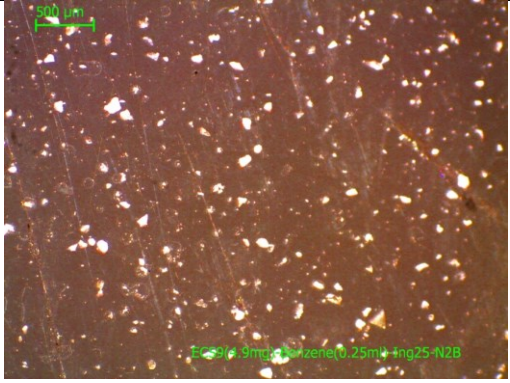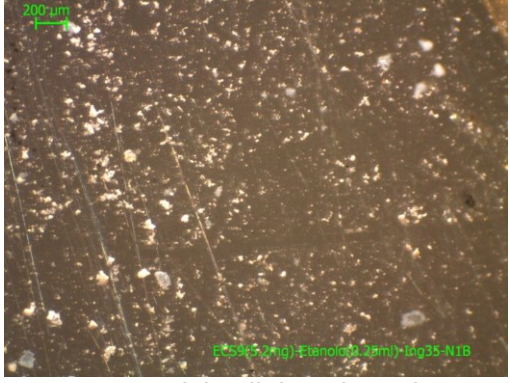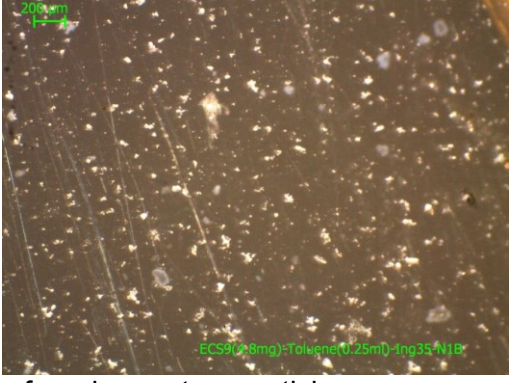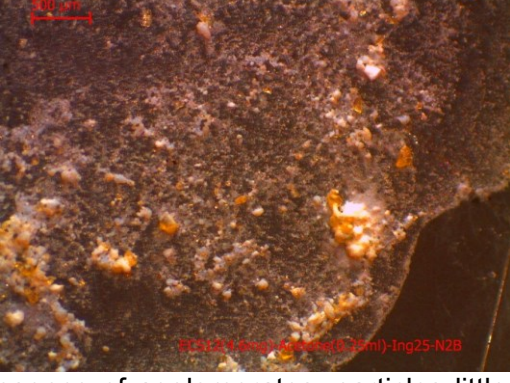
Powder	mg	Solvent	ml	Film quality
				little selected, fine particles generate a partial continuity zone
ECS 13	10.2	Ethanol	0.01	 presence of agglomerates, particles from on average to little selected, however there is a continuous film with the presence of holes
ECS 14	11.2	Ethanol	0.01	 presence of agglomerates, little selection of the particles, continuous film with holes
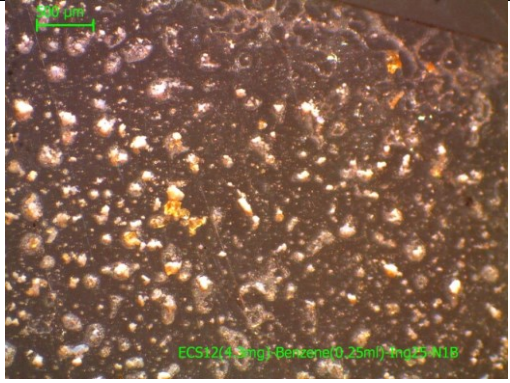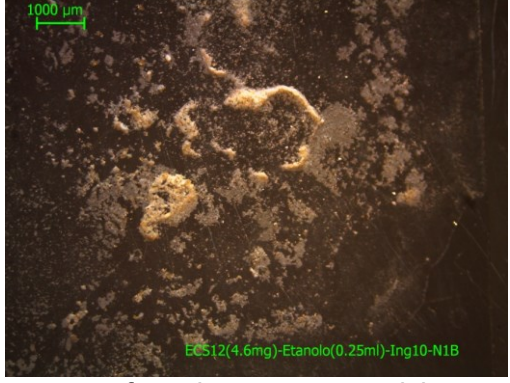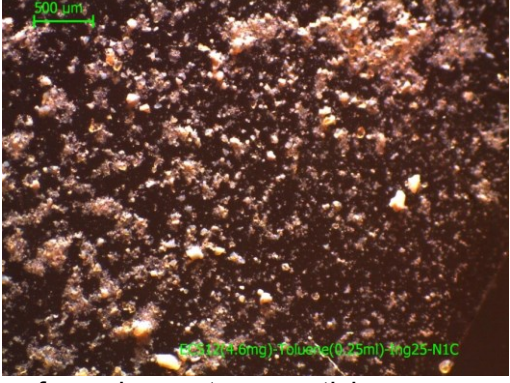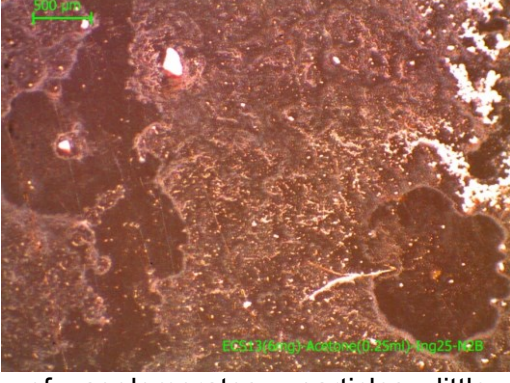
Table B2: Solubility tests
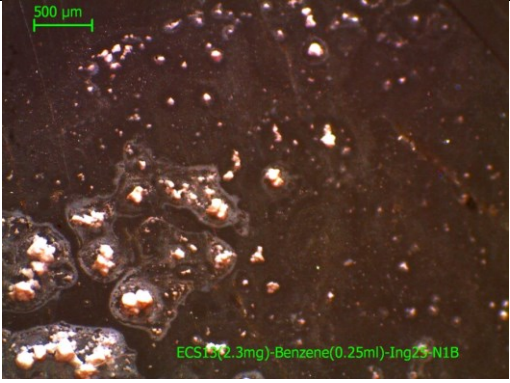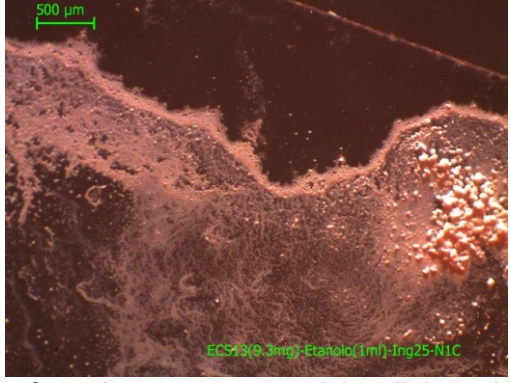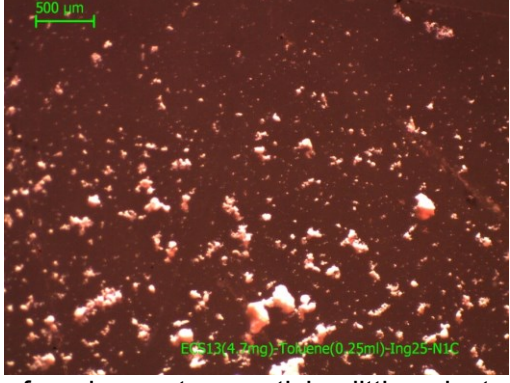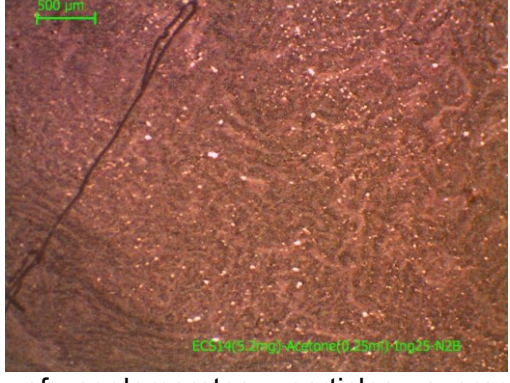
Powder	mg	Solvent	ml	Film quality
ECS 4	4.9	Acetone	0.25	 presence of agglomerates, particles well-selected, not continuous film but with veins

	5.4	Benzene	0.25	
				presence of agglomerates, particles on average-little selected, not continuous film
	5	Chloroform	0.25	
				presence of agglomerates, particles on average-little selected, not continuous film
	3.2	Ethanol	0.25	
				presence of agglomerates, particles well-selected, the presence of veins give a certain continuity
ECS 5	5	Acetone	0.25	
				presence of agglomerates, particles little selected, not a continuous film, likely presence of a thin film

	4.7	Benzene	0.25	
				presence of agglomerates, particles on average-little selected, possible presence of a thin film
	10.3	Ethanol	0.5	
				strong presence of agglomerates, particles strongly little selected, films variously continuous
	4.9	Toluene	0.25	
				present some agglomerates, particles on average selected, maybe there is a thin film
ECS 9	4.8	Acetone	0.25	
				presence of agglomerates, particles on average-little selected, not continuous film, likely presence of a thin film

	4.9	Benzene	0.25	
				rare agglomerates, particles on average-little selected, non-continuous film, possible presence of a thin
	5.2	Ethanol	0.25	
				rare agglomerates, particles little selected, non-continuous film, possible presence of a thin
	4.8	Toluene	0.25	
				presence of agglomerates, particles on average selected, "film" is not continuous, possible presence of a thin film
ECS 12	4.6	Acetone	0.25	
				strong presence of agglomerates, particles little selected, partially continuous "film" with veins, possible presence of a thin film

	4.3	Benzene	0.25	 presence of agglomerates, particles little selected, "film" is not continuous
	4.6	Ethanol	0.25	 strong presence of agglomerates, particles on average-little selected, in general "film" is not continuous, presence of a thin film
	4.6	Toluene	0.25	 presence of agglomerates, particles on average-little selected, "film" is not continuous
ECS 13	6	Acetone	0.25	 presence of agglomerates, particles little selected, continuity generated by a background pasta consists of a dense network of veins

	2.3	Benzene	0.25	presence of agglomerates, particles little selected, "film" is not continuous, possible presence of a thin film
	9.3	Ethanol	1.0	presence of agglomerates, particles little selected, the presence of thick veins give continuity
	4.7	Toluene	0.25	presence of agglomerates, particles little selected, "film" is not continuous, likely presence of a thin film
ECS 14	5.2	Acetone	0.25	presence of agglomerates, particles averagely well-selected, continuous film made of a very dense tangle of veins
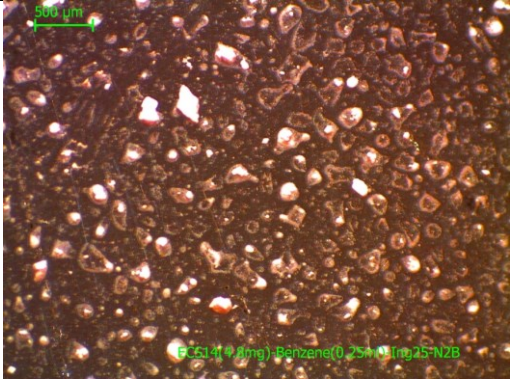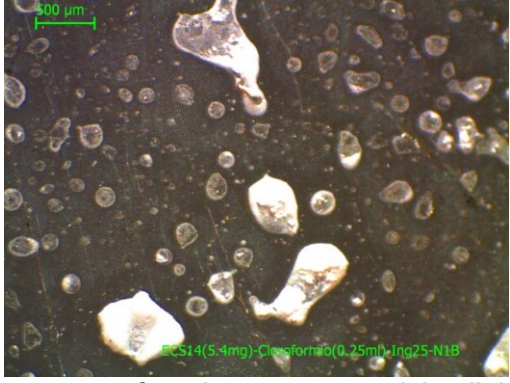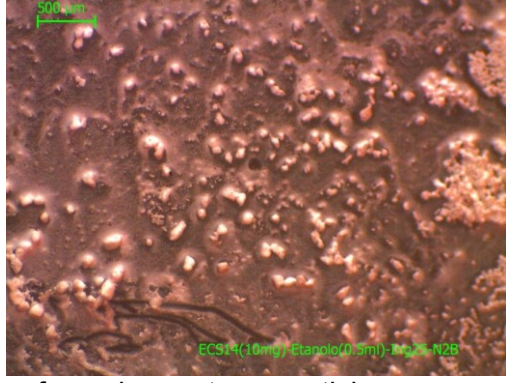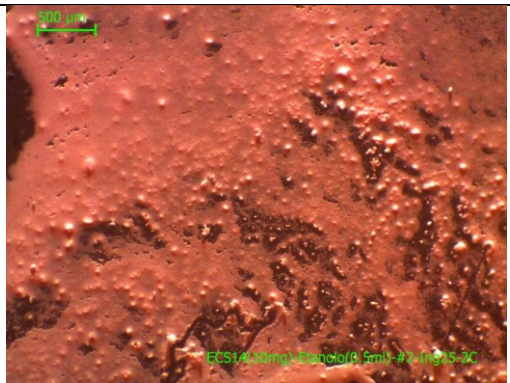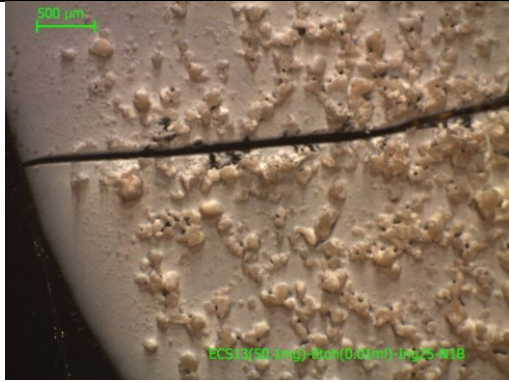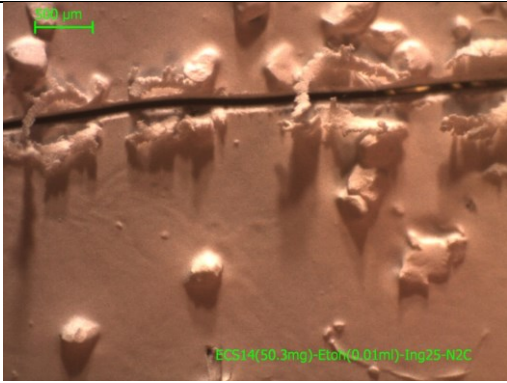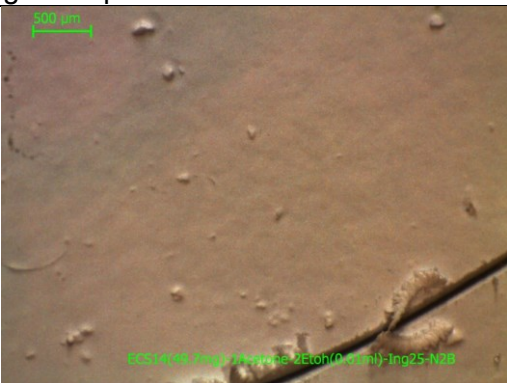
	4.8	Benzene	0.25	
				dubious presence of agglomerates, particles little-average selected, "film" is not continuous
	5.4	Chlorofor m	0.25	
				dubious presence of agglomerates, particles little-average selected, "film" is not continuous, possible presence of thin film
	10	Ethanol	0.5	
				presence of agglomerates, particles on average-little selected, the film is made from a background paste characterized by a dense network of veins which creates continuity
	10	Ethanol-2	0.5	
				presence of agglomerates, particles averagely well-selected, continuous film with the presence of veins and holes

Table B3: Role of ethanol and acetone (glass-optical microscope)

Powder	mg	Solvent	ml	Film quality
ECS 13	49.2	Acetone	10	presence of agglomerates and/or aggregates: the distinction is impossible, the film is on average-well selected, its thickness appears substantially uniform and continuous
	50.1	Ethanol	10	presence of agglomerates consisting of a low number of little packaged aggregates, so weakly bound. The particles (or aggregates) are on average-selected. The deposition deviates from a uniform thickness because of the many agglomerates and aggregates. The film appears continuous
	49.2	(1)Acetone (2)Ethanol	(1) 10 (2) 10	presence of agglomerates characterized by elongated shapes. The aggregates are on average well-selected. The film is almost uniform in thickness. The deposition deviates from a uniform thickness because of the aggregates. The film is continuous with the exception of grooves that could give discontinuities

	50.1	(1)Ethanol (2)Acetone	(1) 10 (2) 10	presence of clusters of small size and low concentration. The aggregates are well selected. The deposition is almost uniform. Presence of small agglomerates and aggregates. This film is characterized by a surface consisting of small cells of polygonal shape. However the layer appears continuous
ECS 14	49.7	Acetone	10	It was not possible to deposit the suspension due to the high viscosity of the same
	50.3	Ethanol	10	presence of corpuscles which are to be classified as aggregates due to their shape, this coul mean that particles are very little selected. The deposition is not uniform because of the presence of corpuscles. These particles are embedded in a background paste which constitutes the film of uniform thickness. In this background pasta one can see the veins
	49.7	(1)Acetone (2)Ethanol	(1) 10 (2) 10	presence of corpuscles which are to be classified as aggregates (or particles). The presence of aggregates determines a powder on average - well selected. The deposition is characterized by an almost uniform thickness. Presence of small particles (presumably
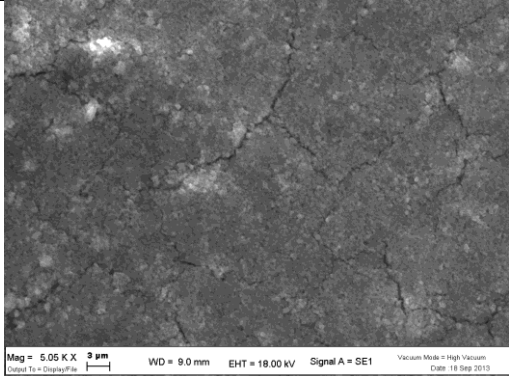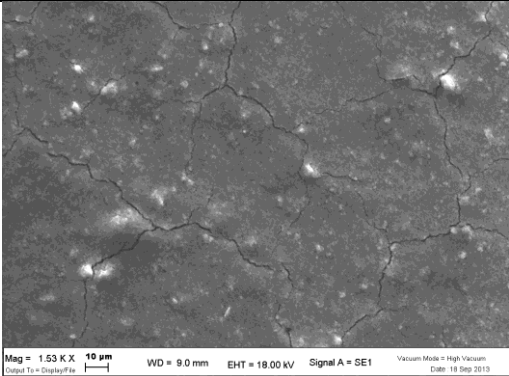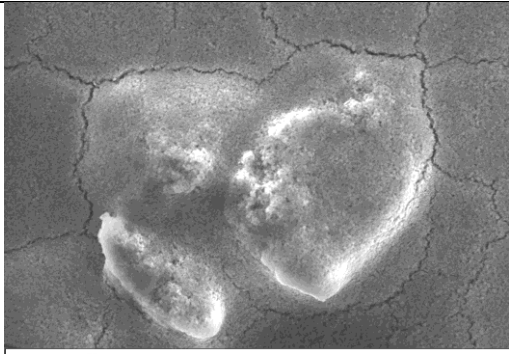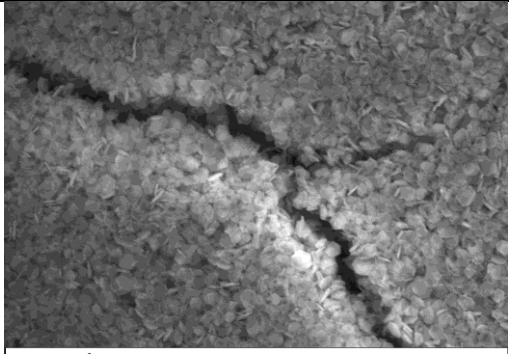
				aggregates) on the film which is characterized by a slightly pitted surface. However the layer appears continuous
	50.3	(1)Ethanol (2)Acetone	(1) 10 (2) 10	absence of aggregates or agglomerates (excluding 3 or 4 tiny corpuscles), so particles are very well selected to fine elements. The deposition is characterized by a uniform thickness, film appears perfectly continuous
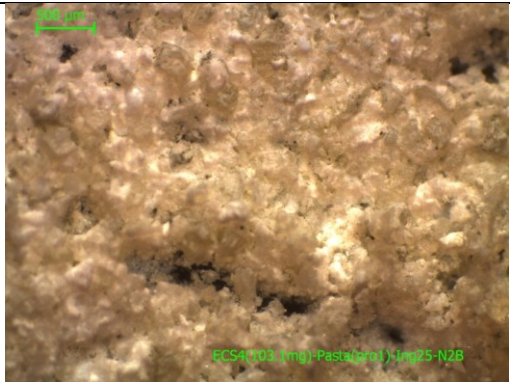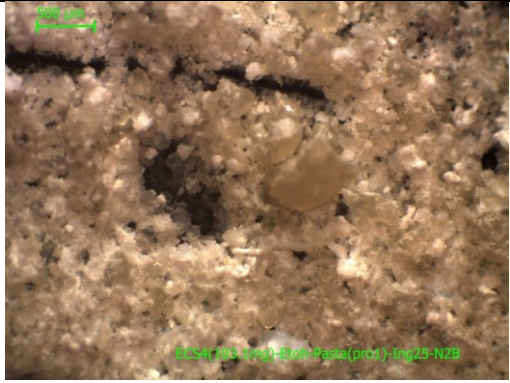
Table B4: Role of ethanol and acetone (silicon-SEM)
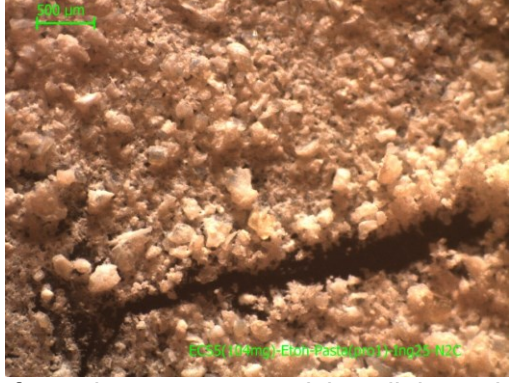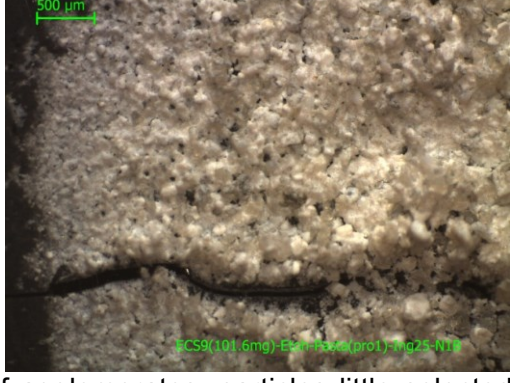
Powder	mg	Solvent	ml	Film quality
ECS 13	49.2	(1)Acetone (2)Ethanol	(1) 10 (2) 10	presence of aggregates, while agglomerates are in minimal amount. The individual particles are not clearly distinguishable. However the material is on average-well selected. Film has uniform thickness and it is made of a continuous layer with corpuscles deposited above, this continuity is characterized by cracking
	50.1	(1)Ethanol (2)Acetone	(1) 10 (2) 10	presence of aggregates, agglomerates do not seem to be present, except in small quantities. The individual particles are not clearly distinguishable,
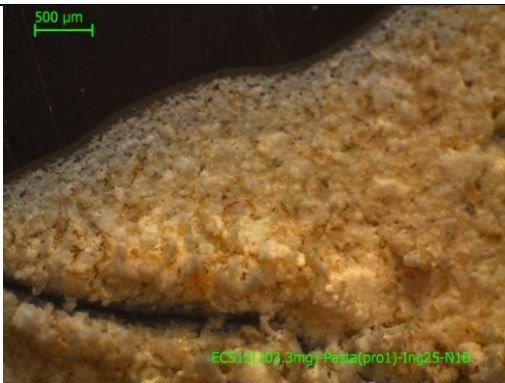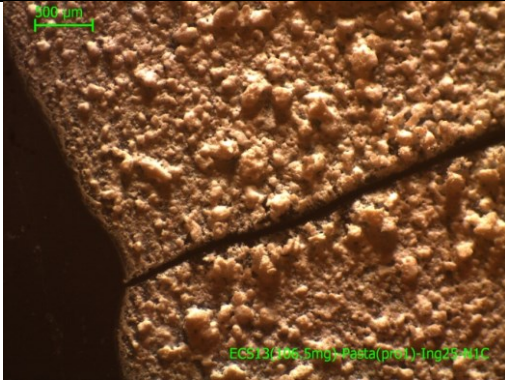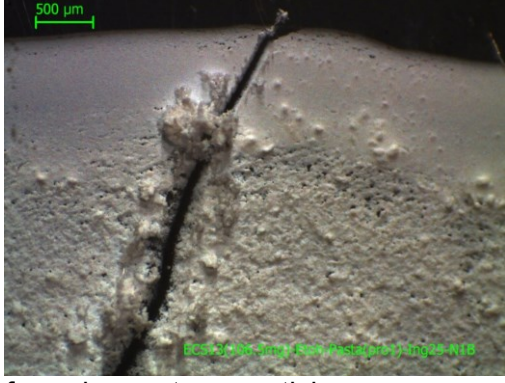
				however the material is well selected. The film is made of a continuous layer with corpuscles which are distributed on the surface of the film. Film of uniform thickness, with small cracks
ECS 14	49.7	(1)Acetone (2)Ethanol	(1) 10 (2) 10	one can appreciate agglomerates, particles are very well selected. The film has uniform thickness, there is some corpuscle attributable to aggregates. The continuity is altered by a network of cracks
	50.3	(1)Ethanol (2)Acetone	(1) 10 (2) 10	one can appreciate agglomerates, particles are very well selected. The film has uniform thickness, there is some corpuscle attributable to aggregates. Present a surface defect in the form of rectangle (it may have been created at the moment of deposition, by contact with some instrument). The continuity is altered by a network of cracks

ECS as functional materials for screen printing paste preparation

Table B5: Complete paste formulation (glass-optical microscope)

Powder	mg	Solvent	ml	Film quality
Organic vehicle with glass frit			/	The pure organic vehicle with glass frit appears almost transparent. The presence of frit induces a decrease in transparency. The film appears well-uniform and well adherent.
ECS 4	103.1	Paste	/	strong presence of agglomerates, particles little selected, substantially continuous film with presence of holes
	103.1	EtOH-Paste	25	presence of agglomerates, particles little selected, the variable continuity of the film and substantial presence of holes

ECS 5	104	Paste	/
			presence of agglomerates, particles little selected, substantially continuous film with presence of holes
	104	EtOH-Paste	25
			presence of agglomerates, particles little selected, poor continuity due to the presence of holes
ECS 9	101.6	Paste	/
			presence of agglomerates, particles little selected variable continuity due to holes
	101.6	EtOH-Paste	25
			presence of agglomerates, particles little selected, the film is characterized by a certain continuity, but with the presence of holes

ECS 12	103.3	Paste	/	presence of agglomerates, particles little selected, "film" continuous, but the presence of holes
	103.3	EtOH-Paste	25	presence of agglomerates, particles on average selected, the "film" appears continuous but there are small holes and some fracture
ECS 13	106.5	Paste	/	strong presence of agglomerates, particles little selected, film with a not complete continuity due to the presence of holes
	106.5	EtOH-Paste	25	presence of agglomerates, particles on average selected, substantially continuous film with the presence of holes
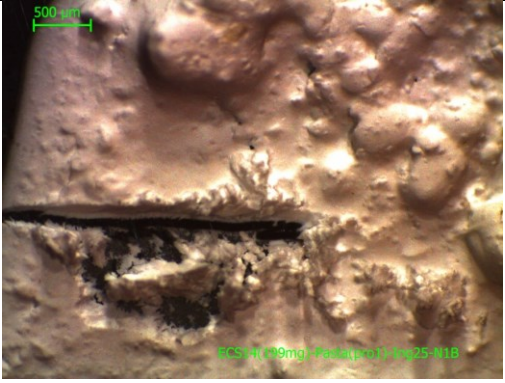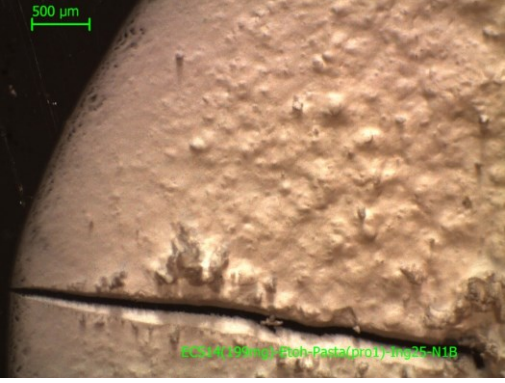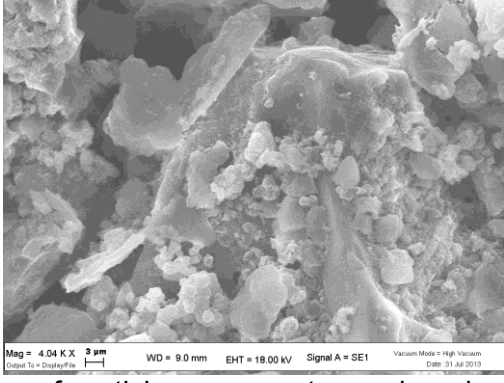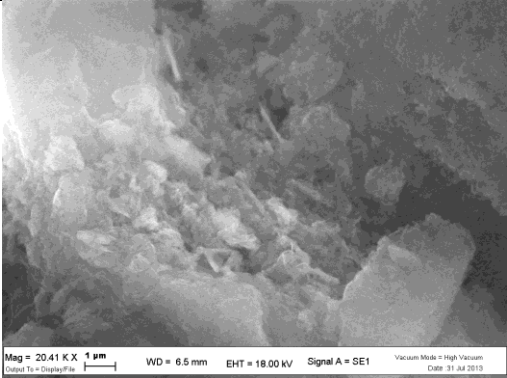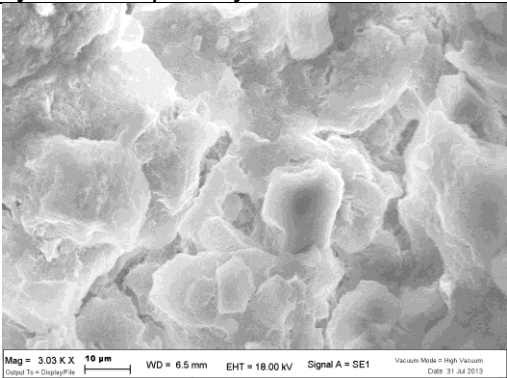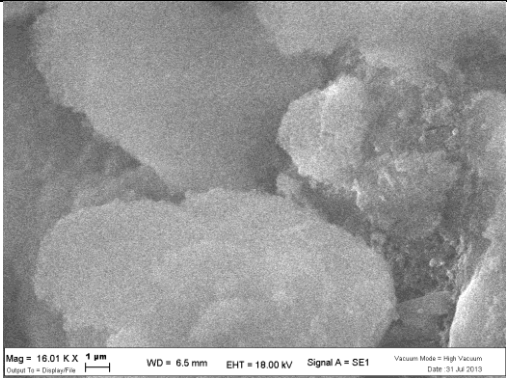
Powder	mg	Solvent	ml	Film quality
ECS 14	199	Paste	/	presence of aggregates and probably also agglomerates, it seems being a poor selection. Rough surface, the film appears continuous
	199	EtOH-Paste	50	presence of aggregates, agglomerates and probably, this aspect suggests lack of selection. Rough surface, anyway the film appears continuous

Table B6: Complete paste formulation (silicon-SEM)

Powder	mg	Solvent	ml	Film quality
ECS 4	103.1	EtOH-Paste	25	presence of particles, aggregates and agglomerates, the particles appear extremely poorly selected. The film is not uniform (this aspect also appears in photographs optical microscope). The surface is discontinuous with the presence of holes, this aspect is due to the presence of coarse elements, which create non-contact areas also not filled by finer elements

ECS 5	104	EtOH-Paste	25	
				presence of particles, aggregates and agglomerates. The particles are poorly selected. The film does not present an uniform thickness, this aspect is due to poor particle-size selection. The possible surface continuity is interrupted by fractures and holes
ECS 9	101.6	EtOH-Paste	25	
				presence of particles, aggregates agglomerations (it appears difficult to distinguish particle and aggregates). The particles are poorly selected. The film does not present an uniform thickness, due to the presence of coarse elements. Compromised continuity of the film for the presence of fractures and holes
ECS 12	103.3	EtOH-Paste	25	
				presence of particles, aggregates and agglomerates (it is difficult to distinguish between individual particles and aggregates). The particles are poorly selected. The film does not present an uniform thickness due to the presence of coarse elements. The possible surface continuity is compromised by the presence of coarse elements, which create vacuum zones unfilled or in part filled by finer elements
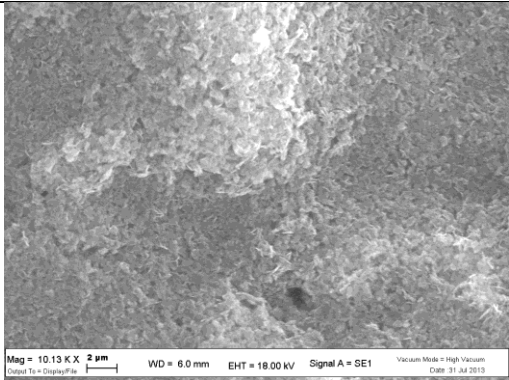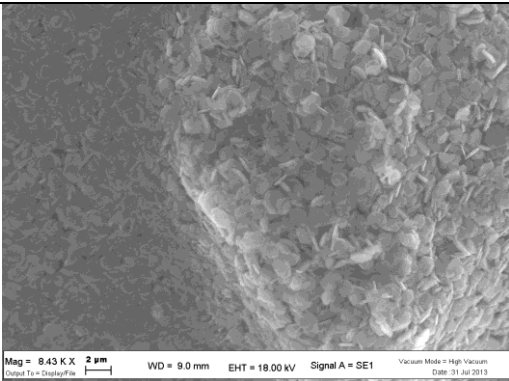
Powder	mg	Solvent	ml	Film quality
ECS 13	106.5	EtOH-Paste	25	 presence of particles, aggregates and agglomerates. The particles are well selected. The film appears nearly uniform thickness, although the presence of coarse elements alters in some areas that characteristic. The presence of fractures makes discontinuous the film
ECS 14	199	EtOH-Paste	50	 the entire surface one can observe lumps, for which the particles seem adherent but not fused, and then are to be classified as agglomerates. To take into account the low presence of aggregates. However, the particles are very well selected. The film presents a non-uniform thickness due to the presence of agglomerates. The surface would appear continuous, but the presence of fractures alters the continuity

Table B7: Formulation without organic vehicle

Powder	mg	Solvent	ml	Film quality
ECS 13	50.5	Ethanol	0.05	 presence of agglomerates, particles on average-little selected, the film does not present an uniform thickness: rough surface, continuously interrupted by the presence of many small holes
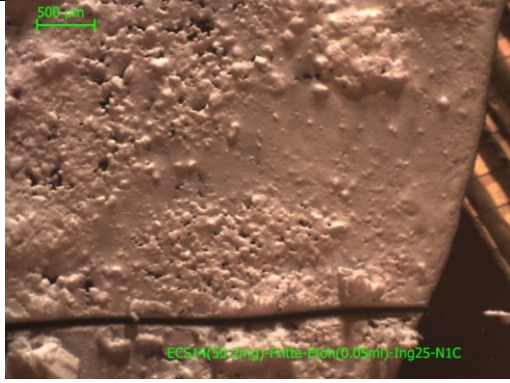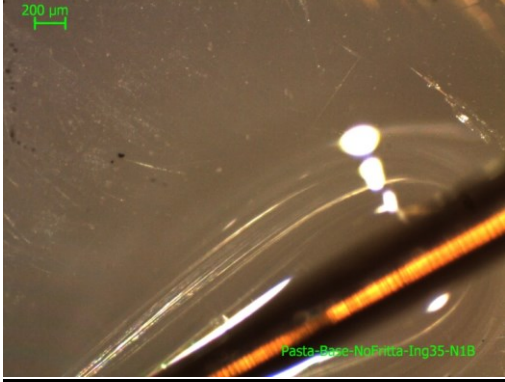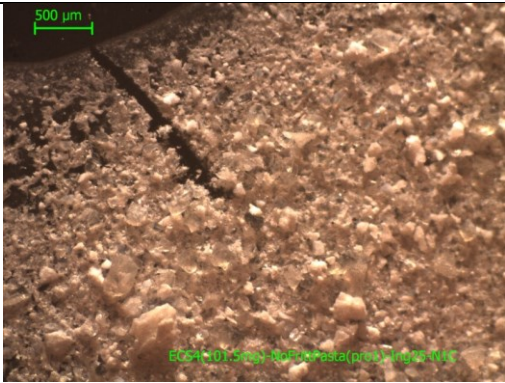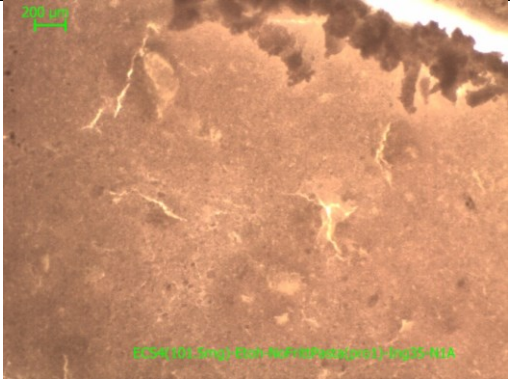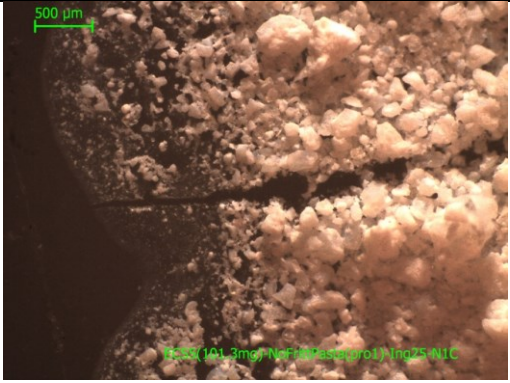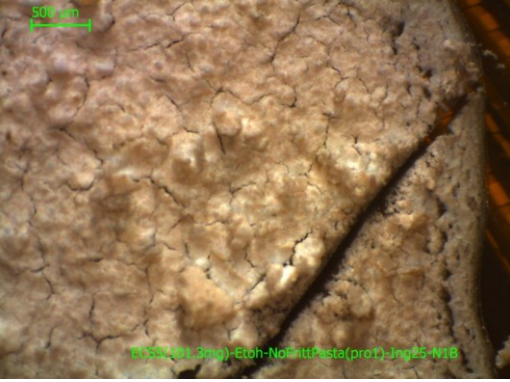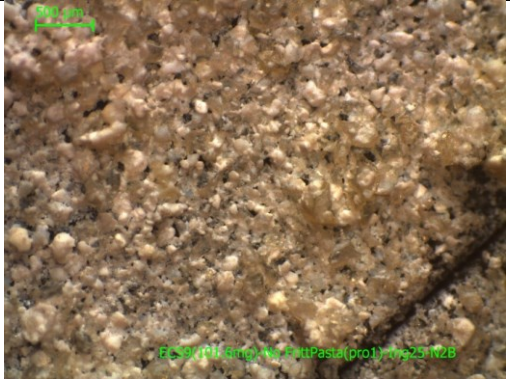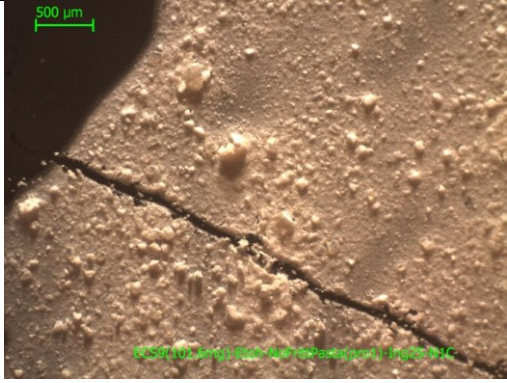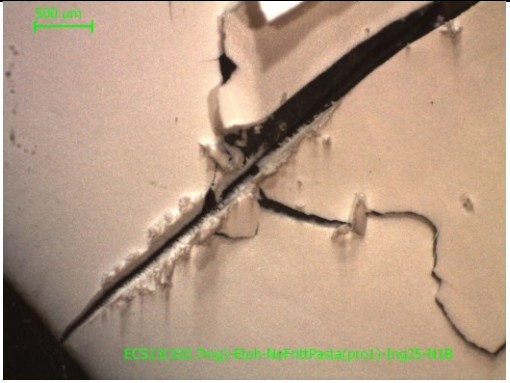
ECS 14	50.5	Ethanol	0.05	
				presence of agglomerates, particles very little selected, the film does not present an uniform thickness, it is continuous in some areas, whereas in other areas holes of different sizes and shapes present

Table B8: Formulation without glass frit (glass-optical microscope)

Powder	mg	Solvent	ml	Film quality
Organic vehicle with glass frit			/	
				the pure organic vehicle without glass frit appears very transparent. The contact between a steel tip and the film highlights a certain tension surface of the latter, which in fact appears gelatinous. The film has a very uniform thickness and it is well adherent.
ECS 4	101.5	Paste without frit	/	
				presence of agglomerates, particles little selected, cleaner film than those containing glass frit, substantially continuous, presence of holes
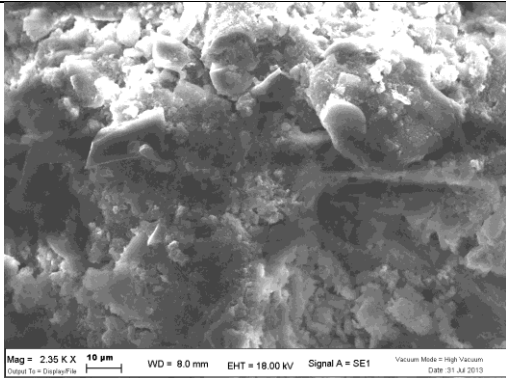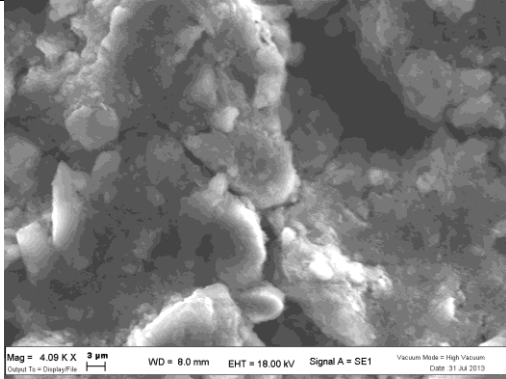
	101.5	EtOH-Paste without frit	10	
				presence of agglomerates and/or aggregates, particles on average well-selected, continuous surface with small fractures
ECS 5	101.3	Paste without frit	/	
				presence of agglomerates, particles strongly little selected, which make the surface extremely rough, strong presence of holes that makes the film poorly continuous
	101.3	EtOH-Paste without frit	10	
				presence of agglomerates and/or aggregates, particles well selected with a few exceptions, surface continuity interrupted by small fractures
ECS 9	101.6	Paste without frit	/	
				presence of agglomerates, particles little selected, the "film" is not continuous, strong presence of holes which increase towards the edge
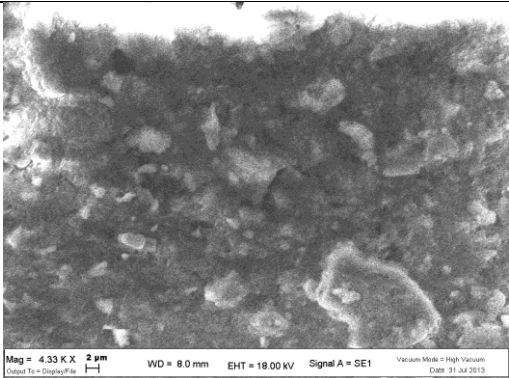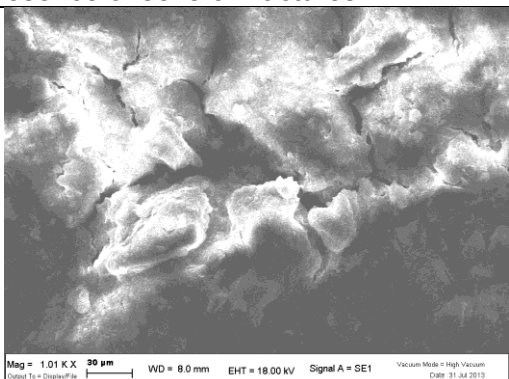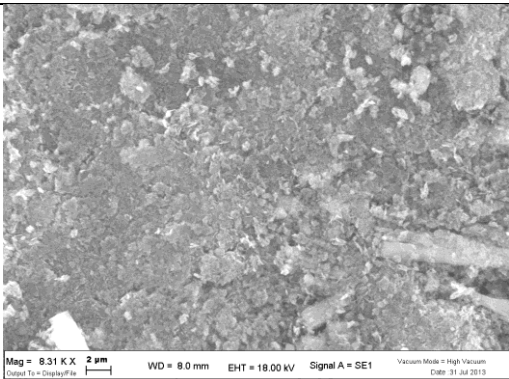
	101.6	EtOH-Paste without frit	10	
				presence of aggregates or perhaps also agglomerates, particles appear on average selected: relatively fine dimensions, with the exception of some aggregate. The film has not an uniform thickness: areas of low thickness, areas of high thickness, fractures in the areas of high thickness interrupt the continuity of the surface
ECS 12	100.8	Paste without frit	/	
				strong presence of agglomerates, particles little selected, the "film" is continuous but with the presence of holes
	100.8	EtOH-Paste without frit	10	
				poor presence of agglomerates, the particles appear on average well-selected, with the exception of some aggregates, there are areas of different thickness, continuous film with the exception of fractures in the area with greater thickness

ECS 13	102.7	Paste without frit	/	strong presence of agglomerates, particles very little selected, low continuity of the "film" for the presence of holes
	102.7	EtOH-Paste without frit	10	complete absence of agglomerates: the material has been fully unbundled, the film has uniform thickness, smooth surface. The continuity would be perfect, but the presence of significant fractures radially arranged dissect the film, also causing detachment of flakes from the support
ECS 14	102.8	Paste without frit	/	presence of agglomerates, particles are very little selected. The "film" is not of uniform and continuous due to the presence of holes
	102.8	EtOH-Paste without frit	10 µl	

| | | | | some rare lump on the surface, if it is not possible to define aggregates and/or agglomerates, these lumps may still be regarded as defects. Excluding these defects particles are indistinguishable even at high magnification, the material has been fully unbundled, very well selected. Uniform thickness, smooth surface, except for the rare defects of the lumps, and perfectly continuous |

Table B9: Formulation without glass frit (silicon-SEM)

Powder	mg	Solvent	ml	Film quality
ECS 4	101.5	EtOH-Paste without frit	10	presence of particles, aggregates and agglomerates. The particles appear extremely poorly selected. The film does not present an uniform thickness. The presence of particles/aggregates would affect the uniformity. The surface is fairly constant, the presence of fractures and holes due to not completely fill of the voids left by the larger particles/aggregates alters the continuity
ECS 5	101.3	EtOH-Paste without frit	10	presence of particles, aggregates and few agglomerates. The particles appear little - on average selected. The film does not present an uniform thickness, due to the presence of elements with coarse dimensions. The possible surface continuity is interrupted by a dense presence of fractures

ECS 9	101.6	EtOH-Paste without frit	10	
				presence of particles/aggregates (from the photos it is impossible to distinguish between the two types of elements) and agglomerates. The particles/aggregates appear little selected. The film does not present an uniform thickness, this aspect is due to the presence of coarse elements. The surface continuity is significantly affected by the presence of several fractures
ECS 12	100.8	EtOH-Paste without frit	10	
				the photo looks very poor presence of individual particles. There are unitary elements as aggregates, however agglomerations do not seem substantial. The film does not present an uniform thickness. In addition there are aggregates and/or agglomerates that make the surface rough. Some fractures in the areas with greater thickness make the surface discontinuous
ECS 13	102.7	EtOH-Paste without frit	10	
				presence of particles, which are often organized into aggregates or agglomerates. The particles are well selected. The film does not present an uniform thickness due to the presence of coarse elements which alter the flatness. The good granulometric selection, consisting of fine elements could guarantee a continuity, thanks to
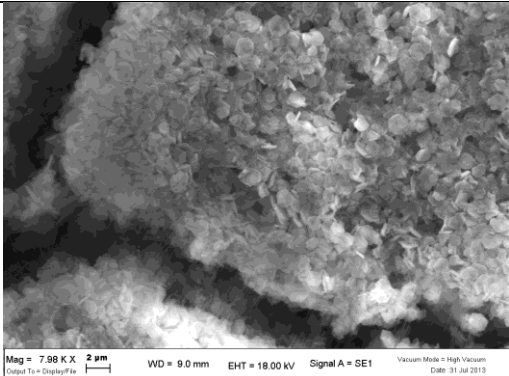
Powder	mg	Solvent	ml	Film quality
				the absence of holes, fractures decrease the continuity of the film
ECS 14	102.8	EtOH-Paste without frit	10	on the surface it can be noted that the particles seem adherent but not fused, and then are to classified as agglomerates, then the presence of aggregates has to be taken into low consideration. The particles are very well selected. The film appears non-uniform thickness due to the presence of agglomerates. The surface would appear continuous, but the presence of fractures alters the continuity

Table B10: Zeolites-Formulation without glass frit (glass-optical microscope)

Powder	mg	Solvent	ml	Film quality
ZY 1	100.1	EtOH-Paste without frit	10	absence of aggregates, well-selected particles; the film is continuous with uniform thickness. The continuity is not perfect due to cracks present mainly in the central area and the average of the deposition; the film looks adherent.
ZY 2	103.5	EtOH-Paste without frit	10	absence of aggregates, well-selected particles;

				the film is continuous with uniform thickness; the film looks adherent.

Table B11: Depositions on alumina substrates of pastes containing ECS 14.
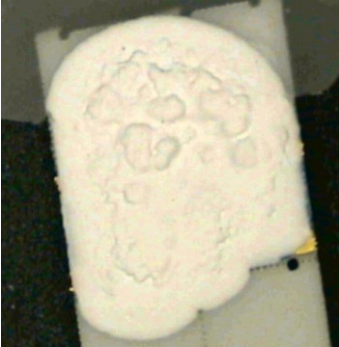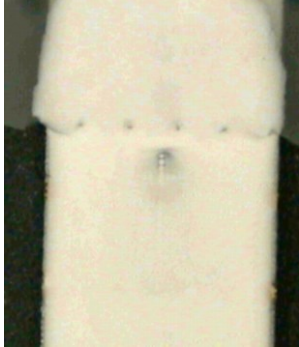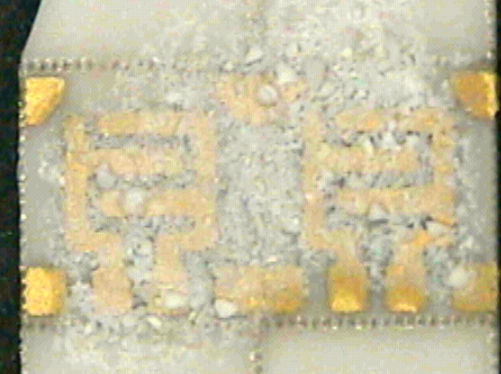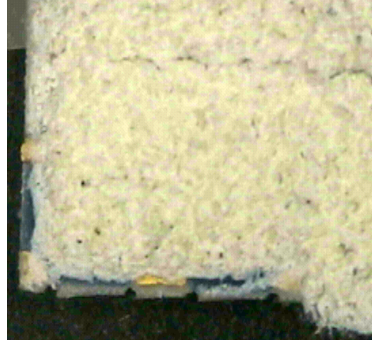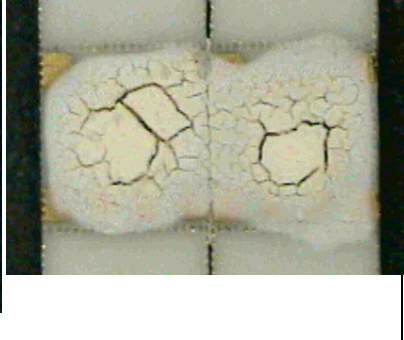
ECS 14		
PASTE + Ethanol	PASTE WITHOUT GLASS FRIT	PASTE WITHOUT GLASS FRIT + Ethanol

Table B12: Depositions on alumina substrates of pastes containing ECS 4.
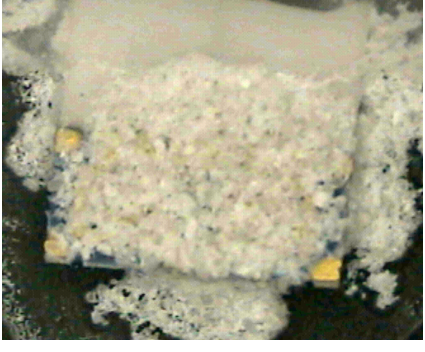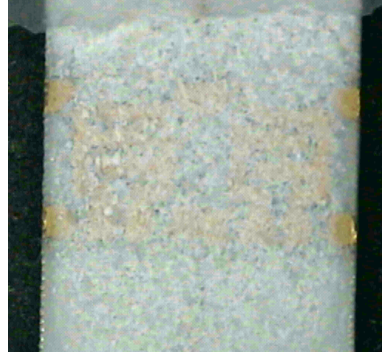
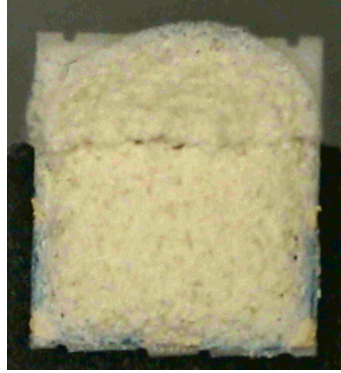| ECS 4		
PASTE + Ethanol	PASTE WITHOUT GLASS FRIT	PASTE WITHOUT GLASS FRIT + Ethanol

Table B13: Depositions on alumina substrates of pastes containing ECS 5.

ECS 5		
PASTE + Ethanol	PASTE WITHOUT GLASS FRIT	PASTE WITHOUT GLASS FRIT + Ethanol

Table B14: Depositions on alumina substrates of pastes containing ECS 9.
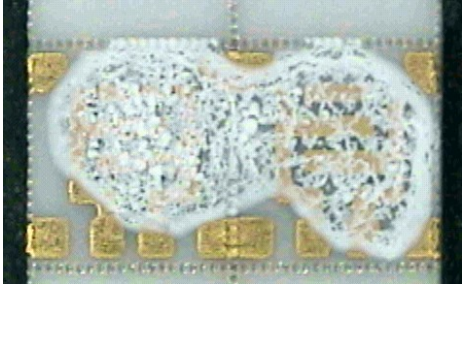
ECS 9		
PASTE + Ethanol	*PASTE WITHOUT GLASS FRIT*	*PASTE WITHOUT GLASS FRIT + Ethanol*

Table B15: Depositions on alumina substrates of pastes containing ECS 12.

ECS 12		
PASTE + Ethanol	*PASTE WITHOUT GLASS FRIT*	*PASTE WITHOUT GLASS FRIT + Ethanol*

Table B16: Depositions on alumina substrates of pastes containing ECS 13.
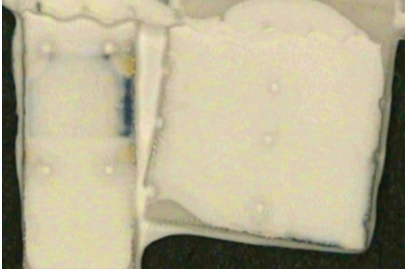
ECS 13		
PASTE + Ethanol	*PASTE WITHOUT GLASS FRIT*	*PASTE WITHOUT GLASS FRIT + Ethanol*

Table B17: Depositions on alumina substrates of pastes containing zeolites.

ZY1 PASTE WITHOUT GLASS FRIT + Ethanol	ZY2 PASTE WITHOUT GLASS FRIT + Ethanol

Appendix C

The abstracts of papers and conference contributions published during the PhD, and not included in this thesis, are showed to follow.

[J01] *V. Guidi, M.C. Carotta, B. Fabbri, S. Gherardi, A. Giberti, C. Malagù, Array of sensors for detection of gaseous malodors in organic decomposition products, Sensors and Actuators B 174 (2012) 349– 354*

Sensing of typical gaseous pollutants and malodors as a result of decomposition of organic compounds via chemoresistive gas sensors has been addressed. Screen-printed films of a solid solution of mixed Sn and Ti oxides, of mixed W and Sn oxides, and ZnO have been selected for the purpose. We demonstrated that the choice of these films for this specific use leads to an improvement in selective detection of such gases under either dry or wet condition. An array of such sensors is shown to be suitable for implementation of deconvolution algorithms because it makes it easier the concentration data processing.

[J02] *A. Giberti, M.C. Carotta, B. Fabbri, S. Gherardi, V. Guidi, C. Malagù, High-sensitivity detection of acetaldehyde, Sensors and Actuators B 174 (2012) 402– 405*

A set of sensors based on nanostructured single and mixed metal oxides has been prepared and employed in acetaldehyde detection within 0.1–10 ppm, this range being useful for many applications. Electrical characterization has been performed in laboratory at several working temperatures, in order to obtain the optimal operating condition. ZnO working within 450–550 °C, was found to best respond to acetaldehyde. The response vs. concentration curves for all the sensors was a power law with an exponent of 0.5, compatible with the oxidation of acetaldehyde catalyzed by the surface. A decay in the sensor response to acetaldehyde due to humidity was observed and discussed.

[J03] *B. Fabbri, S. Gherardi, A. Giberti, V. Guidi, C. Malagù, Sensing of gaseous malodors characteristic of landfills and waste treatment plants, JOURNAL OF SENSORS AND SENSOR SYSTEMS 3, 61–67, 2014*

We approached the problem of sensing gaseous pollutants and malodors originating as a result of
decomposition of organic compounds via chemoresistive sensors. A set of four screen-printed films based on two types of mixed tin and titanium oxides, mixed tungsten and tin oxides, and zinc oxide has been tested vs. the main gaseous components of malodors. N-butanol was also considered because of its importance as a reference gas in the odorimetric intensity scale. We found that, under proper working conditions, the films can sensitively detect such gases either in dry or in wet environments, within the range of concentrations of interest for their monitoring. We also demonstrated that the array is robust under solicitation by harmful interference gases such as CO, C_6H_6, NO_2 and NO.

[J04] *A. Giberti, B. Fabbri, A. Gaiardo, V. Guidi, C. Malagù, Resonant photoactivation of cadmium sulfide and its effect on the surface chemical activity, Applied Physics Letters 104, 222102 (2014)*

Photo-enhanced surface chemical activity of cadmium sulfide gives rise to a wide class of surface-dependent phenomena, such as heterogeneous photocatalysis, chemoresistivity, and chemiluminescence, which have several technological and scientific applications. In this work, the
photochemical properties of nanostructured cadmium sulfide films are investigated by means of electrical conductance measurements in controlled atmosphere, while irradiated by light of wavelengths ranging from 400 to 645 nm. Chemisorption of benzene, carbon monoxide, methane,
ethanol, and hydrogen sulfide onto CdS surface has been analyzed as a function of the wavelength, in a gas concentration range of the order of parts per million. It resulted that the increase of photoconductance with gas adsorption is resonant with the bandgap energy. It turns out that this resonant enhancement of the surface chemical activity can be of advantage for all the optical and chemical mechanisms that depend upon it. An interpretation of these results, in terms of electronic optical transitions and Fermi level shift induced by light, is proposed.

[J05] *C. Malagu', B. Fabbri, S. Gherardi, A. Giberti, V. Guidi, N. Landini, G. Zonta, Chemoresistive gas sensors for detection of colorectal cancer biomarkers, Sensors 2014, 14, 18982-18992*

Numerous medical studies show that tumor growth is accompanied by protein changes that may lead to the peroxidation of the cell membrane with consequent emission of volatile organic compounds (VOCs) by breath or intestinal gases that should be seen as biomarkers for colorectal cancer (CRC). The analysis of VOCs represents a non-invasive and potentially inexpensive preliminary screening technique. An array of chemoresistive gas sensors based on screen-printed metal oxide semiconducting films has been selected to discriminate gases of oncological interest, e.g., 1-iodononane and benzene, widely assumed to be biomarkers of colorectal cancer, from those of interference in the gut, such as methane and nitric oxide.

[J06] *A. Giberti, D. Casotti, G. Cruciani, B. Fabbri, A. Gaiardo, V. Guidi, C. Malagù, G. Zonta, S. Gherardi, Electrical conductivity of CdS films for gas sensing: Selectivity properties to alcoholic chains, Sensors and Actuators B 207, (2014) 504-510*

Nanophased cadmium sulfide powder was synthesized with a simple route and characterized with thermal, structural and morphological analysis. Conductometric gas sensors based on thick films of synthesized CdS were fabricated by means of screen-printing technology and their sensing properties were tested on a selection of alcohols, aldehydes, ketones and other gaseous compounds. We found that, at working temperature of 300◦C, the CdS films show a strong selectivity vs alcohols, proving that they can efficiently detect alcohols in mixtures where aldehydes and other interferers are present. The response was found to be proportional to the length of the alcoholic chain, and a possible sensing mechanism that accounts for this property was proposed.